Three-dimensional Image Classification Using Hierarchical Spatial Decomposition: A Study Using Retinal Data

Thesis submitted in accordance with the requirements of
the University of Liverpool for the degree of Doctor in Philosophy
by

Abdulrahman Abdulaziz A Albarrak

February 3, 2015

Abstract

This thesis describes research conducted in the field of image mining especially volumetric image mining. The study investigates volumetric representation techniques based on hierarchical spatial decomposition to classify three-dimensional (3D) images. The aim of this study was to investigate the effectiveness of using hierarchical spatial decomposition coupled with regional homogeneity in the context of volumetric data representation. The proposed methods involve the following: (i) decomposition, (ii) representation, (iii) single feature vector generation and (iv) classifier generation. In the decomposition step, a given image (volume) is recursively decomposed until either homogeneous regions or a predefined maximum level are reached. For measuring the regional homogeneity, different critical functions are proposed. These critical functions are based on histograms of a given region. Once the image is decomposed, two representation methods are proposed: (i) to represent the decomposition using regions identified in the decomposition (region-based) or (ii) to represent the entire decomposition (whole image-based). The first method is based on individual regions, whereby each decomposed sub-volume (region) is represented in terms of different statistical and histogram-based techniques. Feature vector generation techniques are used to convert the set of feature vectors for each sub-volume into a single feature vector. In the whole image-based representation method, a tree is used to represent each image. Each node in the tree represents a region (sub-volume) using a single value and each edge describes the difference between the node and its parent node. A frequent sub-tree mining technique was adapted to identified a set of frequent sub-graphs. Selected sub-graphs are then used to build a feature vector for each image. In both cases, a standard classifier generator is applied, to the generated feature vectors, to model and predict the class of each image. Evaluation was conducted with respect to retinal optical coherence tomography images in terms of identifying Age-related Macular Degeneration (AMD). Two types of evaluation were used: (i) classification performance evaluation and (ii) statistical significance testing using ANalysis Of VAriance (ANOVA). The evaluation revealed that the proposed methods were effective for classifying 3D retinal images. It is consequently argued that the approaches are generic.

Acknowledgements

Of all the fantastic and fabulous people involved, I would like to express my deepest gratitude to my first supervisor, Prof. Frans Coenen, who has been abundantly helpful and has offered invaluable assistance, support, caring, patience, and guidance throughout my Ph.D. It is my privilege to have worked with him. Deepest gratitude is also due to my second supervisor, Dr. Yalin Zheng, without whose knowledge and assistance this research would not have been successful.

I would like to express my deepest gratitude to my family. They were always supporting me and encouraging me with their best wishes.

Special thanks also go to my colleague, Mr. Nattapon Boonarpha, for his collaborative research work and his scanning of the images. Special thanks also to all the staff in the Department of Computer Science at The University of Liverpool and the St. Paul's Eye Unit at the Royal Liverpool University Hospital who have been helpful whenever needed. Not forgetting my fellow colleagues in Room 2.11 who always encouraged each other either directly or indirectly; my prayers go to all of you to succeed in everything that you do.

I would like to thank the Royal Embassy of Saudi Arabia, more specially the Cultural Bureau in London, for providing me with the opportunity to conduct my Ph.D. study.

Contents

List of Figures

List of Tables

List of Algorithms

Notation

The following notations and abbreviations are found throughout this thesis:

2D Two Dimensional.
3D Three Dimensional.
AMD Age-related Macular Degeneration.
ANOVA Analysis Of Variance.
AUC Area Under the receiver operating Curve.
DM Data Mining.
DL Dictionary Learning.
FSM Frequent Sub-tree Mining.
IM Image Mining.
k-NN k-Nearest Neighbour.
KDD Knowledge Discovery in Databases.
KDI Knowledge Discovery in Images.
NB Naive Bayes classifier.
RB Region-Based.
SVM Support Vector Machine.
TCV Ten-fold Cross Validation.
VOI Volume Of Interest.
WIB Whole Image-Based

Chapter 1

Introduction

1.1 Overview

The past decade has seen the rapid development of three-dimensional (3D) imaging acquisition technologies. This recent innovation has highlighted the need for more advanced techniques to analyse such 3D image data. The potential for such techniques is further highlighted by progress in the amount of computational power and storage that is now available. There are a number of application domains where 3D images are regularly used. One important domain is the medical domain where many different types of images are used to support the prediction and management of diseases and conditions.

Knowledge Discovery in Databases (KDD), or simply Knowledge Discovering in Data, is a computer science technology directed at turning low-level data into high-level knowledge [46]. More formally KDD can be described as the non-trivial process of identifying valid, novel, potentially useful, previously unknown, and ultimately understandable patterns and useful information from data. The data mining element of the KDD process can be argued to be the most significant element of the entire process; it is where the desired knowledge discovery is actually undertaken. Data mining is thus concerned with the specific task of extracting hidden patterns and/or other useful information from the input data. Various techniques, from various disciplines, have been proposed with which to conduct the data mining [36].

Data mining has traditionally been applied to straightforward tabular (database) style data. However, there are many applications where we might wish to apply the concept of data mining but the data is not naturally in a tabular format. One such application domain is image mining, the extraction of useful information and patterns from collections of images. Image mining, or Knowledge Discovery in Images (KDI), encompasses processes outside of the normal scope of KDD. In this context, KDI uses approaches from image processing, computer vision, image retrieval, and image understanding, as well as data mining approaches, in order to discover relevant knowledge from images.

One common image mining task is image classification. Classification can be defined as the process of automatically creating a piece of software, called a classifier, which can be used to categorise unseen data. Classifiers are typically built using a pre-labelled *training set* and their effectiveness is typically established by applying it to a *test set* whose labels are known (thus the actual labels can be compared with the derived labels). In the case of image classification, a classifier might be built for the purpose of disease/no-disease categorisation of medical images ("normal" versus "abnormal"). This type of image classification is known as whole-image classification in contrast to other types of classification where the task is to base the classification on some object contained within an image.

Image mining is typically directed at two-dimensional (2D) images; however, as noted above, recent technology exists whereby we can acquire 3D images (volumes). Volumetric 3D image mining has received much less attention than 2D image mining [6, 104, 149, 142]. This is largely because 3D image mining is a much more resource intensive task than 2D image mining. In the context of image classification 3D image classification is therefore a challenging task. However, 3D image classification provides a solution to the need for advanced techniques with which to analyse 3D image data as noted at the start of this section.

The subject matter for this thesis is thus 3D (volumetric) medical image classification. The main issue with 3D image classification is not so much the data mining techniques to be applied, these are frequently well understood, but the preprocessing of the 3D data so as to enable the application of data mining techniques. The challenge here is to translate the input data into some appropriate representation compatible with the data mining techniques to be adapted, while at the same time ensuring that no key elements are lost, elements that may be significant with respect to effective 3D image classification. This thesis proposes a number of approaches to deal with the problem of 3D image classification founded on the idea of hierarchical spatial decomposition. The justification for this is presented in Section 1.3 below. Note that we can identify two broad mechanisms for using 3D hierarchical decomposition in the context of 3D volume classification. We can represent the decomposition using regions identified in the decomposition (region-based) or we can represent the entire decomposition (whole image-based).

To act as a focus for the research, the work has been directed at the detection of retinal diseases such as Age-related Macular Degeneration (AMD) in 3D volumes produced using Optical Coherence Tomography (OCT). Analogous to ultrasound, OCT is a relatively new imaging technology that can produce cross-sectional views of a retina at a high level of resolution and speed. AMD is a condition typically contracted in old age, which leads to irreversible vision loss at its advanced stages [21, 66].

The rest of this introductory chapter is organised as follows. First additional dis-

cussion concerning the motivation for the work is presented in Section 1.2. The specific "research question", and associated research issues, are presented in Section 1.3. Section 1.4 outlines the research methodology adopted to address the research question and issues, including the adopted evaluation strategy. Section 1.5 then highlights the research contribution of the work, and Section 1.6 presents some of the published work resulting from the research presented in this thesis. Section 1.7 reviews the structure of the rest of this thesis.

1.2 Motivations

The main aim of the investigation presented in this thesis is to find efficient and accurate approaches to represent 3D images using the concept of hierarchical spatial decomposition, which will enable reliable classification with respect to real-world problems. Most of the research on volumetric date analysis to date has tended to focus on feature extraction [32, 129, 139], image segmentation [55, 58, 136] and image alignment and registration [93] rather than classification. There is very little published work on the classification of volumetric data [1, 127]. In practice, at least with respect to the medical image mining domain, this tends to be done by hand; although there are various tools in current use to support 3D image analysis and diagnosis, these tend not to fully automate the process. The automated diagnosis of diseases using 3D data, even if only coarsely achieved, would clearly ease the time resource required to process such images. Areas where automated diagnosis would be of particular value are in screening programmes where large quantities of image data need to be processed in such a way that patients can receive results during the same consultation in which the data is acquired (point of care diagnosis). Examples include breast and prostrate cancer screening, although this is usually done using 2D images. In the case of 3D volumetric imaging, the problem is more acute as there is much more data to consider; 3D data sets tend to be an order of magnitude larger than 2D data sets. One type of screening programme where 3D images are regularly used are retina screening programmes. For example, screening programmes for the detection of AMD are currently under consideration given the global ageing population. Another example is screening programs for diabetics who are frequently screened for diabetic retinopathy using 3D retinal images.

In the medical domain there are a number of technologies typically used to generate 3D volumes; these include: Cone Beam Computed Tomography (CBCT), Magnetic Resonance Imagery (MRI) and Optical Coherence Tomography (OCT). The focus of the research is thus the detection of AMD in 3D OCT. The motivations for choosing this application domain as a "driver" for the research described in this thesis are as follows:

1. Little work has been reported for AMD detection in terms of volumetric data

mining applied to 3D OCT image data, although there have been a number of reported studies with respect to macular disease diagnosis using 2D OCT images [49, 88]. Most reported work on OCT image analysis is directed at retinal layer segmentation [70, 150], vessel segmentation [71], image enhancement [81] and noise reduction [110].

2. With the increasing widespread use of 3D OCT techniques many clinicians have found that they are "overwhelmed" by the quantity of data available for analysis. They are limited by time and resources. There is also a lack of automated diagnosis tools; most existing tools are directed at supporting the analysis, such as tools for retinal thickness measurement. In practice, subjective assessment is the mainstay. Although the clinicians do an outstanding job the process is subject to human error and skill. Therefore, automated diagnosis tools, founded on the technology proposed in this thesis, are desirable; not only to provide for better patient management but also to provide for staff training.

3. More generally, Computer-Aided Diagnosis (CAD) is an important element of many branches of medical care, not just in the case of 3D retinal diagnosis. Generally applicable approaches to support automate CAD are therefore desirable.

4. Intuitively, for many medical applications (including retinal image diagnosis), being able to use 3D data sets to support the diagnosis is likely to be much more effective than when using 2D data sets. It is anticipated that volumetric data is likely to reveal more information about the scanned objects than 2D data.

1.3 Research Questions and Issues

Given the research motivation presented in Section 1.2 above the work described in this thesis is targeted at an investigation of techniques to facilitate the diagnosis of 3D medical images. More specifically, the work is directed at the development of various ways to represent 3D volumes so that efficient and effective 3D classifiers can be generated using hierarchical spatial decomposition techniques to represent 3D images for classification. Thus the overarching research question addressed by this thesis is:

> *Is it possible to devise hierarchical spatial decomposition-based representation methods, suited to the classification of volumetric data, in such a way that effective classification performance can be achieved given the significant size and complexity of volumetric data sets?*

The reasons for adapting a decomposition approach are as follows:

- The decomposing of a space into subspaces helps to identify the most significant localised patterns in the context of the subspace; whereas otherwise, by considering the space in its entirety, localised patterns may be missed. Note that in the

context of data mining the patterns we are interested in generally tend to be a description or a model of a subset of the data [35].

- Hierarchical decomposition allows for a more "complete" analysis in that the analysis can be directed at different levels of the decomposition.

- There is evidence to suggest that image representation methods that rely on localised features tend to produce better performance than those that use global features. Examples of such localised methods include: (i) Scale-Invariant Feature Transform (SIFT) [90, 91, 92], (ii) Histograms of Oriented Gradients (HOGs) [25], and (iii) Local Binary Patterns (LBPs) [98] and their extension to 3D [40, 119, 123, 157].

- Hierarchical decomposition analysis allows for the identification of regions with similar (homogeneous) properties, properties that may be significant with respect to classification of the volume under consideration.

- Spatial relationships between regions can be maintained. Regions that share the same parent remain identifiable.

- Once the decomposition has been established it can be used in a variety of different ways; in other words, decomposition is a versatile technique. Principally we can choose to represent the decomposition in its entirety (whole image-based) or we can consider individual regions within the decomposition in isolation (region-based).

A central issue with respect to representations that are founded on the concept of hierarchical spatial decomposition is the termination condition for the decomposition (the so called "critical function"). Critical functions normally operate according to the "homogeneity" of individual regions. A further issue is the "overlap problem" where a particular object of interest is held in different parts of the decomposition; the object of interest overlaps several identified regions. The research presented in this thesis investigates various techniques to decompose the image by considering different approaches to ensure the homogeneity of the decomposed regions.

The above research question thus encompasses five subsidiary research questions:

1. **What is the most appropriate method to decompose images?** A number of different mechanisms for decomposing volumes can be identified although prior to the research described in this thesis it was unclear as to which was the most appropriate.

2. **Once a volume has been decomposed, is it better to represent the volume in terms of the individual decomposed regions (region-based)**

or in terms of the entire decomposition (whole image-based)? This is the most significant subsidiary research question, whose resolution is central to the work described in this thesis.

3. **With respect to the use of either region-based or whole image-based representation, what is the most appropriate representation for encapsulating the decomposition to support the desired classification?** The issue here is that some image representation techniques result in a more classification effective representation than others.

4. **Given a particular representation what is the most effective way of generating a single feature vector for each image?** Most classifier generation mechanisms ultimately operate using a feature vector representation. Thus regardless of what decomposition representation is adapted it needs to be eventually translatable into a feature vector form. The best process for this is unclear.

5. **What is the most appropriate mechanism for conducting volumetric classification?** Different image representations, even when features are translated into a feature vector representation, will be compatible with different classification techniques; however, it is unclear what the most appropriate technique for each representation is with respect to the representation proposed in this thesis.

1.4 Research Methodology

To provide answers to the above central research question posed by this thesis, and the subsidiary questions, the adapted research methodology was broadly to consider and evaluate a number of hierarchical spatial decomposition techniques, each operating in a different manner.

To this end it was first necessary to collect OCT training and test data; this was obtained from the Royal Liverpool University Hospital (RLUH), which has a well-established eye unit, St. Paul's Eye Unit. Specialist staff at St. Paul's were also able to comment on the utility of the proposed approaches. The obtained raw image data required preprocessing, due to some unwanted content, and alignment. These images were then used to investigate the effectiveness of spatial decomposition as the basis upon which different ideas concerning decomposition based techniques, to support 3D volume analysis, were founded. With respect to the decomposition process different critical functions were used to determine different regional homogeneity. Once the images had been decomposed, the effect of using two different categories of hierarchical spatial decomposition representation were investigated and evaluated: (i) region-based and (ii) whole image-based. Different techniques within each representation method were also investigated. The various representations ultimately, of course, had to result

in some form of feature vector representation as this is the standard input format for most classifier generators (as noted above). Because ultimately a feature vector representation would need to be derived, feature selection and generation strategies were considered.

What ever the case the generated feature vectors could then be fed into a classifier generator, for which purpose a number of different classifier generators were considered and evaluated. The process of generating a classifier thus comprises different stages and at each stage there are different techniques that can be used. Therefore the evaluation of each stage was conducted by considering the proposed techniques for the stage in question while using a fixed set of techniques for the remaining stages. For each stage two types of evaluation were conducted: (i) individual performance evaluation, and (ii) statistical significance testing. Ten-fold Cross Validation (TCV) was used, whereby the image data set is randomly divided into ten sub-sets (each with the same number of images for each class). Each technique was then tested ten times, on each occasion with a different tenth as the test set. TCV is a well-established technique with respect to determining the effectiveness of classifiers. On each iteration the following was recorded: (i) accuracy, (ii) sensitivity, (iii) specificity, (iv) Positive Predictive Value (PPV), (v) Negative Predictive Value (NPV), (vi) Area Under the receiver operator characteristic Curve (AUC) and (vii) Equal Error Rate (EER). For the second type of evaluation, the ANalysis Of VAriance (ANOVA) statistical significance test was used.

1.5 Contributions

This thesis makes a number of contributions and these are summarised in this section. Firstly, the work demonstrates that it is possible to improve the performance of 3D image classification by adapting hierarchical spatial decomposition based representation methods. It is argued that by decomposing regions down to homogeneous regions, it is possible to produce effective solutions to the 3D classification problem (various ways to extract homogeneous regions are introduced in this thesis). By hierarchical spatial decomposition, the multi-scale aspects of an image can further be characterised by considering a representation such as the tree-based representation where tree mining techniques can be applied. In addition, various approaches are employed to represent the images by associating the proposed decomposition methods with different representations. After the decomposition process, it is important to examine the significance of each decomposed region with respect to the rest of the images. In this thesis, a number of techniques are proposed to identify the discriminative regions which are significant with respect to individual class labels.

Given the above, the main technical and practical contributions of the work presented in this thesis can be summarised as follows:

1. A novel and effective approach to 3D image classification using spatial decomposition for generating classifiers applicable to 3D volumetric data.
2. Two methods for representing volumetric data within the context of spatial decomposition: (i) region-based and (ii) whole image-based.
3. A mixed oct and quad decomposition mechanism specifically designed for retinal OCT data volumes.
4. Four histogram-based critical functions for regional homogeneity, namely:
   (a) Euclidean Distance (ED)
   (b) Kullback-Leibler divergence (KLD)
   (c) Dynamic Time Warping (DTW)
   (d) Longest Common Subsequence (LCS).
5. A dictionary learning mechanism based on homogeneous regions.
6. In the context of the whole image-based methods, a novel mechanism for generating a feature vector representation from a graph (where the graph represents a hierarchical decomposition) based on the concept of frequent sub-graph mining. Note that with respect to the work presented in this thesis different critical functions are used while previous authors, such as [59], only used one critical function. It should also be noted that in [59] only 2D images were considered while in this thesis 3D images were used.

In addition to the above, the work also makes a number of application-dependent contributions in the context of 3D OCT retinal image analysis and AMD detection, namely:

1. A set of techniques to support automated screening for retinal diseases such as AMD and diabetic retinopathy.
2. With respect to (1), a set of techniques that can be easily extended to encompass generic Computer-Aided Diagnosis (CAD).

1.6 Published Work

Some of the materials described in this thesis have been published previously. This section provides a brief summary of these publications:

1. *Abdulrahman Albarrak, Frans Coenen and Yalin Zheng (2011). Identifying Age-related Macular Degeneration In Volumetric Retinal Images. Ophthalmic Image Analysis Workshop Proceeding. University of Liverpool, pp. 53-58.* This paper investigated some statistical-based representation techniques which are applicable with respect to the region-based representation presented in Chapter 5.

2. *Abdulrahman Albarrak, Frans Coenen, Yalin Zheng and Wen Yu (2012). Volumetric Image Mining Based on Decomposition and Graph Analysis: An Application to Retinal Optical Coherence Tomography. 13th IEEE International Symposium on Computational Intelligence and Informatics (CINTI 2012), Budapest, Hungary, pp. 263-268.* This paper studied the effect of using the whole image representation in terms of a tree structure. The effect of a number of proposed critical functions was also considered. The work described in this paper was used as the foundation for the work presented in Chapter 7.

3. *Abdulrahman Albarrak, Frans Coenen and Yalin Zheng (2013). Classification of Volumetric Retinal Images Using Overlapping Decomposition and Tree Analysis. The 26th IEEE International Symposium on Computer-Based Medical Systems (CBMS 2013), University of Porto, Porto, Portugal, pp. 11-16.* An enhanced method with respect to the previous paper was illustrated. The effect of the boundary on the decomposition was considered. The content of this paper was also used with respect to the work in Chapter 7.

4. *Abdulrahman Albarrak, Frans Coenen and Yalin Zheng (2013). Age-related Macular Degeneration Identification In Volumetric Optical Coherence Tomography Using Decomposition and Local Feature Extraction. The 17th Annual Conference in Medical Image Understanding and Analysis (MIUA 2013), University of Birmingham, pp. 59-64.* This paper presented a method for region-based representation whereby each region was represented in terms of histograms. The work described in this paper was used for Chapter 5.

5. *Abdulrahman Albarrak, Frans Coenen and Yalin Zheng (2014). Dictionary Learning-based Volumetric Image Classification for The Diagnosis of Age-related Macular Degeneration. The 10th International Conference on Machine Learning and Data Mining (MLDM 2014), St. Petersburg, Russia, pp. 272-284.* This paper improved the previous paper by adapting a feature selection mechanism to be used with region-based representation. The content of this paper was also used in Chapter 5. Note that this paper was nominated for the best paper award at the conference.

6. *Abdulrahman Albarrak, Frans Coenen and Yalin Zheng (2014). Dictionary Learning Meets Homogeneous Decomposition for Image Classification: A Study Using Volumetric Retinal Image Data. (In preparation for submission to Medical Image Analysis).* This paper compares region-based representation methods (Chapters 5 and 6) with the whole image-based representation methods (Chapter 7) with respect to the use of a number of proposed critical functions.

1.7 Outline of Thesis

The remainder of this thesis is organised in the following way. Chapter 2 presents a literature review and some background material to the work. Chapter 3 begins by describing the application domain with which the proposed decomposition based techniques were evaluated. The chapter also introduces the image data sets and reviews the required preprocessing. The different proposed approaches for decomposing the volumes of interest are presented in Chapter 4. The two categories for representing the hierarchical spatial decompositions considered in this thesis (region-based and whole image-based) are then presented, and individually evaluated, in the following chapters: region-based representation methods are considered in Chapter 5 and evaluated in Chapter 6, and whole image-based methods are described and evaluated in Chapter 7. In Chapter 8 some comparative discussion concerning the overall best method is presented. Finally, Chapter 9 presents some conclusions and the main findings of the work presented in this thesis, and some possible directions for future work.

Chapter 2

Literature Review and Previous Work

2.1 Overview

This chapter presents an overview of previous work relevant to the work presented later in this thesis. Broadly the work described falls under the "umbrella" of Knowledge Discovery in Images (KDI). This chapter thus commences with a review of KDI in Section 2.2. KDI can be viewed as form of Knowledge Discovery in Data but applied to images. KDI describes a group of techniques used to automatically analyse and discover useful knowledge and patterns within collections of images (or in some cases single images) [9, 34]. As such, KDI is a multi-step process aimed at building sophisticated models of image data. One of these steps is the data mining step which is the part of the KDI process where the knowledge and patterns of interest are discovered. The remaining steps are concerned with the preprocessing and post processing of the input and output data. With respect to the mining step, within the KDI processes, there are a number of different types of task that this step encompasses such as: clustering, pattern identification and classification [130]. The work described in this thesis is directed at image classification.

Although directed at image classification, the central theme of this thesis is image decomposition to support image classification. Section 2.3 therefore reviews the current "state-of-the-art" with respect to image decomposition. Once a given image has been decomposed there are two methods whereby the image can be represented. We can either represent the image in terms of the sub-images (regions) into which it has been decomposed, in which case each image is represented as a collection of sub-images, or we can represent the entire image in terms of its decomposition, in other words as some form of tree structure. Techniques suitable for representing regions within a decomposition are thus reviewed in Section 2.4, while techniques for representing the entire decomposition in the form of some sort of tree structure are reviewed in Section 2.5.

Regardless of whether a region or a whole image-based representation is used, ultimately we wish to produce a feature vector representation as this is the input format typically required by most classification systems. Feature vector generation, in the context of existing work, is therefore considered in Section 2.6. Once the desired feature vector representation has been generated the classification process can be commenced. A review of popular classifier generation methods, particularly those employed with respect to the work described in this thesis, is thus presented in Section 2.7. To measure the effectiveness of a generated classifier there are many well established metrics that can be used. These are therefore described in Section 2.8. Finally, Section 2.9 presents a summary of the material presented in this chapter.

Table 2.1: Terminology used throughout this thesis

Term	Description
Classifier	A software system employed to predict the class of an image.
Decomposition	The process of dividing an image into a set of regions (sub-images).
Feature	A characteristic of an image that can be used to differentiate between images (also sometimes referred to as an attribute). Each feature will have a range of values associated with it, which may be either discrete or continuous.
Feature Space	A n dimensional space where each dimension represents a feature. A given image or region described in terms of n feature values will be located somewhere in this space.
Feature Vector	A vector comprised of a set feature values describing the location of an image in a given feature space.
Voxel	The atomic element of an image volume whose location may be indicated in terms of three dimensional coordinates. A voxel is akin to a pixel in 2D space.

Table 2.2: Basic notation used throughout this thesis

Notation	Description
I_n	An image n in the dataset I.
C_n	The class label for image n in the dataset I.
$X \times Y \times Z$	The size of an image, where X, Y and Z are the width, height, and depth of the image respectively.
$I_n(x, y, z)$	A voxel within an image of a given x, y, z location, where $x \in X$, $y \in Y$ and $z \in Z$.
AIV_i	The average intensity value of a region i.
$d(i, j)$	A function to measure the difference or similarity between two given vectors or values i, j.

Table 2.1 gives some basic definitions of the terminology used in this chapter and in the rest of this thesis. Table 2.2 presents the notation regularly used throughout the rest of this chapter and the remainder of this thesis.

2.2 Knowledge Discovery in Images

As noted in the introduction to this chapter, the field of Knowledge Discovery in Images (KDI) is a specialised variant of the more general field of Knowledge Discovery in Databases (KDD). The distinction between KDI and KDD is thus discussed in Subsection 2.2.1. Subsection 2.2.2 then presents a categorisation of the application-dependent objectives of KDI and this is followed in Subsection 2.2.3 by a general review of the KDI process.

2.2.1 Distinction Between KDI and KDD

The fundamental distinction between KDD and KDI is that the latter is intended to be applied specifically to image data, while KDD has much more general applicability. KDD is defined as the process of identifying useful knowledge from data, while data mining is the sub-process within the overall KDD process concerned with the actual identification of hidden information. The focus of KDI is to support the automated extraction of information from images (as opposed to data in general). KDI is thus concerned with methods for mapping low-level features in images to descriptions where the relationships between them are hidden [64]. KDD is concerned with knowledge discovery in (relational) databases, while KDI is concerned with knowledge discovery in image data. However, there are some significant differences between relational databases and image databases which in turn require that some sub-processes within the overall KDI process need to be different to the corresponding processes found in KDD. Thus this section reviews the distinctions between image data and tabular data so as to highlight the differences between the KDI and KDD processes. The differences between relational databases and image databases data may be summarised as follows [60, 154]:

1. **Absolute versus relative values:** Usually, in relational databases values are meaningful on their own, such as the value for an attribute age. In contrast, the intensity value of an image pixel/voxel does not reveal much information on its own unless the neighbouring context is considered. Therefore, individual intensity values need to be considered with respect to their neighbours.

2. **Spatial information (independent versus dependent position):** It is very important to extract image features by considering the positional relationships of each intensity value with respect to its neighbouring context before mining the patterns of the images, as the spatial position indicates useful information such as the connectivity of the object, texture, shape and colour which may indicate a change in the region. In addition, in 3D images, the depth information should also be taken into consideration. It is not possible to form precise interpretations

of an image without considering this spatial information. In relational databases, there is no need to consider such spatial relationships.

3. **Unique versus multiple interpretation:** In tabular data, the data has a unique interpretation. In contrast, in the case of images it may be the case that the same region can have multiple interpretations. A robust feature extraction method which can cope with this issue therefore needs to be used.

From the above, the main distinction between KDI and KDD is that image data tends to be very unstructured while the tabular data to which KDD is normally applied tends to be highly structured. Thus a variety of processes, from across different disciplines (such as image processing and computer vision [85]), are needed to realise KDI. Feature extraction is one of the most dominant problems in KDI [34]. This issue will therefore be discussed in further detail in Section 2.4.

2.2.2 Objectives of KDI

This subsection considers the distinctions between KDI and KDD further by considering the objectives of KDI in comparison with KDD. At a high level the application-dependent objectives of both KDD and KDI can be characterised as being either: (i) descriptive knowledge discovery or (ii) predictive knowledge discovery [128]. In the case of KDI the focus of descriptive knowledge discovery is on how to describe or represent image data in as concise a manner as possible while at the same time ensuring that key elements of the data are not lost (so that previously hidden knowledge can be readily identified). In descriptive knowledge discovery the aim is to understand the content, differences and similarities of the given image data. For instance, an image may be represented in terms of features, such as texture or shape, so as to form a meaningful description. These descriptions can then be used to compare between images. In the KDD techniques applied to relational databases, descriptive knowledge discovery is not a significant issue because each value is meaningful in its own right, while in KDI descriptive knowledge discovery is a significant issue because individual values are not meaningful in their own right.

Predictive knowledge discovery, in turn, is concerned with identifying patterns that can lead to the establishment of prediction models that can be used with respect to previously unseen image data. For example, the construction of classifiers from medical image data that can be used to predict the presence or absence of some condition or disease. Thus the work described in this thesis falls into the second category, although it can be argued that to produce an effective classifier an effective representation of the data is first required (thus descriptive knowledge discovery).

2.2.3 KDI Process

The KDI process comprises a sequence of steps similar to those found in KDD [75, 80]. The precise sequence and nature of these steps varies across KDI application domains and KDI methodologies. In the context of the work described in this thesis (which is directed at 3D image classification), the KDI process is considered to comprise the following sequence of steps:

1. **Preprocessing Phase**
   (a) **Dataset creation:** This step is essentially concerned with image acquisition.
   (b) **Preparation:** Preparation of the 3D image data so as to remove unwanted structure, such as noise, so as to enhance the image quality.
   (c) **Image representation:** The encapsulation of the key elements (features) of a given set of images (volumes)
   (d) **Feature vector generation:** Generation of a set of feature vectors describing the image data. Note that feature vector generation may also require the application of "reduction methods" so as to reduce the complexity/size of the feature space. This may only be needed if the quantity of generated feature vectors cannot be handled within the image mining.
2. **Data Mining Phase**
   (a) **Image mining:** The step in which the actual knowledge discovery is undertaken (classifier generation with respect to the work described in this thesis).
3. **Post Processing and Usage Phase**
   (a) **Evaluation:**: The evaluation of the discovered knowledge (the generated classifier).
   (b) **Usage:** Application of the discovered knowledge (usage of the generated classifier to label previously unseen volumes)

Note that the above is divided into three phases: (i) preprocessing, (ii) mining and (iii) post-processing and usage. Each of these phases is discussed in further detail in the following three subsections.

2.2.3.1 The KDI Preprocessing Phase

The KDI preprocessing phase is of great significance with respect to the quality of the data mining conducted in the following phase. The phase commences with image acquisition. Broadly, the 3D image sets of interest can be viewed as digital representations

of objects acquired by some process. The image acquisition process can be affected by factors such as: (i) noise, (ii) resolution and (iii) configuration settings. As a result, the nature of the acquired images is often changeable. Therefore, various preliminary processes need to be applied to the images such as colour equalisation, noise removal, and image alignment (registration) [154].

The next step is to represent an image in some way. Image representation in the specific context of the work described later in this thesis is discussed in Sections 2.4 and 2.5. Whatever the case, the nature of the chosen image representations is critical to the effectiveness of the nature of the KDI to be applied [5, 8]. The general aim is to represent image data in terms of a set of features. In the context of the work described in this thesis, the identified set of features should be compatible with the concept of a feature vector representation. The challenges are firstly how best to decide what features are most appropriate to the selected KDI task and secondly how best to extract the desired features. Typically, depending on the application domain, we wish to preserve one or more of the following: contextual information, spatial information, texture and connectivity.

There are a variety of ways that we might represent image data. A growing amount of research has focused on building "local" based image representations. The term "local" in the context of representation refers to the building of descriptors for parts (sub-images) of the whole image (i.e. a local grouping of pixels/voxels). Local based image representations are thus concerned with features that describe a small region within an image instead of a whole image. Local invariant features have proven effective for a range of computer vision problems over the last decade [151]. Local image based representation requires that the given image is first decomposed into a collection of sub-images/sub-volumes (called regions). Mechanisms for this are well understood. The main issue is how to select a representation for the identified regions that allows them to be used to discriminate between images. For classification purposes each image should be represented in a way that makes its label distinguishable from other class labels.

Once we have described our image set in terms of a set of appropriate features the next step is typically to generate a set of feature vectors. The objective of feature vector generation is to include only the most relevant features. Thus in this stage irrelevant or redundant features are removed [12]. In the case of image classification we also wish to retain features with a high discriminatory power.

2.2.3.2 The KDI Mining Phase

As already noted above, Image Mining (IM) is the core of KDI. Recall that IM is the sub-process within the overall KDI process concerned with the actual discovery of knowledge, the remaining steps are all concerned with the preprocessing of image data

so that IM can be applied and the post-processing of the discovered knowledge so that it can be used with respect to some application domain context. The challenge of IM is how to effectively extract the desired knowledge [60]. IM, like data mining in general, makes use of techniques taken from a number of different domains including: machine learning, statistics and artificial intelligence [11, 102].

In the context of image classification the goal of the IM is classifier generation. The input to the classifier generator is a set of training images $I = \{I_1, ..., I_n\}$, with the associated training labels $C = \{c_1, ...c_n\}$. The output is a mapping of the input to the set of class labels: $f : \chi \rightarrow C$.

2.2.3.3 The KDI Post Processing and Usage Phase

On completion of the IM phase the acquired knowledge can be applied. In the case of image classification this means the application of the generated classifier to real-life data. Prior to this it is useful to obtain some level of confidence in the generated classifier. This is typically done by applying the classifier to pre-labelled test data. There are a number of different evaluation metrics that can be used to measure the performance of a classifier. Further details concerning these metrics are presented in Section 2.8.

2.3 Hierarchical Spatial Decomposition

The work described in this thesis is directed at image representations for classification founded on the idea of hierarchical decomposition. Image decomposition has been used in various application domains [118]: such as computer graphics [63, 65], volume rendering [42, 120], modelling and animation [17], segmentation [87, 141] and Geographic Information Systems [10]. In [133] an edge detection algorithm was proposed using image decomposition.

The basic idea is to decompose a given image I_n into a set of sub-images (called regions in this thesis). Image decomposition offers a number of advantages that can be summarised as follows (see also [13, 137, 144]):

1. General applicability.
2. Provides for a more effective representation (than other methods) because it allows for the capture of regionalised details.
3. Fast computation of image properties due to applying representation methods to small regions.
4. Supports different forms of image representation at both the local (region) level and the global level.

5. Provides for a simplification of the space.

6. In many cases obviates the need for computationally expensive processes such as segmentation.

7. Reduces problems associated with occlusion because of the use of smaller regions instead of the whole image

The process of decomposition has to satisfy a number of conditions in order to ensure that appropriate regions are identified. These are itemised in [137] as follows:

1. **Repeatable**: The same regions should be identified in different conditions.

2. **Robust**: The decomposition should be robust against factors such as occlusion, clutter, noise and blur.

3. **Homogeneity**: The identified regions should, in some sense, be homogeneous.

4. **Invariant**: The decomposition should be invariant against transformations and deformations.

5. **Distinctive**: Allow for individual regions to be matched to similar regions in other images.

6. **Quantity**: Result in a sufficient number of regions with respect to the envisioned application.

7. **Efficient**: Operate in an efficient manner.

There are various different spatial decomposition methods that can be found in the literature. Subsection 2.3.1 below provides an overview of some of the most popular methods. One of the issues with hierarchical decomposition is deciding when to stop. One approach is to define a maximum "level" for the decomposition. However, on its own, this might result in unnecessary decomposition. A more efficient approach is to cease decomposing a branch whenever a homogeneous region is arrived at. There are various mechanisms for measuring regional homogeneity, usually expressed in terms of what is referred to as a *critical function*, and these are reviewed in Subsection 2.3.2.

2.3.1 Spatial Decomposition Methods

From the literature two approaches to spatial decomposition can be identified: (i) segmentation-based and (ii) grid-based. In the segmentation-based approach the image is divided into objects (for example, organs in the case of medical applications), while in the grid-based approach the image is divided into regularly shaped sub-spaces [13]. Thus in the segmentation-based approach the regions are non-uniform objects

which, as the name suggests, requires recourse to segmentation algorithms. Popular segmentation techniques used for this purpose are Watershed [23] and Superpixel [114]. The disadvantages of segmentation-based approaches are:

1. Good-quality images are required. Image blurring can make it difficult to identify image boundaries and consequently the segmentation process is less accurate [95]. One potential solution is to use the concept of "region isophotes" to handle problems associated within boundary blurring [103].

2. Many very small objects may be identified. One idea whereby this issue may be addressed is to use some threshold, such as the "Maximally Stable" condition used in [94], but this in turn means that the segmentation does not necessarily cover the whole image.

The advantage of the segmentation-based approaches is that the "overlap" problem found in grid-based representations does not occur. This is where an object of interest is distributed over a number of different regions dispersed across the decomposition, which in some cases can hinder further analysis. It is the view of the author that the disadvantages associated with segmentation-based decomposition outweighed the advantages, and thus the work described in this thesis is directed at grid-based decomposition techniques.

The principal advantage of grid-based decomposition is that it operates without the need for segmentation. From the literature we can identify two popular forms of grid-based decomposition: (i) fixed-sized "window" and (ii) quadtree. In the first method, a predefined rectangular window is passed over the image and used to extract regions from the image [149]. In the quadtree-based image decomposition technique the image is iteratively decomposed into smaller and smaller regions. One popular method is the Spatial Pyramid (SP) approach [82, 83] where at each level of decomposition each region is iteratively divided into four sub-regions. Figure 2.1(a) shows how the image is decomposed. Another example can be found in [88] where the concept of a Multi-Scale Spatial Pyramid (MSSP) was used. Quadtree decomposition offers the advantage that the property of being hierarchical can be used with respect to later processing, although the "overlap" problem remains. The approach adopted in this thesis is the quadtree-based spatial decomposition approach, although in 3D the phrase octree based spatial decomposition should be used [115, 121, 131]. One proposed solution to the overlap problem is the Overlapped Multi-Scale Spatial Pyramid (OMSSP) presented in [146] and illustrated in Figure 2.1(b), where the image is resized between different levels and overlapping blocks are used to try to cover the overlapping regions.

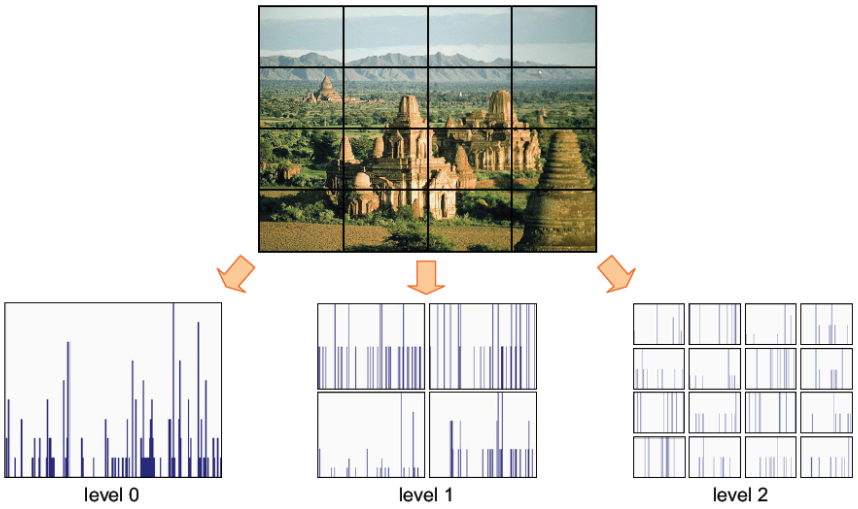

(a) Spatial pyramid representation [83]

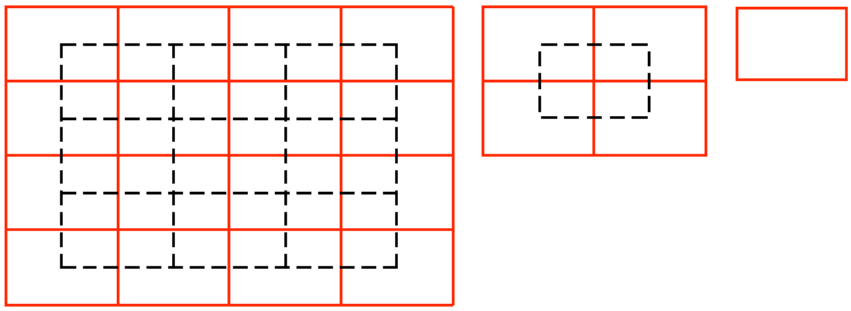

(b) Overlapped MSSP representation where the red lines indicate the overlapped regions [146]

Figure 2.1: Forms of grid decomposition.

2.3.2 Regional Homogeneity

As noted above, homogeneity is an important issue in the context of image decomposition. With respect to image decomposition, homogeneity is measured using what is referred to as a "critical function". Most existing critical functions are typically intended for use with segmentation-based methods [135]. These methods are applied to extract homogeneous regions (segments). In order to determine the homogeneity of a region, statistical features of the region or edges are taken into consideration [41]. In the literature, there are two common examples of critical functions based on statistical features: (i) Average Intensity Values (AIV) (mean) [59] and (ii) Kendall's Coefficient Concordance (KCC) [153]. With respect to edge information proposed methods are prone to failure when the adapted edge detection mechanism fails to identify all edges, leading to over/under-segmentation [41].

The use of the AIV function is well described in [59] where it was used in the con-

text of 2D image decomposition. The AIV value of each region is computed before decomposition. Then the region is decomposed and the AIV for each child sub-region is computed. Following this, a difference function is constructed to compute the "distance" $d(AIV_p, AIV_i) = AIV_p - AIV_i$ between the parent region AIV_p and the AIV of each child region AIV_i. The square root of the sum of the distances between the parent region and the child regions is then computed. The homogeneity ω of the parent volume is calculated using Equation 2.1, where s is the number of child regions, AIV_p indicates the parent AIV and AIV_i the AIV for each child region. If the value of ω is less than a predefined threshold the region is considered to be homogeneous and therefore the decomposition process is stopped. A similar approach using the mean intensity value was used with respect to the region growing method described in [30]. AIV was included as a feature in the MPEG-7 algorithm [147].

$$\omega = \frac{1}{s} \sum_{i=1}^{s} \sqrt{(AIV_p - AIV_i)^2} \tag{2.1}$$

KCC was proposed in [153] where it was used to assess the homogeneity of regions in functional MRI (fMRI) images. KCC is a time-series based method for measuring the relationships between each voxel and its neighbours. In the context of 3D volumes KCC operates as follows. First, for each voxel in a decomposed region, a time series involving the intensity values of the voxel's nearest neighbours is formed. Then the KCC is applied on the generated time series to check the homogeneity of the region. KCC is calculated using Equation 2.2.

$$KCC = \frac{\sum(R_i^2 - n\bar{R}^2)}{1/12K^2(n^3 - n)} \tag{2.2}$$

where R_i is the sum of the ith time series for the ith voxel, $\bar{R} = \frac{(n+1)K}{2}$, $\bar{R}$ is the mean of each time series, K is the size of the time series (number of selected neighbours for each voxel) and n is the number of voxels in a given region. The resulting KCC value has a range of 0 to 1, where 1 indicates a completely homogeneous region and 0 an entirely un-homogeneous region.

Note that AIV and KCC are both used later in this thesis for comparison with the author's own proposed critical functions.

2.4 Region-based Representation

Once an image has been decomposed, either the individual region represented by each node, or the decomposition as a whole, needs to be translated into a representation compatible with classifier generation. Whole image-based representation methods are discussed in the following section. This section deals with previous work that lends itself to individual region representation (although clearly these representations could

equally well be applied in the context of whole, non-decomposed, image representation). From the literature, two categories of region-based representation can be identified: (i) statistical-based techniques and (ii) histogram-based techniques. Two types of statistical-based techniques can also be identified: (i) first-order and (ii) second-order [134]. In the case of first-order methods, images are described using statistical functions such as mean, variance, energy and standard deviation of the image's intensity values.

With respect to the second-order methods, the relationship between the intensity value of each pixel with respect to those of its neighbours is taken into consideration [134]. In other words, relative location information is used. One example of a second-order method is where the concept of a co-occurrence matrix [44, 49] is used to enumerate the number of times two intensity values appear in an image within a certain distance and a direction of each other. A Voxel Co-occurrence Matrix (VCM) is used in the same manner as a pixel co-occurrence matrix but with respect to 3D images [44]. In a VCM matrix, the rows and the columns represent intensity values and a field represents the frequency that an intensity value in the ith row was adjacent to the intensity value in the jth column. The adjacency is defined by a displacement distance d and angle. After computing VCM, various statistical functions can be applied to this matrix, such as angular second moment, contrast, correlation and variance. Another example of a second-order method is where run-length encoding matrices are used. These are matrices that hold information about the set of consecutive intensity pixels/voxels that have the same values [43, 132]. A Voxel Run-Length Matrix (VRLM) is the 3D form of a pixel run-length matrix. In a VRLM matrix, the rows represent intensity values, the columns represent the length of the run and the fields show the frequency of a specific intensity value in adjacent pixels/voxels in a specific direction. Similar to VCM, in the case of the VRLM matrix, different functions may be applied, such as, short/long run emphasis, length nonuniformity, run percentage and so on.

Regardless of whether first-order or second-order statistical methods are used, the generated statistics describe individual features which in turn can be used to define a feature space from which feature vectors can be extracted.

In the case of the histogram-based methods, there are a number of techniques that can be adapted: (i) simple histograms, (ii) Histograms of Oriented Gradients (or HOGs), (iii) histograms of Local Binary Patterns (LBPs) and (iv) histograms of Local Phase Quantisation (LPQ). In the case of simple histograms, the x-axis represents the values for some image features and the y-axis a count of the number of times that each feature value occurs. Often the attribute-values are grouped into sub-ranges referred to as "bins". The simplest form of histogram image representation is where the x-axis represents intensity values. The histogram thus represents the number of times each intensity value, or group of intensity values, appears. The disadvantages of such simple histograms are: (i) significant information is lost, such as spatial information, because

only the frequency of the intensity values are considered; and (ii) invariant problems, especially when two images have similar content but with different resolutions (in which case different histograms will be produced).

A more advanced histogram-based method is the use of Histograms of Oriented Gradients (or HOGs) [24]. Using HOGs the changes in the intensity values of the region, with respect to either the azimuth and/or zenith direction, are computed and referred to as *gradients*. In order to compute a gradient at each location the difference between the "left" and "right" neighbouring intensity values, in a given direction, is calculated. Following this, the angles between the image gradients are computed and stored in what are called "orientation" bins. The gradient magnitudes in each orientation bin are accumulated. In the generated histogram, the x-axis represents directions and the y-axis the sum of the gradient magnitudes.

In order to generate LBPs, each pixel/voxel is compared to its immediate neighbours. For each comparison a one is stored if the intensity value of the pixel/voxel is greater than the neighbour, otherwise a zero is stored. The generated binary number from the sequence of neighbours then describes an integer value. In the generated histogram, the x-axis represents the computed integer values and the y-axis the frequency with which they occur. In order to generate a robust representation, it is desirable to compute rotation invariant LBPs. With respect to 2D images it is straightforward to calculate rotation invariant LBPs because each location has only eight immediate neighbours. With respect to 3D images the generation of 3D rotation invariant LBPs (26 neighbours in contrast to 8 neighbours) is computationally expensive. To address this issue Zhao and Pietikainen [157] proposed the use of Three Orthogonal Plane LBPs (LBP-TOP). The LBP-TOP representation considers the calculation of LBPs only with respect to neighbouring voxels located in the XY, XZ and YZ planes. A combination of HOG and LBP (HOG-LBP) has also been proposed and found to be a robust representation [143].

The concept of histograms of Local Phase Quantisation (LPQ) was proposed in [101]. LPQ uses low frequency local Fourier transforms whereby a histogram of the quantised Fourier transform can be generated [99]. At each image location, a Short-Term Fourier Transform (STFT) is applied with respect to the immediate neighbours. Then the resulting values are quantised (a value of one is used if the value is bigger than or equal to zero, otherwise a value of zero is used). In this manner a binary encoding is computed for each image location which can then be interpreted as an integer value between 0-256 ($b = \sum_{i=0}^{8} q_i 2^{i-1}$, where q_i is the quantised value of a neighbouring pixel/voxel). Histograms describing the number of times that each integer value occurs are then computed, one per image.

2.5 Whole Image-Based Representation

An alternative to representing individual regions is to represent the decomposition in its entirety, for example as some form of tree which can eventually be translated into a feature vector format (again to ensure compatibility with the data mining techniques to later be applied). There are a variety of mechanisms whereby this can be achieved that have been reported in the literature; however, hierarchical decomposition techniques naturally lend themselves to tree representations where the nodes represent regions. The question is then what features to store at the tree nodes (and by extension the links connecting the nodes); in other words, what information should the tree hold?

There has been a substantial amount of work directed at tree based representations of space but mostly directed at 2D space such as [31] and [59]. In [31] a quad tree representation was used to encapsulate a 2D representation of the Corpus Callosum, the part of the brain that connects the left and right hand sides of the brain. The shape of the Corpus Callosum was extracted from MRI scan data. In this case, the data stored at the tree nodes was either the digit 1 or the digit 0, 1 indicating that the associated region was part of the Corpus Callosum and 0 indicating it was not. The work of [59] is particularly relevant with respect to the work described in this thesis because a hierarchical representation was used to describe 2D retinal images. In this case, each node held the mean intensity values of all the pixels in the associated region [59].

What is interesting about tree representations is that a tree is a type of graph and therefore graph mining techniques can be applied. For example, frequently occurring sub-graphs (sub-trees) can be used as attributes in a feature space model. Both [31] and [59] experimented with this idea. A similar idea is adapted with respect to the work described in this thesis and hence graph mining is considered in some further detail below in Subsection 2.6.2.

2.6 Feature Vector Generation

As already noted the feature vector format is the standard format used in data mining. The format initially requires the generation of a feature space. In some cases, this is straightforward; in others, it is not so straightforward. Thus in the case of the region-based representations considered in this thesis the feature space of interest is formed by identifying a set of features of interest across the regions. Whatever the case, for reasons of computational efficiency, it is often necessary to reduce the number of dimensions in a given feature space. There are a variety of techniques whereby this can be achieved and these are discussed in Subsection 2.6.1. In the whole image-based representation where the decompositions as represented as a graph, extracting a feature space is not so straightforward. Techniques for identifying a feature space with a graph representation

are therefore discussed in Subsection 2.6.2.

2.6.1 Feature Vector Generation for Region-based Methods

Two commonly used methods used to reduce the dimensionality of a given feature space are: (i) Principal Component Analysis (PCA) and (ii) the coding-pooling framework. In PCA [69] orthogonal linear transforms are applied to the set of feature vectors, forming a new set of vectors according to the variance of the feature vectors. PCA is used to transform a feature space into lower-dimensional space. PCA operates by first calculating the Eigenvectors and Eigenvalues for the new space. Feature vectors are then generated using the list of Eigenvectors. They are sorted and a specific number of Eigenvectors are chosen. There is an assumption that an Eigenvector with a larger Eigenvalue indicates that this Eigenvector is significant, so Eigenvectors with the largest Eigenvalues are selected to represent the image [146].

In the coding-pooling framework the coding element consists of identifying a subset of vectors (the "dictionary"). The pooling element is then used to generate a single feature vector guided by the dictionary where feature vectors linked to the same vector in the dictionary are combined. The coding should operate so that the selected vectors include the most representative features. There are different ways of conducting the coding, of note are: (i) Vector Quantization (VQ), (ii) Sparse Coding (SC), (iii) Locality-constrained Linear Coding (LLC), (iv) Improved Fisher Kernel Encoding (IFK) and (v) SuperVector encoding (SV).

Lazebnik et al. [82] proposed the use of Vector Quantization (VQ) for feature selection. VQ is essentially a clustering technique. In the context of region-based representation methods K-means is applied to a random sub-set of regions extracted from the training images to form the dictionary. The dictionary in this case thus consists of cluster centres. The dictionary typically comprises between 200 to 400 cluster centres. Alternatively, Sparse Coding (SC) or Locality-constrained Linear Coding (LLC) may be used to form the dictionary. SC tries to find a feature vector that best represents a group of feature vectors by measuring the "response" of the vector to the group. In the case of region-based representation methods, this group of feature vectors is extracted from the whole set of given feature vectors across all images [149]. In order to reduce the computing time, SC may be applied to a random sample of feature vectors. LLC may be used as an alternative to SC to achieve the same result [142]. Improved Fisher Kernel Encoding (IFK) [105] is another method used for generating dictionaries. Here, given a set of feature vectors, the feature vectors' distributions are computed using a Gaussian Mixture Model (GMM) (based on the Maximum Likelihood (ML) estimation) to identify a feature vector-specific distribution. In order to distinguish between different image signatures, L2 normalisation is applied to the feature vector-specific distribution to form the "Fisher vector signature" aimed at encapsulating class-

specific information. Similar to IFK, SuperVector (SV) encoding was used in [158]. Instead of GMM as in IFK, K-means clustering was computed. Then the clusters were improved by using upper bounds aimed at minimising the error using the Euclidean distance between feature vectors and their means. In [62] an experiment is reported that compares the operation of different coding methods; FK proposed in [105] was shown to outperform the rest.

With respect to the pooling element of the coding-pooling framework, the aim is to map each feature vector with its equivalent vector in the dictionary in order to form a single feature vector. There are two common methods for achieving this, average and maximum pooling. In "average pooling", the average values between similar feature vector elements in the dictionary are computed and then used to form a new feature vector. Following this, a long global feature vector is generated by concatenating the new feature vectors for each image. The resulting feature vector is then normalised [82]. One example of maximum pooling is Multi-scale Spatial Maximum Pooling (MSMP) [149]. MSMP recursively computes the histograms of the maximum values for a given set of vectors and their association with elements in the dictionary. Feature vectors in neighbouring regions are recursively united by getting the maximum values of each element. This process of combing feature vectors is applied until a final single feature vector is reached.

2.6.2 Feature Vector Generation for Whole Image-based Methods

As noted above, the generation of feature vectors from tree-based representations is more challenging than in the case of region-based representation methods. One approach, used in [59] in the context of 2D retinal images and in [89] with respect to MRI brain scan data, is to first identify frequently occurring sub-graphs in the tree data using some appropriate search method. Various Frequent Sub-Graph (FSG) mining techniques can be used for this purpose. One of the most commonly used is the graph-based Substructure pattern mining (gSpan) algorithm [148]. The gSpan algorithm uses a Depth First Search (DFS) approach to identify frequent sub-graphs (sub-trees). A sub-graph is said to be frequent according to a "support threshold" σ. In the case of the tree representations considered in this thesis, each identified frequent sub-tree is then conceptualised as a dimension within a feature space. Sub-graphs may be ranked according to some weighting measure as suggested in [15] and the top K sub-graphs selected. This later approach was adapted in [59] in the context of 2D retinal images.

2.7 Classifier Generation Techniques

From the literature we can identify a great many proposed classifier generation algorithms. The most common techniques include: (i) Support Vector Machines (many

"kernel" variations can be identified), (ii) clustering (variations of the KNN algorithm) and (iii) probability based. Examples of each were adapted with respect to the work described in this thesis for evaluation purposes.

The Support Vector Machine (SVM) method was introduced in [7, 20, 138]. The basic idea is to fit a *hyperplane* to data contained in a multi-dimensional space that serves to divide the data into two classes. SVMs thus operate in a similar manner to perceptrons. The difference between a perceptron and an SVM is the "kernel trick" whereby data that could not be discriminated is translated into a further dimension so that a hyperplane can be fitted. The advantage of SVM is that application of a kernel function makes the data linearly separable, which leads to a robust classification. One of the main disadvantages of SVMs is that they are essentially binary classifiers. If we wish to apply the technique for multi-class classification a collection of "one against all" SVMs must be adapted. However, in our case, a binary classification is only used. Another disadvantage is that SVMs are essentially a "black box" method; it is difficult to derive an explanation for a particular classification.

The most common clustering-based classifier is the K-Nearest Neighbours (KNN) technique. KNN was proposed by [38] and is both a clustering and classification technique [86]. The learning part is the most important element in this method. A KNN cluster configuration is typically generated by considering a training set record by record. The first record defines the initial cluster. Further records are then assigned to this cluster according to a distance function. If the distance of a new record to the centre of the cluster is too great, a new cluster is created for the new record. The process continues until all records in the training set have been assigned, at which point we have K clusters. The centroid of each cluster then defines a class. The class definitions can then be used to classify new records. Distance-based comparisons such as Euclidean distance are used for this purpose [52]. However, the method is not very resilient to noise. Although there have been some attempts to enhance the method by including (for example) weighting factors [2], the accuracy of this method tends not to be as good as that associated with other classification techniques.

The most commonly used example of a probability-based classifier is the Bayesian Network (BN). BN is founded on acyclic graphs where the nodes are the attribute variable values and the edges describe the probabilistic relationships between the variables. Each node is associated with a probability distribution derived from the dependency between the node and its ancestors [46]. There are two main components for BN: a directed acyclic graph and a set of probability tables linked to each variable. The probabilities are derived from pre-labelled training data. Given a particular set of variable values the network can be used to determine the class label to be associated with this set. BNs have been shown to work well, but computational complexity remains an issue.

2.8 Evaluating Classification Algorithms

This section discusses the evaluation metrics used to measure the quality of classification algorithms. The significance is that these are used later in this thesis in the context of the proposed techniques. The effectiveness of a generated classifier is typically measured by applying it to pre-labelled test data so that generated class labels can be compared to the known class labelling. In the context of research into classification algorithms, classifier generation and testing are often combined into a single process. One commonly adopted approach is to use a Ten-fold Cross Validation (TCV) technique whereby the training and test data is combined to form a single pre-labelled data set. The classifier generation and evaluation is then conducted ten times, on each occasion using a different tenth of the concatenated dataset as the test set. In this section, two types of evaluation are presented: (i) classifier performance evaluation (Subsection 2.8.1) and (ii) statistical significance testing (Subsection 2.8.2).

2.8.1 Evaluating Performance of Classifiers

Various metrics can be used to evaluate the performance of a classifier. One commonly used technique with respect to binary (positive-negative) classification is to use a "confusion matrix" of the form shown in Table 2.3. The confusion matrix records the number of: (i) True Positives (TP), the number of records for which the classifier correctly predicts the positive class; (ii) False Positives (FP), the number of records for which the classifier wrongly predicts the positive class; (iii) False Negatives (FN), the number of records for which the classifier wrongly predicts the negative class; and (iv) True Negatives (TN), the number of records for which the classifier correctly predicts the negative class. Using a confusion matrix, a number of measures can be computed as follows:

1. **Accuracy (Acc)** measures the probability that an unseen record is classified correctly, $Acc = \frac{TP+TN}{TP+TN+FP+FN}$.
2. **Sensitivity (Sen)** (also referred to as the True Positive Rate (TPR) or recall) is the probability that a positive record is classified correctly, $Sen = \frac{TP}{TP+FN}$.
3. **Specificity (Spec)** or True Negative Rate (TNR) is the probability that a negative record is classified correctly, $Spec = \frac{TN}{TN+FP}$.
4. **False Positive Rate (FPR)** is the probability that a positive record is classified incorrectly, $FPR = 1 - Spec$.
5. **Positive Predictive Value (PPV)** or precision is the probability that a positive predication is correct, $PPV = \frac{TP}{TP+FP}$.

6. **Negative Predictive Value (NPV)** is the probability that a predication is negative when an image is negative, $NPV = \frac{TN}{TN+FN}$.

7. **Area Under the receiver operator characteristic Curve (AUC)** which indicates the relative relationship between True Positive Rate (TPR) and the False Positive Rate (FPR) [33]. The AUC value for a given classifier is computed using the Receiver Operating Characteristic (ROC) curve. The Receiver Operating Characteristic (ROC) curve is the plot of FPR on the x-axis against TPR on the y-axis for the classifier giving all the test instances. Figure 2.2(a) shows an example ROC graph.

8. **Equal Error Rate (EER)** is used to measure the error when TPR equals FPR (as in Figure 2.2(b)) [122]. In general, the classifier with the lowest EER is most accurate.

Table 2.3: Confusion matrix

		Actual Class		
		Positive (P)	Negative (N)	Total
Predicted Class	Positive ($\hat{P}$)	True Positive (TP)	False Positive (FP)	TP + FP
	Negative ($\hat{N}$)	False Negative(FN)	True Negative (TN)	FN+TN
	Total	TP + FN	FP + TN	

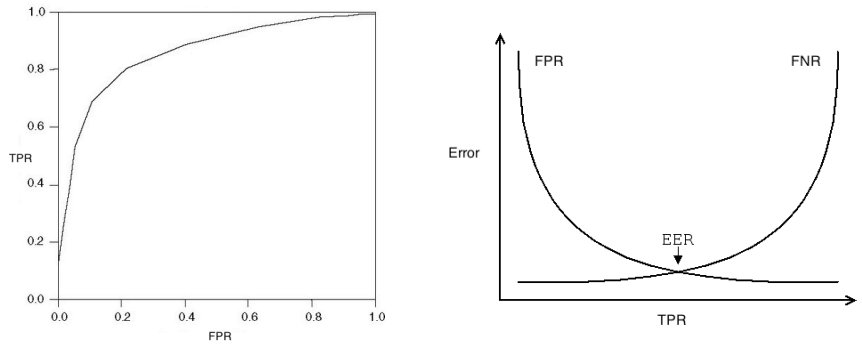

(a) ROC (b) EER

Figure 2.2: A diagram showing an example plot of ROC and EER.

2.8.2 Statistical Significance Testing

Given two classifiers and when using the above metrics one classifier is bound to be better than the other. The question is: is this statistically significant or not? ANalysis Of VAriance (ANOVA) is a common statistical method used to compare the statistical significance of the operation of groups of classifiers. More specifically, ANOVA is used to determine whether the null hypothesis (that there is no statistical distinction between

the operation of the classifiers) holds or not. If the null hypothesis can be rejected, then a post-hoc test can be employed to identify the classifiers whose operation is statistically different from others [29].

With respect to the work described in this thesis, a group of k classifiers with associated n results (e.g accuracy or AUC) is given and the objective is to determine whether the operation of any of these k classifiers is statistically significant from the rest. In our case, different techniques to decompose the image are proposed and tested with different parameters. The goal of using ANOVA is thus to determine whether, although one result is better than another, there is a statistical difference between the operation of the techniques or not. The processes for conducting ANOVA uses the following equations [67, 124, 125]:

1. The Total Sum of Squares (SS_T).

$$SS_T = \sum X_T^2 - \frac{(\sum X_T)^2}{N}$$

   where $N = \sum_{i=n}^{k} n_i$ (the total number of results), n_i is the number of results associated with the ith classifier, X is a particular result (expressed in terms of (say) accuracy or AUC), X_T is the set containing all the results from all the group of classifiers.

2. The Between-Groups Sum of Squares (SS_{BG}), which indicates the statistical changes between the k groups.

$$SS_{BG} = \sum_{j=1}^{k} \left[\frac{(\sum X_j)^2}{n_j} \right] - \frac{(\sum X_T)^2}{N}$$

3. The Within-groups Sum of Squares (SS_{Error}), which describes the amount of change within each of the k groups (error).

$$SS_{Error} = \sum_{j=1}^{k} \left[\sum X_j^2 - \frac{(\sum X_j)^2}{n_j} \right] = SS_T - SS_{BG}$$

4. Between-groups degrees of freedom (df_{BG}).

$$df_{BG} = k - 1$$

5. Within-groups degrees of freedom (df_{Error}).

$$df_{Error} = N - k$$

6. Total degrees of freedom (df_T).

$$df_T = N - 1$$

7. Mean Square Between-Groups (MS_{BG}).

$$MS_{BG} = \frac{SS_{BG}}{df_{BG}}$$

8. Mean Square Within-Groups (MS_{Error}).

$$MS_{Error} = \frac{SS_{Error}}{df_{Error}}$$

9. F ratio (F)

$$F = \frac{MS_{BG}}{MS_{Error}}$$

10. Probability value (Prob or p-value) is the probability that the observed F ratio (F) is statistically significant taking into consideration the degrees of freedom df_{BG}, df_{Error} using the F Cumulative Distribution Function (FCDF).

If the p-value is less than or equal to a threshold α (usually $\alpha = 0.05$) the null hypothesis can be rejected and this indicates there is a statistical significance between the groups. To determine the significant differences between different classifiers, a post-hoc test can then be conducted. In this thesis Tukey's Honestly Significant Difference (HSD) Post-Hoc Test is applied, which indicates the differences between algorithm performance. In order to apply HSD, the Standard Error (SE) is computed for the results of each classifier using Equation 2.3. Then the q statistic between two classifiers is computed (Equation 2.4, where $m\bar{k}_1$ and $m\bar{k}_2$ are the means of the results for the given two classifiers). Then the q statistic is compared to q_α, which is the critical q value with respect to the significance level α, and if $q > q_\alpha$. Finally, the HSD is calculated using Equation 2.5, indicating the minimum difference between the two classifiers' means [67].

$$SE = \sqrt{\frac{MS_{Error}}{n}} \tag{2.3}$$

$$q_\alpha = \frac{m\bar{k}_1 - m\bar{k}_2}{SE} \tag{2.4}$$

$$HSD = q_\alpha SE \tag{2.5}$$

In order to determine the range of values of each classifier's outcome, presented for example in terms of accuracy or AUC values, the Confidence Interval (CI) is computed. From the given sample (classification results of each technique), CI shows the range of values that the classifier will produce. The CI is computed in the form of $(1 - \alpha)$ where $\alpha \in [0, 1]$. It is common to set the value of α to 0.05, where this results in 95% CI (1- 0.05). CI is expressed in terms of a lower and upper bound, CI_{lower} and CI_{upper} calculated as shown in Equations 2.6 and 2.7; where S_k is the set of samples

for the classifier k, $\bar{k}$ is the means of the classifier results, σ is the variance, u is the true distribution mean and Z_p the probability value computed using Equation 2.8 [67].

$$CI_{lower} = \bar{k} - Z_p \frac{\sigma(k)}{\sqrt{\mid S_k \mid}} \tag{2.6}$$

$$CI_{upper} = \bar{k} + Z_p \frac{\sigma(k)}{\sqrt{\mid S_k \mid}} \tag{2.7}$$

$$Z_p = \frac{\bar{k} - u}{\alpha / \sqrt{\mid S_k \mid}} \tag{2.8}$$

In order to provide a better understanding of the above statistical significance testing methods, two simple examples are provided here using the data presented in Tables 2.4 and 2.5. With reference to the tables, each column represents a classifier and each row a set of classification results. The ANOVA for the data presented in Table 2.4 is conducted using the following: $SS_T = (25511 + 42919 + 34968 + 34817) - \frac{(357+463+418+417)^2}{5\times5\times5\times5}$ = 1.2638e+03, $SS_{BG} = (\frac{357^2}{5} + \frac{463^2}{5} + \frac{418^2}{5} + \frac{417^2}{5}) - \frac{(357+463+418+417)^2}{5\times5\times5\times5}$ =1.1349e+03, SS_{Error} = 1.2638e+03 - 1.1349e+03 = 128.8000, $df_T = (5 \times 5 \times 5 \times 5) - 1 = 19$, $df_{BG} = 4 - 1 = 3$, $df_{Error} = (5 \times 5 \times 5 \times 5) - 4 = 16$, $MS_{BG} = \frac{1.1349e+03}{3} = 378.3167$, $MS_{Error} = \frac{128.8000}{16} = 8.05$, $F = \frac{378.3167}{8.05} = 46.9959$ and p-value = 3.7064e-08. With respect to Table 2.5 the ANOVA is conducted using the following: SS_T = 194.2000, SS_{BG} = 5.8000, SS_{Error} = 188.4000, df_T = 19, df_{BG} = 3, df_{Error} = 16, MS_{BG} = 1.9333, MS_{Error} = 11.7750, F = 0.1642 and p-value =0.9189. The analysis in both cases is summarised in Tables 2.6 and 2.7; note that this is the manner in which ANOVA results will be presented later in this thesis. The p-value for results presented in Table 2.4 is less than 0.05 (3.7064e-08), indicating that there is a statistically significant difference between the operation of the classifiers. However, in the case of the data presented in Table 2.5 the results are not statistically different as the p-value is 0.9189 (p-value $> \alpha = 0.05$). The post-hoc test for the classifiers in Table 2.4 is conducted because there is a statistical difference between them. Figure 2.3(a) shows a boxplot of the significant difference between the groups where the x-axis represents the results and the y-axis lists the groups. The lines represent the "comparison interval" around the mean of each group and the dot in the middle of the line is the mean of each group. When the lines of two groups do not overlap, the two groups are significantly different. Figure 2.3(b) shows boxplot of the confidence interval for each group where the notch in each box represents the 95% confidence intervals (top is the CI_{upper} and the bottom is the CI_{lower}).

Table 2.4: Example accuracy classification results where there is statistical difference in the operation of the classifiers.

	Classifier Number			
	1	**2**	**3**	**4**
Accuracy	70	90	85	88
	75	92	82	85
	71	89	87	80
	72	95	81	82
	69	97	83	82

Table 2.5: Example accuracy classification results where there is not a statistical difference in the operation of the classifiers.

	Classifier Number			
	1	**2**	**3**	**4**
Accuracy	90	80	85	88
	79	81	82	85
	88	84	87	80
	84	83	81	82
	78	84	83	82

Table 2.6: ANOVA results for the example results in Table 2.4.

Source	SS	df	MS	F	p-value
Between-Groups	1.1349e+03	3	378.3167	46.9959	3.7064e-08
Error	128.8000	16	8.0500		
Total	1.2638e+03	19			

Table 2.7: ANOVA results for the example results in Table 2.5.

Source	SS	df	MS	F	p-value
Between-Groups	5.8000	3	1.9333	0.1642	0.9189
Error	188.4000	16	11.7750		
Total	194.2000	19			

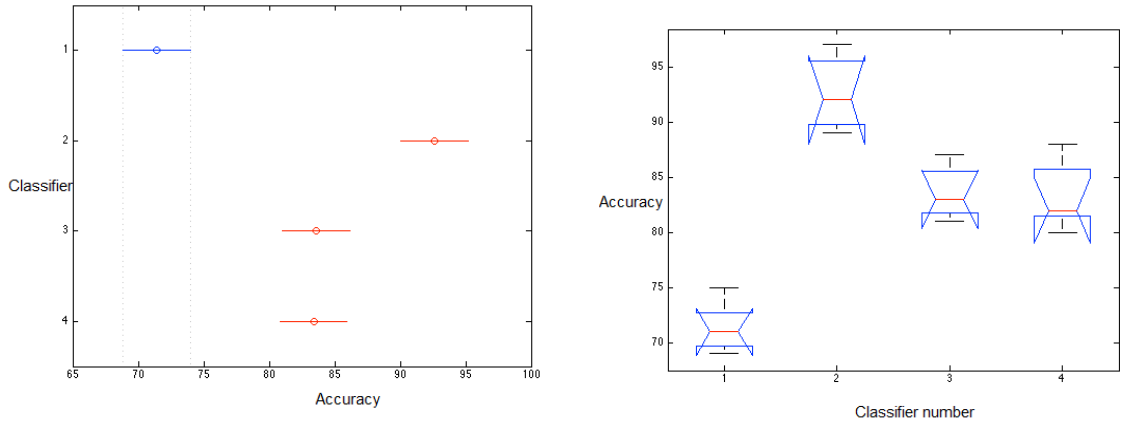

(a) Significance differences

(b) Confidence interval

Figure 2.3: The statistical differences and confidence intervals for the example results in Table 2.4.

2.9 Summary

In this chapter, an overview concerning the previous work related to knowledge discovery in images, and image mining, was presented. Some related work about hierarchical spatial decomposition was also presented. Following this, a review of the selected methods for image representation, feature vector generation and classification was included. Finally, some selected mechanisms for evaluating classifiers were summarised. These evaluation methods will be used later in this thesis. In the following chapter, the retinal image analysis application domain will be presented including a review of previous research related to this domain.

Chapter 3

Application Domain and Dataset

3.1 Overview

This chapter introduces the application domain used to evaluate the different hierarchical spatial (volumetric) decomposition based representation methods proposed in this thesis in the context of classification. For the evaluation the proposed methods were applied to 3D retinal images obtained using Optical Coherence Tomography (OCT). More specifically, the proposed methods were applied to 3D retinal image datasets in order to determine whether they featured Age-related Macular Degeneration (AMD) or not. AMD in 3D OCT image data was selected as the application domain for this thesis because: (i) OCT is a commonly used 3D imaging technique and (ii) AMD is one of the leading causes of worldwide vision loss in people aged over 50 years. Due to the global ageing population, AMD is affecting a significant number of people especially in Western countries. For instance, according to [111], in the U.S. at least 1.7 million people have lost vision because of AMD. Every year, AMD effects more than 165,000 people in the USA; 16,000 of them will lose their vision completely. Therefore, AMD is clinically significant, and automated detection of AMD is desirable. At present, there is a lack of automated AMD detection tools. Notwithstanding the above, it should also be noted that the methods proposed in this thesis will be equally applicable to other 3D image analysis domains.

The rest of this chapter is organised as follows. Section 3.2 provides an overview of the structure of the eye and the retina and then describes AMD. In Section 3.3 the basic principles of OCT scanning are presented. Section 3.4 reviews existing classification techniques that have been applied to retinal images. In Section 3.5 the 3D OCT retinal dataset considered in this thesis is described. Section 3.6 then describes the necessary preprocessing steps applied to this data so as to be compatible with the proposed decomposition techniques.

3.2 The Human Eye and the Retina

In this section, we present the main structure of the human visual system, the eye and the retina. Vision dominates our perception of the world surrounding us. In the human visual system, eyes are the organs by which we see the nearby environment. The eye has three main layers (see Figure 3.1): (i) the external layer including the sclera and the cornea, (ii) the intermediate layer consisting of two parts: anterior (iris and ciliary body) and posterior (the choroid), and (iii) the internal layer, the retina, which is the main part of the eye. There are three parts of the eye that are filled with fluid: (i) the Anterior chamber between the cornea and the iris, (ii) the Posterior chamber between the iris, the zonule fibers and the lens and (iii) the Vitreous between the lens and the retina. Light penetrates and is focused through the cornea and lens and then impinges on the retina [76].

The retina is the only layer in the eye that contains neurons and is actually part of the central nervous system. The retina has the main task of processing the visual information received by the light-sensitive neurons (photoreceptors) in order to pass them onto the brain. Retinal tissues translate light energy into a complex series of neural signals in the visual pathway through the optic nerve. This is achieved by a process known as phototransduction. During phototransduction photoreceptor cells transform photons of light into neural signals [113]. Before visual information reaches the brain, the retina codes it into channels. Each channel carries a special type of visual information. The visual information in each channel is then analysed in the brain [112]. The brain gives the interpretation for such visual information, resulting in the perception of vision [100, 108, 113]. Conditions such as AMD and diabetic retinopathy affect the operation of the retina.

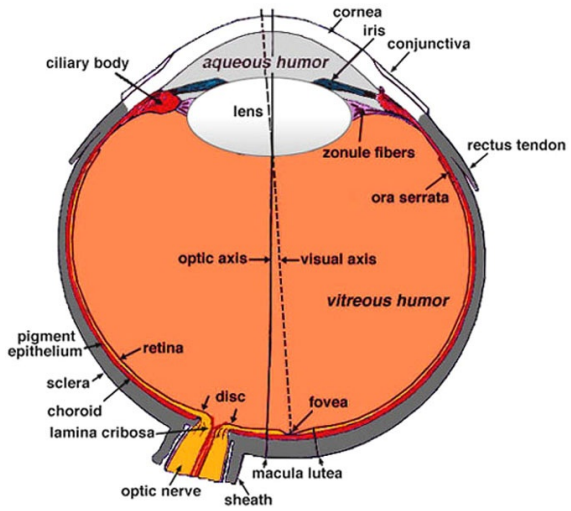

Figure 3.1: Section of human eye [76].

3.2.1 Anatomy of the Retina

The size of the retina is approximately 0.5 mm^2 [77]. The retina has five types of neurons: (i) photoreceptors, (ii) bipolar cells, (iii) ganglion cells, (iv) horizontal cells and (v) amacrine cells. These neurons are stacked in different layers [108]. From the outer-side to inside, the retina has ten layers (see Figure 3.2(a)) [108, 113]: (i) the Retinal Pigment Epithelium (RPE), which is a mono-cell layer with various visual functions such as reducing backscattering of light that enters the eye; (ii) the Photoreceptor Cell Layer (PCL), where the photoreceptor cells (referred to as "rods" and "cones") are special sensor cells containing photopigments that absorb photons of light; (iii) the External Limiting Membrane (ELM); (iv) the Outer Nuclear Layer (ONL); (v) the Outer Plexiform Layer (OPL); (vi) the Inner Nuclear Layer (INL); (vii) the Inner Plexiform Layer (IPL); (viii) the Ganglion Cell Layer (GCL); (ix) the Nerve Fibre Layer (NFL); and (x) the Internal Limiting Membrane (ILM). In a normal retina, these layers are connected and there is interaction between them [113]. In the presence of conditions such as AMD gaps appear between retina layers.

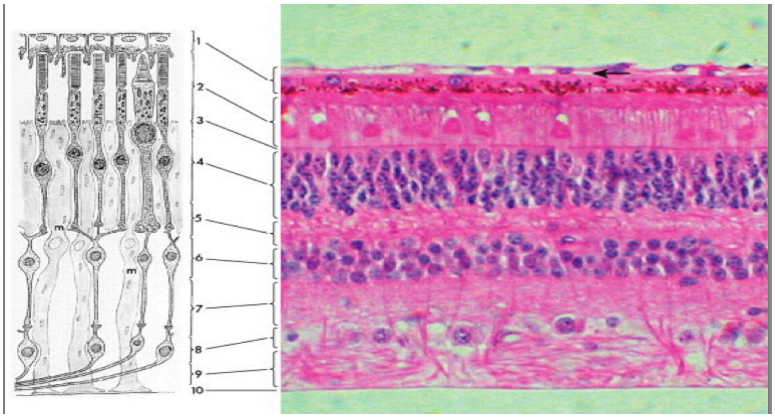

(a) Schematic showing the retinal layers

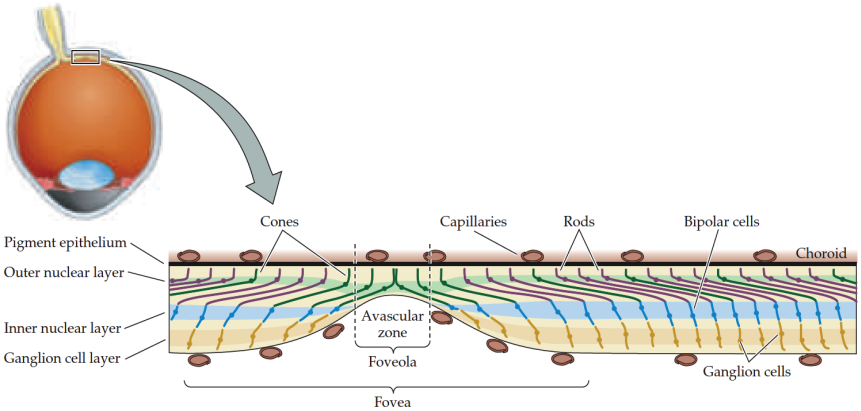

(b) A diagram showing the fovea

Figure 3.2: A schematic of the retinal layers and the fovea [113].

The macula or the macula lutea is the centre part of the retina (shown in Figure 3.1) which includes the fovea. Clinically, the term fovea refers to the very centre of the retina and is an area of horizontal diameter of approximately 1.5 mm. The fovea is a shallow depression where there are only photoreceptors cells, allowing light to pass unobstructed (Figure 3.2(b)). Light reaches the photoreceptor cells through the fovea directly without the interference of any other retinal cells or blood or vessels. The fovea has the highest concentration of sensory cells, making it specialised for discrimination of detailed visual information and colour vision [113].

3.2.2 Age-related Macular Degeneration

AMD is a macular disease that can result in severe vision loss in people aged 50 years or over. It is the most common worldwide disease that leads to blindness [107]. AMD occurs when the macula becomes damaged or infected. In the early stage of AMD, patients may notice a blurring of central vision when doing tasks such as reading and/or driving. In the late stages, complete loss of vision may occur [108]. Figure 3.3 illustrates the difference between a normal eye and an eye with AMD from the patient's viewpoint (a) (a), the location of the problem (b) and the structure of the eye (c).

AMD results in damage to the retina, causing RPE atrophy which leads to: (i) a change in the shape of the retina, (ii) RPE detachment and (iii) other abnormalities such as "drusen" (which are extra accumulations in the eye) and fluid within the retina [66]. Drusen appear as "dots" within retina images, whose colours range from white to yellow in colour fundus photographs. Drusen can be defined as being "hard" or "soft" [27]. If there is only a small number of hard drusen in the retina, then this is not diagnosed as a sign of AMD because this is normal for people over 50 [66].

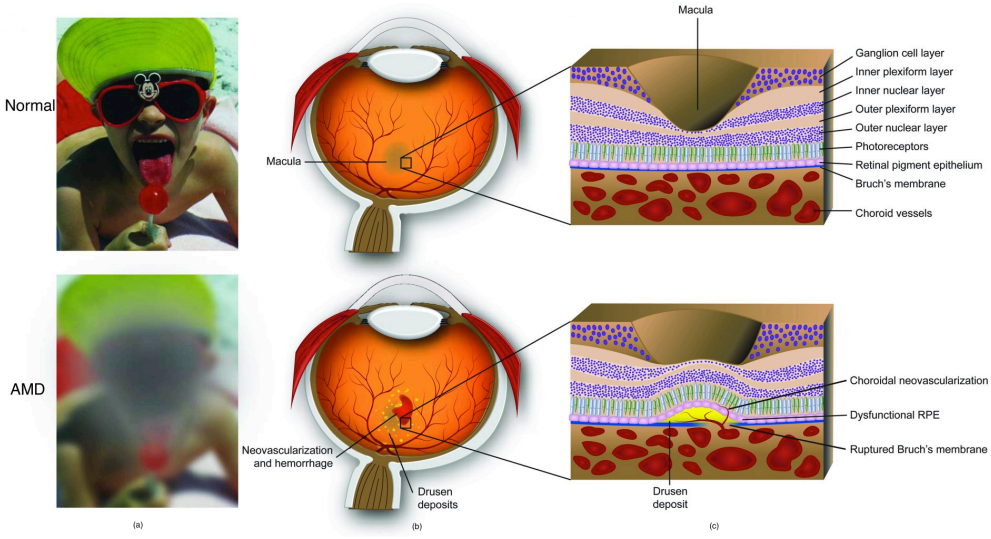

Figure 3.3: Illustration of the difference between (a) normal and AMD vision, (b) a normal and an AMD eye (drusen present in the macula) and (c) a normal retina and an AMD retina [16].

3.3 Optical Coherence Tomography

Optical Coherence Tomography (OCT) was invented by Huang et al. [61]. OCT is a 3D imaging technique that is used to digitally capture, with a high level of resolution, the inner structure of objects. OCT makes use of low-coherence light and ultra-short laser pulses in order to detect the spatial position of tissue and resolve depth information. The use of light waves enables acquisition of images (volumes), with a very high level of resolution, that can reveal the fine detail of internal structures. 3D volumes are generated from a series of 2D OCT "slices" referred to as B-scans. OCT has been widely used in ophthalmological and skin examination.

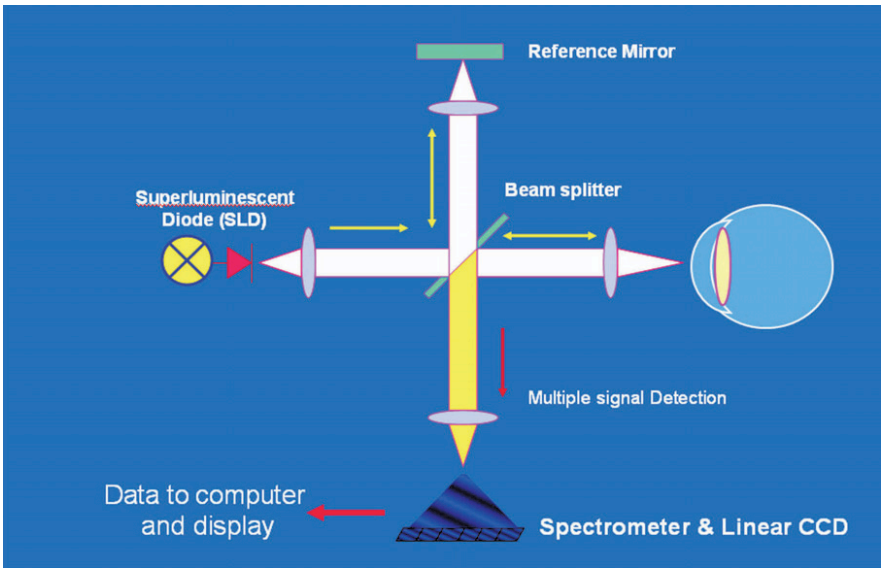

Figure 3.4: An example of an OCT scanner system, where CCD is the Charge-Coupled Device [22].

Spectral Domain OCT (SD-OCT) is currently the most commonly used form of OCT [106]. Figure 3.4 shows a diagram illustrating how an OCT system works. SD-OCT has four main components: (i) a light source, (ii) a reference mirror, (iii) a beam splitter and (iv) a spectrometer. SD-OCT relies on low-coherence interferometry where Super-Luminescent Diodes (SLD) produce a light. The beam splitter is used to split the light omitted by SLD into two paths. The first path is to the reference mirror and the second path is to the object to be scanned (the retina in our case). The reflected lights from the two paths are detected by using multiple signal detection to form an inteferometric signal [45]. Spectrometer and linear CCD cameras are used to measure the depth information from the inteferometric signal using the Fast Fourier-Transform [37]. It has been suggested that the Signal-to-Noise ratio (SNR) in SD-OCT is improved in comparison to other forms of OCT so that the quality of the scanned images is enhanced and the noise level is reduced [96, 145]. SNR of 80 decibel (dB)

or above is generally accepted rate while the typical SNR value for SD-OCT is 110 dB [152].

In the context of retinal analysis, OCT images provide useful information whereby ophthalmologists can conduct non-invasive examinations. OCT has been found to be very accurate and sensitive owing to the fact that the reflected optical signals are grouped by their speed; the exact depth of a scanned object can thus be obtained. Since OCT relies on light reflection, the optical features can be clearly identified [61].

OCT images give more precise information about scanned objects than other scanning techniques such as fundus images. In the context of retinal imagery, an OCT scan allows for different views of the retina. This in turn helps eye examination as clinicians can view various structures within the eye from different angles. In the context of the work described in this thesis, OCT allows for the identification of the different layers of the retina. OCT has thus provided ophthalmologists with significantly more detail concerning the retina than was available using 2D images.

3.3.1 Retinal OCT Images

In order to distinguish between "normal" eyes and diseased eyes, the anatomy of the retina is typically considered. It is thus important to be able to recognise the different parts of the eye, such as the RPE and the choroid, in order to know if the retina is healthy or not. The contour of the retina and the foveal depression are important anatomical elements used when analysing retinal data. Figure 3.5 illustrates ten different retinal layers within an example OCT image. In a healthy eye, the retinal layers are connected and there is no space between the layers but in a diseased eye separations between layers tend to appear. The appearance of such undesirable spaces typically indicates the presence of fluid between the layers involved.

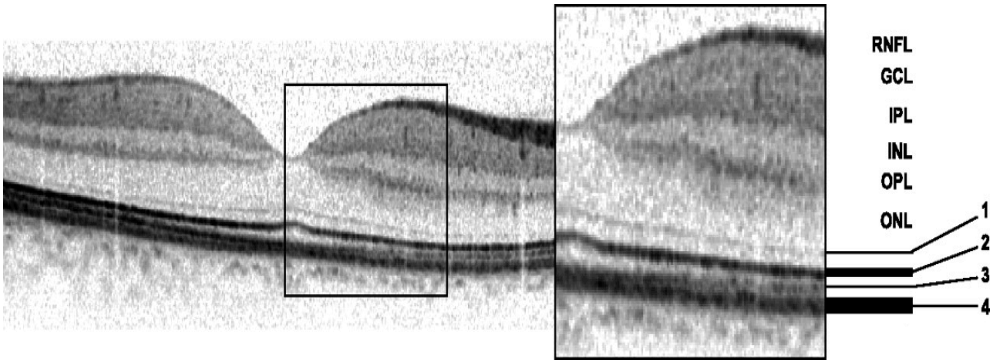

Figure 3.5: An OCT image showing different retinal layers [39].

3.3.2 AMD in 3D OCT

So far OCT is the only imaging technique that can show the cross-sectional details of the retina and the choroid, where most indicators of AMD (if any) will be located, while the use of 2D fundus images are limited in terms of location [74]. AMD is typically identified in retinal OCT images by visual inspection. A normal retinal volume has smooth and connective tissue layers whilst an AMD retinal volume has disrupted layers and other abnormal patterns. Figure 3.6 shows two 3D OCT volumes. Note that one side is longer than the other; this is significant with respect to the decomposition techniques presented later in this thesis. Figure 3.6(a) shows a normal OCT retinal image where the retina features smooth contours and a regular arrangement of individual retinal layers. Figures 3.6(b) and (c) show examples of OCT retinal images with AMD, showing the abnormal change in the retina associated with AMD where fluid and detachment of the retina cause the layers of the retina to separate from one another.

There are some distinct features of AMD that can be found in OCT images such as: (i) disturbance of the RPE layer underneath the neuro-retina due to the presence of drusen, pigment epithelium detachment, geographic atrophy or membrane changes; (ii) disruption of layered neuro-retinal tissue; (iii) the presence of intra- and sub-retinal fluid and (iv) retinal thickening. From Figure 3.6, it can be seen that there are notable distinctions between the normal and the AMD volumes. The normal volume features smooth and connected layers. However, the AMD volume features thickening of the RPE layer, intra-retinal fluid, PED and some unusual texture patterns.

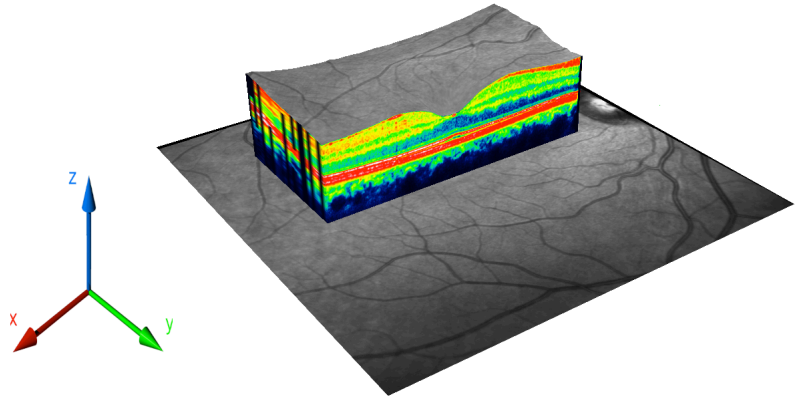

(a) A 3D OCT of a normal eye

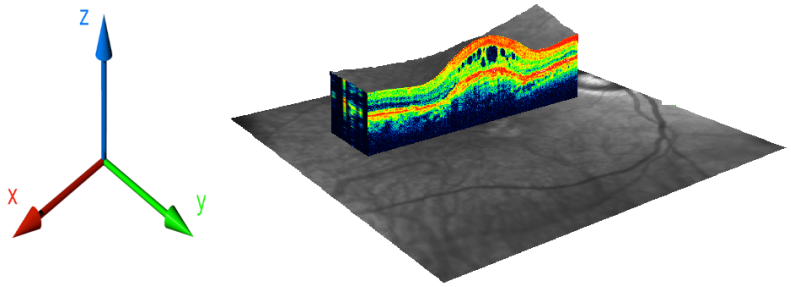

(b) An early stage of a 3D OCT of an AMD eye

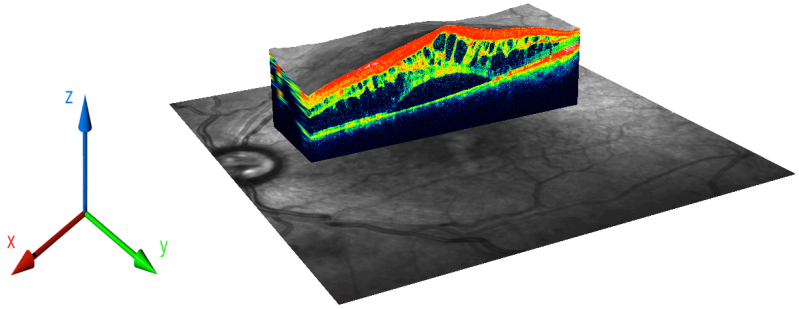

(c) An advanced stage of a 3D OCT of an AMD eye

Figure 3.6: Examples of 3D OCT images from the RLUH data set used in this thesis showing the difference between a "normal" and an AMD retina.

3.4 Classification of Retinal Images

In this section, we review the classification techniques which have been used as retinal disease diagnosis tools. From the literature, most of the current disease diagnosis tools are focused on 2D image data. Two examples can be found in [49] and [88] which used statistical-based methods. In addition, a study was conducted in [59] proposing a tree-based method. In [109] a 3D OCT retinal image classifier was proposed.

In [49] a statistical-based method was applied to a global representation. A co-

occurrence matrix was used to represent the OCT image features. Then statistical functions were used to extract the features of the co-occurrence matrix; features such as energy, entropy, correlation, local homogeneity and inertia. In addition, the Discrete Fourier Transform (DFT) was computed over the frequency of the image. A Mahalanobis distance-based method was applied to measure the similarities between image features and a Bayesian classifier was used to differentiate between features. However, this study was again applied only to 2D OCT retinal image slices.

The study conducted in [88] implemented a classifier for OCT images for classifying different retinal diseases, including AMD, in 2D OCT image slices. The classification process comprised three steps. The first step was image preprocessing (noise removal and image alignment). During noise removal, a threshold and median filter were applied. Following this, a morphological operator was used to remove unwanted objects. During image alignment, a least square curve fitting based-method was applied to a curve which represented the middle of the retina, the objective being to flatten the main region. This alignment process was introduced in order to build a representation for the same area. In the next step, the flattened image was represented using a Multi-Scale Spatial Pyramid (MSSP) up to three levels. MSSP is a region-based technique, where each region is recursively divided into four regions. The local descriptors of each region in each level of the MSSP were generated using a Local Binary Pattern (LBP) histogram. Then the dimensionality of the set of LBP histograms, for the whole set of regions, was reduced by the means of Principal Component Analysis (PCA). All the LBPs were added together, leading to a global feature descriptor. In the third step, the RBF kernel-based SVM classifier was applied to the global descriptor in order to categorise the diseases. One of the limitations with this approach is that it does not consider the complete set of slices available in a 3D OCT image. Only a single 2D foveal slice is used and it is selected manually.

The work described in [59] proposed a whole image-based representation which was applied to 2D fundus retinal images. The image was hierarchically decomposed down to a predefined level whilst taking into consideration a critical function for checking the homogeneity of each region. A graph was then built. A sub-graph mining technique was applied to this graph so as to extract the most important patterns according to their frequency. Then a feature vector was generated using the most frequent sub-graphs. The generated feature vectors were fed into a classifier such as KNN or SVM. In this thesis we compare the operation of the proposed 3D hierarchical decomposition based representation methods to the method proposed in [59].

The study conducted in [109] proposed a method for 3D OCT retinal classification. The retinal layers were segmented using a multi-scale 3D graph algorithm. A set of sub-volumes were generated, one sub-volume per layer. A set of statistical features was generated for each sub-volume. These features included intensity distribution, run

length and co-occurrence matrices and wavelet. These feature were fed into a KNN classifier.

3.5 3D Retinal Image Datasets

In this section, we describe the dataset used to assess the performance of the proposed hierarchical 3D representation approaches to support the volumetric classification presented in this thesis. A dataset comprising 140 3D OCT volumes was used, 68 "normal" (control) volumes and 72 AMD volumes. The size of each volume was approximately 1024×496 pixels $\times 19$ slices representing a $6 \times 6 \times 2$ mm retinal volume. Different types of AMD are included in the dataset, namely classic AMD, Occult AMD and RAP AMD. For evaluation purposes, these types of AMD images were merged because the work described in this thesis is directed at binary (disease versus no-disease) classification. All the images were obtained from the Royal Liverpool University Hospital (RLUH) under ethical approval. These images were labelled by trained clinicians.

In the work presented, the high-definition spectral domain OCT SD-OCT was used. System specifications includes a 5 m depth resolution, a 20 m transversal resolution and a scanning speed of 40,000 A-scans per second. The system allowed for the scanning of the ocular fundus using two different macular cube protocols, namely the $1024 \times 496 \times 19$, covering a volume of 6,000x6,000x2,000 m^3.

The OCT data was collected from patients with AMD and healthy control volunteers attending St Pauls Eye Unit within the Royal Liverpool University Hospital. The study was approved by the UK Research Ethics Committee and the institutional review board at the Royal Liverpool University Hospital. The study was undertaken in accordance with the tenets of the Helsinki Declaration. Written informed consent was obtained from all the patients prior to the enrolment.

3.6 3D OCT Preparation

Due to the nature of the OCT image acquisition process, the captured individual images often had different orientations, and included "speckle" noise and unwanted structures. Therefore, some image preprocessing (cleaning) was required to improve, correct and enhance the quality of the images and reference the images to a common coordinate system prior to the application of any further processing. The preprocessing comprised two steps: (i) removing unwanted structures from the input retinal images and (ii) flattening of the retinal layers (as proposed in [88]). The result of the preprocessing of each volume is a Volume Of Interest (VOI) encompassing the flattened retina. Detail concerning the two steps is presented in the following two subsections.

3.6.1 Unwanted Structure Removal

In order to remove unwanted structures from the input retinal images, an approach was proposed combing: (i) a segmentation based method and (ii) the application of morphological operators.

The segmentation based method was applied to separate the retina from the rest of the image. One of the advanced techniques directed at solving the image segmentation problem is the split Bregman method [47]. This algorithm is an extension of the Rudin-Osher-Fatemi (ROF) algorithm [116] and considers the problem as a L1-regularised optimisation problem based on Total Variation (TV).

The morphological operators were applied to further enhance the quality of the image and obtain a single connected area. Morphological operations are defined as "neighbourhood operations" whereby a mask or a template with specific shape (e.g. rectangle or square) and size (called the Structuring Element (SE)) is defined for comparing the value of each voxel with its neighbours (within the mask). With respect to morphological operators, a voxel or pixel with intensity of 0 is considered black and all the other values are white. The SE is used to specify a neighbourhood relative to a reference voxel (centre voxel). The reason behind using morphological operators is that they rely on the concept of "connectedness", whereby the connectivity between the voxels of the image is taken into consideration [4].

There are two basic morphological operators, namely dilation and erosion. Morphological dilation is a process used to augment white regions in an input image by adding white voxels around the edges of the white regions, or to the holes within individual regions, so that holes in a single region and gaps between different regions are filled. Thus during this process some of the black voxels (zero values) will be converted to white object voxels (non-zero values). The size and the shape of SE plays an essential role in determining which black voxels to leave unchanged and which to change to white voxels. Morphological erosion is a process by which some of the white voxels in an input image are converted to black voxels (thus the reverse of morphological dilation). Again the SE is used to determine which white voxels to keep and which white voxels to erode [4, 48]. A Disc-shaped Structuring Element (DSE) was employed with respect to the morphological operators used in the research described in this thesis.

In addition to dilation and erosion operators, two extension morphological operators, based on the dilation and erosion operators, were employed with respect to the research described in this thesis: (i) closing operator and (ii) opening operator. The first performed morphological closing and was used to eliminate small holes inside the retina caused by applying the split Bregman or which were originally present within the image (indicating fluid or detachment in the retina). Morphological closing comprises the morphological dilation followed by morphological erosion. The morphological closing was guided by a DSE with a radius of 15 voxels. The second operator was a

morphological opening operator, which was applied in order to remove the small parts of the image not connected to the main retina (and to fill some gaps). In this case, the morphological opening was controlled by a DSE with a radius of 5 voxels (in 3D).

3.6.2 Retinal Layer Flattening

In this subsection, the method used to implement a uniform alignment for the images, referred to as "flattening" in [88], is described. This is required because of the OCT settings used during the scanning of retinal images (volumes). Images may not all be referenced to the same "horizon". The images therefore need to be aligned so that the adapted feature extraction methods can be roughly applied to the same region across the entire 3D image set. Figures 3.7(a) and 3.8(a) show an example of a retinal image where the retina is not flattened. In this thesis, each slice in a given retina volume is flattened using a second-order polynomial least-square curve fitting procedure [88] according to the nature of the mean surface of the retina (defined according to the top and bottom retina surfaces). In order to do this, we select the slice where the top and bottom surfaces of the volume (retina) are furthest apart and consider these two layers in terms of two vectors made up of voxel values. These two vectors are used to define the "middle" vector, which is then used as a reference for flattening the entire retinal volume. Figures 3.7(b) and 3.8(b) illustrate the retinal image after the processing.

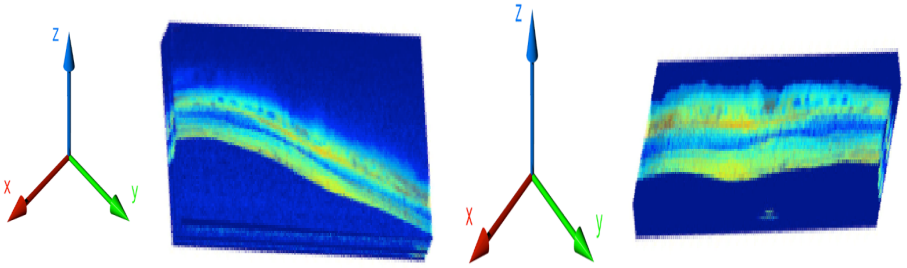

(a) Given 3D OCT (b) After applying the Preprocessing

Figure 3.7: Examples of 3D OCT image before and after applying the preprocessing.

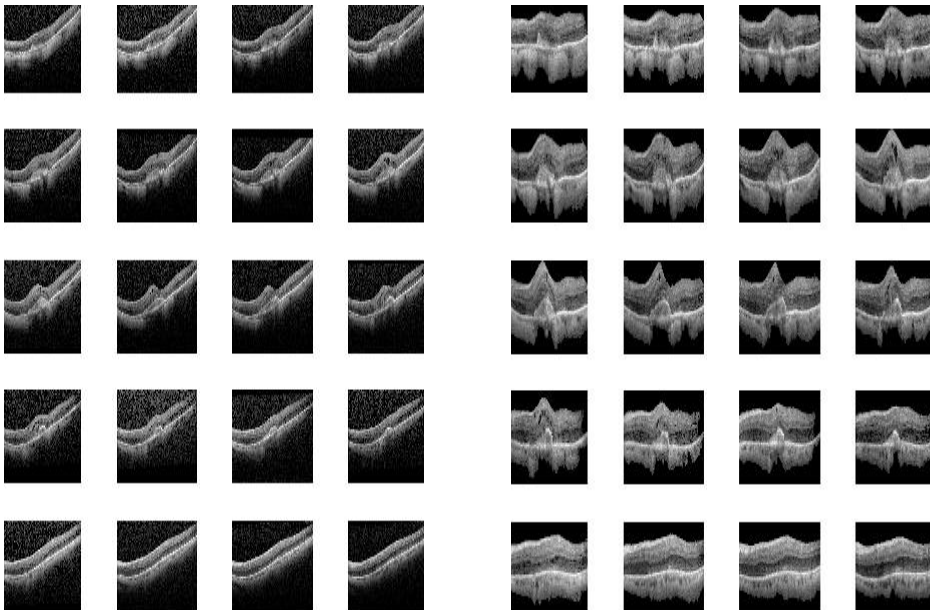

(a) A set of slices for Figure 3.7(a) (b) A set of slices for Figure 3.7(b)

Figure 3.8: Examples of a set of slices for Figure 3.7.

3.7 Summary

This chapter firstly presented an overview of the eye, the retina and AMD. The OCT 3D imaging technique was then described. This was followed by discussion of the dataset used to evaluate the proposed approaches described later in this thesis together with the preprocessing applied to this data so as to identify VOI. In the following chapter, the proposed hierarchical decomposition is presented as applied to the extracted VOI.

Chapter 4

Volumetric Decomposition

4.1 Overview

As stated in Section 1.3 of the introductory chapter, the proposed 3D volumetric mining methods rely on the concept of hierarchical spatial decomposition. In the literature review chapter (Subsection 2.3.1), we identified two types of decomposition methods: (i) segmentation based and (ii) grid based. In Subsection 2.3.1, it was argued that segmentation based methods were inappropriate and that grid based methods were more desirable in the context of 3D volumes. The proposed volumetric decomposition methods are thus presented in this chapter, starting with an overview in Section 4.2. As noted earlier in this thesis, an important issue in hierarchical decomposition is when to stop the decomposition. One common approach, and that adapted with respect to the work described in this thesis, is to use what is called a "critical function". Section 4.3 describes a number of critical functions for measuring the homogeneity of regions (sub-volumes in 3D space) including a number proposed by the author. Section 4.4 presents a method for addressing the boundary issue associated with hierarchical decomposition. A summary concerning this chapter is presented in Section 4.5.

4.2 The Proposed Hierarchical Spatial Decomposition

The problem considered in this section is how to decompose an image in a way that each decomposed region can be used to form a meaningful representation (discussed in more detail in the following chapters). As the name suggests, hierarchical decomposition proceeds in a recursive manner. In the case of 2D space we can think of the decomposition in terms of a quadtree and in 3D space in terms of an octree. In both cases, the root node represents the entire volume and the remaining nodes the decomposed sub-spaces and regions. In the case of 2D decomposition, the space is recursively decomposed into four sub-spaces. In the case of 3D decomposition the space is recursively decomposed into eight regions. Hierarchical decomposition usually assumes that the shape to be decomposed is symmetric (a square in 2D or a cube in 3D). However, in Chapter 3 it

was noted that the retinal volumes of interest are rectangular in shape with one side being much shorter than the other two; thus "traditional" octree decomposition will result in some very "thin" regions. This phenomena is illustrated in Figure 4.1 where it can be observed that the depth of the volume (z axis) is significantly smaller than its width and the height. Consequently, an alternative form of hybrid decomposition is proposed more suited to the nature of the retinal volumes of interest.

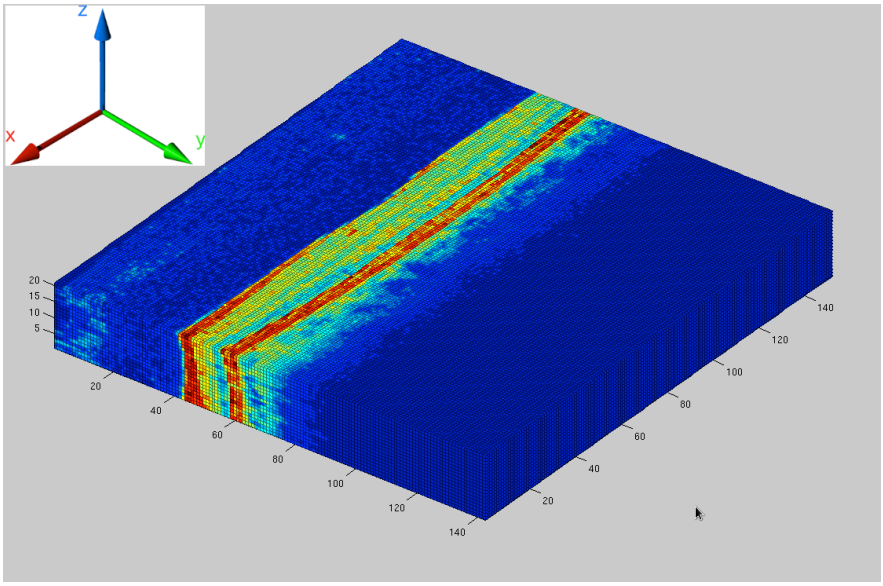

Figure 4.1: Example of a 3D OCT volume showing the size in 3 dimensions (140 (x) $\times$ 140 (y) $\times$ 20(z)).

Given a retinal VOI to be decomposed we commence, at the first level, by dividing it into eight regions. The resulting nodes are then the "children" of the root node. These children nodes are then recursively decomposed into sets of four regions (as opposed to eight) until some chosen maximum level is reached or homogeneous volumes are arrived at as defined by a critical function. The aim of a critical function, as noted above, is to determine whether a given region is, in some sense, homogeneous. If it is then the region is not decomposed further. Consequently, the resulting decomposition (tree) may not be balanced (later in this thesis some evaluation is presented between balanced tees generated without the use of a critical function and unbalanced trees generated using a critical function; thus use of critical functions versus their non use).

Algorithm 4.1 describes the proposed decomposition process. The retinal image and the chosen maximum level, $maxLevel$, are the given inputs. The output is a tree data structure T. We indicate the child i of a node in the tree t using the notation $t.i$. The root of the tree is t. The algorithm commences by first assigning the whole volume to t (line 2). There is then a test (line 3) in case the $maxLevel$ is 1 or the entire volume is homogeneous (an unlikely event). If the $maxLevel$ has not been reached and the volume is not homogeneous it is decomposed into eight sub-volumes (line 5)

using the OctDecomposedVolume() function. Each of these eight sub-volumes, if not homogeneous, is then decomposed further (line 9) using a quad tree decomposition (using the QuadDecomposedVolume() function). In the quadtree decomposition, the z dimension is ignored. This is done using the *decompose* procedure (line 15 to 23). The decomposition continues in this manner until either the maximum level or non-homogeneous regions are reached. Various critical functions will be described in detail in the following section, Section 4.3. The identified regions are stored in a hierarchical manner in order to allow for various types of representation to be used.

Algorithm 4.1 Pseudocode for the proposed hierarchical spatial decomposition method

Input: VolumetricData, maxLevel
Output: Tree data structure T

```
 1: level = 1
 2: t ← VolumetricData
 3: if level < maxLevel and not Homogeneous(t) then
 4:    level = level +1
 5:    t.1 ... t.8 ← OctDecomposedVolume(t)
 6:    if level < maxLevel then
 7:       for i = 1 to i=8 do
 8:          if not Homogeneous(t.i) then
 9:             decompose(t.i,level+1)
10:          end if
11:       end for
12:    end if
13: end if
14: exit with T
15: Procedure decompose (s,level)
16: s.1 ... s.4 ← QuadDecomposedVolume(s)
17: if level < maxLevel then
18:    for i = 1 to i=4 do
19:       if not Homogeneous(s.i) then
20:          decompose(s.i,level+1)
21:       end if
22:    end for
23: end if
```

4.3 Critical Functions for Regional Homogeneity

Measuring region homogeneity is an important aspect of hierarchical decomposition and the proposed decomposition described above. The basic idea is to employ a function that serves to minimise the number of regions that are generated during the decomposition without losing significant information. In the context of this thesis the term *Homogeneity*, with respect to 3D regions, refers to the situation where a region's voxels are in some sense uniform. To this end, as already noted, a critical function is used (the

function *Homogeneous* in the algorithm presented in Algorithm 4.1). In this thesis, we rely on the assumption that if there is no difference between the new decomposed regions and their parent volume then the decomposition is not required and the parent region can be considered to be a homogeneous region. In our proposed method, a distance measure was used to compare the homogeneity of the immediate region and the parent region. In order to apply a critical function, the current region is first decomposed and then the relationships between the new regions and the parent are checked. A threshold value t is used to decide whether each region, in comparison with its parent region, is homogeneous or not; if so the decomposition is accepted, otherwise the parent region is decomposed further.

In this section, seven different critical functions are presented. Two of these have been previously proposed with respect to other applications while the remainder are mechanisms that, although they are used elsewhere for alternative comparisons, have been specifically derived with respect to the work described. The two existing critical functions that have been identified from the literature are:

1. Average Intensity Value (AIV) [59], and
2. Kendall's Coefficient Concordance (KCC)[153]

The five that have been adapted by the author are:

1. Gray Level Co-occurrence Matrix (GLCM)
2. Euclidean Distance (ED)
3. Kullback-Leibler divergence (KLD)
4. Dynamic Time Warping (DTW)
5. Longest Common Subsequence (LCS)

The above defined functions can be categorised as being either: (i) intensity value based or (ii) histogram based. The intensity value based methods are: (i) AIV, (ii) KCC and (iii) GLCM. The rest are histogram based. With respect to the intensity value based methods, the simplest approach is to use a first-order statistical function such as the mean value of the intensity values of each region as in AIV. In more advanced techniques, a second-order statistical method could be employed. Time series-based methods are another option which can be used where the voxel intensity values compared to the set of values for their neighbours are represented as a time series.

In the histogram-based method, a histogram is generated for each region. Then a distance function is used to measure the differences between two regions' histograms. If the distance is less than a given threshold t, then the decomposition stops. Euclidean

Distance and Kullback-Leibler divergence are simple ways to compare two histograms by taking into account the difference between each histogram value (bin). Alternatively, time series-based approaches may be employed to measure the differences between two histograms. DTW and LCS are two time series based techniques. Note that for the purpose of this thesis the size of the histograms used, n, was set to 256.

Each of the considered critical functions is described in some further detail below. Note that in the description, where appropriate, Hp is the histogram of the parent and Hc is the histogram of the child (region), n is the length of the histograms. Note that AIV and KCC were previously described in Section 2.3.2, but have been briefly included here for reasons of completeness.

1. **Average Intensity Value (AIV).** AIV was used by Hijazi et al. [59]. AIV is the mean of the intensity of the volume. AIV is an example of a first-order statistical function. The AIV is computed for the parent region and the child nodes. Then the difference between the AIV values is computed. If the generated distances are less than a given threshold t then the decomposition is stopped. Recall that this method was fully described in Section 2.3.2.

2. **Kendall's Coefficient Concordance (KCC).** KCC indicates homogeneity without the need to decompose an image further because it compares each voxel with its neighbours. Recalling the discussion in Section 2.3.2, the KCC value ranges from between 0 and 1 [153]. The higher is the KCC value the more homogeneous the region. If the KCC value is close to one, then the space has a complete agreement between its elements, which means it is completely homogeneous. In our case, a threshold value t was used to determine if the region should be decomposed further or not. If KCC is less than a specified threshold t then the decomposition is valid and the child regions are added to the collection of regions in the level and the decomposition continues. Although KCC has been previously used for regional homogeneity to determine the similarity of regions in images, it has not been previously used in the same context as in this thesis (image classification).

3. **Gray Level Co-occurance Matrix (GLCM).** The use of GLCM or Voxel Co-occurrence Matrix (VCM) is another option for deciding if a set of regions, generated by decomposing an immediate parent volume, is homogeneous or not. A GLCM is a second-order statistical function. Recall the discussion in Section 2.4, in a GLCM matrix the number of times that the frequency of two intensity values are neighbours is counted within a certain distance and direction. The values recorded along the GLCM leading diagonal indicate the frequency of neighbours having the same intensity value. Thus if the values of the GLCM diagonal are higher than rest of the matrix then this indicates regional homogeneity. The

desired GLCM matrix is first extracted and then the GLCM diagonal is checked. The average value recorded along the diagonal then indicates whether the region is homogeneous or not according to Equation 4.1 [54]. In order to distinguish between the use of VCM as a region representation and a critical function, in the remainder of this thesis we will refer to a 3D GLCM as voxel Co-occurrence Matrix (VCM) for region representation and GLCM as a critical function. The VCM concept is discussed further in Subsection 5.2.2.1 in the context of the region representation technique.

$$GLCMhomogeneity = \sum_{i,j} \frac{GLCM(i,j)}{1+|i-j|} \tag{4.1}$$

Using Equation 4.1, if the calculated $GLCMhomogeneity$ value is great than a given threshold t, then the region is homogeneous and so it is not divided further.

4. **Euclidean Distance (ED).** Using the Euclidean Distance (ED) critical function, the differences between bin values of two histograms to be compared are accumulated. Equation 4.2 illustrates how ED is computed where hc_i is the histogram of the ith child region and hp is the histogram of the parent region. If the calculated ed values for the parent and all child region are less than a given threshold t, then the region is homogeneous and so it is not divided further.

$$ed(hc_i, hp) = \sqrt{\sum_{j=1}^{size} (hc_{i_j} - hp_j)^2} \tag{4.2}$$

5. **Kullback-Leibler divergence (KLD).** Kullback-Leibler divergence (KLD) is another way of comparing two vectors. KLD [68] is used to quantify the distance between two distributions. In our case, the two distributions are the histograms of the parent and the child region. Equation 4.3 is used to compute the KLD value. If all calculated KLD values for all the children regions are less than a given threshold t, then the region is homogeneous and so it is not divided further.

$$KLD = (KL1 + KL2)/2 \tag{4.3}$$

$$KL1 = \sum_{j=1}^{size} (hp_j \times (log(hp_j) - log(hc_{i_j}))) \tag{4.4}$$

$$KL2 = \sum_{j=1}^{size} (hc_{i_j} \times (log(hc_{i_j}) - log(hp_j))) \tag{4.5}$$

6. **Dynamic Time Warping (DTW).** DTW is a time series based method. In DTW, the Euclidean distance between the elements of the two given series is computed and fed into a grid matrix G. The best match between the elements of the two series is the warping path. The warping path should minimise the total cumulative Euclidean distance between the two series. In this thesis, the work presented in [72] was used where a bounding measure for DTW was proposed. Equation 4.6 illustrates this bounding measure. The optimal warping path between the two sequences (histograms) hp and hc_i minimises the total cumulative distance within the boundary. The assumption is that if the DTW value is small then there is homogeneity between two histograms. Therefore, if all calculated DTW values for all the child regions are less than a threshold t the region is considered to be homogeneous and so it is not decomposed further.

$$DTW(hp, hc_i) = \sqrt{\sum_{j=1}^{n} \begin{cases} (hc_{i_j} - U_j)^2 & if \quad hc_{i_j} > U_j \\ (hc_{i_j} - L_j)^2 & if \quad hc_{i_j} < L_j \\ 0 & otherwise \end{cases}} \tag{4.6}$$

In Equation 4.6, $U_i = max(hp_{i-r} : hp_{i+r})$ and $L = min(hp_{i-r} : hp_{i+r})$ are some Upper and Lower bounds respectively and $\forall\ U_i \geq hp_i \geq L_i$, r is the "reach", which is the maximum number of elements covered in the grid.

7. **Longest Common Subsequence (LCS).** LCS is a more advanced method than DTW used with respect to time series domains. LCS computes the similarities between two series located within a region of a size $\delta \times \epsilon$. The Longest Common Subsequence (LCS) time series analysis technique [140] is used to establish the similarity between histograms using the Minimum Bounding Envelope (MBE). When the MBE is used, only the elements of the two series included in the region controlled by δ, ϵ is considered and the rest are ignored. Equations 4.8 and 4.7 show how the MBE LCS is computed where n is the size of the two histograms hp and hc_i. The advantage offered by the LCS mechanism, compared to other time series mechanisms, is that it reduces the complexity of the problem by using an upper and lower Minimum Bounding Envelope (MBE) so as to estimate the similarities within the MBE (as in Equation 4.7). This difference between each histogram value (bin) is only considered if it is within the MBE region as described by Equation 4.7. In the equation, if the difference between each histogram values (bins) is within the MBE region, then the LCS is recursively called with the "head bin" of the given two histograms (in $LCS_{\delta,\varepsilon}(hp_{|hp|-1}, hci_{|hc_i|-1})$) removed and otherwise the the LCS function is called again twice, once with the top bin of the hp removed and once with hc_i; and then the maximum value is selected. This is recursively run until the two histograms are empty. If the calculated distance $D_{\delta,\epsilon}(hp, hc_i)$ (Equation 4.8) values between the parent histogram hp and all the

children histograms hc_i are less than a threshold t, then the region is considered homogeneous (and not decomposed further).

$$LCS_{\delta,\varepsilon}(hp, hc_i) = \begin{cases} 0 & if hp \text{ or } hc_i \text{ is empty} \\ 1 + LCS_{\delta,\varepsilon}(hp_{|hp|-1}, hci_{|hc_i|-1}) & if \mid hp_{|hp|} - hc_{|hc_i|} \mid < \varepsilon \\ & \mid |hp| - |hc_i| \mid \leq \delta \\ max\{LCS_{\delta,\varepsilon}(hp_{|hp|-1}, hc_i), LCS_{\delta,\varepsilon}(hp, hci_{|hc_i|-1}), & otherwise \end{cases} \tag{4.7}$$

$$D_{\delta,\epsilon}(hp, hc_i) = 1 - \frac{lcs_{\delta,\epsilon}(hp, hc_i)}{n} \tag{4.8}$$

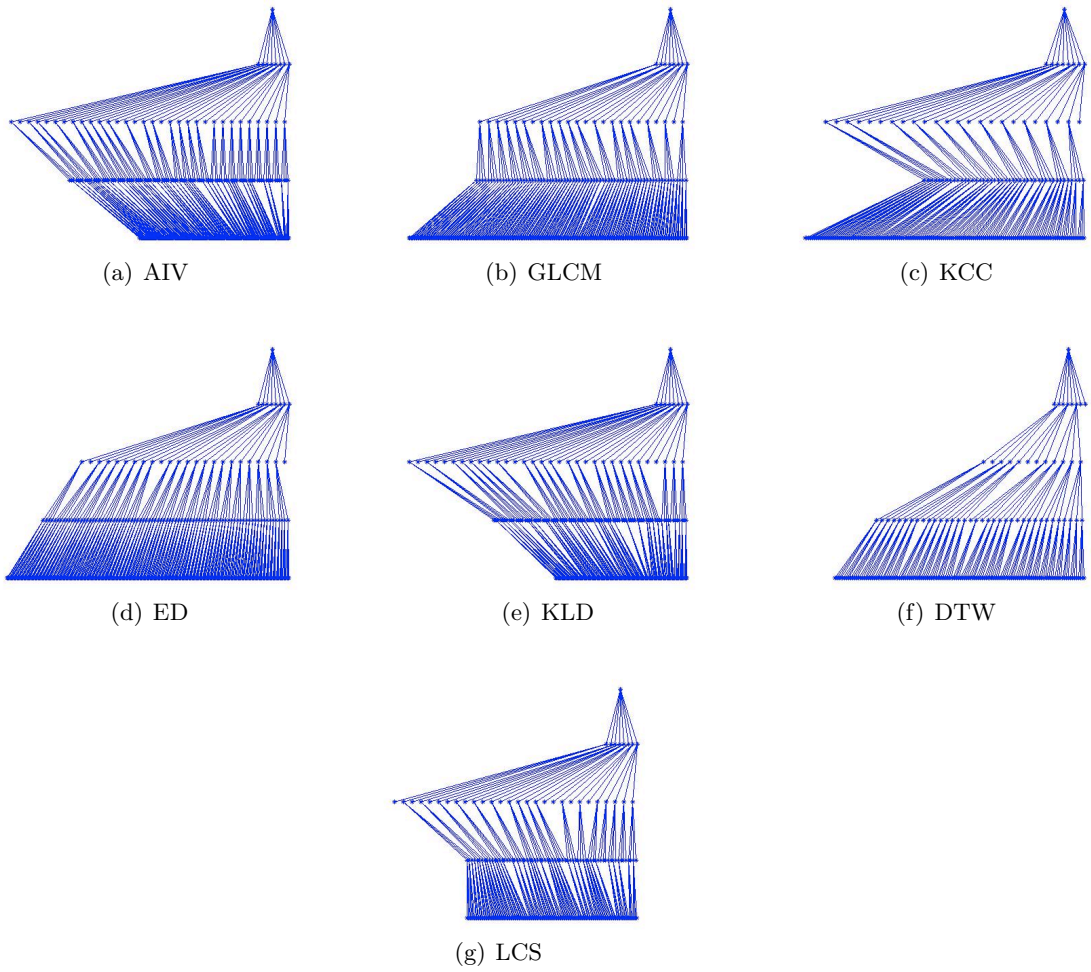

(a) AIV (b) GLCM (c) KCC

(d) ED (e) KLD (f) DTW

(g) LCS

Figure 4.2: Illustration of the effect of the seven different critical functions considered in this thesis when applied to decompose the volume in Figure 4.1.

In order to illustrate the comparative operation of each critical function, they were used to perform the decomposition of the 140 pixel × 140 pixel × 20 slice retinal OCT volume given in Figure 4.1 (which was decomposed using Algorithm 4.1). Figure 4.2

depicts the seven trees that resulted. From the figure, it can be noted, from the general shape of the trees, that there are clear differences between the operation of the critical functions. For example, from the third level (the root is level one) it can be noticed that in some cases the regions are decomposed further, and in other cases not. The above critical functions are evaluated in further detail later in this thesis with respect to the different representations proposed, both region-based and whole image-based.

4.4 Decomposition Methods and the Boundaries

When an image is decomposed, there is a possibility that a boundary region is included between two regions; a connected region that exists in more than one region at a given level of decomposition. In this thesis, we also refer to this issue as the "boundary problem". In this thesis, other than standard (oct-trees) decomposition, we also proposed overlapping (non-tree) decomposition. The later is illustrated in Figure 4.3(b) and (c). For comparison purposes, standard decomposition is shown in Figure 4.3(a). In the case of standard decomposition, the given volume is divided into eight regions. The whole volume is considered as the only region at the first level. The eight regions at the second level of decomposition are then considered as the children regions. In the overlapping decomposition, an overlapping volume is included as a ninth region. This is included in order to cover the part of the image located at the region intersection of the standard decomposition, where boundary regions are most likely to occur. The children regions, in each case, are then recursively decomposed into further groupings of five regions (four regions plus an overlapping region).

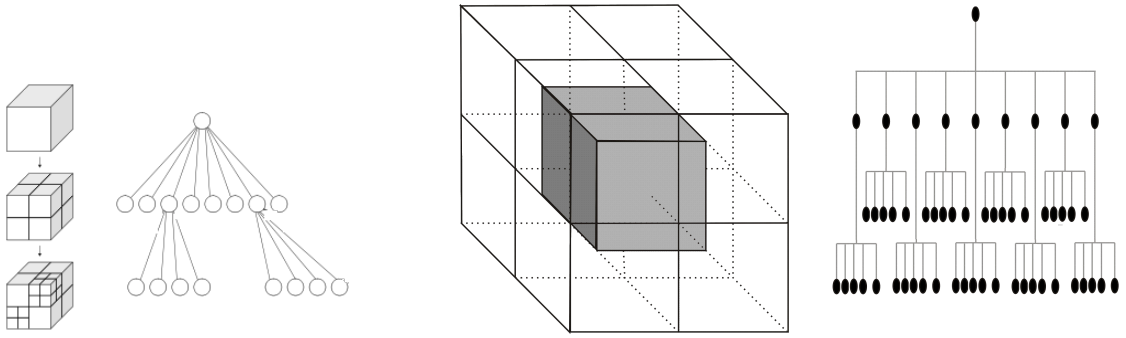

(a) Standard decomposition (b) Overlapped decomposition (c) Nine tree

Figure 4.3: Standard volumetric decomposition versus the overlapping volumetric decomposition.

4.5 Summary

In this chapter, the proposed hierarchical spatial decomposition algorithms have been described. For reasons of both efficiency and effectiveness it is desirable to decompose

the image down to homogeneous regions. For this purpose, a set of associated critical functions for measuring the regional homogeneity were considered. A mechanism for addressing the overlap problems, non-tree decomposition, was also presented. In the following chapter (Chapter 5), the proposed region-based representation methods are considered. These are evaluated in Chapter 6. Chapter 7 presents the proposed whole image-based representation methods.

Chapter 5

Classification Based on Decomposition and Region-based Volumetric Representation

5.1 Overview

This chapter presents the procedure for building 3D (volumetric) image classifiers using Region-Based (RB) representation methods. Recall that the basic idea of the region-based representation method is to form a description for each region (node in the decomposition) in terms of a feature vector format. Figure 5.1 presents a schematic of the region-based volumetric classification process presented in this chapter. From the figure, it can be seen that the process comprises four stages commencing with decomposition (as described in the foregoing chapter), the result of which is a tree where the nodes represent the individual regions. Next the regions are represented in a format that will provide for the generation of feature vectors. As will be seen later in this chapter, a number of alternative formats may be adapted. However, as discussed previously in Section 2.4 these formats can be characterised as being either: (i) statistical or (ii) histogram-based techniques. A set of techniques for both the statistical and histogram-based formates will be described in this chapter and will be evaluated in the following chapter. More formally, a given image I_n is decomposed into a set S_n of r regions $S_n = \{s_1, \ldots s_r\}$ where the regions are at a number of different levels of decomposition. The regions S_n are then represented using one of the techniques presented in this chapter to form a set of r feature vectors. The third stage is feature vector generation; the objective being to represent each image in terms of a single feature vector subscribing to some global set of features (feature space). The final stage is classifier generation. Referring back to the KDI process presented in Subsection 2.2.3, the first three stages belong to the KDI preprocessing phase while the last stage belongs to the KDI mining phase.

The rest of the chapter is structured as follows. First of all, the region-based

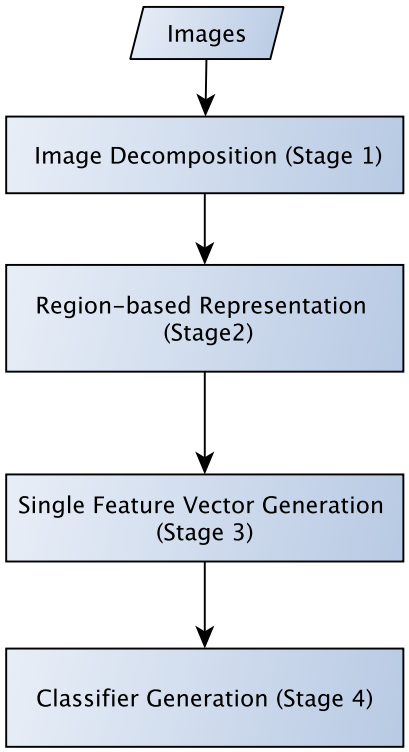

Figure 5.1: Overview of the region-based classification process.

representations proposed in this thesis are presented. Statistical-based techniques are described in Section 5.2 and histogram-based techniques in Section 5.3. Section 5.4 describes different techniques whereby a single feature vector for each image can be generated. In Section 5.5 the classification techniques applied to these feature vectors are briefly considered (they were introduced in Chapter 2). A summary concerning this chapter is provided in Section 5.6.

5.2 Statistical-Based Representation Techniques

As noted above, regions identified at nodes in the decomposition can be represented using either statistical based techniques or histogram-based techniques. This section considers the first of these while the following section considers the second. Essentially, statistical-based representation techniques, as the name suggests, are founded on the use of statistical functions to extract representative values that can be used to describe individual regions. As also noted in Section 2.4, the statistical functions that can be used can be characterised as being either: (i) First-Order Representation (FOR) or (ii) Second-Order Representation (SOR) [134]. The distinction is that first-order statistical functions are applied directly to the region of interest while second-order functions are applied to a matrix intermediate representation of the region (generated using informa-

tion such as the relative position and spatial relationship of each voxel making up the region and its associated intensity with respect to each voxel's "neighbourhood"). The first-order statistical techniques used with respect to the work described in this thesis are presented in Subsection 5.2.1 below, while the second-order adapted techniques are presented in Subsection 5.2.2.

5.2.1 First-Order Representation (FOR)

In this subsection, we describe the adapted First-Order Representation (FOR) techniques used to represent each region. The symbols used for FOR are listed in Table 5.1. The first-order statistical functions that have been derived from the literature [50, 53, 73, 84, 155] are listed below.

Table 5.1: Symbols used for FOR

Symbols	Description
S	A decomposed region.
(x, y, z)	the location coordinates of a voxel.
$S(x, y, z)$	The intensity value of a voxel in a given x, y, z location.
$sizeof(S)$	The number of voxels in a region S.
$\text{remove}_S(\text{x,y})$	To return a vector after removing x and y elements from the vector S.
$max(S)$	The maximum intensity value in a region S.
$min(S)$	The minimum intensity value in a region S.
$\mu(S)$	The mean intensity value of a given region S.
$std(S)$	The standard deviation of a region S.

1. **Angular Second Moment (ASM)**: $f_{ASM} = \sum_x \sum_y \sum_z S(x, y, z)^2$
2. **Entropy (E)**: $f_E = -\sum_x \sum_y \sum_z S(x, y, z) \log(S(x, y, z))$
3. **Mean (μ)**: $f_\mu = \frac{1}{sizeof(S)} \sum_x \sum_y \sum_z S(x, y, z)$
4. **Median (M)**: $f_M = middle(sort(S))$. The voxels' intensity values of region S are sorted and the middle value selected as the median.
5. **Trimmed Mean (TM)**: $f_{TM} = mean(remove_S(max(S), min(S)))$. The Mean of the intensity values is computed after discarding the highest and lowest intensity values associated with the voxels in a region S.
6. **Geometric Mean (GM)**: $f_{GM} = \left[\prod_x \prod_y \prod_z S(x, y, z)\right]^{1/max(S)}$
7. **Harmonic Mean (HM)**: $f_{HM} = \frac{max(S)}{\sum_x \sum_y \sum_z 1/S(x,y,z)}$
8. **Range (R)**: $f_R = max(S) - min(S)$. The difference between the maximum and the minimum intensity values of the region S.

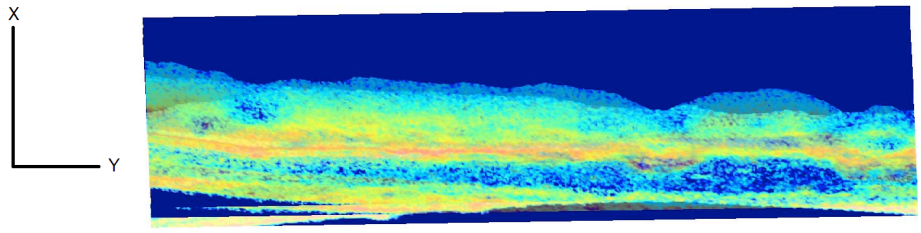

Figure 5.2: Example of a region (S), where the colour represents the intensity value.

9. **InterQuartile Range (IQR)**: The intensity values of voxels in a region S sorted and the difference between the values of the first and the third quartiles calculated.
10. **Standard deviation (std)**: $f_{std} = (\frac{1}{sizeof(S)} \sum_x \sum_y \sum_z (S(x,y,z) - \mu(S))^2)^{1/2}$
11. **Variance (V)**: $f_V = \frac{1}{sizeof(S)} \sum_x \sum_y \sum_z (S(x,y,z) - \mu(S))^2$
12. **Central Moments (CM)**: $f_{CM_o} = \sum_x \sum_y \sum_z (S(x,y,z) - \mu(S))^o$, where o is the order of the moments. Note that in this thesis five values for o were used: $\{3,4,5,6,7\}$.
13. **Skewness (S)**: $f_S = \frac{\sum_x \sum_y \sum_z (S(x,y,z) - \mu(S))^3}{std(S)^3}$.
14. **Kurtosis (K)**: $f_K = \frac{\sum_x \sum_y \sum_z (S(x,y,z) - \mu(S))^4}{std(S)^4}$.

Each function described above gives an output of one value. The collected values can be stored in a vector of length 18 (including five CM values), one per region. Figure 5.2 shows an example region with the associated FOR values given in Table 5.2. (Note that the example region presented in Figure 5.2 will be revisited later in this chapter.)

5.2.2 Second-Order Representation (SOR)

As noted above, SOR uses second-order statistical functions whereby first-order style statistical functions are applied to a matrix intermediate representation that describes the relationship between "neighbourhoods" of voxels. Two types of matrix were used with respect to the work described in this thesis: (i) the Voxel Co-occurrence Matrix (VCM) and (ii) the Voxel Run-Length Matrix (VRLM) [134]. These were originally proposed in the context of 2D image representations, but in this thesis they have been adapted for use with respect to 3D volumes in the context of spatial decomposition (recall that the concept of VCM was introduced in Section 2.4). The first, together with the statistical functions that might be applied, is described in Subsection 5.2.2.1 below, the second is described in Subsection 5.2.2.2. The advantage offered by the use of these kinds of matrices is that they reduce the dimensionality of the given 3D image to a 2D matrix by considering only the relationships between the image voxels'

Table 5.2: FOR values for the region presented in Figure 5.2.

Function	Value
f_{ASM}	5071388
f_E	0.4634
f_μ	0.7246
f_M	0
f_{TM}	0.2916
f_{GM}	0
f_R	15
f_{IQR}	0
f_V	5.3671
$f_{CM(3)}$	39.1555
$f_{CM(4)}$	337.5897
$f_{CM(5)}$	3.0151e+03
$f_{CM(6)}$	2.7993e+04
$f_{CM(7)}$	2.6844e+05
f_S	3.1491
f_K	11.7195

intensity values (instead of the intensity values themselves). The single value outcomes from application of the first-order style statistical functions to the intermediate matrix representation are again used to form a feature vector representation (one for each region). The statistical functions used are presented at the end of this subsection.

In 2D images, a pixel has eight immediate neighbours defined by a displacement distance d and "azimuth" direction with respect to the angle between the x and y axises in this thesis referred to as Φ with respect to a pixel of interest. In 3D images, a voxel has 26 immediate neighbours, as illustrated in Figure 5.3(a) defined by: (i) a displacement distance d; and (ii) a direction described in terms of a pair of displacement angles Φ, as the "azimuth" direction, and Θ as the "zenith" direction with respect to the z axis for each voxel, as shown in Figure 5.3(b). The complete set of definitions for the 26 neighbours to a voxel in a 3D space, in terms of d, Φ and Θ, is given in Table 5.3.

5.2.2.1 Voxel Co-occurrence Matrix (VCM)

The VCM concept was introduced in Sections 2.4 and again in Section 4.3 in the context of critical functions for regional homogeneity. Recall that the idea of the VCM matrix is founded on the concept of the Grey-Level Co-occurrence Matrix (GLCM) as used in the context of 2D image analysis [53]. Typically, a number of GLCMs are generated, each defined by a azimuth angle (Φ) and distance (d). The rows and columns in each GLCM represent intensity values, and the fields represent intensity value pairings. The value of each field is the frequency of occurrence for a particular pairing. Table 5.4 shows an example region with intensity values (1, 2 and 3) and its GLCM for $d = 1$

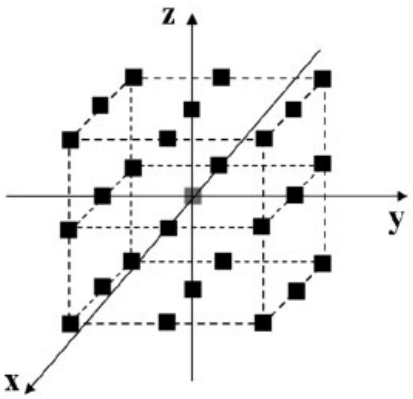

(a) The 26 immediate neighbours for a voxel in 3D space

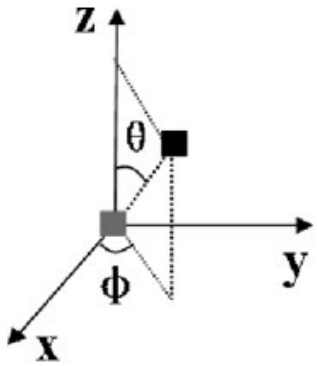

(b) Definition of the azimuth angle Φ and the zenith angle Θ

Figure 5.3: Illustration of neighbours and directions of a voxel in a 3D region [18].

Table 5.3: The possible 26 displacement vectors that can be associated with a voxel [18].

Displacement distance (d)	Direction (Φ, θ)
$\pm(d, 0, 0)$	$(0, 90)$
$\pm(0, d, 0)$	$(90, 90)$
$\pm(0, 0, d)$	$(0, 90)$
$\pm(d, d, 0)$	$(45, 90)$
$\pm(-d, d, 0)$	$(135, 90)$
$\pm(0, d, d)$	$(90, 45)$
$\pm(0, d, -d)$	$(90, 135)$
$\pm(d, 0, d)$	$(0, 45)$
$\pm(d, 0, -d)$	$(0, 135)$
$\pm(d, d, d)$	$(45, 54.7)$
$\pm(-d, d, d)$	$(135, 54.7)$
$\pm(d, d, -d)$	$(54, 125.3)$
$\pm(-d, d, -d)$	$(135, 125.3)$

and $\Phi = 0$.

Table 5.4: Illustration of how to generate a GLCM from a region ($d = 1$ and $\Phi = 0$). In the region, there are 3 intensity values (1,2, and 3).

Region				GLCM			
1	1	2	2	i/j	1	2	3
1	1	2	2	1	4	2	0
3	3	1	1	2	0	2	0
3	3	1	1	3	2	0	2

Thus when generated, a GLCM matrix holds the frequencies of neighbouring intensity values (for a particular value of d and Φ) which in turn can be interpreted as the second-order conditional probability of each intensity value over the complete range of intensity values. With respect to the work described in this thesis, the GLCM ideas was adapted to produced the concept of the VCM, the 3D extension of a GLCM where direction is specified in terms of an azimuth Φ and a zenith angle Θ. Equation 5.1 illustrates how a VCM is generated. The symbols used are given in Table 5.5.

$$VCM(i,j,d_x,d_y,d_z) = \sum_{x=1}^{X}\sum_{y=1}^{Y}\sum_{z=1}^{Z}\begin{cases}1 & if S(x,y,z) = i \ \ and \ \ S(x+d_x, y+d_y, z+d_z) = j \\ 0, & otherwise\end{cases} \tag{5.1}$$

From Equation 5.1 it can be seen that many VCMs could be computed from the same data by varying the value d with respect to three dimensions (x, y, z) (d_x, d_y, d_z). A total of 13 (26 if both directions, plus and minus are considered) matrices can be generated for a given value of d. However, in this research, for simplicity one VCM matrix is generated by summing up of all the possible VCMs. After computing the VCM matrix, the following statistical functions are applied [53, 73]:

Table 5.5: Symbols used for VCM

Symbols	Description
i, j	The i, j row and column respectively of the VCM matrix.
N_g	The maximum value included in intensity values of the region.
$VCM(i,j)$	The VCM with i and j intensity values.
υ	The mean value of the VCM matrix.
υ_i	The means of VCM row i.
υ_j	The means of VCM column j .
σ_i	The standard deviations of VCM row i.
σ_j	The standard deviations of VCM column j .
$max(VCM)$	The maximum value of $VCM(i,j)\ \forall\ i,j$.

1. Angular Second Moment (ASM): $f_{ASM} = \sum_i \sum_j VCM(i,j)^2$.

2. Contrast (c): $f_C = \sum_{n=1}^{N_g} n^2 \left\{ \sum_{i=1}^{N_g} \sum_{j=1}^{N_g} VCM(i,j) \right\}$, where $|i-j| = n$.

3. Correlation (CO): $f_{CO} = \frac{\sum_i \sum_j (ij) VCM(i,j) - \upsilon_i \upsilon_j}{\sigma_i \sigma_j}$.

4. Sum of squares (Variance (V)): $f_V = \sum_i \sum_j (i-\upsilon)^2 VCM(i,j)$.

5. Inverse Difference Moment (IDM): $f_{IDM} = \sum_i \sum_j \frac{1}{1+(i-j)^2} VCM(i,j)$.

6. Sum Average (SA): $f_{SA} = \sum_{i=2}^{N_g} i VCM_{x+y}(i)$,
   where $VCM_{x+y}(s) = \sum_{i=1}^{N_g} \sum_{j=1}^{N_g} VCM(i,j) \quad s.t \;\; i+j = s$.

7. Sum Entropy (SE): $f_{SE} = \sum_{i=2}^{2N_g} VCM_{x+y}(i) \log VCM_{x+y}(i)$.

8. Sum Variance (SV): $f_{SV} = \sum_{i=2}^{2N_g} (i - f_S E)^2 VCM_{x+y}(i)$.

9. Entropy (E): $f_E = -\sum_i \sum_j VCM(i,j) \log(VCM(i,j))$.

10. Difference Entropy: $f_{DE} = \sum_{i=0}^{N_{g-1}} VCM_{x-y}(i) \log VCM_{x-y}(i)$, where $VCM_{x-y}(s) = \sum_{i=1}^{N_g} \sum_{j=1}^{N_g} VCM(i,j) \quad s.t \;\; i-j = s$.

11. Difference Variance (DV): f_{DV} =variance of VCM_{x-y}.

12. Maximal Correlation Coefficient (MCC): f_{MCC}=(second eigenvalue of Q)$^{1/2}$, where Q(i, j)=$\sum_k \frac{VCM(i,k)VCM(j,k)}{VCM_x(i)VCM_j(k)}$.

13. Information Measures of Correlation (IMC): $f_{MCC} = \frac{f_E - XY1}{\max(HX,HY)}$, $f_{IMC} = (1 - \exp[-2.0(XY2 - f_E)^{1/2}])$ where: (i) HX and HY are the entropies of VCM_x and VCM_y and (ii) $XY1 = -\sum_i \sum_j VCM(i,j) \log \{VCM_x(i)VCM_y(j)\}$ and $XY2 = -\sum_i \sum_j VCM_x(i)VCM_y(j) \log \{VCM_x(i)VCM_y(j)\}$.

14. Dissimilarity (D): $f_D = \sum_i \sum_j |(i-j)| VCM(i,j)$.

15. Inverse Difference: $f_{ID} = \sum_i \sum_j \frac{1}{1+(i-j)} VCM(i,j)$.

16. Maximum Probability (MP): $f_{MP} = max(VCM)$.

17. Inverse Difference Normalised (IDN): $f_{IDN} = \sum_i \sum_j \frac{VCM(i,j)}{1+|i-j|^2/N_g^2}$.

18. Autocorrelation (A): $f_A = \sum_i \sum_j (ij) VCM(i,j)$.

19. Cluster Shade (CS): $f_{CS} = \sum_i \sum_j (i+j-\upsilon_i-\upsilon_j)^3 VCM(i,j)$.

20. Cluster Prominence (CP): $f_{CP} = \sum_i \sum_j (i+j-\upsilon_i-\upsilon_j)^4 VCM(i,j)$.

Thus, after applying the above set of functions to a VCM matrix, a set of 20 values are generated for each region (node in the decomposition tree). These values are used to produce a feature vector formate. Table 5.6 shows an example set of "VCM" values for the region in Figure 5.2.

Table 5.6: SOR values for the region presented in Figure 5.2 generated using a VCM

Function	Value
f_{ASM}	0.01
f_C	11.23
f_{CO}	0.36
f_V	58.93
f_{IDM}	0.2916
f_{SA}	1.36
f_{SE}	11.23
f_{SV}	1.99
f_E	4.25
f_{DE}	0.06
f_{DV}	1.99
f_{MCC}	0.51
f_{IMC}	0.46
f_D	2.35
f_{ID}	0.46
f_{MP}	3.1491
f_{IDN}	0.96
f_A	49.12
f_{CS}	-22.19
f_{CP}	1.01e+03

5.2.2.2 Voxel Run-Length Matrix (VRLM)

The concept of the VRLM is founded on the Grey Level Run-Length Matrix (GLRLM); the relationship is similar to that between a GLCM and a VCM as described in the foregoing section. A GLRLM holds the run information for each region. A "run" in this context is a set of consecutive, collinear, image intensity pixels/voxels that have the same values. The length of the run is the number of adjacent pixels/voxels that have the same value. A 2D $GLRLM(\Phi)$ matrix includes a run of length j in a certain direction in the column and in the row is the associated intensity value i [43, 132]. Table 5.7 shows an example of GLRM for angle $\Phi = 0$. A $VRLM(\Phi, \Theta)$ is a volumetric extension to the GLRLM. As in the case of VCM, VRLM is defined in term of two displacement angles Φ and Θ.

Table 5.7: Illustration of how to generate a GLRLM from a region. In the region, there are three intensity values (1,2, and 3), the GLRLM for $\Phi = 0$.

Region			
2	2	2	2
1	1	2	2
3	3	3	1
3	3	1	1

GLRLM			
i/j	1	2	3
1	2	0	0
2	1	0	1
3	1	1	0

Again, as in the case of VCM, one VRLM is computed which is the sum of all the

13 (26 if both directions, plus and minus, are considered) VRLMs. The following five statistical function were extracted from a VRLM matrix, defined as suggested in [43] and used to define a feature vector (the symbols used are given in Table 5.8).

Table 5.8: Symbols used for VRLM.

Symbols	Description
i	The i is the intensity value.
j	The j is the length of the run.
N_g	The maximum value included in intensity values of the region.
VRLM(i,j)	The VRLM with intensity value i and run length j.
N_r	The maximum run length in the given VRLM.

1. Short Runs Emphasis (SRE): $f_{SRE} = \sum_{i=1}^{N_g} \sum_{j=1}^{N_r} \frac{VRLM(i,j)}{j^2} / \sum_{i=1}^{N_g} \sum_{j=1}^{N_r} VRLM(i,j)$.
2. Long Runs Emphasis (LRE): $f_{LRE} = \sum_{i=1}^{N_g} \sum_{j=1}^{N_r} j^2 VRLM(i,j) / \sum_{i=1}^{N_g} \sum_{j=1}^{N_r} VRLM(i,j)$.
3. Gray Level Nonuniformity (GLN): $f_{GLN} = \sum_{i=1}^{N_g} (\sum_{j=1}^{N_r} VRLM(i,j))^2 / \sum_{i=1}^{N_g} \sum_{j=1}^{N_r} VRLM(i,j)$.
4. Run Length Nonuniformity (RLN): $f_{RLN} = \sum_{j=1}^{N_g} (\sum_{i=1}^{N_r} VRLM(i,j))^2 / \sum_{i=1}^{N_g} \sum_{j=1}^{N_r} VRLM(i,j)$.
5. Run Percentage (RP): $f_{RP} = \sum_{i=1}^{N_g} \sum_{j=1}^{N_r} VRLM(i,j) / VRLM$.

In addition, emphasis functions are used [19, 26]. An emphasis function is used to characterise the frequency. The emphasis functions used were as follows:

6. Low Gray-Level Run Emphasis (LGRE): $f_{LGRE} = \frac{1}{N_r} \sum_{i=1}^{N_g} \sum_{j=1}^{N_r} \frac{VRLM(i,j)}{i^2}$.
7. High Gray-Level Run Emphasis (HGRE): $f_{HGRE} = \frac{1}{N_r} \sum_{i=1}^{N_g} \sum_{j=1}^{N_r} VRLM(i,j) i^2$.
8. Short Run Low Gray-Level Emphasis (SRLGE): $f_{SRLGE} = \frac{1}{N_r} \sum_{i=1}^{N_g} \sum_{j=1}^{N_r} \frac{VRLM(i,j)}{i^2 \cdot j^2}$.
9. Short Run High Gray-Level Emphasis (SRHGE): $f_{SRHGE} = \frac{1}{N_r} \sum_{i=1}^{N_g} \sum_{j=1}^{N_r} \frac{VRLM(i,j) \cdot i^2}{j^2}$.
10. Long Run Low Gray-Level Emphasis (LRLGE): $f_{LRLGE} = \frac{1}{N_r} \sum_{i=1}^{N_g} \sum_{j=1}^{N_r} \frac{VRLM(i,j) \cdot j^2}{i^2}$.
11. Long Run High Gray-Level Emphasis (LRHGE): $f_{LRHGE} = \frac{1}{N_r} \sum_{i=1}^{N_g} \sum_{j=1}^{N_r} VRLM(i,j) \cdot i^2 \cdot j^2$.

All these statistical functions were applied to each VRLM. Each one of the functions resulted in a singe value. Each set of values was then combined into a single feature vector representing each region. Table 5.9 shows a set of example values generated using these statistical functions when applied to a VRLM generated with respect to the region in Figure 5.2.

Table 5.9: SOR values for the region presented in Figure 5.2 generated using a VRLM .

Function	Value
f_{SRE}	2.64
f_{LRE}	6.25
f_{GLN}	8.63
f_{RLN}	2.01e+05
f_{RP}	33.98
f_{LGRE}	9.57
f_{HGRE}	1.06e+04
f_{SRLGE}	1.62
f_{SRHGE}	4.95
f_{LRLGE}	4.80e+02
f_{LRHGE}	1.34

5.3 Histogram-based Techniques

In the histogram-based techniques, as the name suggests, histograms are used to represent the occurrence counts for individual values (or bins of values) associated with some attribute (such as intensity values). A histogram is generated with respect to the intensity values of each decomposed region. With respect to the work described in this thesis, four different types of histogram were considered: (i) Histograms of Oriented Gradients (HOG), (ii) Histograms of Local Binary Pattern (LBP), (iii) a combination of HOG and LBP and (iv) Local Phase Quantisation (LPQ). These histogram techniques were selected because, as reported in the literature, they tend to be effective and generate discriminative representations (see discussion presented previously in Section 2.4). These histogram techniques are presented in more detail in the following subsections, Subsections 5.3.1 to 5.3.4. (The effectiveness of each histogram representation in the context of image classification will be measured in the next chapter.)

5.3.1 Histograms of Oriented Gradients (HOG)

The HOG concept was introduced in Section 2.4. Recall that a HOG [24] records the changes of image intensity values. HOGs are the core of the successful Scale-Invariant Feature Transform (SIFT) algorithm [90] used for computer vision applications.

In order to generate a HOG representation the changes in the intensity values of the region, with respect to the azimuth and zenith directions, are computed. These values are referred to as *gradients*. In order to compute the gradient at each location in the region the differences between the "left" and "right" neighbouring intensity values, in a given direction, are calculated. For an region, I, the gradient at each voxel, $\nabla(x, y, z)$, is computed using Equation 5.2.

$$\nabla I(x, y, z) = \frac{\partial I}{\partial x}\mathbf{i} + \frac{\partial I}{\partial y}\mathbf{j} + \frac{\partial I}{\partial z}\mathbf{k} \tag{5.2}$$

In Equation 5.2, $\frac{\partial I}{\partial x}$, $\frac{\partial I}{\partial y}$, and $\frac{\partial I}{\partial z}$ are partial derivatives along the x, y and z direction respectively. Figure 5.4 shows the region presented in Figure 5.2 in terms of difference in gradient. Each location is represented using an arrow indicating the gradient change. These partial derivatives are usually estimated by finite difference schemes such as the forward difference form.

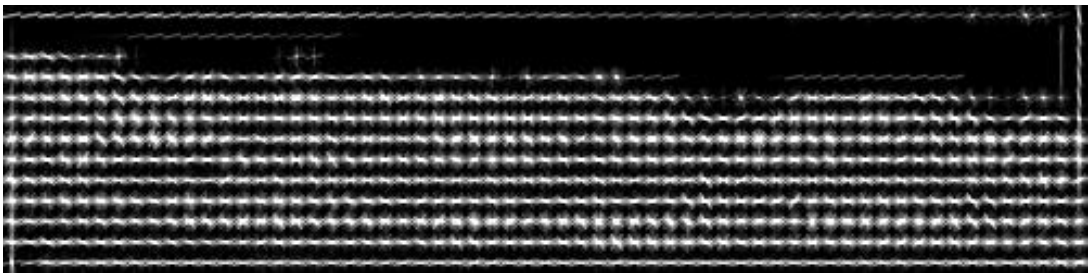

Figure 5.4: Example of gradients with respect to the region presented in Figure 5.2.

The "angles" in each location of the region $\theta(x, y, z)$ are extracted using Equation 5.4 [90, 123]. These angles give values of between 0 and 2π. In order to fix the number of bins in each histogram, the number of angles was set to 8 and the angles quantised using $angle = 2 * \pi/8$. For each quantised angle a between 0 and 8, $h = cos(\theta(x, y, z) - angle(a))^{\alpha}$, where α is constant and set to 9 [126] forming an orientation histogram for each angle a as $hist(a) = hist(a) + (h. * magnitude)$. The histogram is then normalised. Table 5.10 shows example values for the 8 bins extracted from the region presented in Figure 5.2.

$$|\nabla I(x, y, z)| = \sqrt{(\frac{\partial I}{\partial x})^2 + (\frac{\partial I}{\partial y})^2 + (\frac{\partial I}{\partial z})^2} \tag{5.3}$$

$$\theta(x, y, z) = atan2(\frac{\partial I}{\partial z}, \sqrt{(\frac{\partial I}{\partial x})^2 + (\frac{\partial I}{\partial y})^2}) \tag{5.4}$$

Table 5.10: Example values for 8 bins generated using HOG with respect to the region presented in Figure 5.2.

Bins	1	2	3	4	5	6	7	8
Values	1.08	9.37	2.70	1.42	0	8.02	2.07	1.13

5.3.2 Histograms of Local Binary Pattern (LBP)

The basic idea of a LBP was introduced in Section 2.4. The idea is to compare the intensity value of a voxel with the intensity values of its neighbours [56]. Equation 5.5 shows how the LBP is computed in 2D, where v_i is the intensity value of the ith neighbour, v_c is the value for the centre voxel and n is the number of considered

neighbours. In each comparison, a binary value is generated and the concatenation of binary values are converted to a decimal number.

$$LBP_n(x,y) = \sum_{i=1}^{n} f(v_i - v_c))^{2^i}, \quad f(s) = \begin{cases} 1, & s \geq 0 \\ 0, & otherwise \end{cases} \tag{5.5}$$

Due to the possibility that any rotation of the image will change the LBP pattern, there is a need to generate an invariant LBP representation technique. With respect to 2D, each pixel has only eight neighbours (as noted in Section 2.4) so generating such invariant LBP values is not computationally expensive. However, with respect to 3D images, there are 26 neighbours so generating an invariant LBP representation is time consuming and complex. Various approaches have been suggested to cope with this issue: (i) [156] proposed the use of Three Orthogonal Planes LBPs (LBP-TOP), where the calculation of LBPs is only considered with respect to neighbouring voxels located in the XY, XZ and YZ planes, and (ii) [3] proposed the use of Discrete Fourier Transforms LBPs (LBP-DFT). The problem with LBP-TOP is that it only considers the voxels located in the three planes and thus generates three feature vectors, one feature vector per plane, for each image. The problem with LBP-DFT is the time complexity required to calculate the DFT for each location. An alternative LBP approach to address the invariant problem is to use Centre-Symmetric LBP (CSLBP) [57]. CSLBP represents the image by quantising the LBP. The positive aspects of CSLBP are: (i) it derives invariant LBP, (ii) it requires less computational time than other invariant LBP algorithms and (iii) it forms a single feature vector for each region, which is better than LBP-TOP [156]. Equation 5.6 shows how the representation is computed, where n is the number of neighbours (26) and v_i and $v_{i+(n/2)}$ are the opposite voxels to each other around the centre voxel. In CSLBP, each neighbour is compared with its neighbour around the centre voxel so that it ensures the invariant condition is satisfied. In this thesis, given the above identified advantages, CSLBP will be used. Table 5.11 shows an simple example for generating a CSLBP code. Table 5.12 shows example values generated using CSLBP with respect to the region presented in Figure 5.2.

$$CSLBP(x,y,z) = \sum_{i=0}^{(n/2)-1} f(v_i - v_{i+(n/2)})^{2^i} \tag{5.6}$$

Table 5.11: Illustration of how to generate a CSLBP from a region. In the region, there are three intensity values (1,2, and 3).

Region				CSLBP			
1	1	2	2	0	0	0	0
1	1	2	2	0	13	9	0
3	3	1	1	0	12	8	0
3	3	1	1	0	0	0	0

Table 5.12: Example values of eight bins generated using CSLBP with respect to the region presented in Figure 5.2.

Bins	1	2	3	4	5	6	7	8
Values	5.46	-1.93	2.04	1.92	1.32	2.03	1.56	1.89

5.3.3 HOG and LBP Combination (HOG-LBP)

An alternative to using either HOGs or LBPs is to combine the two as described in [143]. The process is as follows:

1. First the LBP value is computed for each voxel of the given region. LBP values in this case serve as a filter which normalises the region against noise as LBP compares the voxel's value to its neighbours.

2. HOG is applied to the LBP code. In this case, both LBP and HOG consider the immediate neighbours so that applying HOG to LBP will allow us to have a representation that will cover a wider region from the centre voxel.

3. HOG histogram generation.

Table 5.13 shows an example of eight bin values for a HOG-LBP extracted from the region presented in Figure 5.2.

Table 5.13: Example values of eight bins generated using HOG-LBP with respect to the region presented in Figure 5.2.

Bins	1	2	3	4	5	6	7	8
Values	2.85	2.24	6.21	3.71	1.03	2.03	2.46	4.7

5.3.4 Histograms of Local Phase Quantisation (LPQ)

Table 5.14: Symbols used for Local Phase Quantisation (LPQ)

Symbols	Description
$N_{x,y,z}$	The set of neighbouring voxels' values where the centre is $S(x, y, z)$.
μ	A specific intensity value.
$f_{x,y,z}$	A vector involving all the intensity values of the neighbouring voxels in $N_{x,y,z}$.
$F_{x,y,z}$	The Fourier Transform (FT) applied to a set of $S(x, y, z)$ neighbours.

As noted in in Section 2.4, Local Phase Quantisation (LPQ) is based on the Fourier Transform (FT) at low frequency whereby a histogram of the quantised low phase of the FT is computed [101]. Table 5.14 illustrates some of the symbols used with respect

to LPQ. At each $\{x, y, z\}$ coordinate location the Fourier Transform (FT) is applied on the set of neighbouring voxel values $N_{x,y,z}$ with respect to the 13 available 3D directions (see Subsection 5.2.2). Given a voxel at location $\{x, y, z\}$, the FT for this voxel, $FT_{x,y,z}$, is generated with respect to the 13 directions, forming 13 values. In order to generate a single value for each voxel, the $FT_{x,y,z}$ values are quantised by generating a binary code ($b_{x,y,z}$) for each element using Equation 5.7. In this case, there are 13 elements associated with $FT_{x,y,z}$, thus when the binary code is translated into a decimal number a large number will be generated. Therefore, a dimensionality reduction technique is applied so as to avoid the inefficiency of generating large histograms (a histogram with 2^{13}). Principal Component Analysis (PCA) was applied to reduce the number of elements in $FT_{x,y,z}$ and then the top L highest values for the eigenvectors V associated with $FT_{x,y,z}$ were selected to get $G_{x,y,z} = [v_1, \ldots, v_L]^T FT_{x,y,z}$. Following this, G_x was quantised using Equation 5.8, where $q_x(j)$ is the jth value in G_x, to generate a binary code for each voxel. Then an integer value derived from the binary code for each voxel was generated using Equation 5.7. Finally a histogram of the integer values of b_x was calculated from each location x. This histogram then describes a feature vector with 2^L bins. Table 5.15 shows an example of LPQ code generation. Table 5.16 shows an example of eight bin values for LPQ generated for the region presented in Figure 5.2.

$$b_{x,y,z} = \sum_{j=1}^{L} q_{x,y,z}(j) 2^{j-1} \tag{5.7}$$

$$q_{x,y,z}(j) = \begin{cases} 1, & g_{x,y,z}(j) \geq 0 \\ 0, & otherwise \end{cases} \tag{5.8}$$

Table 5.15: Illustration of how to generate a LPQ for a region. In the region, there are three intensity values (1, 2 and 3).

Region				LPQ			
1	1	2	2	215	215	95	62
1	1	2	2	229	95	94	14
3	3	1	1	109	93	14	134
3	3	1	1	61	60	148	132

Table 5.16: Example values for eight bins generated by LPQ for the region in Figure 5.2.

Bins	1	2	3	4	5	6	7	8
Values	1.09	9.28	7.82	4.32	1.28	1.37	4.93	2.25

5.4 Single Feature Vector Generation (Stage 3)

Stage 3 of the region-based classification process (Figure 5.1) comprises feature vector generation. Recall that with respect to the volumetric region-based representations

under discussion in this chapter each region is represented by a feature vector leading to a set of feature vectors describing each image. In order to classify images using a traditional form of classifier, a single feature vector for each image is required as input. The problem in our case is that the number of feature vectors can be different between images. In this section, we describe the adapted techniques whereby a single feature vectors can be generated. The objective is to generate the most discriminative feature vector from a given set of such vectors that describes the image in a manner best suited to classification. This process can be achieved using either: (i) dimensionality reduction or (ii) feature selection. In the case of dimensionality reduction, the set of feature vectors generated describing a single image is considered without taking into consideration the feature vectors associated with other images in the image set, while when using feature selection-based techniques the whole dataset of feature vectors is considered. The advantage of feature selection is that the selected feature vectors should maximise the discriminative power as each region is considered with respect to other classes in the dataset. In this thesis, two examples (one for each technique) of feature generation will be employed. Further detail concerning the two adapted feature generation techniques is presented in the following two subsections.

5.4.1 Dimensionality Reduction

One technique for reducing the size of a feature vector representation is to apply some form of dimensionality reduction, the process of either removing unwanted or superfluous dimensions from the feature space or combining dimensions. The issue is determining which dimensions to remove. There are a number of mechanisms whereby this can be achieved; one popular mechanism, and that adopted with respect to the work presented in this thesis, is Principal Component Analysis (PCA) [69]. The concept of PCA was presented in Subsection 2.6.1. The basic idea is to identify a set of eigenvectors and their associated values. An eigenvector with a high associated value is considered more significant than Eigenvectors with a low associated value. Therefore, eigenvectors are sorted in a descending order and the top k selected; for the work in this thesis $k = 40$ was found to be the most appropriate value. The identified eigenvector values are then used to form a single feature vector $FV(i)$ per image i [146] .

5.4.2 Feature Selection

As noted in Subsection 2.6.1, feature selection is a technique used to choose a subset of feature vectors from a large collection of feature vectors. The selected subset is used to form a single feature vector for each image. One of the exemplar feature selection techniques is dictionary learning. In the dictionary, a subset of feature vectors is selected and used to generate a single feature vector. A dictionary in this case refers to a repository of feature vectors that most effectively summarises the whole set of

images.

With respect to the work described in this thesis, the Improved Fisher Kernel (IFK) encoding [105] was used for dictionary feature selection purposes. IFK is used to encode the dictionary learning estimating the distribution of feature vectors. IFK relies on the Gaussian Mixture Model (GMM) to form the dictionary (we refer to this process as IFK-GMM). The dictionary in this context is defined in terms of a clustering of the whole set of feature vectors for the dataset. The process has the two steps: (i) the Gaussian Mixture Model (GMM) is used to model the distribution of the given feature vectors for a whole set of images so forming a dictionary and (ii) the Fisher Kernel approach is used to encode the information about the distribution.

In IFK-GMM, GMM is first applied to the whole sets of feature vectors N with a required number of clusters K. Let $X = \{\mathbf{x_1}, \ldots, \mathbf{x_N}\}$ be the whole sets of feature vectors corresponding to all the decomposed regions of the whole dataset. The distribution of the feature vectors is estimated using the GMM; a mixture of K multivariate Gaussian distributions, where K is the number of desired elements in the dictionary. For a sample $\mathbf{x}$ the conditional probability $p(\mathbf{x}|\Lambda)$ is calculated as follows:

$$p(\mathbf{x}|\Lambda) = \sum_{k=1}^{K} w_k g(\mathbf{x}|\boldsymbol{\mu}_k, \boldsymbol{\Sigma}_k) \tag{5.9}$$

$$g(\mathbf{x}|\boldsymbol{\mu}_k, \boldsymbol{\Sigma}_k) = \frac{1}{\sqrt{(2\pi)^D \det \boldsymbol{\Sigma}_k}} \exp\left[-\frac{1}{2}(\mathbf{x} - \boldsymbol{\mu}_k)^T \boldsymbol{\Sigma}_k^{-1}(\mathbf{x} - \boldsymbol{\mu}_k)\right] \tag{5.10}$$

where w_k, $\boldsymbol{\mu}_k$ and $\boldsymbol{\Sigma}_k$ are the prior probability, mean, and covariance matrix of the Gaussian g_k. D is the number of dimensions of the feature vector describing a sub-volume. The GMM can be described by the parameters $\Lambda = \{w_k, \boldsymbol{\mu}_k, \boldsymbol{\Sigma}_k, k = 1, \ldots, K\}$. In general, the parameters Λ are unknown at the beginning and have to be learnt by maximising the log-likelihood of the data X. This is usually conducted using the Expectation Maximisation (EM) algorithm (interested readers are referred to the original paper for further details [28]).

Once the GMM parameters are learnt, Improved Fisher Kernel Encoding (IFK) [105] is used to encode all the features of an image. The reasons for using IFK are: (i) it has been shown to perform well with respect to other image classification applications [62], and (ii) the anticipated relatively small size of dictionary required to represent all the possible features. More specifically, IFK forms the gradients of the mean $G^N_{\boldsymbol{\mu},i}$ and standard deviation $G^N_{\boldsymbol{\sigma},i}$ of Gaussian i for feature vectors $i = 1 \ldots K$ as in Equations 5.12 and 5.13.

$$\gamma_n(i) = \frac{w_i \mu_i(x_n)}{\sum_{j=1}^{K} w_j \mu_j(x_n)} \tag{5.11}$$

$$G^N_{\boldsymbol{\mu},i} = \frac{1}{N\sqrt{w_i}} \sum_{n=1}^{N} \gamma_n(i)\left(\frac{x_n - \boldsymbol{\mu_i}}{\boldsymbol{\sigma_i}}\right) \tag{5.12}$$

$$G^N_{\boldsymbol{\sigma},i} = \frac{1}{N\sqrt{2w_i}} \sum_{n=1}^{N} \gamma_n(i)[\frac{(x_n - \boldsymbol{\mu_i})^2}{\boldsymbol{\sigma_i}^2} - 1] \tag{5.13}$$

Finally, the single feature vector is formed by concatenating the two gradients ($G^N_{\boldsymbol{\mu},i}$ and $G^N_{\boldsymbol{\sigma},i}$). All the generated single feature vectors for each image will be of the same size, $2 * K * D$, where D is the dimension of the feature vector and K is the number of elements (feature vectors) in the dictionary.

5.5 Classifier Generation (Stage 4)

The final stage, Stage 4, of the region-based classification process is concerned with the classifier generation. From the foregoing, a single feature vector $FV(i)$ is used to describe each data volume i (retinal volume with respect to the motivation for this thesis) where each volume is made up of a number of features. For training purposes, each feature vector $FV(i)$ was combined with a class label $c_i \in \{-1, 1\}$. The class label in our case is in a binary form where +1 indicates a retina with AMD, and -1 a normal retina. The resulting representation is compatible with a number of classifier generators.

In order to evaluate the seven region-based representations (FOR, SOR-VCM, SOR-VRLM, HOG, LBP, HOG-LBP and LPQ), three classifier generators were employed: (i) Support Vector Machines(SVM), (ii) k-Nearest Neighbours (KNN), and (iii) Bayesian Networks (BN). The implementations for these classifiers were taken from Weka [51]. For SVM, the Library for Support Vector Machines (LIBSVM) package [14] is used. The outcomes of the evaluation are presented in the following chapter.

5.6 Summary

The general process for generating region-based representations advocated in this chapter comprises a four-stage process: (i) image decomposition to produce a set of regions, (ii) feature vector generation for each region, (iii) a single feature vector and (iv) classifier generation applied to the complete set of single feature vectors. Two types of region-based techniques were considered: (i) statistical-based techniques and (ii) histogram-based techniques. With respect to the statistical-based techniques, two approaches were considered: (i) First-Order Representation (FOR) and (ii) two Second-Order Representation (SOR) using VCM and VRLM. With respect to the histogram-based techniques, four approaches were considered: (i) HOG, (ii) LBP, (iii) HOG-LBP and (iv) LPQ. For stage three, two feature vector generation techniques were proposed: (i) dimensionality reduction and (ii) feature selection. An evaluation of the techniques described in this chapter is presented in the following chapter.

Chapter 6

Evaluation of Classification Performance Using Region-Based Volumetric Representations

6.1 Overview

In the previous chapter (Chapter 5), a four-stage region-based process for generating binary classifiers for application to volumetric data, specifically retinal volumes, was described. The four stages were: (i) image decomposition to produce a set of regions, (ii) region representation, (iii) single feature vector generation (feature vector combination) and (iv) classifier generation. In this chapter, the evaluation of this process is presented in terms of the different techniques that can be used at each stage.

Image decomposition (Stage one) was presented in Chapter 4 where it was noted that an important aspect of image decomposition is the use of critical functions to establish regional homogeneity. Recall that seven critical functions were considered:

1. Average Intensity Value (AIV).
2. Kendall's Coefficient Concordance (KCC).
3. Gray Level Co-occurrence Matrix (GLCM).
4. Euclidean Distance (ED).
5. Dynamic Time Warping (DTW).
6. Longest Common Subsequence (LCS).
7. Kullback-Leibler divergence (KLD).

Of which the last five were adapted by the author with respect to volumetric decomposition. In this chapter, we compare between these different critical functions and

different forms of decomposition in terms of classification effectiveness. For the experiments the threshold value t used with the critical functions, as presented in Section 4.3, was set to 0.5. This value was selected because experiments conducted using the whole image-based representation indicated that this produced the best classification outcomes. The details of these experiments is not reported in the main body of this thesis; however, for completeness, it has been included in Appendix A. In Chapter 4, two forms of decomposition, standard and overlapping, were also discussed.

With respect to region representation (Stage two), seven representation techniques were proposed in Chapter 5 as follows:

1. First-Order Representation (FOR).
2. Voxel Co-occurrence Matrix (VCM).
3. Voxel Run-Length Matrix (VRLM).
4. Histograms of Oriented Gradients (HOG).
5. Histograms of Local Binary Pattern (LBP).
6. A combination of HOG and LBP (HOG-LBP).
7. Local Phase Quantisation (LPQ).

Of which the first three are statistical representations (2 and 3 are second-order statistical representation or SOR) and the remaining four are histogram based representations. Note that each of the above resulted in a feature vector representation, one for each identified region (node) in the decomposition.

With respect to Stage three (feature vector combination for single feature generation), two mechanisms were proposed:

1. A dimensionality reduction-based method using Principal Component Analysis (PCA).
2. A feature selection-based method using Improved Fisher Kernel (IFK).

The result in each case was a single feature vector representing an entire volume (made up of regions). In terms of IFK, as described in Subsection 5.4.2, different dictionary sizes could be used. Thus for the evaluation presented in this chapter we compare between the operation of a range of dictionary sizes (32, 64, 128, 256 and 512).

The final stage of the process (Stage four) was classifier generation. As noted previously, there are a great many binary classifier generators available that operate using a feature vector representation. Three were considered with respect to the work described in this thesis:

1. Support Vector Machines (SVM).
2. K-Nearest Neighbour (KNN).
3. Bayesian Networks (BN).

As noted in the previous chapter, these were selected because they tended to produce good results when used with other related application domains and because their usage is widely reported in the literature. For the SVM classifier, the complexity constant was set to one and the linear polynomial kernel was used with a coefficient value of one. For KNN, the number of nearest neighbours (k) was set to one.

Given the above, the different techniques can be combined to give 4 (levels) $\times$ 2 (standard and overlapping decomposition) $\times$ 7 (critical functions) $\times$ 7 (region representation techniques) $\times$ 2 (single feature vector generation techniques) $\times$ 3 (classifiers) $= 2,352$ different ways whereby region-based volumetric classification can be achieved. The combination of these techniques forms as a set of $3,528$ ($4 \times 2 \times 7 \times 7 \times 3$) classification results if we include the option of not using a critical function at all. Experiments were undertaken with respect to all these combinations; however, for ease of presentation these are reported in this chapter by considering the alternatives with respect to each stage (decomposition, region representation, feature vector generation and classification) in isolation. In each case, a constant set of techniques for the remaining stages was typically used; these were selected according to their anticipated best performance.

The overall objectives of the evaluation presented in this chapter were as follows:

1. **Stage 1**: To determine if the use of a critical function produces a more effective classification than when a critical function is not used, and if so to determine which critical function produced the best classification results; and to determine whether standard or overlapping decomposition was more appropriate.
2. **Stage 2**: To determine the most appropriate region-based representation technique in terms of classification effectiveness.
3. **Stage 3**: To determine which single feature vector generation mechanism produced the best result and whether using feature selection improves the outcome.
4. **Stage 4**: To identify the most appropriate classifier to be applied (out of the three different generators considered).

The experiments conducted with respect to each stage fell into two categories: (i) classifier performance evaluation and (ii) statistical significance testing. The evaluation metrics used for classifier performance evaluation were: (i) Accuracy (Acc.), (ii) Sensitivity (Sen.), (iii) Specificity (Spec.), (iv) Positive Predictive Value (PPV), (v) Negative Predictive Value (NPV), (vi) Error Equal Rate (EER) and (vii) Area Under the Curve

(AUC) of the receiver operating characteristic as defined in Subsection 2.8.1. Ten-fold Cross Validation (TCV) was used throughout. Significance testing was conducted using ANalysis Of VAriance (ANOVA). This aim was to check whether there is a statistical significance between results in terms of AUC. Recall that the ANOVA procedure was described in Subsection 2.8.2. Using this procedure, the results concerned with the analysis of a particular stage were grouped together and ANOVA testing applied, resulting in a p-value in each case. The p-values indicate the level of significance; a result was considered to be significant if the associated p-value was below 0.05. Tukey's Honestly Significant Difference (HSD) Post-Hoc Test was then applied to determine whether there were any significant differences between the operation of the classifier performances (as also described in Subsection 2.8.2). The dataset used was the 3D OCT retinal image data set introduced in Section 3.5.

In the remainder of this chapter the evaluation results, with respect to each stage and each of the above objectives, are presented and discussed in Sections 6.2 to 6.5 below. A summary of the main findings of the conducted evaluation is presented at the end of this chapter in Section 6.6.

6.2 Decomposition (Stage One)

From the foregoing, the aim of the reported experiments presented in this section was to determine the best decomposition method in the context of classification performance. More specifically, the objectives were:

1. To determine whether a better result is produced when using a critical function to support the decomposition than when not using a critical function.
2. If the use of a critical function is desirable which, out of the seven functions considered, produced the best results.
3. In the context of the critical functions considered (and no critical function), which is the best level of decomposition to use.
4. To determine whether standard or overlapping decomposition is more desirable.

For the performance evaluation the following techniques were used with respect to the stages not considered in this section (representation, feature vector generation and classification): (i) the HOG region-based representation, (ii) dimensionality reduction using PCA and (iii) SVM classifier generation. Four levels of decomposition (L) were considered, 3, 4, 5 and 6. These levels were selected because preliminary experiments had indicated that these tended to produce good classification results. As noted in the introduction to this chapter, and in line with the experiments conducted with respect to stages two, three and four reported later in this chapter, two sets of experiments

are reported on in this section: (i) classifier performance in Subsection 6.2.1 and (ii) statistical significance testing in Subsection 6.2.2.

6.2.1 Classifier Performance in the Context of Decomposition

Tables 6.1 and 6.2 show the decompositions results obtained in the context of classification performance. Best average results are highlighted in bold font. The first set of rows, labelled "0NCF", gives the results obtained when no critical function was used. The column labelled "L" indicates the level of decomposition. Table 6.1 gives the results obtained using standard decomposition while Table 6.2 provides the results using overlapping decomposition. From the tables, it can be observed that a good overall performance was recorded.

When comparing the use of a critical function with not using a critical function the best AUC value obtained using 0NCF was 0.97, while the best critical function AUC result was 0.98; thus not a significant difference between the two. However, when no critical function was used no best average value was recorded. Out of the seven critical functions considered AIV, KCC and ED all produced a best AUC value of 0.98. GLCM produced the worst performance. Overall, a marginal argument can be made that the use of a critical function produces a better classification result, and therefore a better decomposition, than when no critical function is used. A marginal argument can also be made that use of the ED and LCS critical functions was the most effective because they produced the best average accuracy, EER and AUC values with standard and overlapping decomposition. Recall that the ED and LCS critical functions were proposed by the author.

Table 6.3: The number of occasions when the best recorded AUC value from Tables 6.1 and 6.2 with respect to level of decomposition L and type of decomposition (standard or overlapping) was recorded

L	Standard	Overlapping	Totals
3	2	$2\frac{5}{6}$	$4\frac{5}{6}$
4	3	$2\frac{2}{6}$	$4\frac{2}{6}$
5	2	$1\frac{5}{6}$	$3\frac{5}{6}$
6	1	2	3
Totals	8	8	16

In the context of the standard versus overlapping decomposition, the results in Tables 6.1 and 6.2 indicate that better AUC results were generated using the overlapping decomposition. This is probably because the overlapping decomposition alleviates the boundary problem encountered when undertaking image decomposition. From the tables, the best recorded AUC value for the standard decomposition was 0.94 while the best for the overlapping decomposition was 0.98.

In the context of the most appropriate level of decomposition, Table 6.3 summarises

Table 6.1: Classifier performance results using standard decomposition, the HOG region-based representation, dimensionality reduction using PCA and SVM classification in the context of decomposition (Stage 1) using: (i) a range of decomposition levels, (ii) a number of critical functions (including no critical function).

CF	L	Acc	Sen	Spec	PPV	NPV	EER	AUC
0NCF	3	89.29%	92.06%	87.01%	85.29%	93.06%	0.14	0.89
	4	92.86%	95.31%	90.79%	89.71%	95.83%	0.10	0.93
	5	92.14%	95.24%	89.61%	88.24%	95.83%	0.11	0.92
	6	92.14%	95.24%	89.61%	88.24%	95.83%	0.11	0.92
	Ave.	91.6%	94.46%	89.25%	87.87%	95.13%	0.11	0.91
AIV	3	92.86%	98.33%	88.75%	86.76%	98.61%	0.12	0.93
	4	91.43%	96.67%	87.50%	85.29%	97.22%	0.13	0.91
	5	91.43%	93.75%	89.47%	88.24%	94.44%	0.11	0.91
	6	91.43%	93.75%	89.47%	88.24%	94.44%	0.11	0.91
	Ave.	91.78%	95.62%	88.79%	87.13%	96.17%	0.11	0.91
KCC	3	90.00%	95.00%	86.25%	83.82%	95.83%	0.14	0.9
	4	93.57%	98.36%	89.87%	88.24%	98.61%	0.11	0.93
	5	89.29%	94.92%	85.19%	82.35%	95.83%	0.16	0.89
	6	92.14%	95.24%	89.61%	88.24%	95.83%	0.11	0.92
	Ave.	91.25%	95.88%	87.73%	85.66%	96.52%	0.13	**0.93**
GLCM	3	89.29%	92.06%	87.01%	85.29%	93.06%	0.14	0.89
	4	87.14%	90.32%	84.62%	82.35%	91.67%	0.16	0.87
	5	91.43%	95.16%	88.46%	86.76%	95.83%	0.12	0.91
	6	91.43%	95.16%	88.46%	86.76%	95.83%	0.12	0.91
	Ave.	89.82%	93.17%	87.13%	85.29%	94.09%	0.13	0.89
ED	3	92.86%	98.33%	88.75%	86.76%	98.61%	0.12	0.93
	4	92.14%	98.31%	87.65%	85.29%	98.61%	0.13	0.92
	5	94.29%	100.00%	90.00%	88.24%	100.00%	0.11	0.94
	6	93.57%	98.36%	89.87%	88.24%	98.61%	0.11	0.93
	Ave.	93.21%	**98.75%**	89.06%	87.13%	**98.95%**	0.11	**0.93**
DTW	3	89.29%	92.06%	87.01%	85.29%	93.06%	0.14	0.89
	4	92.86%	95.31%	90.79%	89.71%	95.83%	0.10	0.93
	5	91.43%	95.16%	88.46%	86.76%	95.83%	0.12	0.91
	6	90.71%	93.65%	88.31%	86.76%	94.44%	0.12	0.91
	Ave.	91.07%	94.04%	88.64%	87.13%	94.79%	0.12	0.91
LCS	3	92.86%	98.33%	88.75%	86.76%	98.61%	0.12	0.93
	4	93.57%	96.83%	90.91%	89.71%	97.22%	0.10	0.93
	5	94.29%	98.39%	91.03%	89.71%	98.61%	0.09	0.94
	6	94.29%	98.39%	91.03%	89.71%	98.61%	0.09	0.94
	Ave.	**93.75%**	97.98%	**90.43%**	**88.97%**	98.26%	**0.10**	**0.93**
KLD	3	90.71%	93.65%	88.31%	86.76%	94.44%	0.12	0.91
	4	92.86%	95.31%	90.79%	89.71%	95.83%	0.10	0.93
	5	92.14%	93.85%	90.67%	89.71%	94.44%	0.10	0.92
	6	92.14%	93.85%	90.67%	89.71%	94.44%	0.10	0.92
	Ave.	91.96%	94.16%	90.11%	**88.97%**	94.78%	**0.1**	0.92

Table 6.2: Classifier performance results using overlapping decomposition, the HOG region-based representation, dimensionality reduction using PCA and SVM classification in the context of decomposition (Stage 1) using: (i) a range of decomposition levels, (ii) a number of critical functions (including no critical function).

CF	L	Acc	Sen	Spec	PPV	NPV	EER	AUC
0NCF	3	93.57%	98.36%	89.87%	88.24%	98.61%	0.11	0.93
	4	95.71%	100.00%	92.31%	91.18%	100.00%	0.08	0.96
	5	96.43%	98.46%	94.67%	94.12%	98.61%	0.06	0.96
	6	97.14%	100.00%	94.74%	94.12%	100.00%	0.06	0.97
	Ave.	95.71%	99.2%	92.89%	91.91%	99.3%	0.07	0.95
AIV	3	97.86%	98.51%	97.26%	97.06%	98.61%	0.03	0.98
	4	95.71%	100.00%	92.31%	91.18%	100.00%	0.08	0.96
	5	94.29%	98.39%	91.03%	89.71%	98.61%	0.09	0.94
	6	93.57%	98.36%	89.87%	88.24%	98.61%	0.11	0.93
	Ave.	95.35%	98.81%	92.61%	91.54%	98.95%	0.07	0.95
KCC	3	97.86%	97.10%	98.59%	98.53%	97.22%	0.01	0.98
	4	95.71%	96.97%	94.59%	94.12%	97.22%	0.06	0.96
	5	97.86%	100.00%	96.00%	95.59%	100.00%	0.04	0.98
	6	95.00%	96.92%	93.33%	92.65%	97.22%	0.07	0.95
	Ave.	96.6%	97.74%	95.62%	95.22%	97.91%	**0.04**	**0.96**
GLCM	3	94.29%	96.88%	92.11%	91.18%	97.22%	0.08	0.94
	4	94.29%	98.39%	91.03%	89.71%	98.61%	0.09	0.94
	5	95.71%	98.44%	93.42%	92.65%	98.61%	0.07	0.96
	6	96.43%	98.46%	94.67%	94.12%	98.61%	0.06	0.96
	Ave.	95.18%	98.04%	92.80%	91.91%	98.26%	0.07	0.95
ED	3	97.86%	98.51%	97.26%	97.06%	98.61%	0.03	0.98
	4	96.43%	97.01%	95.89%	95.59%	97.22%	0.04	0.96
	5	95.71%	95.59%	95.83%	95.59%	95.83%	0.04	0.96
	6	95.71%	96.97%	94.59%	94.12%	97.22%	0.06	0.96
	Ave.	**96.42%**	97.02%	**95.89%**	**95.59%**	97.22%	**0.04**	**0.96**
DTW	3	94.29%	100.00%	90.00%	88.24%	100.00%	0.11	0.94
	4	96.43%	98.46%	94.67%	94.12%	98.61%	0.06	0.96
	5	97.14%	100.00%	94.74%	94.12%	100.00%	0.06	0.97
	6	97.14%	100.00%	94.74%	94.12%	100.00%	0.06	0.97
	Ave.	96.25%	**99.61%**	93.53%	92.65%	**99.65%**	0.07	**0.96**
LCS	3	95.71%	95.59%	95.83%	95.59%	95.83%	0.04	0.96
	4	97.14%	98.48%	95.95%	95.59%	98.61%	0.04	0.97
	5	95.71%	98.44%	93.42%	92.65%	98.61%	0.07	0.96
	6	95.00%	98.41%	92.21%	91.18%	98.61%	0.08	0.95
	Ave.	95.89%	97.73%	94.35%	93.75%	97.91%	0.05	**0.96**
KLD	3	96.43%	98.46%	94.67%	94.12%	98.61%	0.06	0.96
	4	96.43%	100.00%	93.51%	92.65%	100.00%	0.07	0.96
	5	95.71%	98.44%	93.42%	92.65%	98.61%	0.07	0.96
	6	95.00%	98.41%	92.21%	91.18%	98.61%	0.08	0.95
	Ave.	95.89%	98.82%	93.45%	92.65%	98.95%	0.07	0.95

the results obtained. The table lists the number of occasions, from Tables 6.1 and 6.2, when a best AUC value was recorded with respect to each value for L and the type of decomposition (standard or overlapping). From the summary, it can be seen that best AUC results were most frequently obtained with $L = 3$, with $L = 4$ giving a close second best performance. However, there is no clear best value for L.

6.2.2 Decomposition Significance Testing

Other than that, the use of critical function was beneficial to inspection of the results presented in Tables 6.1 and 6.2, using the HOG representation, PCA and SVM classifier generation, suggesting that there is no significant difference with respect to the operation of the different decomposition techniques considered although some produced better results than the others. This subsection reports on the ANOVA that was applied to all the generated results (including results using all other combination of the proposed techniques not included in Section 6.2.1) to determine if there was any statistically significant difference in the operation between the different techniques considered in this section.

As already noted in the previous subsection, 64 different combinations of techniques were considered: 4 (levels) $\times$ 2 (standard and overlapping decomposition) $\times$ 8 (critical functions) = 64 combinations. ANOVA was applied to check if there was any significant difference between the operation of these 64 different techniques. The analysis was conducted with respect to AUC values.

In the context of comparing the use of the critical functions against each other and without a critical function (0NCF), Table 6.4 shows the ANOVA table (more detail about ANOVA was presented in Subsection 2.8.2). The ANOVA table has six columns:

1. **Source**: The source of variation in terms of: (i) the differences between groups (Between-Groups), and (ii) the change within each group (Error).
2. **SS**: The sum of squares value for each source.
3. **df**: The degrees of freedom for each source.
4. **MS**: The mean square value associated with each source.
5. **F**: The F ratio of the mean square values.
6. **p-value**: The p-value obtained by the cumulative distribution function of F.

From the table, it can be noted that the calculated p-value (2.8315e-20) is less than 0.05, indicating that there is indeed a statistical significance between the results obtained. From the table, $Error_{SS} = 14.02$, indicating that there are a wide range of values for each critical function but with a smaller range in terms of the difference between critical functions (Between-Groups$_{SS} = 0.7024$).

Figure 6.1(a) shows the significant difference between the results of the critical functions where the x-axis represents the AUC results and the y-axis lists the methods. The lines represent the "comparison interval" around the AUC mean of each group (critical function); the dot in the middle of each line makes the mean of each group. When the lines of two methods do not overlap, the operation (in terms of AUC) between the two methods can be said to be significantly different.

Figure 6.1(b) shows boxplots of the confidence intervals for each method. In the diagram, the x-axis lists the methods and the y-axis the AUC value. The red line in each box represents the median value of the AUC results while the top and bottom of the box represent the 75% and 25% quartile of the AUC results. The notch in each box represents the 95% confidence intervals of the measured median value. The whiskers mark the highest/lowest AUC values of each group of AUC results that are within 1.5 times the interquartile range of the box edges. The red plus signs represent the outliers beyond the data range. When the notches of two methods do not overlap, the medians of them will be significantly different at the 0.05 significance level. From both figures it can be observed that:

1. The results obtained using 0NCF were statistically different from the results obtained using critical functions (except for the DTW and GLCM critical functions) where the range of AUC results for 0NCF were less than the results of the proposed critical functions, a lower mean (0.86) than the critical functions and a lower median (0.87) than the rest of the critical functions. This result supports the conjecture that the use of critical functions for measuring the regional homogeneity produces a more concise and descriptive representation.

2. The AUC results recorded using the ED critical function were statistically different from those recorded using 0NCF, DTW, GLCM, KCC and KLD because the range of the confidence interval for the ED result was higher than the other critical functions.

3. The LCS results were not statistically different from AIV, ED and KCC but were statistically different from the other critical functions.

4. The AUC results obtained using GLCM were statistically different from AIV, ED and LCS.

5. The results obtained using KCC were statistically different from ED, DTW and 0NCF.

6. The KLD results were statistically different from the 0NCF, ED and LCS results.

In the context of level of decomposition, the ANOVA table presented in Table 6.5 shows that there was a statistical significance between the results obtained for the

Table 6.4: ANOVA table for comparing critical functions

Source	SS	df	MS	F	p-value
Between-Groups	0.7024	7	0.1003	15.7415	2.8315e-20
Error	14.0246	2200	0.0064		
Total	14.7271	2207			

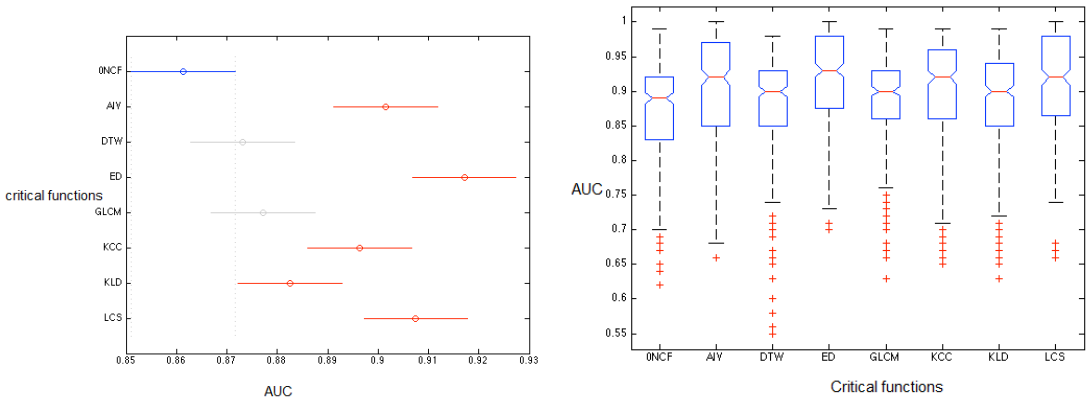

(a) Significance differences

(b) Confidence intervals

Figure 6.1: Significance differences and confidence intervals for comparing critical functions

different levels of decomposition in the context of the recorded AUC values (the p-value was 6.9209e-04). Note that in the table the groups are the techniques used with respect to each level. From the table, it can be seen that the range of values was wide (Error$_{SS}$=14.69), while the difference in values between the groups was slightly smaller (Between-Groups$_{SS}$=0.1). The significant difference and confidence interval diagrams shown in Figure 6.2(a) illustrate the significant differences between the levels of decomposition. From the figure, it can be observed that the AUC results obtained using $L = 3$ were statistically different from those obtained using $L = 5$ and $L = 6$; while the AUC results obtained using $L = 4$ were not statistically different from the others because the range of recorded AUC results overlaps with the ranges of the results associated with the other groups. The confidence intervals shown in Figure 6.2(b) reveal that there was a similarity between the results with slight improvement with respect to $L = 5$, which had a slightly higher median AUC result of 0.91, thus contradicting the previously conducted but less sophisticated, analysis presented in Table 6.3.

In terms of comparing standard and overlapping decomposition, Table 6.6 gives the ANOVA table, where the p-value of 1.7955e-25 indicates that there was a statistical difference between the standard and overlapping decomposition, as also demonstrated in Figure 6.3. From the table, it can be seen that there was similarity between the results of the standard and overlapping decomposition as Between-Groups$_{SS}$=0.6906

Table 6.5: ANOVA table for comparing levels of decomposition

Source	SS	df	MS	F	p-value
Between-Groups	0.1099	3	0.0366	5.7014	6.9209e-04
Error	14.6999	2288	0.0064		
Total	14.8098	2291			

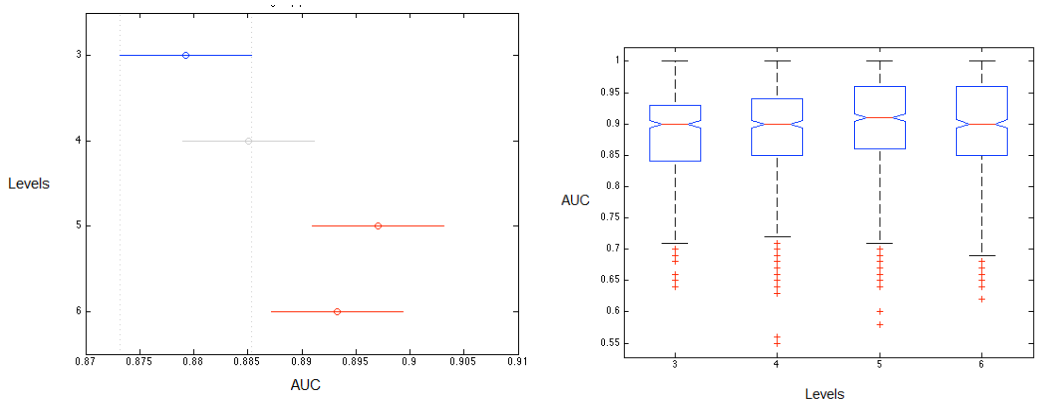

(a) Significance differences

(b) Confidence intervals

Figure 6.2: Significance differences and confidence intervals for comparing levels of decomposition

which is slightly low. The table revels also that the differences within each decomposition method with Error_{SS}=14.1132 were higher than between groups, indicating that there were large differences between the classification results. The confidence interval, shown in Figure 6.3, indicates that the overlapping decomposition outperformed the standard decomposition in a statistically significant manner, thus confirming the earlier conclusions presented in Subsection 6.2.1.

Table 6.6: Comparison of decomposition techniques

Source	SS	df	MS	F	p-value
Between-Groups	0.6906	1	0.6906	111.4646	1.7955e-25
Error	14.1132	2278	0.0062		
Total	14.8038	2279			

Thus in conclusion we can consider that the best critical function to use is either the ED or LCS critical function together with $L = 5$ and overlapping decomposition. Note that both ED and LCS are amongst the critical functions proposed by the author.

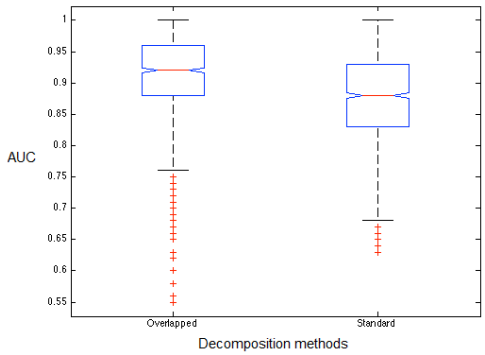

Figure 6.3: Confidence intervals for overlapping with standard decomposition.

6.3 Region Representation (Stage Two)

In this section, the results obtained comparing the operation of the seven proposed region-based representation techniques are considered. Recall that the objective was to identify the most appropriate region representation in the context of classification performance based on the decomposition process. As in the previous section, results with respect to both classification performance and significance testing are presented (Subsections 6.3.1 and 6.3.2 respectively). For the performance evaluation, four levels of decomposition were again considered, $L = 3$, $L = 4$, $L = 5$ and $L = 6$, together with the ED critical function and overlapping decomposition because the experiments presented in the previous section (and others not specifically reported in this thesis) indicated that these later two worked well. Although in the previous section it was demonstrated that $L = 5$ tended to produced a best performance, the reason for using a range of levels with respect to the experiments reported here was because it was conjectured that the operation of the different region representation techniques might be affected by the nature of the level of decomposition used. As previously, with respect to the other two stages not considered in this section (feature vector generation and classification), dimensionality reduction using PCA and SVM classification were adapted.

6.3.1 Classifier Performance in the Context of Region Representation

In this section, we present the results obtained to compare the operation of the seven proposed region-based representation techniques. The results are presented in Table 6.7. Out of the seven representation techniques considered, the results presented in the table indicate that the HOG representation method produced the best results with a best average AUC of 0.96. From the table, the best accuracy and AUC value were produced using the HOG representation with $L = 4$ (97.14% and 0.97 respectively). Overall, use of the HOG representation produced the average best results with respect

to the all the metrics considered.

Considering the three statistical representations (FOR, VCM and VRLM), they produced a similar performance to each other. With respect to the FOR representation, it is interesting to note that when a higher level of decomposition was used a better performance was obtained. The AUC with respect to FOR representation when $L = 3$ was 0.83 while for $L = 6$ the AUC was 0.92. It was conjectured that this was because FOR can produce a better performance with smaller regions than with larger regions.

With respect to the histogram based representation techniques (HOG, LBP, HOG-LBP and LPQ) the best performing method as already noted above was HOG. The lowest recorded AUC using the HOG representation was 0.96 while the lowest recorded AUC for LBP, HOG-LBP and LPQ were 0.8, 0.84, and 0.73 respectively. When comparing the LBP and HOG-LBP results, HOG-LBP produced better average results where the average AUC for HOG-LBP is 0.85 while the average AUC for LBP is 0.82. It was conjectured that this was because of the positive effect of combing the HOG and LBP representations. With respect to the LPQ representation, the recorded performance was worse than that for the LBP and HOG-LBP representation. It was conjectured that this was because LPQ generated less effective histograms when a higher level of decomposition is used than in the case of LBP and HOG-LBP. The AUC for LPQ with $L = 3$ was 0.94 while with $L = 6$ it was 0.75. This is because LPQ is based on the Fourier Transform which is a more effective representation when larger regions are used, but the effectiveness is decreased when smaller regions are used. However, when using the HOG representation the changes in the intensity values of the regions (sub-volumes) in different directions are considered. The HOG representation improved the discriminative power when applied to homogeneous and small regions as in the case of the proposed decomposition. The reason is that the HOG representation uses the gradient (change) in the intensity value even when the region is small; while other representation techniques, such LPQ which relies on the frequency of the neighbours, tend to work better with larger regions.

6.3.2 Region Representations Significance Testing

The objective of this subsection is to consider whether the result presented above, that HOG representation is the most effective, is indeed statistically significant. ANOVA was conducted using seven groups, where each group represents the AUC results for a specific region representation. The results from the ANOVA, as shown in Table 6.8, demonstrated that there was a statistical difference in the effectiveness of the seven representations (from Table 6.8 it can be seen that the p-value was 3.4274e-119 which is less than 0.05). From the table, it can also be seen that the difference between the groups and within the groups were very similar (Between-Groups$_{SS}$ = 2.5 and Error$_{SS}$ = 2.2).

Table 6.7: Classifier performance results using overlapping decomposition, an ED critical function, dimensionality reduction using PCA and SVM classification in the context of region representation methods (Stage 2) using: (i)) a range of decomposition levels (L), (ii) the seven region-based representation techniques.

Method	L	Acc	Sen	Spec	PPV	NPV	EER	AUC
FOR	3	82.86%	81.43%	84.29%	83.82%	81.94%	0.16	0.83
	4	84.29%	83.82%	84.72%	83.82%	84.72%	0.16	0.84
	5	95.00%	94.20%	95.77%	95.59%	94.44%	0.04	0.95
	6	92.14%	92.54%	91.78%	91.18%	93.06%	0.09	0.92
	Ave.	88.57%	87.99%	89.14%	88.60%	88.54%	0.11	0.88
VCM	3	87.86%	86.96%	88.73%	88.24%	87.50%	0.12	0.88
	4	90.00%	89.71%	90.28%	89.71%	90.28%	0.10	0.9
	5	85.71%	84.29%	87.14%	86.76%	84.72%	0.14	0.86
	6	85.71%	84.29%	87.14%	86.76%	84.72%	0.14	0.86
	Ave.	87.32%	86.31%	83.32%	87.84%	86.80%	0.12	0.87
VRLM	3	85.71%	86.36%	85.14%	83.82%	87.50%	0.16	0.86
	4	84.29%	84.85%	83.78%	82.35%	86.11%	0.17	0.84
	5	85.71%	86.36%	85.14%	83.82%	87.50%	0.16	0.86
	6	85.71%	86.36%	85.14%	83.82%	87.50%	0.16	0.86
	Ave.	85.35%	85.98%	84.80%	83.45%	87.15%	0.16	0.85
HOG	3	97.86%	98.51%	97.26%	97.06%	98.61%	0.03	0.98
	4	96.43%	97.01%	95.89%	95.59%	97.22%	0.04	0.96
	5	95.71%	95.59%	95.83%	95.59%	95.83%	0.04	0.96
	6	95.71%	96.97%	94.59%	94.12%	97.22%	0.06	0.96
	Ave.	**96.42%**	**97.02%**	**95.89%**	**95.59%**	**97.22%**	**0.04**	**0.96**
LBP	3	86.43%	83.56%	89.55%	89.71%	83.33%	0.11	0.87
	4	82.86%	80.56%	85.29%	85.29%	80.56%	0.15	0.83
	5	80.00%	77.03%	83.33%	83.82%	76.39%	0.17	0.8
	6	80.00%	77.03%	83.33%	83.82%	76.39%	0.17	0.8
	Ave.	82.32%	79.54%	85.37%	85.66%	79.16%	0.15	0.82
HOG-LBP	3	87.86%	94.74%	83.13%	79.41%	95.83%	0.18	0.88
	4	84.29%	91.07%	79.76%	75.00%	93.06%	0.21	0.84
	5	85.00%	91.23%	80.72%	76.47%	93.06%	0.20	0.85
	6	85.00%	91.23%	80.72%	76.47%	93.06%	0.20	0.85
	Ave.	85.53%	92.06%	81.08%	76.83%	93.75%	0.19	0.85
LPQ	3	94.29%	94.12%	94.44%	94.12%	94.44%	0.06	0.94
	4	72.86%	66.67%	84.00%	88.24%	58.33%	0.17	0.73
	5	75.00%	68.97%	84.91%	88.24%	62.50%	0.16	0.75
	6	75.00%	68.97%	84.91%	88.24%	62.50%	0.16	0.75
	Ave.	79.28%	74.60%	87.06%	89.71%	69.44%	0.13	0.79

Figure 6.4(a) shows the significant differences and confidence intervals between the region-based representation methods. From the figure, it can be seen that the operation of three of the methods was not statistically different from each other: LBP-HOG, VCM and VRLM - but they are different from the rest of the representation methods. A statistical difference in operation can be noted between FOR, LPQ, LBP and HOG. The results from the confidence interval diagram (Figure 6.4(b)) indicate that the LPQ results had the lowest median AUC value (0.7), while the HOG representation produced the highest median AUC value (0.9). From Figure 6.4(b), it can be seen that the HOG representation has the narrowest confidence interval, which is indicative of the effectiveness of the representation. Overall, the statistical significance result confirms the results presented in the previous subsection that the HOG representation is the most appropriate with respect to the proposed 3D image classification based on spatial decomposition and region-based representation.

Table 6.8: Comparison of region-based representation methods.

Source	SS	df	MS	F	p-value
Between-Groups	2.5743	6	0.4290	140.7131	3.4274e-119
Error	2.2837	749	0.0030		
Total	4.8580	755			

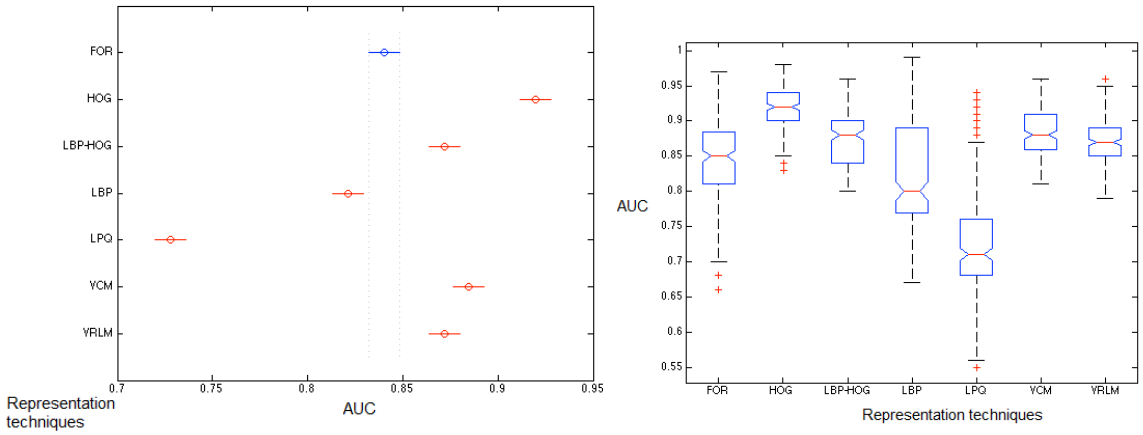

(a) Significance differences

(b) Confidence intervals

Figure 6.4: Significance differences and Confidence intervals for comparing representation techniques.

6.4 Single Feature Vector Generation (Stage Three)

In this section, the results obtained using the proposed process with respect to the single feature vector generation methods are considered. Recall that two methods were

considered: (i) a dimensionality reduction based technique using Principal Component Analysis (PCA) and (ii) a feature selection based technique using the Improved Fisher Kernel (IFK). For the evaluation, four levels of decomposition were again considered, $L = 3$, $L = 4$, $L = 5$ and $L = 6$, together with the LCS critical function, overlapping decomposition and the HOG representation technique because the experiments presented in the previous section (and others not specifically reported in this thesis) indicated that these produced "best" results. With respect to the classification stage, SVM classification was again adapted. As before, two sets of experiments were conducted: (i) classifier performance (described in Subsection 6.4.1) and (ii) significance testing (described in Subsection 6.4.2). Recall (Subsection 5.4.2) that the IFK feature selection technique required the dictionary size K to be pre-specified. The experiments conducted to evaluate the use of IFK therefore used a range of K values ($\{32, 64, 128, 256, 512\}$). The objectives of the comparison were as follows:

1. To determine which feature selection technique, PCA or IFK, served to produce the best classification performance.

2. In the context of the IFK feature selection technique, to determine the effect of using different dictionary sizes (defined by the parameter K).

6.4.1 Classifier Performance in the Context of Single Feature Vector Generation

In this section, we compare between the performance of PCA and IFK in terms of classification effectiveness. In addition, we compare classification performance with respect to different dictionary sizes K when using IFK.

Table 6.9 presents the comparison between the results using PCA and IFK ($K = 32$). From the table, it can be seen that the best classification results when using IFK were accuracy of 99.29% and AUC of 0.99, while the best accuracy for PCA was 97.14% and the best AUC value was 0.97. Overall, IFK produced the best average results with respect to all the metrics considered. It is conjectured that this was because the IFK-based technique selects feature vectors to be included in the single feature vector by considering the entire collection of feature vectors for the entire collection of images, while PCA considers each image individually. The results of all experiments using IFK are presented in Appendix A.3.

Considering the most appropriate dictionary size (K) with respect to the IFK single feature vector generation method, the results obtained are presented in Table 6.10. In the table, for the evaluation the following techniques were used: (i) overlapping decomposition, (ii) a range of decomposition levels, (iii) the LCS critical function, (iv) the HOG region-based representation and (v) SVM classification. From the table, it can be seen that all the dictionary sizes produced good performance results. The average

Table 6.9: Classifier performance results using overlapping decomposition, a LCS critical function, the HOG region-based representation and) SVM classification in the context of single feature vector generation (Stage 3) using: (i) a range of decomposition levels (L), (ii) PCA and IFK (with $K = 32$) feature selection.

Method	L	Acc	Sen	Spec	PPV	NPV	EER	AUC
PCA	3	95.71%	95.59%	95.83%	95.59%	95.83%	0.04	0.96
	4	97.14%	98.48%	95.95%	95.59%	98.61%	0.04	0.97
	5	95.71%	98.44%	93.42%	92.65%	98.61%	0.07	0.96
	6	95.00%	98.41%	92.21%	91.18%	98.61%	0.08	0.95
	Ave.	95.89%	97.73%	94.35%	93.75%	97.91%	0.05	0.96
IFK	3	95.71%	98.44%	93.42%	92.65%	98.61%	0.07	0.96
	4	97.86%	98.51%	97.26%	97.06%	98.61%	0.03	0.98
	5	97.14%	98.48%	95.95%	95.59%	98.61%	0.04	0.97
	6	99.29%	98.55%	100.00%	100.00%	98.61%	0.00	0.99
	Ave.	**97.5%**	**98.49%**	**96.65%**	**96.32%**	**98.61%**	**0.03**	**0.97**

results for the dictionary size of $K = 128$ were the best with accuracy of 98.57% and AUC of 0.98. From the table, it can be seen that $K = 128$ produced the best average results with respect to all the evaluation metrics considered. From the table, it can also be seen that there was a relationships between the dictionary size and the level of decomposition. For example, the most effective results are generated for small dictionary sizes such as $K = 32, 64$ with higher levels of decomposition such as $L = 5, 6$. This is because when a larger K is used the IFK will required more feature vectors; a higher level of L will ensure that there is a large selection to choose from.

Table 6.10: Classifier performance results using overlapping decomposition, a LCS critical function, the HOG region-based representation and (v) SVM classification in the context of the IFK single feature generation method with (i) a range of dictionary sizes and (ii) a range of decomposition levels.

k	L	Acc	Sen	Spec	PPV	NPV	EER	AUC
32	3	95.71%	98.44%	93.42%	92.65%	98.61%	0.07	0.96
	4	97.86%	98.51%	97.26%	97.06%	98.61%	0.03	0.98
	5	97.14%	98.48%	95.95%	95.59%	98.61%	0.04	0.97
	6	99.29%	98.55%	100.00%	100.00%	98.61%	0.00	0.99
	Ave.	97.5%	98.49%	96.65%	96.41%	98.61%	0.035	0.97
64	3	97.86%	98.51%	97.26%	97.06%	98.61%	0.03	0.98
	4	97.86%	98.51%	97.26%	97.06%	98.61%	0.03	0.98
	5	99.29%	100.00%	98.63%	98.53%	100.00%	0.01	0.99
	6	97.86%	97.10%	98.59%	98.53%	97.22%	0.01	0.98
	Ave.	98.21%	98.53%	97.93%	97.79%	98.61%	0.02	0.98
128	3	99.29%	100.00%	98.63%	98.53%	100.00%	0.01	0.99
	4	99.29%	100.00%	98.63%	98.53%	100.00%	0.01	0.99
	5	97.86%	100.00%	96.00%	95.59%	100.00%	0.04	0.98
	6	97.86%	95.77%	100.00%	100.00%	95.83%	0.00	0.98
	Ave.	**98.57%**	**98.94%**	**98.31%**	**98.16%**	**98.95%**	**0.01**	**0.98**

256	3	95.71%	96.97%	94.59%	94.12%	97.22%	0.06	0.96
	4	97.86%	97.10%	98.59%	98.53%	97.22%	0.01	0.98
	5	95.71%	94.29%	97.14%	97.06%	94.44%	0.03	0.96
	6	99.29%	100.00%	98.63%	98.53%	100.00%	0.01	0.99
	Ave.	97.14%	97.09%	97.23%	97.06%	97.22%	0.02	0.97
512	3	95.00%	96.92%	93.33%	92.65%	97.22%	0.07	0.95
	4	100.00%	100.00%	100.00%	100.00%	100.00%	0.00	1.00
	5	98.57%	97.14%	100.00%	100.00%	97.22%	0.00	0.99
	6	97.14%	100.00%	94.74%	94.12%	100.00%	0.06	0.97
	Ave.	97.67%	98.51%	97.01%	96.69%	98.61%	0.03	0.97

6.4.2 Single Feature Vector Generation Significance Testing

The results presented in Subsection 6.4.1 above using PCA and IFK single feature vector generation suggest that there is a significant difference, in terms of classification effectiveness, between the two techniques. In this section, the results from an ANOVA for comparing the two techniques are presented to demonstrate whether there was indeed a statistically significant difference between the two techniques or not. In addition, a second ANOVA is presented compare between the effect of using different IFK dictionary sizes with respect to classification performance in the context of AUC.

With respect to the comparison of PCA and IFK (with $K = 32$) Table 6.11 sows the ANOVA result. From the table, it can be seen that the ANOVA confirms that there is indeed a statistical difference between the operation of the PCA and IFK single feature vector generation methods in terms of classifier performance ($p-value = 2.106e-211$). Figure 6.5 shows the confidence interval diagram comparing the results of PCA and IFK, from which it can be clearly seen that the operation of the IFK techniques is statistically better than the operation of the PCA technique. As noted above, it is conjectured that this is because IFK generates the feature vector for each image with respect to the entire images collection, whilst the PCA methods consider the set of regions for each image individually.

Table 6.11: Comparing IFK and PCA-based methods.

Source	SS	df	MS	F	p-value
Between-Groups	4.73	1	4.73	1255.37	2.106e-211
Error	7.14	1894	0.00377		
Total	11.87	1895			

With respect to experiments conducted to identify the most appropriate dictionary size (K), the ANOVA result is presented in Table 6.12. From the table, it can be seen that the difference in operation resulting from using different dictionary sizes is not statistically significant ($p - value = 0.7106 > 0.05$). From the table, it can also be noted that the difference between the groups, where each group represents the results

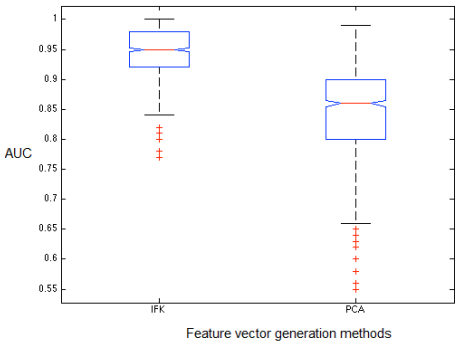

Figure 6.5: Confidence intervals for comparing single feature vector generation techniques.

using a particular dictionary size K, is very small (Between-Groups$_{SS} = 0.0030$) while the difference within each group is slightly higher with Error$_{SS} = 1.2460$. From Figure 6.6, it can be seen that there were no major differences between the confidence intervals associated with the different dictionary sizes where all the medians of the results are above 0.9 of AUC. It seems that $K = 128$ was slightly better than the rest because it has a shorter interval and all the result range above 0.86.

Table 6.12: Comparing different dictionary size K in IFK.

Source	SS	df	MS	F	p-value
Between-Groups	0.0030	4	7.4372e-04	0.5342	0.7106
Error	1.2460	895	0.0014		
Total	1.2490	895			

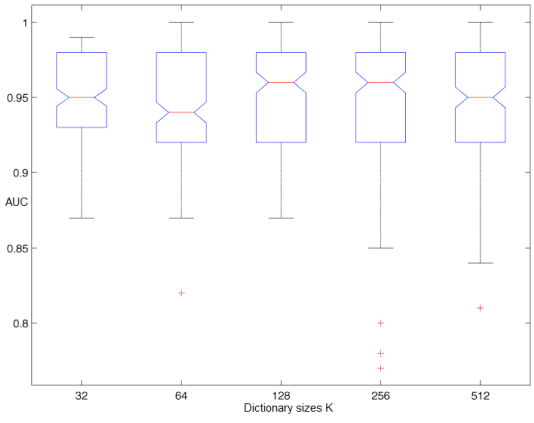

Figure 6.6: Confidence intervals for comparing different dictionary sizes K when using IFK single feature vector generation.

6.5 Stage Four Evaluation: Classifier Generation

In this section, the results obtained from the evaluation conducted to compare the operation of the proposed process using different classification methods are presented. Recall that three classifier generators were considered: (i) SVM, (ii) KNN and (iii) BN. For KNN $K = 1$ was used. The objective of the evaluation was to determine which is the best classifier generator in the context of the proposed methods for 3D classification using hierarchical spatial decomposition. As before, two sets of experiments were conducted: (i) classifier performance evaluation (Subsection 6.5.1) and (ii) statistical significance testing (Subsection 6.5.2). For the performance evaluation, four levels of decomposition were again considered, $L = 3$, $L = 4$, $L = 5$ and $L = 6$, together with the KLD critical function, overlapping decomposition, the HOG region representation method and IFK feature selection (with $K = 32$) because the above reported experiments indicated that these were the most appropriate techniques with respect to each of the previous classification stages. For the significance testing, all the results obtained using each classifier were used.

6.5.1 Classifier Performance in the Context of Classifier Generation

Table 6.13 shows the classification results obtained using each classifier generation method and the four different values for L considered in order to show a range of results for each classifier. From the table, it can be seen that, in general, the classification results obtained using SVM and BN were better than those obtained using KNN. From the table, it can also be seen that best average results were obtained using SVM classifier generation with respect to all the evaluation measure considered (best recorded AUC of 0.99).

6.5.2 Classifier Generation Significance Testing

This subsection presents the results obtained from the statistical significance testing with respect to the classifier generation results presented above. Three groups are identified, one for each of the classifier generators considered. Table 6.14 shows the ANOVA results obtained. From the table, it can be seen that the calculated p-value was 5.7819e-06, indicating that there is a statistical significance between the operation of the classifiers. There was a small difference between the results as indicated by the Between-Groups$_{SS}$ value which equates to 0.1552. The significance difference and confidence interval diagrams given in Figures 6.7(a) and 6.7(b) indicate that there was a statistically significant difference in operation between the BN and KNN classifiers, and between the SVM and KNN classifiers. There was no statistically significant difference in operation between the SVM and BN classifiers. From Figure 6.7(b), it can be seen that when using the SVM classifier the highest median and data range was recorded,

Table 6.13: Classification results using a LCS critical functions, the HOG region-based representation, IFK feature selection (with $K = 32$) in the context of classifier generation (Stage 4) using: (i) a range of decomposition levels (L), (ii) three classifier generators (SVM, NB and KNN).

CF	L	Acc	Sen	Spec	PPV	NPV	EER	AUC
SVM	3	97.86%	97.10%	98.59%	98.53%	97.22%	0.01	0.98
	4	99.29%	100.00%	98.63%	98.53%	100.00%	0.01	0.99
	5	98.57%	100.00%	97.30%	97.06%	100.00%	0.03	0.99
	6	98.57%	100.00%	97.30%	97.06%	100.00%	0.03	0.99
	Ave.	**98.57%**	**99.27%**	**97.95%**	**97.79%**	**99.3%**	**0.02**	**0.98**
KNN	3	94.29%	95.45%	93.24%	92.65%	95.83%	0.04	0.96
	4	98.21%	100.00%	96.64%	96.32%	100.00%	0.03	0.99
	5	97.86%	100.00%	96.00%	95.59%	100.00%	0.04	0.98
	6	95.36%	99.20%	92.26%	91.18%	99.31%	0.08	0.97
	Ave.	96.43%	98.66%	94.53%	93.93%	98.78%	0.04	0.97
BN	3	94.05%	95.43%	92.83%	92.16%	95.83%	0.04	0.97
	4	98.57%	100.00%	97.30%	97.06%	100.00%	0.00	0.99
	5	98.10%	100.00%	96.43%	96.08%	100.00%	0.04	0.99
	6	96.43%	99.48%	93.89%	93.14%	99.54%	0.06	0.98
	Ave.	96.78%	98.72%	95.11%	94.61%	98.84%	0.03	**0.98**

while when using the KNN classifier the lowest median was recorded. The BN classifier had the smallest confidence interval and data range associated with it.

Table 6.14: Comparing classifiers.

Source	SS	df	MS	F	p-value
Between-Groups	0.1552	2	0.0776	12.1246	5.7819e-06
Error	14.6545	2289	0.0064		
Total	14.8098	2291			

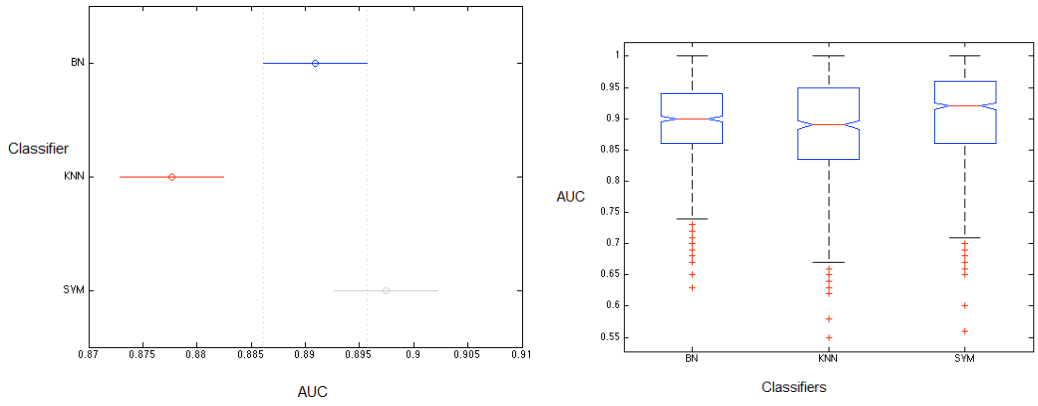

(a) Significance differences

(b) Confidence intervals

Figure 6.7: Significance differences and confidence intervals for comparing classifiers.

6.6 Summary and Conclusions

This chapter has reported on the evaluation of the proposed region-based volumetric representations in terms of classification effectiveness using the AMD data sets introduced earlier. The process involved four stages each with a number of potential techniques associated with it. The evaluation was therefore conducted by considering the techniques available at each stage in isolation with a fixed set of techniques for the remaining stages.

According to the results provided in this chapter, the main findings can be summarised as follows:

1. Regional homogeneity (measured using a critical function) in the decomposition process plays an important role in image classification. The classification results with respect to methods using the five critical functions identified, namely AIV, ED, KCC, KLD and LCS, outperformed the results obtained when no critical function (0NCF) was used. The best critical functions were LCS and ED.

2. Overlapping decomposition was more effective than the standard decomposition.

3. The results produced using the HOG region-based image representation were statistically the best among the seven different representations considered.

4. In terms of single feature vector generation methods, feature selection using IFK with $K = 128$ outperformed the PCA dimensionality reduction based method.

5. Use of the BN and SVM classifier generators produced results that were better than the results produced using KNN classification.

Table 6.15 summarises the best four combinations of techniques in terms of AUC (arguably the best overall measure). For reference later in this thesis, the techniques have been labelled as follows: (i) RB_1, (ii) RB_2 (iii) RB_3 (iv) RB_4.

For completeness, Table 6.16 summarises the classification results obtained with respect to the best four combinations of techniques presented in Table 6.15. From the tables, it can be seen that the best results in terms of accuracy reached 99.29% with respect to RB_1 and in terms of AUC reached 0.99 with respect to RB_1 and RB_2.

The following chapter considers and evaluates the proposed whole image-based representations using the concept of hierarchical spatial decomposition.

Table 6.15: Best four performing combinations of techniques as identified in the foregoing evaluation.

Identifier	Image Decomposition	Region Representation	Feature Selection	Classification
RB_1	overlapping decomposition, L=5, ED critical function	HOG representation	IFK with $K = 128$	SVM classifier
RB_2	overlapping decomposition, L=5, ED critical function	HOG representation	IFK with $K = 128$	BN classifier
RB_3	overlapping decomposition, L=5, LCS critical function	HOG representation	IFK with $K = 128$	SVM classifier
RB_4	overlapping decomposition, L=5, LCS critical function	HOG representation	IFK with $K = 128$	BN classifier

Table 6.16: Summary of evaluation results obtained using the four best techniques identified in Table 6.15

Label	Acc	Sen	Spec	PPV	NPV	EER	AUC
RB_1	99.29%	98.55%	100.00%	100.00%	98.61%	0.00	0.99
RB_2	98.57%	99.01%	98.17%	98.04%	99.07%	0.02	0.99
RB_3	97.86%	100.00%	96.00%	95.59%	100.00%	0.04	0.98
RB_4	97.62%	99.49%	95.98%	95.59%	99.54%	0.04	0.98

Chapter 7

Classification Based on Decomposition and Whole Image-Based Representation

7.1 Overview

This chapter discusses the proposed procedure for building 3D (volumetric) image classifiers using Whole Image-Based (WIB) representation methods, as opposed to the region based methods described in Chapter 5. Note that the distinction between the RB and the WIB methods is that using the RB methods each region was represented individually while WIB the all the regions are considered. Recall that the decomposition results in a hierarchy, which for practical purposes is best encapsulated in the form of some kind of tree structure. In the case of the work described in this thesis, hybrid quad/oct-trees and non-trees were used, quad/oct-tress when using a standard decomposition and non-trees when using an overlapping decomposition. Recall that non-trees were introduced as a potential solution to the boundary problem often encountered as a result of decomposition (see Section 4.4). Broadly, the idea behind the work presented in this chapter is to apply frequent sub-graph mining techniques to a set of trees representing images so as to identify a set of frequently occurring sub-graphs that in turn can be used to define a feature space from which feature vectors can be generated (one per input image) which can then be input to a classifier generator.

A schematic of the entire process is presented in Figure 7.1. From the figure, it can be seen that the process comprises five stages: (i) image decomposition, (ii) tree conceptualisation, (iii) frequent sub-graph mining, (iv) feature vector generation and (v) classifier generation. The image decomposition element was previously described in Chapter 4. This work is inspired by [59] where Frequent Sub-graph Mining (FSM) is applied (Stage 3) to the tree representing the image set so as to identify frequently occurring sub-graphs. The identified set of frequent sub-graphs is then used (Stage 4) to define a feature space from which a set of binary-valued feature vectors (one

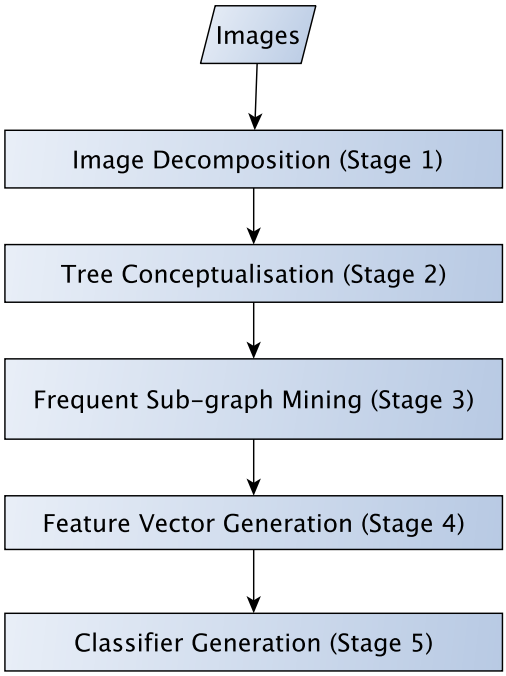

Figure 7.1: Schematic illustrating the whole image-based representation approach to image classification.

per volume) is drawn. The identified set of feature vectors is then used to generate a classifier (Stage 5).

The rest of this chapter is organised as follows. First the adapted tree conceptualisation is presented in Section 7.2. Section 7.3 describes the frequent sub-graph mining process and Section 7.4 the feature vector generation process. Classifier generation is briefly discussed in Section 7.5. The evaluation of the proposed WIB technique is then presented in Section 7.6. Section 7.7 discuses the reported results and presents a summary of the work described in this chapter.

7.2 Tree Conceptualisation (Stage Two)

Decomposition techniques tend to operate in a top-down manner (either breadth first or depth first) and thus lend themselves to tree storage structures, quad trees in the case of 2D data and oct-trees in the case of volumetric data. In the case of the overlapping decomposition, the boundary region is included as presented in Section 4.4 leading to nine regions (hence a non-tree). In the context of the region based representation techniques, the nature of this tree conceptualisation was not of significance; it was the regions identified by the nodes in the tree that were of importance. In the case of the WIB representation techniques considered in this chapter, the structure of the tree is of significance as is the nature of the node and edge labelling. More formally, a tree

T is a 4-tuple $T = (N, E, nl, el)$, where N is the set of nodes (representing regions), $E \subseteq N \times N$ is the set of edges, nl is the set of node labels, and el is the set of edge labels. The node label is a single value representing each node (region). The edge label is typically a mapping between the parent and child node. In the generated tree, every newly generated node is connected to an existing parent node with an edge having a label that indicates the relationship between the parent node and the child node. The edge labels are also single values. On completion, each node in the tree will describe a region in terms of a node label.

Algorithm 7.1 describes the process of adding node and edge labels to trees, generated as part of a decomposition, so that Frequent Sub-graph Mining (FSM) can be applied. The input for the algorithm is a decomposed image (represented as a tree) generated using Algorithm 4.1 previously presented in Section 4.2. The notation $n.nodeLabel$ is used to indicate the node label belonging to node n, n_i to indicate the ith child node from node n, and $n.edgeLabel_i$ to indicate the edge label for the edge connecting a current node to a child node n_i. The functions *nodeLabel* (line 6) and *edgeLabel* (line 9) are used to generate node and edge labels as appropriate; these functions are discussed further in Subsections 7.2.1 and 7.2.2 below. Of course, this process could have been integrated with the decomposition process, but the labelling is not required in the case of the region based representations.

Algorithm 7.1 Pseudocode for the tree labelling.

Input: An image decomposed into a tree t
Output: The labelled tree G_i

```
1:  max = Number of regions (Children) per node.
2:  Start
3:      treeLabelling(t)
4:  End
5:  Function treeLabelling(n)
6:  n.nodeLabel ← nodeLabel(n)
7:  if n has child nodes  then
8:    for i = 1 to max do
9:      n.edgeLabel_i ← edgeLabel(i)
10:     treeLabelling(n_i)
11:   end for
12: end if
13: End Function
```

7.2.1 Node Labels

We refer to the different types of values that may be associated with a node as *node features*. The node features are used to form node labels. The selection of appropriate node features plays an important role in the context of the effectiveness of whole image tree representations. In the Average Intensity Values (AIVs), the mean of the intensity

values of the pixels (voxels) making up the region represented by a tree node, were used to label the nodes. This is probably the simplest way of assigning labels to nodes. However, it is conjectured here that such mean values for regions do not provide a sufficient description of content. Instead, for the work described in this thesis, the *Kurtosis* of each region is used as the node label. Kurtosis measures the "peakedness" of a distribution (an intensity histogram in our case). In other words, Kurtosis describes the shape of a distribution [79]. In this case, Kurtosis represents the distribution of the histogram of the region. Kurtosis is calculated as follows (Equation 7.1):

$$Kurtosis = \frac{\frac{1}{n}\sum_{i=1}^{n}(h_i - \overline{h})^4}{(\frac{1}{n}\sum_{i=1}^{n}(h_i - \overline{h})^2)^2} \tag{7.1}$$

where h is the histogram vector associated with the region/volume represented by a given node, $\overline{h}$ is the mean of h and n is the number of bins in h.

Later on in this chapter we compare between both these node labelling techniques. However, in order to not confuse AIV node labelling with the critical function of the same name, for the rest of this thesis the term "mean" node labelling will be used to indicate AIV node labelling.

7.2.2 Edge Labels

Using tree-based image representations, the edge features used are typically defined in terms of some node feature similarity measure describing the similarity between a parent-child node coupling. Edge features are essential for the envisioned volumetric tree classification as they are used, together with the node labels, for distinguishing between sub-graphs (sub-trees). With respect to the work described in this thesis, edge labels are defined in terms of the Kullback-Leibler Divergence (KLD) [68] between parent node pairs. The concept of KLD was introduced in Section 4.3 in terms of histogram based critical functions. KLD is a measure of the similarity between the parent and the child node intensity histograms for the regions/volumes they represent. Essentially, KLD measures the divergence between the two histograms. Thus KLD was used to generate edge labels in a similar manner to that with which it was used to determine the intensity homogeneity between parent-child node pairs during the decomposition process (as described in Section 4.3). Recall that Equations 4.4 to 4.3, presented in Section 4.3, demonstrated how the KLD measure is generated. Alternatives to using KLD include ED, DTW and LCS as also introduced in Section 4.3. These were not selected because the KLD measure indicates the likelihood ratio between two distributions (in our case histograms of nodes) and if two distributions are identical then the KLD value is zero while the other techniques compute the average difference between each histogram value (bin).

7.3 Frequent Sub-graph Mining (Stage Three)

After trees of the form described in the foregoing section have been generated, one tree per image, the next stage is to generate the feature vector representation so that the salient features of the tree collection are preserved. In this case, the salient features of interest are deemed to be frequently occurring sub-graphs; sub-graphs that represent common structures that occur across the tree represented data set as a whole. A sub-graph is deemed to be "frequent" if its occurrence count is greater than some threshold value σ. The occurrence count for a sub-graph is the number of trees in the input data in which the sub-graph occurs (one count per tree in the input data). The value for σ is thus expressed in terms of a proportion of the total number of trees considered. Usually σ is set to a low value so as to ensure that nothing is missed; however the consequence of this is that many frequent sub-graphs may be identified (hence some form of feature selection may need to be applied).

From the literature, the advocated method for identifying frequently occurring sub-graphs in a collection of trees is to apply a Frequent Sub-graph Mining (FSM) algorithm. With respect to the work described in this thesis, the well-known frequent sub-graph mining the graph-based Substructure pattern mining (gSpan) [148] algorithm was employed, although alternative FSM algorithms could equally well have been used. Formally:

Definition Given two trees $T' = (N', E', nl', el')$ and $T = (N, E, nl, el)$, T' is a sub-graph of T ($T' \subseteq T$) if $N' \subseteq N$, $E' \subseteq E$, $nl' \subseteq nl$ and $el' \subseteq el$.

7.4 Feature Vector Generation (Stage Four)

Having identified a set of frequently occurring sub-graphs, the sub-graphs were then used to define a feature space where each identified sub-graph represents a dimension within that space and each dimension can have the values 0 or 1 (exists or does not exist). However, using algorithms such as gSpan, as noted above, many frequent sub-graphs may be identified (especially if a low σ value is used), which in turn may hinder both efficiency and effectiveness. To reduce the number of features included in the feature space representation, some form of feature selection can be applied.

With respect to the work described in this thesis, feature selection was conducted by allocating a *gain* value to each sub-graph s. Gain is essentially a measure of the discriminative power of individual features (an important concept in the context of classification) and is calculated as shown in Equation 7.3 [78, 97, 117], where n is the total number of training images, $c_i \in \{-1, 1\}$ is the class label of the image and $M(s, g_n)$ is a function to match a sub-graph s to the graph g_n generated for the image i_n. Each sub-graph gain $g(s)$ is computed and if the gain is less than a threshold α then the

sub-graph is ignored.

$$Match(sg, t_n) = \begin{cases} 1, & if \quad sg \subseteq t_n \\ -1, & otherwise \end{cases} \tag{7.2}$$

$$gain(sg) = \sum_{i=1}^{n} c_i Match(sg, t_i) \tag{7.3}$$

Algorithm 7.2 Pseudocode for the proposed feature vector generation for the whole image-based methods

Input: A set of Trees T, Set of class label C, Set of Sub-Graphs SG, gainThreshold

Output: FV

```
1: M = |SG| × |T|
2: for each i = 1 to |T| do
3:    for each l = 1 to |SG| do
4:       M_{l,i} ← Match(sg_l, t_i)
5:    end for
6: end for
7: g = vector of size |T|
8: for each l = 1 to |SG| do
9:    for each i = 1 to |T| do
10:      g(i) = c_i × M_{l,i}
11:   end for
12:   gain(l) = Σ_{i=1}^{|T|} g(i)
13:   if gain(l) > gainThreshold then
14:      IncludedSubgraphs ← sg_l
15:   end if
16: end for
17: for each i = 1 to |T| do
18:   for each l = 1 to |IncludedSubgraphs| do
19:      if Match(IncludedSubgraphs_l, t_i) then
20:         FV(i, l) ← 1
21:      else
22:         FV(i, l) ← 0
23:      end if
24:   end for
25: end for
```

Algorithm 7.2 describes the process used to generate a feature vector for each image. The input to the algorithm is: (i) a set of trees T (one tree per image), (ii) the set of classes $C \in \{-1, 1\}$, (iii) a set of identified frequent sub-graphs SG (identified using the gSpan algorithm in the case of the work presented in this thesis) and (iv) a gain threshold. A matrix M is then built with rows I representing the number of individual trees (images) and columns L representing the identified frequent sub-graphs (lines 2 to 6). Note that a matrix intersection is indicated using the notation $M_{i,j}$. The function

Match (line 4) is used to determine if the sub-graph sg is in the given tree t_n. The match function is defined in Equation 7.2. The output of the match function is fed into the matrix M. A vector g is then built with the same size as $|T|$, the size of the set of columns (lines 9 to 11). The vector g holds the multiplication of the class label, $c_i \in C$, (-1 or +1), by the corresponding matched graph $M_{i,j}$ for each sub-graph j, where i is the ith tree and j is the jth sub-graph. Then we calculate the gain as in Equation 7.3 for each sub-graph (from line 12) by summing the value of the vector g. If the gain for a sub-graph is greater than a given threshold (line 13) then the sub-graph is included in the set of sub-graphs. Finally, the feature vector FV for each image is formed. If the included sub-graph l is found in the tree of the image i then the $FV(i, l)$ holds the value 1 and otherwise the value 0 (from line 17 to line 25).

7.5 Classifier generation (Stage Five)

Once a set of feature vectors has been generated these can be used as input to a supervised learning algorithm provided that we have a known class label for each vector; in other words, we need to have a *training set*. With respect to the evaluation presented later in this thesis, the same AMD dataset as used to evaluate the region-based representation was used. Also, as in the case of the region-based methods, three classifier generation techniques were experimented with: (i) Support Vector Machine (SVM), (ii) K-Nearest Neighbours (KNN) and (iii) Bayesian Network (BN), all provided within the Weka machine learning workbench [51].

7.6 Evaluation

From the foregoing, a five-stage process for generating binary classifiers using the whole image-based representation method for application to volumetric data was described. The five stages were: (i) image decomposition, (ii) tree conceptualisation, (iii) frequent sub-graph mining, (iv) feature vector generation (one per image) and (v) classifier generation.

Image decomposition was discussed in Chapter 4 where it was noted that an important aspect is the use of critical functions to establish regional homogeneity. For the experimentation reported in this chapter, the five critical functions (out of the total of seven critical functions considered in this thesis) that produced the best results with respect to the region-based representation (discussed in the previous chapter, Chapter 6) were used. Recall that these were:

1. Average Intensity Value (AIV).
2. Kendall's Coefficient Concordance (KCC).
3. Euclidean Distance (ED).

4. Longest Common Subsequence (LCS).

5. Kullback-Leibler divergence (KLD).

As before, a range of levels of decomposition was considered with respect to the reported evaluation from $L = 3$ to $L = 6$, and both standard an overlapping decomposition was used.

With respect to tree representation (Stage two) two node labellings were considered in Section 7.2.1 as follows:

1. Mean (as used in [59]).

2. Kurtosis.

Recall that only one edge-labelling mechanism was proposed.

Regarding the frequent sub-graph mining (stage three), only one algorithm is used, the gSpan [148] algorithm described in Section 7.3. In the experiment, the threshold value σ for the frequent sub-graph mining as presented in Section 7.3 was set to 20%. This relatively low value was selected so as to ensure that a reasonably large number of sub-graphs were selected. In stage four, one technique is again proposed for feature vector generation with $gainThreshold = 0$ as presented in Section 7.4. This value was selected because if the gain for a graph is zero then the sub-graph is found in both class labels.

The final stage of the process (Stage 5) was classifier generation. As noted previously, there are a great many binary classifier generators that operate using a feature vector representation. Three were considered with respect to the evaluation described in this chapter (and the foregoing chapter):

1. Support Vector Machines(SVM).

2. K-Nearest Neighbour (KNN).

3. Bayesian Networks (BN).

These were selected for the same reason that they were used with respect to the experiments used to evaluate the operation of the region-based representation techniques; because: (i) they tend to produced good results with respect to other application domains and (ii) their usage is widely reported in the literature. With respect to the SVM classifier, the complexity constant was set to one and the linear polynomial kernel was used with a coefficient value of one. For the KNN classifier, the number of nearest neighbours (k) was set to one.

Given the above, the different techniques whereby whole image-based volumetric classification can be achieved can be combined in: 4 (levels of decomposition) $\times 2$ (types

of decomposition) ×5 (critical functions) ×2 (labellings) ×3 (classifiers) = 240 different manners (fewer techniques than in the case of the region-based representation methods).

As in the previous chapter, this chapter presents an evaluation of these different combinations in the context of the AMD detection application that has acted as a focus for the work described in this thesis. The objectives of the evaluation were (in the context of the relevant stage in the proposed process) as follows:

1. **Stage 1**
   (a) To determine the best critical function.
   (b) To determine whether standard or overlapping decomposition was more appropriate.
   (c) To determine which level of decomposition produced the most effective classification results.
2. **Stage 2**: To determine the most appropriate node labelling in terms of classification effectiveness.
3. **Stage 5**: To identify the most appropriate classifier to be applied (out of the three different mechanisms considered)

In the context of stage one, the option of not using a critical function was not considered because previous work with respect to region-based methods had already demonstrated that this did not work well. As before, the adapted evaluation strategy was to consider each of the above objectives in turn with respect to the applicable techniques for the stage in question, while using a constant set of techniques for the remaining stages. As in the previous chapter, two styles of evaluation were conducted: (i) classifier performance evaluation and (ii) significance testing. The individual evaluation metrics with respect to the classifier performance evaluation were again: (i) Accuracy (Acc.), (ii) Sensitivity (Sen.), (iii) Specificity (Spec.), (iv) Positive Predictive Value (PPV), (v) Negative Predictive Value (NPV), (vi) Error Equal Rate (EER) and (vii) Area Under the Curve (AUC) of the receiver operating characteristic as defined in Subsection 2.8.1. Ten-fold Cross Validation (TCV) was used throughout. ANalysis Of VAriance (ANOVA) was applied to the recorded AUC values for the statistical significance testing in the same manner as presented in the previous chapter. Some of the results that were obtained are presented in the main body of this chapter while the rest of the results can be found in Appendix B. More specifically, the evaluation results, with respect to each of the above objectives, are presented and discussed in Sections 7.6.1 to 7.6.3 below.

7.6.1 Decomposition (Stage One)

In this section, the results obtained using the proposed whole image-based representation process, with respect to the five critical functions identified above, are presented.

Recall that the objectives of the evaluation were:

1. To determine which of the five critical functions considered produced the best result.
2. To determine which is the best level of decomposition to use (a range of values were considered).
3. To determine whether standard or overlapping decomposition is more desirable.

7.6.1.1 Classifier Performance in the Context of Decomposition

Tables 7.1 and 7.2 show the results obtained using the WIB approach with respect to the decomposition and in the context of classification performance. The column labelled "L" indicates the level of decomposition. Table 7.1 gives the results obtained using standard decomposition and 7.2 the results using overlapping decomposition. For the evaluation, the following techniques were fixed with respect to the stages not considered in this section (node labelling, FSG and classification): (i) Kurtosis node labelling, (ii) gSpan using $\sigma = 20\%$ and (iii) SVM classification. As in the case of the evaluation conducted with respect to region based techniques, four levels of decomposition were considered, $\{3, 4, 5, 6\}$. In the experiment, the threshold value t with respect to the five critical functions considered was set to 0.5.

Considering the five different critical functions, from both tables it can be seen that the best result, reaching a recorded AUC value of 1.00, was obtained with respect to the LCS and KLD critical functions. Note that both LCS and KLD were proposed by the author. For the LCS critical function, the best result was obtained using $L = 5$ and $L = 6$ in the case of standard decomposition; and $L = 4$, $L = 5$ and $L = 6$ in the case of overlapping decomposition. For the KLD critical function, the best result was obtained using the overlapping decomposition with $L = 5$. LCS and KLD were more effective because they were better in terms of comparing between histograms of regions, leading to a better method in identifying homogeneous regions. In general, it can be observed that the LCS critical function was very effective in comparison to the other critical functions considered. The lowest recorded result was obtained using the KCC critical function, standard decomposition and $L = 4$ (Accuracy = 75.00%, EER = 0.29 and AUC = 0.75). The results of using the AIV critical function with average AUC of 0.87 were slightly better than KCC with 0.8 and ED with 0.86 with respect to both decomposition types. Recall that the LCS and KLD were among the critical functions proposed by the author.

Regarding the difference between the standard and the overlapping decomposition, from Tables 7.1 and 7.2 the results using overlapping decomposition produced a better performance than in the case of the standard decomposition, thus confirming the results obtained using the region-based representation presented in Chapter 6. For example,

using $L = 3$, the best AUC result using standard decomposition was 0.81 while the best result using overlapping decomposition was 0.94. The best KLD AUC result for standard decomposition was 0.90 with $L = 3$ and an average of 0.86, while for the overlapping decomposition it was 1.00 and the average was 0.97.

With respect to level of decomposition, as in the case of the region-based methods, there was not a discernible difference between the results obtained using different levels of decomposition. For example, the AUC results using $L = 3$ and $L = 5$ using standard decomposition and KLD were the same. Table 7.3 shows the number of occasions that the best AUC was recorded with respect to each level of decomposition. From the table, the best overall level was $L = 5$ (Recall that $L = 5$ also performed well with respect to region-based methods).

Table 7.1: Classifier performance results in the context of decomposition (Stage 1) using: (i) standard decomposition with decomposition threshold $t = 0.5$, (ii) a range of decomposition levels (L), (iii) a number of critical functions, (iv) Kurtosis node labelling and (v) SVM classification.

CF	L	Acc	Sen	Spec	PPV	NPV	EER	AUC
AIV	3	82.86%	83.82%	81.94%	81.43%	84.29%	0.18	0.83
	4	86.43%	85.92%	86.96%	87.14%	85.71%	0.13	0.86
	5	81.43%	78.21%	85.48%	87.14%	75.71%	0.15	0.81
	6	88.57%	87.50%	89.71%	90.00%	87.14%	0.10	0.89
	Ave.	84.82%	83.86%	86.02%	86.42%	83.21%	0.14	0.87
KCC	3	80.71%	77.92%	84.13%	85.71%	75.71%	0.16	0.81
	4	75.00%	80.70%	71.08%	65.71%	84.29%	0.29	0.75
	5	86.43%	89.23%	84.00%	82.86%	90.00%	0.16	0.86
	6	80.71%	80.28%	81.16%	81.43%	80.00%	0.19	0.81
	Ave.	80.71%	82.03%	80.09%	78.92%	82.5%	0.2	0.80
ED	3	89.29%	95.08%	84.81%	82.86%	95.71%	0.15	0.89
	4	90.71%	90.14%	91.30%	91.43%	90.00%	0.09	0.91
	5	78.57%	80.30%	77.03%	75.71%	81.43%	0.23	0.79
	6	85.71%	86.76%	84.72%	84.29%	87.14%	0.15	0.86
	Ave.	85.32%	88.07%	84.46%	83.57%	88.57%	0.15	0.86
LCS	3	90.71%	90.14%	91.30%	91.43%	90.00%	0.09	0.91
	4	98.57%	98.57%	98.57%	98.57%	98.57%	0.01	0.99
	5	100.00%	100.00%	100.00%	100.00%	100.00%	0.00	1.00
	6	100.00%	100.00%	100.00%	100.00%	100.00%	0.00	1.00
	Ave.	**97.32%**	**97.17%**	**97.46%**	**97.50%**	**97.14%**	**0.05**	**0.97**
KLD	3	90.00%	92.42%	87.84%	87.14%	92.86%	0.12	0.9
	4	83.57%	84.06%	83.10%	82.86%	84.29%	0.17	0.84
	5	83.57%	84.06%	83.10%	82.86%	84.29%	0.17	0.84
	6	85.71%	87.88%	83.78%	82.86%	88.57%	0.16	0.86
	Ave.	85.75%	87.10%	84.45%	83.93%	87.50%	0.15	0.86

Table 7.2: Classifier performance results in the context of decomposition (Stage 1) using: (i) overlapping decomposition with decomposition threshold $t = 0.5$, (ii) a range of decomposition levels (L), (iii) a number of critical functions, (iv) Kurtosis node labelling and (v) SVM classification.

CF	L	Acc	Sen	Spec	PPV	NPV	EER	AUC
AIV	3	89.29%	87.67%	91.04%	91.43%	87.14%	0.09	0.89
	4	82.86%	81.94%	83.82%	84.29%	81.43%	0.16	0.83
	5	96.43%	95.77%	97.10%	97.14%	95.71%	0.03	0.96
	6	85.00%	83.56%	86.57%	87.14%	82.86%	0.13	0.85
	Ave.	88.39%	87.23%	89.63%	90.00%	86.78%	0.10	0.90
KCC	3	83.57%	82.19%	85.07%	85.71%	81.43%	0.15	0.84
	4	82.14%	83.58%	80.82%	80.00%	84.29%	0.19	0.82
	5	85.00%	84.51%	85.51%	85.71%	84.29%	0.14	0.85
	6	83.57%	84.06%	83.10%	82.86%	84.29%	0.17	0.84
	Ave.	83.57%	83.58%	83.62%	83.57%	83.57%	0.16	0.83
ED	3	90.00%	88.89%	91.18%	91.43%	88.57%	0.09	0.9
	4	87.86%	87.32%	88.41%	88.57%	87.14%	0.12	0.88
	5	85.00%	84.51%	85.51%	85.71%	84.29%	0.14	0.85
	6	84.29%	85.29%	83.33%	82.86%	85.71%	0.17	0.84
	Ave.	86.57%	86.50%	87.17%	87.14%	86.42%	0.13	0.86
LCS	3	99.29%	100.00%	98.59%	98.57%	100.00%	0.01	0.99
	4	100.00%	100.00%	100.00%	100.00%	100.00%	0.00	1.00
	5	100.00%	100.00%	100.00%	100.00%	100.00%	0.00	1.00
	6	100.00%	100.00%	100.00%	100.00%	100.00%	0.00	1.00
	Ave.	**99.82%**	**100.00%**	**99.64%**	**99.64%**	**100.00%**	**0.00**	**0.99**
KLD	3	92.86%	92.86%	92.86%	92.86%	92.86%	0.07	0.93
	4	97.14%	97.14%	97.14%	97.14%	97.14%	0.03	0.97
	5	100.00%	100.00%	100.00%	100.00%	100.00%	0.00	1.00
	6	97.86%	98.55%	97.18%	97.14%	98.57%	0.03	0.98
	Ave.	96.96%	97.13%	96.79%	96.78%	97.13%	0.03	0.97

Table 7.3: The number of occasions when the best recorded AUC value from Tables 7.1 and 7.2 was recorded with respect to level of decomposition L and type of decomposition (standard or overlapping).

Level	Standard	Overlapping	Totals
3	1	1	2
4	$\frac{2}{6}$	1	$1\ \frac{2}{6}$
5	$3\frac{2}{6}$	$1\frac{3}{6}$	$4\frac{5}{6}$
6	$1\frac{2}{6}$	$1\frac{3}{6}$	$2\frac{5}{6}$
Totals	5	5	10

7.6.1.2 Decomposition Significance Testing

In this subsection, the reported results from the ANOVA are presented to determine whether the above results are statistically significant or not. The ANOVA table for comparing the critical functions against each other is given in Table 7.4. Note that in

the table, as in the case of Chapter 6, the rows indicate: (i) the differences between groups and (ii) within groups (Error). The column labelling is as follows: (i) SS is the sum of squares of the source, (ii) df is the degree of freedom in the source, (iii) MS is the mean square of the source, and (iv) F is the F ratio. More information about the ANOVA table was described in Section 2.8.2. The most important element of Table 7.4 to note is the p-value (6.3746e-143) which tells use if the groups are statistically significant from each other. The term "groups" in this context refers to the AUC sets of results associated with each critical functions (the AUC results for each critical function are considered to be a group).

From the results it can be seen that the difference between the SS value between groups (Between-Groups$_{SS}$ = 2.4282) and the SS value within each group (Error$_{SS}$ =1.5800) was large. From Table 7.4 it can also be seen that there is a statistical significance between the usage of the critical functions. This can more clearly be observed with respect to Figures 7.2(a) and (b), which show the significant difference and confidence interval diagrams. From Figure 7.2(a) it can be seen that the critical differences between the performances of LCS and AIV, ED, KCC and KLD is significant. The results of ED and KCC were not statistically different. This can be confirmed by reference to Figure 7.2(b) where it can be seen that LCS generated the best AUC results. Thus it can be concluded that the result presented in Subsection 7.6.1.1, where the LCS critical function produced the best performance, is statistically significant. It is interesting to note that the ED critical function, which performed well with respect to the region-based representation methods, did not performed well with respect to the whole image based methods. Recall that LCS also performed well with respect to the region-based methods (second place after ED).

Table 7.4: ANOVA data for critical function comparison

Source	SS	df	MS	F	p-value
Between-Groups	2.4282	4	0.6070	274.7054	6.3746e-143
Error	1.5800	715	0.0022		
Total	4.0082	719			

Regarding the level of decomposition, four levels of decomposition were used in the above reported experiments. ANOVA was applied to each level of decomposition AUC results. The resulting p-value of 0.1246 (>0.05) (see Table 7.5) confirmed that there was no statistically significant difference between the operation of the different levels of decomposition considered (3, 4, 5 and 6). There was a small difference between the groups, with a Between-Groups$_{SS}$= 0.0326 (Table 7.5). Figure 7.3 shows the confidence interval diagrams, where it can be seen that there was similarity between the results associated with the different levels of decomposition. From the figure, it can be seen

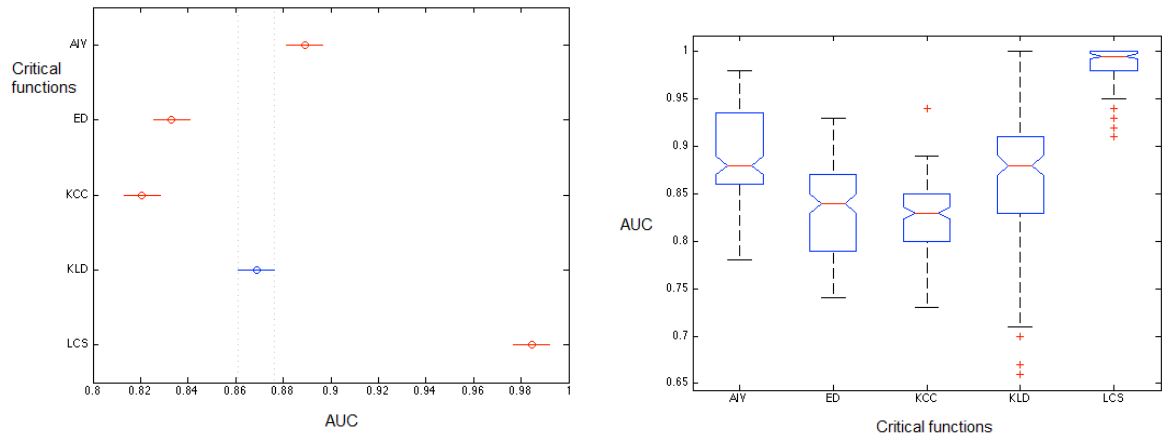

(a) Significance differences

(b) Confidence intervals

Figure 7.2: Significance difference and confidence intervals for comparing critical functions

that there was no significant difference in operation when using either $L = 4$ or $L = 5$. The fact that $L = 6$ produced a slightly better performance than $L = 3$, $L = 4$ and $L = 5$ is not statistically significant.

Table 7.5: ANOVA data for levels of decomposition comparison ($L = \{3, 4, 5, 6\}$)

Source	SS	df	MS	F	p-value
Between-Groups	0.0326	3	0.0109	1.9218	0.1246
Error	4.2466	752	0.0056		
Total	4.2791	755			

In terms of comparing the operation of standard and overlapping decomposition, Table 7.6 gives the ANOVA data, where the calculated p-value (5.7568e-26) indicates that there was a statistical difference in operation between usage of the standard and the overlapping decomposition. Figures 7.4, which shows the confidence intervals, confirms the above observation that using overlapping decomposition produced a significantly better performance than when using standard decomposition.

Table 7.6: ANOVA data for decomposition comparison (standard v. overlapping)

Source	SS	df	MS	F	p-value
Between-Groups	0.5689	1	0.5689	119.6620	5.7568e-26
Error	3.6130	760	0.0048		
Total	4.1818	761			

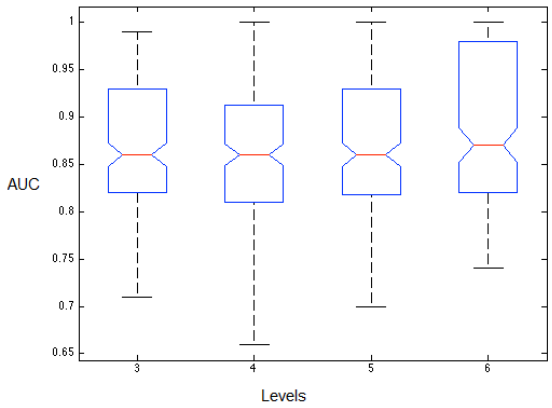

Figure 7.3: Confidence interval diagrams for comparing levels of decomposition ($L = \{3, 4, 5, 6\}$)

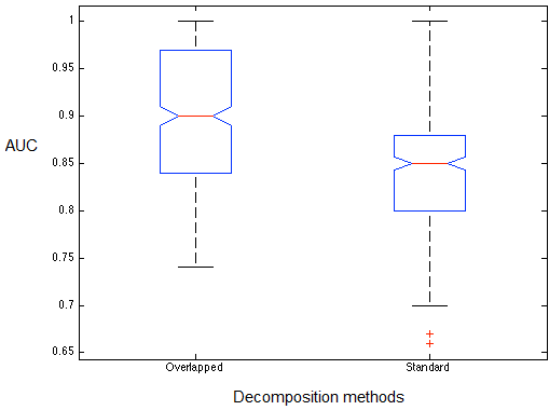

Figure 7.4: Confidence intervals diagrams for decomposition comparison (standard v. overlapping)

7.6.2 Tree Conceptualisation (Stage Two)

In this section, the evaluation results obtained with respect to the proposed node and edge labelling process are considered. Recall that the objective of the evaluation was to determine whether Kurtosis or Mean intensity value node labelling was the most appropriate in the context of classifier performance. As in the foregoing subsection, two forms of testing were conducted: (i) classifier performance testing and (ii) statistical significance testing. The following two subsections present the results associated with each. For the evaluation, the following techniques were fixed with respect to the stages not considered in this section (decomposition, FSG, feature vector generation and classification): (i) the KLD critical function with a threshold of $t = 0.5$ and standard decomposition, (ii) gSpan FSG using $\sigma = 20\%$, (iii) feature selection with $gainthreshold = 0$, and (iv) SVM classifier generation. Four different levels of decomposition ($L = \{3, 4, 5, 6\}$) were used for the experiments because it was thought that the level of decomposition might have an effect on the usage of the considered edge-labelling mechanisms. These techniques were adapted for the same reason as presented in Section 7.6.1.1.

7.6.2.1 Classifier Performance in the Context of Tree Conceptualisation

The results for the classifier performance testing are provided in Table 7.7. From the table, it can be seen that the use of Kurtosis as a node label mechanism improved the overall classification performance compared to Mean labelling regardless of the value of L (the suggestion that the level of decomposition might have an effect was therefore unfounded). The average AUC result for the Mean was 0.79 while the average for the Kurtosis was 0.85. The conjecture (Subsection 7.2.1) that mean intensity node labelling did not provide for a sufficient description was verified.

Table 7.7: Classifier performance results in the context of the edge labelling mechanism used (Stage 2) using: (i) standard decomposition, (ii) a range of decomposition levels, (iii) KLD critical function, (iv) gSpan FSG using $\sigma = 2$ and (v) SVM classification.

CF	L	Acc	Sen	Spec	PPV	NPV	EER	AUC
Mean	3	80.71%	82.09%	79.45%	78.57%	82.86%	0.21	0.81
	4	75.71%	77.27%	74.32%	72.86%	78.57%	0.26	0.76
	5	77.86%	76.71%	79.10%	80.00%	75.71%	0.21	0.78
	6	83.57%	85.07%	82.19%	81.43%	85.71%	0.18	0.84
	Ave.	79.46%	80.28%	78.76%	78.21%	79.96%	0.21	0.79
Kurtosis	3	90.00%	92.42%	87.84%	87.14%	92.86%	0.12	0.9
	4	83.57%	84.06%	83.10%	82.86%	84.29%	0.17	0.84
	5	80.71%	79.45%	82.09%	82.86%	78.57%	0.18	0.81
	6	85.71%	87.88%	83.78%	82.86%	88.57%	0.16	0.86
	Ave.	**84.99%**	**85.95%**	**84.20%**	**83.93%**	**86.07%**	**0.15**	**0.85**

7.6.2.2 Tree Conceptualisation Significance Testing

In this subsection, the results for the significance testing applied to the above results are presented. The resulting ANOVA data is presented in Table 7.8 from which it can be seen that there was a statistically significant difference between the Kurtosis and Means node labelling mechanisms (the p-value was 3.0482e-05). Figure 7.5 shows the confidence interval diagrams. From the figure, it can be seen that the classification performance AUC results produced using Kurtosis node labelling were significantly better than when Mean intensity labelling was used, thus confirming the above result as being statistically significant.

Table 7.8: ANOVA data for edge-labelling comparison (Kurtosis v. Mean)

Source	SS	df	MS	F	p-value
Between-Groups	0.1033	1	0.1033	17.5826	3.0482e-05
Error	4.8546	826	0.0059		
Total	4.9579	827			

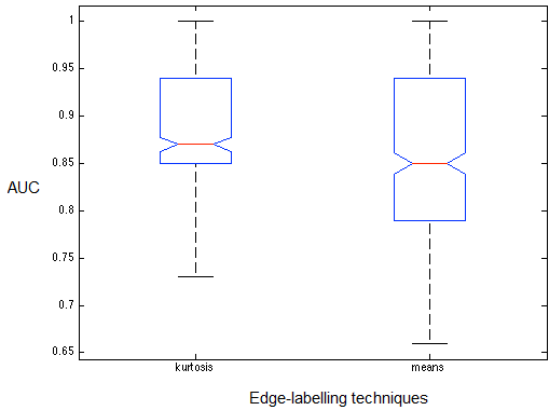

Figure 7.5: Confidence intervals for comparing edge-labelling techniques.

7.6.3 Evaluation of Classifier Generation (Stage Five)

In this section, the results obtained using the proposed process with respect to the three different classifier generation mechanisms (KNN, SVM and BN) are considered. Recall that the objective was to determine which classifier produced the best results. Recall also that in the context of the region-based method the BN and SVM classifier generators produced the best results. Two sets of experiments were again conducted: (i) classifier performance evaluation and (ii) statistical significance testing. For the evaluation, the following techniques were fixed with respect to the stages not consid-

ered in this section: (i) standard decomposition and the KLD critical function with a threshold of $t = 0.5$, (ii) gSpan FSG using $\sigma = 20\%$. A range of values for L were considered ($L = \{3, 4, 5, 6\}$) again because it was conjectured that the level of decomposition would have an effect on the nature of the adapted classifier generator. The results obtained are discussed in the following subsections.

7.6.3.1 Classifier Performance in the Context of Classifier Generation

In this subsection, we present the results obtained using the three classifiers considered: (i) SVM, (ii) KNN and (iii) BN. Table 7.9 presents the results obtained. From the table, it can be seen that the SVM and BN classifier generator tended to produce the best results with respect to the four different decomposition levels considered. The SVM produced the best average results with respect to all the metrics considered. It can also be observed that as the level of decomposition increased the classification performance tended to decrease. All reported AUC results obtained, as shown in the table, were between 0.82 and 0.92.

Table 7.9: Classifier performance results in the context of classifiers generation (Stage 5) using: (i) standard decomposition, (ii) a range of decomposition levels, (iii) KLD critical function and (iv) Kurtosis node labelling.

CF	L	Acc	Sen	Spec	PPV	NPV	EER	AUC
SVM	3	89.29%	88.73%	89.86%	90.00%	88.57%	0.10	0.89
	4	85.00%	82.67%	87.69%	88.57%	81.43%	0.12	0.85
	5	83.57%	78.31%	91.23%	92.86%	74.29%	0.09	0.84
	6	82.14%	80.00%	84.62%	85.71%	78.57%	0.15	0.82
	Ave.	**85.00%**	**82.42%**	**88.35%**	**89.28%**	**80.71%**	**0.15**	**0.85**
KNN	3	88.93%	87.59%	90.37%	90.71%	87.14%	0.11	0.90
	4	80.00%	77.27%	83.33%	85.00%	75.00%	0.22	0.83
	5	81.07%	77.71%	85.37%	87.14%	75.00%	0.22	0.83
	6	80.71%	76.54%	86.44%	88.57%	72.86%	0.20	0.82
	Ave.	82.67%	79.77%	86.37%	87.85%	77.5%	0.18	0.84
BN	3	89.29%	87.67%	91.04%	91.43%	87.14%	0.11	0.92
	4	79.29%	77.33%	81.54%	82.86%	75.71%	0.22	0.83
	5	80.95%	78.26%	84.21%	85.71%	76.19%	0.21	0.84
	6	81.19%	77.18%	86.59%	88.57%	73.81%	0.21	0.83
	Ave.	82.68%	80.11%	85.84%	87.14%	78.21%	0.18	**0.85**

7.6.3.2 Classifier Generation Significance Testing

The test conduced to measure the differences between the operation of the classifiers in the context of the whole image-based methods showed that there was no statistical difference between the classifiers. Table 7.10 presents the calculated ANOVA data. The reported p-value was 0.4920, indicating that there was no difference between the operation of the classifiers. Thus the fact that the BN classifier generator produced

Table 7.10: ANOVA data for classifier generation comparison.

Source	SS	df	MS	F	p-value
Between-Groups	0.0085	2	0.0042	0.7098	0.4920
Error	5.0104	840	0.0060		
Total	5.0188	842			

the best performance, as reported above, is not statistically significant. Because there was no detected significant difference in the operation of the three classifier generators considered, no further analysis was conducted. There was a small difference between the groups with a Between-Groups$_{SS}$= 0.0085 (Table 7.5). Figure 7.6 shows the confidence diagrams showing the similarities between the results obtained using the different classifiers. From the diagram, it can be seen that BN and SVM were slightly better than KNN.

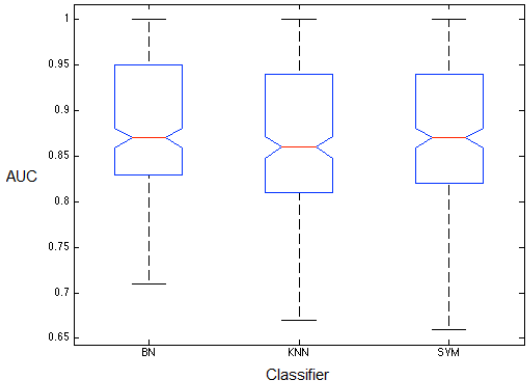

Figure 7.6: Confidence intervals for comparing classifiers.

7.7 Summary and Conclusions

In this chapter, the whole image-based representation mechanism, in the context of AMD classification, has been presented and evaluated. The process comprised five stages: (i) image decomposition, (ii) tree conceptualisation, (iii) frequent sub-graph mining, (iv) feature vector generation and (v) classifier generation. First the images of interest were decomposed into a tree structure. To this end, two different types of decomposition were suggested (standard and overlapping) and the use of six different critical functions (including no critical unction). Nodes were labelled using a single statistical value computed by comparing parent-child regions. The gSpan graph mining algorithm was then applied to generate a set of frequent sub-graphs. These sub-graphs

were then used to form a feature vector for each image. Three classifier generators were considered for the final stage (SVM, KNN and BN).

Table 7.11: Best four performing combinations of techniques as identified in the foregoing evaluation.

Identifier	Image Decomposition	Node Labelling	Feature Selection	Classification
WIB_1	overlapping decomposition, L=6, LCS critical function	Kurtosis node labelling	gSpan FSG using $\sigma = 20\%$	SVM classifier
WIB_2	overlapping decomposition, L=3, LCS critical function	Kurtosis node labelling	gSpan FSG using $\sigma = 20\%$	BN classifier
WIB_3	overlapping decomposition, L=6, KLD critical function	Kurtosis node labelling	gSpan FSG using $\sigma = 20\%$	SVM classifier
WIB_4	overlapping decomposition, L=6, KLD and LCS critical function	Kurtosis node labelling	gSpan FSG using $\sigma = 20\%$	BN classifier

Table 7.12: The best classification results obtained using decomposition and whole image-based methods.

Label	Acc	Sen	Spec	PPV	NPV	EER	AUC
WIB_1	100.00%	100.00%	100.00%	100.00%	100.00%	0.00	1
WIB_2	99.29%	100.00%	98.59%	98.57%	100.00%	0.00	0.99
WIB_3	97.86%	98.55%	97.18%	97.14%	98.57%	0.03	0.98
WIB_4	98.10%	99.03%	97.20%	97.14%	99.05%	0.01	0.98

The evaluation results for the whole image-based representation established that the proposed method produced good classification performances. It was clearly demonstrated that overlapping decomposition produced a much better classification performance than when using standard decomposition. It was also established that the best performing critical function was LCS (which produced an accuracy of 100%, an error rate of 0.00 and an AUC of 1). It is noteworthy that the use of LCS outperformed the use of AIV, as proposed in [59] where work on retina classification was also presented (bit directed at 2D images). In the context of the selected level of decomposition, the overall results demonstrated that six levels of decomposition produced high-performing classifiers. In addition, it was established that node labelling using the Kurtosis measure produced better results than when Means labelling was used. The ANOVA statistical significance testing and the post-hoc test (the Tukey's test) analysis revealed that the results obtained were statistically significant.

The best results from the reported experiments concerning the operation of the proposed whole image-based techniques are summarised. Tables 7.11 gives the best four performing combination of techniques and the associated results obtained. For reference later in this thesis, the techniques have been labelled as follows: (i) WIB_1, (ii) WIB_2 (iii) WIB_3 (iv) WIB_4. From the tables, it can be seen that the best results in terms of accuracy reached 100%. From the given results with respect to the proposed approaches using the decomposition, it can be concluded that: (i) overlapping decomposition is more effective than standard decomposition, and (ii) the LCS and KLD critical functions produced a good performance.

Thus, in summary, the main findings from this chapter are as follows:

1. The LCS critical function contributed to a better whole image-based representation.

2. There were similarities between levels of decomposition with slightly better performance using level 6 of decomposition.

3. Kurtosis node labelling produced better results than Mean node labelling.

4. All the classifiers produced good results although SVM and BN results were slightly better than KNN.

In the next chapter, we compare the obtained results in this chapter with the results from the previous chapter (Chapter 6).

Chapter 8

Discussion

8.1 Overview

This short chapter discusses and compares the operation of the proposed volumetric representation methods, both Region-Based (RB) and Whole Image-Based (WIB), for image classification described in the foregoing chapters. The comparison is conducted in the context of the four best region-based methods and the four best whole image-based representation methods identified in Chapters 6 and 7. The aim of this chapter is to provide a comparison between these two groups of techniques and to compare their operation with other techniques taken from the literature (identified in Chapters 2 and 3). For the evaluation, the AMD data set used previously was again used.

With respect to the RB category, the best identified performing techniques are summarised in Table 8.1. With respect to the WIB category the best identified performing techniques are summarised in Table 8.2. The alternative techniques with which the best four RB and best four WIB techniques were compared were as follows:

1. Voxel Co-occurrence Matrix (VCM) [53, 73].
2. Voxel Run-Length Matrix (VRLM) [19, 26, 43, 132].
3. Histograms of Oriented Gradients (HOG) [24, 90, 123].
4. Histograms of Local Binary Pattern (LBP) [57].
5. A combination of HOG and LBP (HOG-LBP) [143].
6. Local Phase Quantisation (LPQ) [101].

Details of these techniques were presented earlier in the previous work chapter (Section 2.4). These methods have been widely used for image feature extraction. Note that none of these featured any form of decomposition. They have thus been adapted for the purpose of 3D (volumetric) image classification in the research domain of interest with respect to this thesis. The SVM classifier was used with all the given techniques because

Table 8.1: Best four performing combinations of techniques for region-based methods.

Identifier	Image Decomposition	Region Representation	Feature Selection	Classification
RB_1	overlapping decomposition, L=5, ED critical function	HOG representation	IFK with $K = 128$	SVM classifier
RB_2	overlapping decomposition, L=5, ED critical function	HOG representation	IFK with $K = 128$	BN classifier
RB_3	overlapping decomposition, L=5, LCS critical function	HOG representation	IFK with $K = 128$	SVM classifier
RB_4	overlapping decomposition, L=5, LCS critical function	HOG representation	IFK with $K = 128$	BN classifier

it had been shown to produce good performance (see evaluation results presented in Chapters 6 and 7).

Table 8.2: Best four performing combinations of techniques for whole image-based methods.

Identifier	Image Decomposition	Node Labelling	Feature Selection	Classification
WIB_1	overlapping decomposition, L=6, LCS critical function	Kurtosis node labelling	gSpan FSG using $\sigma = 20\%$	SVM classifier
WIB_2	overlapping decomposition, L=3, LCS critical function	Kurtosis node labelling	gSpan FSG using $\sigma = 20\%$	BN classifier
WIB_3	overlapping decomposition, L=6, KLD critical function	Kurtosis node labelling	gSpan FSG using $\sigma = 20\%$	SVM classifier
WIB_4	overlapping decomposition, L=6, KLD and LCS critical function	Kurtosis node labelling	gSpan FSG using $\sigma = 20\%$	BN classifier

With respect to the above, two sets of comparisons are presented. The first set of comparisons is concerned with classifier performance. The second set of comparisons is directed at investigating the run time complexity of the proposed methods (classification efficiency).

The rest of this short chapter is organised as follows. Section 8.2 presents the

comparison in performance between the selected techniques. The time complexity of the selected techniques is then considered in Section 8.3. Some conclusion concerning the results is presented in Section 8.4.

8.2 Comparison Between the Performance of Volumetric Representations

This section compares and discusses the classification results obtained using the best performing techniques identified in the foregoing chapters and the identified techniques from the literature which have been adapted for 3D classification.

Table 8.3 summarises the results obtained; best results highlighted in bold font. The table presents the results in three blocks: (i) classification performance with respect to the alternative methods taken from the literature (no decomposition), (ii) classification performances with respect to the proposed RB methods (with decomposition), and (iii) classification performances with respect to the proposed WIB methods. Note that the best results presented in blocks 2 and 3 are identical; those presented in Tables 6.16 and 7.12.

From the first block of results (results produced using techniques taken from the literature), it can be seen that the best performance was produced using VCM (Acc. = 95.71%, Sen. = 95.59%, Spec. = 95.83%, PPV = 95.59%, NPV = 95.83%, EER = 0.04 and AUC = 0.96). VCM was more effective because feature vectors were generated using different statistical functions for feature extraction. In addition, these statistical functions used were more effective when applied to the VCM matrix. The worst result was obtained using VRLM. This may be because VRLM was less descriptive than the VCM and the rest of the methods.

Comparing these results with the RB and WIB results (blocks 2 and 3), it can be seen that the techniques taken from the literature did not perform as well as the techniques proposed in this thesis. It is argued that this is because these techniques do not use decomposition.

Comparing the RB and WIB results, there were no significant differences between them, although it can be argued that WIB_1 produced the overall best results. Recall that WIB_1 used: (i) overlapping decomposition, with L=6 and LCS critical function, (ii) Kurtosis node labelling, (iii) feature selection FSG (gSpan with $\sigma = 20\%$) and (iv) SVM classifier.

The strengths of the proposed methods are: (i) avoid the use of the segmentation-based methods such as the work in [109] and (ii) the use of decomposition process has improved the classification performance as reported early in this section. Although successfully able to differentiate between AMD and non-AMD volumes, the proposed RB methods associated with the decomposition decreases the performance compared to alternative methods without the the use of decomposition.

Table 8.3: Best classification results for the alternative techniques, RB techniques, WIB techniques.

Method	Acc	Sen	Spec	PPV	NPV	EER	AUC
Classification performance for alternative methods without decomposition							
VCM [53, 73]	95.71%	95.59%	95.83%	95.59%	95.83%	0.04	0.96
VRLM [19, 26, 43, 132]	82.38%	84.95%	80.34%	77.45%	87.04%	0.19	0.84
HOG [24, 90, 123]	94.29%	95.45%	93.24%	92.65%	95.83%	0.07	0.94
LBP[57]	90.00%	89.71%	90.28%	89.71%	90.28%	0.10	0.90
HOG-LBP [143]	89.29%	98.18%	83.53%	79.41%	98.61%	0.17	0.89
LPQ [101]	87.86%	89.23%	86.67%	85.29%	90.28%	0.14	0.88
Classification performance for the proposed region-based representation methods							
RB_1	99.29%	98.55%	**100.00%**	**100.00%**	98.61%	**0.00**	0.99
RB_2	98.57%	99.01%	98.17%	98.04%	99.07%	0.02	0.99
RB_3	97.86%	100.00%	96.00%	95.59%	**100.00%**	0.04	0.98
RB_4	97.62%	99.49%	95.98%	95.59%	99.54%	0.04	0.98
Classification for the proposed whole image-based methods							
WIB_1	**100.00%**	**100.00%**	**100.00%**	**100.00%**	**100.00%**	**0.00**	**1.00**
WIB_2	99.29%	**100.00%**	98.59%	98.57%	**100.00%**	**0.00**	0.99
WIB_3	97.86%	98.55%	97.18%	97.14%	98.57%	0.03	0.98
WIB_4	98.10%	99.03%	97.20%	97.14%	99.05%	0.01	0.98

8.3 Run Time Complexity

In this section, we present the results obtained with respect to a set of run time complexity experiments conducted using the techniques considered in Section 8.2. Experiments were conducted with respect to: (i) the required run time for decomposition, (ii) the required run time for the feature vector generation, (iii) the required run time for classifier generation and (iv) the required total run time. For these experiments, Apple iMac with quad-core Intel Core i5 processor with 12 GB of RAM memory were used. The results obtained are presented in Table 8.4. Again, as in the case of Table 8.3, the table is divided into three blocks.

From the table, it can be seen that the whole image-based methods required significantly more time than the other methods. The reason for this is that when the level of decomposition increases the required computation time becomes an issue with respect to the WIB methods. Recall that the proposed WIB methods rely on the frequent sub-graph mining based approaches, such as gSpan algorithm, to generate feature vectors. The use of gSpan added significantly to the overall run time of the WIB methods especially when the size of the graph is large (recall that the graph size is affected by the level of decomposition). The alternative methods, especially (VCM), required very little run time, largely because they did not involve any decomposition.

When the level of decomposition increases the required computation time becomes an issue with respect to the WIB methods as presented in this section. Recall that the proposed WIB methods rely on frequent sub-graph mining based approaches. One of the issues with graph mining is time complexity. For graph mining algorithms, such as gSpan, required more processing time than the other methods such as IFK for RB

Table 8.4: The average run time in seconds for the identified methods in this chapter. The following are given: Average Decomposition Time (ADT), Average Feature Vector Generation Time (AFVGT), Classifier Generation (CG) and Total Execution Time (TET).

CF	ADT	AFVGT	CG	TET
Alternative methods				
VCM	-	2.31	0.01	2.32
VRLM	-	5.83	0.01	5.4
HOG	-	5.09	0.01	5.1
LBP	-	37.94	0.01	37.95
HOG-LBP	-	42.84	0.01	42.85
LPQ	-	4.71	0.01	4.72
Region-based methods				
RB_1	2.69	4.12	0.31	7.12
RB_2	2.69	4.12	0.82	7.63
RB_3	16.05	3.80	0.26	20.11
RB_4	16.05	3.80	0.75	20.60
Whole image-based methods				
WIB_1	15.63	433.51	0.01	449.15
WIB_2	16.05	4,703.56	0.01	4,719.62
WIB_3	8.75	4208.72	0.01	4,217.48
WIB_4	8.81	378,785.1	0.01	378,793.92

methods, especially when the size of the graph, it depends on the level of decomposition, is increased. Another issue with algorithms such as the gSpan algorithm is the required space complexity especially when considering large trees (high levels of decomposition).

8.4 Summary

In this chapter, we have compared and discussed the operation of the best performing RB and WIB methods with alternative approaches from the literature. Two types of comparison were conducted: (i) in terms of best overall classification performance and (ii) in terms of run time complexity. From the reported results, it can be seen that there is a trade-off between performance and time complexity. Decomposition-based methods performed well but required more time than the alternative methods which did not use decomposition. The whole image-based methods required much more run time than the region-based methods and the alternative methods. An important conclusion from the experiments reported in this chapter is that the use of decomposition produces very good results in the context of the AMD application and with respect to the alternative techniques considered, but requires more run time.

Chapter 9

Conclusion

This chapter summarises the proposed hierarchical spatial decomposition techniques to represent 3D images (volumetric data) for classification purposes presented in this thesis, in particular with respect to their application to 3D OCT retinal images for the detection of AMD. The main findings of the research, the research contributions and their implications are presented in this chapter with respect to the research question and issues identified in Chapter 1. Some recommendations for further research work are also provided.

This chapter is structured as follows. The summary of the proposed techniques is presented in Section 9.1. Section 9.2 then presents the main findings of the research. The research contributions are provided in Section 9.3. Some suggested future research work is proposed in Section 9.4.

9.1 Summary

This thesis has investigated the effectiveness of hierarchical spatial decomposition techniques to support 3D image classification methods. This study set out to determine the effect of the decomposition on image representation methods for image classification. To act as a focus for the work described, the proposed decomposition methods were applied to support the classification of retinal images so as to identify AMD. AMD is an eye disease that may lead to blindness in elderly people. The reported performance of the proposed decomposition methods shows that the hierarchical spatial decomposition helps to derive regions that can be represented better than when no decomposition is used and thus can lead to good classification performance.

The proposed methods served to classify 3D images using various 3D representation methods based on hierarchical spatial decomposition. The proposed process comprised the following stages: (i) preparation presented in Section 3.6, (ii) decomposition in Chapter 4, (iii) representation using region-based in Chapter 5 and whole image-based in Chapter 7, (iv) feature vector generation, (v) classifier generation and (vi) evaluation. In the first stage, the quality of the given images is improved using some preprocessing

such as removing unwanted content, and flattening. The retinal layers are flattened in order to reference the images to some common coordinate system. The preprocessing methods produced a Volume Of Interest (VOI).

In the second stage, each VOI was recursively decomposed until it reached a predefined maximum level of decomposition or a homogeneous region. In order to determine regional homogeneity, seven critical functions were considered: (i) Average Intensity Value (AIV), (ii) Kendall's Coefficient Concordance (KCC), (iii) Gray Level Co-occurrence Matrix (GLCM), (iv) Euclidean Distance (ED), (v) Kullback-Leibler divergence (KLD), (vi) Dynamic Time Warping (DTW) and (vii) Longest Common Subsequence (LCS). These critical function were defined in Section 4.3. Two of the critical functions were proposed by other authors, namely AIV [59] and KCC [153]; the rest were introduced by the author. Four histogram-based critical functions were proposed, namely ED, KLD, DTW and LCS. For the histogram based methods, histograms of each region in the decomposition were generated. Histograms for potential region were then computed. If there was a substantial difference between the two, the decomposition proceeded; otherwise the decomposition was terminated.

Two types of decomposition techniques were also considered: (i) standard and (ii) overlapping. Once the image was decomposed, the decomposition was stored in a tree structure (the decomposition process naturally lends itself to a tree structure).

In the representation stage, two sorts of representation methods were proposed: (i) Region-Based (RB) and (ii) Whole Image-Based (WIB). These two representation methods are central to the contribution of the thesis. A variety of different techniques, and variations of the methods, were considered. What the methods all had in common was that they were all designed to ultimately define a feature space model.

Using these models, feature vector generation methods were applied so as to derive a single feature vector for each image. The set of feature vectors for a collection of images was then input into a classifier generator. For the classification stage, three different classifier generators were considered: (i) SVM, (ii) KNN and (iii) BN.

To evaluate the proposed region-based and the whole image-based methods, two sorts of evaluation were used: (i) classification performance evaluation using different evaluation metrics such as accuracy, equal error rate and AUC, and (ii) statistical significance testing using ANalysis Of VAriance (ANOVA). Ten-fold Cross Validation (TCV) was used throughout.

In the context of the RB methods, two types of techniques were used to represent each region: (i) statistical based and (ii) histogram based. In total, seven techniques were considered:

1. First-Order Representation (FOR),
2. Voxel Co-occurrence Matrix (VCM),

3. Voxel Run-Length Matrix (VRLM),
4. Histograms of Oriented Gradients (HOG),
5. Histograms of Local Binary Pattern (LBP),
6. A combination of HOG and LBP and
7. Local Phase Quantisation (LPQ)

of which the first three were statistical-based and the remainder were histogram-based. With respect to the RB methods, two feature vector generation methods were used to form a single feature vector for each image: (i) a dimensionality reduction-based method using Principal Component Analysis (PCA) and (ii) a feature selection-based method in terms of dictionary learning using Improved Fisher Kernel Encoding (IFK). In the dimensionality reduction-based method, each set of image regions was considered independently without considering the collection of other images' regions, while in the feature selection-based method all the image regions were considered as one set. Once a single feature vector was generated for each image, the set of feature vectors was used for the training and testing of the selected classifier.

The proposed WIB methods relied on graph-mining techniques. Once the images were decomposed, each region was considered as a node label in the tree and the relationships between the parent node and the child node were considered as the edge labels in the tree. The effect of two types of node labelling was compared: (i) using the mean value of each region intensity value as in [59], and (ii) using the kurtosis of the histogram of the intensity values represented by the voxels representing each region represented by each node. Two types of edge labels were also considered: (i) the difference between the parent node and the child node in terms of mean values as in [59] and (ii) using the result of the Kullback-Leibler Divergence (KLD) comparing the histograms of the child node and the parent nodes. Using the WIB approach, each image was represented as a tree with a set of nodes and edges. These trees were fed into a Frequent Sub-graph Mining (FSM) algorithm, namely gSpan [148], to determine the set of frequent sub-graphs contained across the tree represented image set. A feature selection mechanism was used to select a subset from the sub-graphs generated. These sub-graphs were used as the basis for generating a binary-valued feature vector for each image. A value of 1 was used if the sub-graph existed in the generated tree of the image, and a value of 0 if it did not exist. The generated feature vector was then fed into a classifier generator in the same way as for the RB methods.

The different techniques presented in this thesis were compared with each other and alternative techniques taken from the literature. Very positive results were obtained and these are discussed further in the next section.

9.2 Main Findings

This section presents the main findings from the conducted research presented in this thesis. Referring back to Chapter 1, the initial research question was:

> *Is it possible to devise hierarchical spatial decomposition-based representation methods, suited to the classification of volumetric data, in such a way that effective classification performance can be achieved given the significant size and complexity of volumetric data sets?*

The resolution of this research question required that a number of associated research issues be addressed. Each is discussed below:

1. **What is the most appropriate method to decompose images so that homogeneous regions are identified?** The comparison between the results of the proposed approaches presented in this thesis, as given in Chapter 8, indicated that the best way to decompose the image is to use the overlapping decomposition proposed by the author coupled with either the ED or LCS or KLD critical function. The results obtained using this decomposition, using both the RB and WIB methods, indicated that it outperformed the situation where decomposition without a critical function was used (and where alternative critical functions were used).

2. **Once a volume has been decomposed, is it better to represent the volume in terms of the individual decomposed regions (region-based) or in terms of the entire decomposition (whole image-based)?** From the results, both representations performed well.

3. **With respect to the use of either region-based or whole image-based representation, what is the most appropriate representation for encapsulating the decomposition to support the desired classification?** In the case of the RB methods, it was found that the best mechanism for representing regions was using the HOG representation. In the case of the WIB mechanism, it was found that the best ways of encapsulating the decomposition was to use the Kurtosis node labelling.

4. **Given a particular representation, what is the most effective way of generating a single feature vector for each image?** According to the results presented in Chapter 6, the best feature vector generation technique with respect to the RB methods was found to be where the IFK feature selection method (with $K = 128$) was adapted. This was because IFK used the concept of dictionary learning where the selection of the feature vector was based on the entire collection

of feature vectors derived from several images. In the case of WIB methods, the use of the proposed frequent sub-graph mining approach work well.

5. **What is the most appropriate mechanism for conducting volumetric classification?** From the comprehensive comparisons between the results obtained, reported in Subsections 6.5.1 and 7.6.3, the SVM and BN classifiers generated the best classification results with respect to the proposed representation methods.

Returning to the research question posed at the beginning of this thesis in Chapter 1, it is now possible to state that the proposed methods presented in Chapters 5 and 7 can be successfully employed to classify volumetric data sets. The most appropriate approach was to use overlapping hierarchical spatial decomposition coupled with the LCS critical function coupled with WIB representation using: (i) Kurtosis node labelling, (ii) gSpan FSG using $\sigma = 20\%$ and (iii) SVM classifier. With appropriate representation, feature generation methods and classifiers can perform effective classification of 3D images. One of the more significant findings to emerge from this study is that homogeneous decomposition coupled with region-based representation methods and feature selection-based methods using dictionary learning can also form feature vectors that can be classified effectively.

9.3 Research Contributions

The findings from this thesis make several contributions to the current state of the art. These contributions may be summarised as follows:

1. A novel and effective approach to 3D image classification using spatial decomposition for generating classifiers applicable to 3D volumetric data.
2. Two methods for representing volumetric data within the context of spatial decomposition: (i) region-based and (ii) whole image-based.
3. A mixed oct and quad decomposition mechanism specifically designed for retinal OCT data volumes.
4. Four critical functions to derive regional homogeneity associated with the decomposition methods, especially the ED, KLD, DTW and LCS critical functions.
5. A WIB representation method that utilised the concept of frequent sub-graph mining for generating feature vectors to support 3D image classification.
6. Novel approaches to AMD image screening with respect to 3D OCT data.
7. Approaches to support future automated retinal disease screening.

9.4 Future Work

In this section, a number of possible directions for future work are suggested as follows:

1. It would be interesting to consider further alternative mechanisms for conducting the desired decomposition other than using the standard and overlapping decompositions considered in this thesis, such as wavelet or curvelet transforms. This is because wavelet and curvelet transforms are frequency-based methods and spatial decomposition by the means of these methods would lead to homogeneous regions in terms of frequency.

2. The time complexity issue associated with the frequent sub-graph mining techniques is a significant issue. A reasonable approach to address this issue could be to use a heuristic approach for selecting a subset of sub-graphs according to some criteria instead of considering each possible sub-graph. However, in this context it should be noted that efficient sub-graph mining is a substantial area of current research within data mining community.

3. It would also be useful to conduct further research directed at exploring the effect of using RB methods coupled with class-based dictionary learning. The idea here would be to try to remove redundant regions by identifying regions that commonly occur with a specific class and adding these to the dictionary so that regions associated with a specific class are included (assuming they exist).

4. It would be interesting to explore the potential generic nature of the proposed techniques, to assess the effects of the proposed methods on alternative image datasets with different application domains; for example, the classification of MRI brain images for investigating brain disorders.

5. Further research might be directed at investigating the effect of combining the region-based method with the whole image-based methods. The intuition here is that the use of graph mining applied to trees, where each node is represented by one of the region-based methods such HOG, might produce good results. It is suggested that in this case the information held at nodes would be more descriptive than in the case of the current "single value per node" method used in the WIB methods presented earlier in this thesis.

Whatever the case, the work presented in this thesis has provided a sound foundation on which further investigations can be conducted.

Appendix A

Further Results for Region-based Representation Methods

A.1 Overview

In this appendix some additional results are presented with respect to the evaluation of the region-based volumetric representation presented in Chapter 6. Recall that the region-based representation comprised four stages as illustrated previously in Figure 5.1: (i) decomposition, (ii) region representation, (iii) single feature vector generation and (iv) classifier generation. Each of these stages had a number of techniques associated with it. With respect to the third stage, single feature vector generation, two techniques were proposed: (i) dimensionality reduction using Principal Component Analysis (PCA) and (ii) feature selection using the Improved Fisher Kernel (IFK) encoding. For the evaluation presented in Chapter 6 both techniques were evaluated using static techniques for the remaining stages, these were: the LCS critical function, overlapping decomposition, the HOG representation and SVM classification. For completeness in this appendix results from additional experiments with respect to PCA and IFK are presented in Parts A.2 and A.3 respectively. The results presented in this appendix confirm the earlier results that, in the context of the region based representation: (i) overlapping decomposition outperforms standard decomposition, (ii) use of a critical function is more advantageous than when not using a critical function, (iii) the best performing critical functions tend to be ED and LCS, (iv) that the use of IFK is more beneficial than PCA and (v) SVM and BN classification tend to outperform KNN classification.

A.2 Dimensionality Reduction-based Results using PCA

In this part results are presented from additional experiments with respect to dimensionality reduction using PCA that were not included in the main body of the thesis. For comparison purposes the results previously reported have also been included. The

results included in this part are presented in seven different tables (Tables A.1 to A.7) one for each region representation:

1. First-Order Representation (FOR).
2. Voxel Co-occurrence Matrix (VCM).
3. Voxel Run-Length Matrix (VRLM).
4. Histograms of Oriented Gradients (HOG).
5. Histograms of Local Binary Pattern (LBP).
6. A combination of HOG and LBP (HOG-LBP).
7. Local Phase Quantisation (LPQ).

In each table, the standard and overlapping decomposition results with a range of levels, $\{3, 4, 5, 6\}$, are presented as well as the results associated with the use of the seven critical functions. The critical functions were:

1. No critical function (0NCF),
2. Average Intensity Value (AIV),
3. Kendall's Coefficient Concordance (KCC),
4. Gray Level Co-occurrence Matrix (GLCM),
5. Euclidean Distance (ED),
6. Dynamic Time Warping (DTW),
7. Longest Common Subsequence (LCS) and
8. Kullback-Leibler divergence (KLD).

In addition, three classifier generators were used:

1. Support Vector Machines(SVM).
2. K-Nearest Neighbour (KNN).
3. Bayesian Networks (BN).

Table A.1: The results using FOR with PCA.

Method	Classifiers	Acc	Sen	Spec	PPV	NPV	EER	AUC

Standard-0NCF-3L	SVM	70.00%	66.67%	74.19%	76.47%	63.89%	0.27	0.7
	KNN	74.29%	69.05%	82.14%	85.29%	63.89%	0.30	0.72
	BN	77.86%	74.03%	82.54%	83.82%	72.22%	0.16	0.78
Standard-0NCF-4L	SVM	85.71%	85.29%	86.11%	85.29%	86.11%	0.15	0.86
	KNN	83.93%	83.21%	84.62%	83.82%	84.03%	0.16	0.85
	BN	85.95%	85.71%	86.18%	85.29%	86.57%	0.15	0.88
Standard-0NCF-5L	SVM	82.86%	83.33%	82.43%	80.88%	84.72%	0.18	0.83
	KNN	81.79%	81.95%	81.63%	80.15%	83.33%	0.19	0.82
	BN	84.05%	84.42%	83.71%	82.35%	85.65%	0.17	0.86
Standard-0NCF-6L	SVM	83.57%	84.62%	82.67%	80.88%	86.11%	0.18	0.83
	KNN	78.21%	80.00%	76.77%	73.53%	82.64%	0.24	0.81
	BN	81.67%	83.96%	79.83%	76.96%	86.11%	0.22	0.85
Standard-AIV-3L	SVM	74.29%	73.53%	75.00%	73.53%	75.00%	0.26	0.74
	KNN	74.64%	71.52%	78.29%	79.41%	70.14%	0.22	0.75
	BN	79.52%	77.06%	82.18%	82.35%	76.85%	0.23	0.8
Standard-AIV-4L	SVM	87.86%	84.93%	91.04%	91.18%	84.72%	0.09	0.88
	KNN	85.36%	82.31%	88.72%	88.97%	81.94%	0.17	0.87
	BN	88.10%	85.00%	91.50%	91.67%	84.72%	0.08	0.9
Standard-AIV-5L	SVM	90.00%	87.50%	92.65%	92.65%	87.50%	0.08	0.9
	KNN	87.86%	86.96%	88.73%	88.24%	87.50%	0.12	0.89
	BN	88.81%	87.92%	89.67%	89.22%	88.43%	0.11	0.91
Standard-AIV-6L	SVM	90.71%	93.65%	88.31%	86.76%	94.44%	0.12	0.91
	KNN	83.57%	87.50%	80.62%	77.21%	89.58%	0.19	0.87
	BN	83.81%	86.96%	81.36%	78.43%	88.89%	0.11	0.88
Standard-GLCM-3L	SVM	74.29%	70.51%	79.03%	80.88%	68.06%	0.22	0.74
	KNN	76.07%	70.41%	84.68%	87.50%	65.28%	0.28	0.75
	BN	79.05%	74.79%	84.41%	85.78%	72.69%	0.15	0.81
Standard-GLCM-4L	SVM	85.00%	84.06%	85.92%	85.29%	84.72%	0.15	0.85
	KNN	80.00%	78.17%	81.88%	81.62%	78.47%	0.21	0.83
	BN	83.57%	82.30%	84.83%	84.31%	82.87%	0.17	0.87
Standard-GLCM-5L	SVM	90.00%	89.71%	90.28%	89.71%	90.28%	0.10	0.9
	KNN	89.64%	89.05%	90.21%	89.71%	89.58%	0.10	0.9
	BN	90.95%	91.09%	90.83%	90.20%	91.67%	0.08	0.92
Standard-GLCM-6L	SVM	87.14%	86.76%	87.50%	86.76%	87.50%	0.13	0.87
	KNN	82.86%	83.33%	82.43%	80.88%	84.72%	0.18	0.85
	BN	84.76%	86.08%	83.63%	81.86%	87.50%	0.12	0.88
Standard-KCC-3L	SVM	78.57%	75.00%	82.81%	83.82%	73.61%	0.18	0.79
	KNN	76.07%	69.94%	85.98%	88.97%	63.89%	0.28	0.78
	BN	80.71%	75.52%	87.71%	89.22%	72.69%	0.12	0.83
Standard-KCC-4L	SVM	82.86%	85.48%	80.77%	77.94%	87.50%	0.20	0.83
	KNN	81.07%	84.30%	78.62%	75.00%	86.81%	0.22	0.82
	BN	84.29%	85.20%	83.48%	81.86%	86.57%	0.13	0.86
Standard-KCC-5L	SVM	92.86%	96.77%	89.74%	88.24%	97.22%	0.11	0.93
	KNN	92.86%	97.54%	89.24%	87.50%	97.92%	0.11	0.93
	BN	94.05%	96.86%	91.70%	90.69%	97.22%	0.03	0.94
Standard-KCC-6L	SVM	97.14%	97.06%	97.22%	97.06%	97.22%	0.03	0.97
	KNN	94.64%	96.18%	93.29%	92.65%	96.53%	0.07	0.96
	BN	95.24%	95.54%	94.95%	94.61%	95.83%	0.04	0.96
Standard-ED-3L	SVM	82.86%	81.43%	84.29%	83.82%	81.94%	0.16	0.83
	KNN	84.64%	82.07%	87.41%	87.50%	81.94%	0.17	0.84
	BN	87.38%	85.45%	89.37%	89.22%	85.65%	0.11	0.88

Standard-ED-4L	SVM	88.57%	87.14%	90.00%	89.71%	87.50%	0.11	0.89
	KNN	89.29%	86.81%	91.91%	91.91%	86.81%	0.13	0.89
	BN	90.24%	88.26%	92.27%	92.16%	88.43%	0.12	0.91
Standard-ED-5L	SVM	94.29%	92.86%	95.71%	95.59%	93.06%	0.05	0.94
	KNN	92.50%	92.59%	92.41%	91.91%	93.06%	0.07	0.93
	BN	92.14%	91.71%	92.56%	92.16%	92.13%	0.08	0.93
Standard-ED-6L	SVM	92.86%	92.65%	93.06%	92.65%	93.06%	0.07	0.93
	KNN	90.00%	91.54%	88.67%	87.50%	92.36%	0.12	0.91
	BN	90.71%	91.88%	89.69%	88.73%	92.59%	0.11	0.92
Standard-DTW-3L	SVM	72.14%	68.83%	76.19%	77.94%	66.67%	0.25	0.72
	KNN	75.00%	69.64%	83.04%	86.03%	64.58%	0.29	0.74
	BN	78.57%	74.78%	83.16%	84.31%	73.15%	0.16	0.79
Standard-DTW-4L	SVM	85.00%	84.06%	85.92%	85.29%	84.72%	0.15	0.85
	KNN	80.71%	77.33%	84.62%	85.29%	76.39%	0.21	0.83
	BN	84.29%	81.94%	86.76%	86.76%	81.94%	0.13	0.87
Standard-DTW-5L	SVM	90.00%	92.19%	88.16%	86.76%	93.06%	0.12	0.9
	KNN	83.21%	83.46%	82.99%	81.62%	84.72%	0.18	0.87
	BN	85.95%	85.37%	86.51%	85.78%	86.11%	0.14	0.9
Standard-DTW-6L	SVM	87.14%	89.06%	85.53%	83.82%	90.28%	0.15	0.87
	KNN	81.79%	83.46%	80.39%	77.94%	85.42%	0.20	0.84
	BN	84.76%	86.08%	83.63%	81.86%	87.50%	0.12	0.88
Standard-LCS-3L	SVM	78.57%	78.79%	78.38%	76.47%	80.56%	0.23	0.79
	KNN	74.29%	73.19%	75.35%	74.26%	74.31%	0.26	0.76
	BN	78.10%	78.00%	78.18%	76.47%	79.63%	0.22	0.81
Standard-LCS-4L	SVM	85.00%	87.30%	83.12%	80.88%	88.89%	0.18	0.85
	KNN	81.43%	83.33%	79.87%	77.21%	85.42%	0.21	0.83
	BN	82.38%	83.85%	81.14%	78.92%	85.65%	0.21	0.85
Standard-LCS-5L	SVM	90.71%	89.86%	91.55%	91.18%	90.28%	0.09	0.91
	KNN	86.07%	89.43%	83.44%	80.88%	90.97%	0.10	0.88
	BN	87.62%	89.18%	86.28%	84.80%	90.28%	0.10	0.9
Standard-LCS-6L	SVM	90.00%	90.91%	89.19%	88.24%	91.67%	0.11	0.9
	KNN	87.14%	90.32%	84.62%	82.35%	91.67%	0.16	0.88
	BN	87.62%	88.38%	86.94%	85.78%	89.35%	0.11	0.89
Standard-KLD-3L	SVM	82.86%	82.35%	83.33%	82.35%	83.33%	0.17	0.83
	KNN	83.21%	79.87%	87.02%	87.50%	79.17%	0.13	0.83
	BN	84.52%	81.74%	87.56%	87.75%	81.48%	0.13	0.86
Standard-KLD-4L	SVM	90.00%	87.50%	92.65%	92.65%	87.50%	0.08	0.9
	KNN	81.43%	80.88%	81.94%	80.88%	81.94%	0.18	0.86
	BN	85.48%	85.22%	85.71%	84.80%	86.11%	0.15	0.9
Standard-KLD-5L	SVM	89.29%	88.41%	90.14%	89.71%	88.89%	0.10	0.89
	KNN	83.21%	80.69%	85.93%	86.03%	80.56%	0.18	0.86
	BN	85.00%	84.06%	85.92%	85.29%	84.72%	0.15	0.89
Standard-KLD-6L	SVM	85.71%	83.33%	88.24%	88.24%	83.33%	0.12	0.86
	KNN	76.43%	75.00%	77.86%	77.21%	75.69%	0.24	0.81
	BN	78.81%	78.05%	79.53%	78.43%	79.17%	0.21	0.84
Overlapped-0NCF-3L	SVM	70.00%	68.06%	72.06%	72.06%	68.06%	0.29	0.7
	KNN	69.64%	65.27%	76.11%	80.15%	59.72%	0.33	0.7
	BN	74.29%	70.69%	78.72%	80.39%	68.52%	0.20	0.77
Overlapped-0NCF-4L	SVM	77.86%	77.61%	78.08%	76.47%	79.17%	0.23	0.78
	KNN	77.86%	76.06%	79.71%	79.41%	76.39%	0.21	0.78
	BN	82.38%	80.37%	84.47%	84.31%	80.56%	0.19	0.84

Overlapped-0NCF-5L	SVM	77.86%	76.81%	78.87%	77.94%	77.78%	0.22	0.78
	KNN	82.14%	80.28%	84.06%	83.82%	80.56%	0.19	0.8
	BN	85.00%	82.79%	87.32%	87.25%	82.87%	0.16	0.84
Overlapped-0NCF-6L	SVM	81.43%	81.82%	81.08%	79.41%	83.33%	0.20	0.81
	KNN	79.64%	80.62%	78.81%	76.47%	82.64%	0.22	0.8
	BN	82.38%	83.51%	81.42%	79.41%	85.19%	0.15	0.85
Overlapped-AIV-3L	SVM	65.71%	65.15%	66.22%	63.24%	68.06%	0.35	0.66
	KNN	70.36%	68.28%	72.59%	72.79%	68.06%	0.28	0.68
	BN	74.76%	73.56%	75.94%	75.00%	74.54%	0.25	0.74
Overlapped-AIV-4L	SVM	84.29%	82.86%	85.71%	85.29%	83.33%	0.15	0.84
	KNN	81.43%	81.34%	81.51%	80.15%	82.64%	0.18	0.83
	BN	84.05%	83.74%	84.33%	83.33%	84.72%	0.16	0.87
Overlapped-AIV-5L	SVM	83.57%	80.82%	86.57%	86.76%	80.56%	0.14	0.84
	KNN	82.50%	79.59%	85.71%	86.03%	79.17%	0.19	0.83
	BN	85.71%	82.73%	89.00%	89.22%	82.41%	0.11	0.88
Overlapped-AIV-6L	SVM	77.86%	74.67%	81.54%	82.35%	73.61%	0.19	0.78
	KNN	78.21%	75.51%	81.20%	81.62%	75.00%	0.24	0.78
	BN	81.67%	79.81%	83.57%	83.33%	80.09%	0.20	0.84
Overlapped-GLCM-3L	SVM	72.14%	71.01%	73.24%	72.06%	72.22%	0.28	0.72
	KNN	71.07%	66.47%	77.88%	81.62%	61.11%	0.21	0.72
	BN	75.95%	72.10%	80.75%	82.35%	69.91%	0.30	0.78
Overlapped-GLCM-4L	SVM	81.43%	80.00%	82.86%	82.35%	80.56%	0.18	0.81
	KNN	81.07%	77.12%	85.83%	86.76%	75.69%	0.22	0.81
	BN	85.48%	81.78%	89.74%	90.20%	81.02%	0.10	0.87
Overlapped-GLCM-5L	SVM	89.29%	90.77%	88.00%	86.76%	91.67%	0.13	0.89
	KNN	87.14%	89.06%	85.53%	83.82%	90.28%	0.15	0.88
	BN	89.05%	89.90%	88.29%	87.25%	90.74%	0.13	0.91
Overlapped-GLCM-6L	SVM	85.71%	86.36%	85.14%	83.82%	87.50%	0.16	0.86
	KNN	80.71%	82.54%	79.22%	76.47%	84.72%	0.21	0.83
	BN	82.86%	84.38%	81.58%	79.41%	86.11%	0.16	0.86
Overlapped-KCC-3L	SVM	80.71%	79.71%	81.69%	80.88%	80.56%	0.19	0.81
	KNN	82.14%	77.22%	88.52%	89.71%	75.00%	0.22	0.82
	BN	84.76%	80.97%	89.18%	89.71%	80.09%	0.20	0.85
Overlapped-KCC-4L	SVM	86.43%	86.57%	86.30%	85.29%	87.50%	0.14	0.86
	KNN	78.21%	79.07%	77.48%	75.00%	81.25%	0.23	0.82
	BN	81.67%	82.23%	81.17%	79.41%	83.80%	0.21	0.86
Overlapped-KCC-5L	SVM	92.14%	92.54%	91.78%	91.18%	93.06%	0.09	0.92
	KNN	86.43%	89.52%	83.97%	81.62%	90.97%	0.16	0.89
	BN	89.05%	90.72%	87.61%	86.27%	91.67%	0.14	0.92
Overlapped-KCC-6L	SVM	76.43%	77.78%	75.32%	72.06%	80.56%	0.26	0.76
	KNN	75.36%	83.17%	70.95%	61.76%	88.19%	0.29	0.76
	BN	79.05%	83.33%	76.02%	71.08%	86.57%	0.29	0.81
Overlapped-ED-3L	SVM	82.86%	81.43%	84.29%	83.82%	81.94%	0.16	0.83
	KNN	74.64%	69.01%	83.49%	86.76%	63.19%	0.28	0.79
	BN	78.10%	74.14%	82.98%	84.31%	72.22%	0.28	0.83
Overlapped-ED-4L	SVM	84.29%	83.82%	84.72%	83.82%	84.72%	0.16	0.84
	KNN	85.71%	83.80%	87.68%	87.50%	84.03%	0.13	0.85
	BN	87.86%	85.92%	89.86%	89.71%	86.11%	0.13	0.88
Overlapped-ED-5L	SVM	95.00%	94.20%	95.77%	95.59%	94.44%	0.04	0.95
	KNN	87.86%	86.43%	89.29%	88.97%	86.81%	0.13	0.91
	BN	88.33%	87.08%	89.57%	89.22%	87.50%	0.11	0.92

Overlapped-ED-6L	SVM	92.14%	92.54%	91.78%	91.18%	93.06%	0.09	0.92
	KNN	88.21%	87.05%	89.36%	88.97%	87.50%	0.11	0.9
	BN	89.29%	88.41%	90.14%	89.71%	88.89%	0.10	0.91
Overlapped-DTW-3L	SVM	71.43%	70.00%	72.86%	72.06%	70.83%	0.28	0.71
	KNN	68.93%	65.03%	74.36%	77.94%	60.42%	0.33	0.7
	BN	74.05%	70.56%	78.31%	79.90%	68.52%	0.21	0.77
Overlapped-DTW-4L	SVM	78.57%	77.14%	80.00%	79.41%	77.78%	0.21	0.79
	KNN	76.43%	74.65%	78.26%	77.94%	75.00%	0.24	0.78
	BN	80.95%	79.81%	82.08%	81.37%	80.56%	0.19	0.83
Overlapped-DTW-5L	SVM	85.71%	84.29%	87.14%	86.76%	84.72%	0.14	0.86
	KNN	79.64%	76.16%	83.72%	84.56%	75.00%	0.22	0.83
	BN	83.10%	79.30%	87.56%	88.24%	78.24%	0.12	0.87
Overlapped-DTW-6L	SVM	87.86%	89.23%	86.67%	85.29%	90.28%	0.14	0.88
	KNN	79.29%	79.55%	79.05%	77.21%	81.25%	0.22	0.84
	BN	81.43%	81.19%	81.65%	80.39%	82.41%	0.18	0.87
Overlapped-LCS-3L	SVM	75.71%	75.76%	75.68%	73.53%	77.78%	0.25	0.76
	KNN	76.07%	75.56%	76.55%	75.00%	77.08%	0.25	0.76
	BN	79.29%	79.40%	79.19%	77.45%	81.02%	0.19	0.81
Overlapped-LCS-4L	SVM	90.00%	89.71%	90.28%	89.71%	90.28%	0.10	0.9
	KNN	86.79%	85.11%	88.49%	88.24%	85.42%	0.12	0.88
	BN	85.95%	82.81%	89.45%	89.71%	82.41%	0.11	0.89
Overlapped-LCS-5L	SVM	83.57%	82.61%	84.51%	83.82%	83.33%	0.16	0.84
	KNN	75.36%	78.15%	73.29%	68.38%	81.94%	0.22	0.79
	BN	78.10%	80.11%	76.50%	73.04%	82.87%	0.19	0.83
Overlapped-LCS-6L	SVM	85.00%	87.30%	83.12%	80.88%	88.89%	0.18	0.85
	KNN	77.14%	80.51%	74.69%	69.85%	84.03%	0.25	0.81
	BN	80.71%	83.98%	78.24%	74.51%	86.57%	0.14	0.86
Overlapped-KLD-3L	SVM	73.57%	74.60%	72.73%	69.12%	77.78%	0.28	0.73
	KNN	71.07%	67.52%	75.61%	77.94%	64.58%	0.25	0.72
	BN	75.48%	72.85%	78.39%	78.92%	72.22%	0.22	0.78
Overlapped-KLD-4L	SVM	80.71%	78.87%	82.61%	82.35%	79.17%	0.18	0.81
	KNN	79.29%	77.08%	81.62%	81.62%	77.08%	0.22	0.8
	BN	82.86%	80.28%	85.64%	85.78%	80.09%	0.16	0.84
Overlapped-KLD-5L	SVM	88.57%	87.14%	90.00%	89.71%	87.50%	0.11	0.89
	KNN	82.86%	80.56%	85.29%	85.29%	80.56%	0.18	0.86
	BN	86.19%	83.49%	89.11%	89.22%	83.33%	0.11	0.89
Overlapped-KLD-6L	SVM	80.71%	82.54%	79.22%	76.47%	84.72%	0.22	0.81
	KNN	79.64%	82.11%	77.71%	74.26%	84.72%	0.23	0.8
	BN	83.10%	84.10%	82.22%	80.39%	85.65%	0.19	0.85

Table A.2: The results using VCM with PCA.

Method	Classifiers	Acc	Sen	Spec	PPV	NPV	EER	AUC
Standard-0NCF-3L	SVM	91.43%	92.42%	90.54%	89.71%	93.06%	0.10	0.91
	KNN	86.07%	85.40%	86.71%	86.03%	86.11%	0.14	0.89
	BN	88.57%	87.50%	89.62%	89.22%	87.96%	0.11	0.92
Standard-0NCF-4L	SVM	90.00%	90.91%	89.19%	88.24%	91.67%	0.11	0.9
	KNN	84.29%	82.86%	85.71%	85.29%	83.33%	0.15	0.87
	BN	86.67%	84.58%	88.83%	88.73%	84.72%	0.14	0.89

Standard-0NCF-5L	SVM	90.00%	90.91%	89.19%	88.24%	91.67%	0.11	0.9
	KNN	84.64%	83.94%	85.31%	84.56%	84.72%	0.15	0.87
	BN	86.90%	85.65%	88.15%	87.75%	86.11%	0.14	0.9
Standard-0NCF-6L	SVM	90.00%	90.91%	89.19%	88.24%	91.67%	0.11	0.9
	KNN	85.71%	84.29%	87.14%	86.76%	84.72%	0.14	0.88
	BN	88.33%	86.73%	89.95%	89.71%	87.04%	0.12	0.91
Standard-AIV-3L	SVM	90.71%	88.73%	92.75%	92.65%	88.89%	0.08	0.91
	KNN	89.29%	86.30%	92.54%	92.65%	86.11%	0.13	0.9
	BN	90.95%	88.79%	93.20%	93.14%	88.89%	0.10	0.92
Standard-AIV-4L	SVM	92.14%	92.54%	91.78%	91.18%	93.06%	0.09	0.92
	KNN	86.43%	85.00%	87.86%	87.50%	85.42%	0.13	0.89
	BN	89.29%	87.32%	91.30%	91.18%	87.50%	0.12	0.92
Standard-AIV-5L	SVM	89.29%	89.55%	89.04%	88.24%	90.28%	0.12	0.89
	KNN	88.57%	88.24%	88.89%	88.24%	88.89%	0.12	0.89
	BN	90.24%	89.37%	91.08%	90.69%	89.81%	0.10	0.91
Standard-AIV-6L	SVM	92.14%	92.54%	91.78%	91.18%	93.06%	0.09	0.92
	KNN	85.71%	85.82%	85.62%	84.56%	86.81%	0.15	0.89
	BN	89.29%	88.78%	89.77%	89.22%	89.35%	0.11	0.93
Standard-GLCM-3L	SVM	88.57%	90.62%	86.84%	85.29%	91.67%	0.14	0.88
	KNN	86.07%	85.93%	86.21%	85.29%	86.81%	0.14	0.87
	BN	87.86%	87.32%	88.37%	87.75%	87.96%	0.12	0.9
Standard-GLCM-4L	SVM	92.14%	90.14%	94.20%	94.12%	90.28%	0.06	0.92
	KNN	87.50%	84.35%	90.98%	91.18%	84.03%	0.15	0.9
	BN	89.76%	86.76%	93.03%	93.14%	86.57%	0.12	0.92
Standard-GLCM-5L	SVM	92.14%	93.85%	90.67%	89.71%	94.44%	0.10	0.92
	KNN	90.36%	90.37%	90.34%	89.71%	90.97%	0.10	0.91
	BN	92.38%	92.16%	92.59%	92.16%	92.59%	0.08	0.93
Standard-GLCM-6L	SVM	89.29%	90.77%	88.00%	86.76%	91.67%	0.13	0.89
	KNN	87.50%	88.55%	86.58%	85.29%	89.58%	0.14	0.88
	BN	89.52%	89.60%	89.45%	88.73%	90.28%	0.10	0.91
Standard-KCC-3L	SVM	90.71%	91.04%	90.41%	89.71%	91.67%	0.10	0.91
	KNN	88.21%	86.52%	89.93%	89.71%	86.81%	0.11	0.89
	BN	89.76%	88.52%	91.00%	90.69%	88.89%	0.09	0.91
Standard-KCC-4L	SVM	95.71%	94.29%	97.14%	97.06%	94.44%	0.03	0.96
	KNN	92.86%	92.65%	93.06%	92.65%	93.06%	0.07	0.94
	BN	93.81%	92.79%	94.81%	94.61%	93.06%	0.06	0.95
Standard-KCC-5L	SVM	95.71%	95.59%	95.83%	95.59%	95.83%	0.04	0.96
	KNN	95.36%	95.56%	95.17%	94.85%	95.83%	0.05	0.96
	BN	95.95%	95.61%	96.28%	96.08%	95.83%	0.04	0.96
Standard-KCC-6L	SVM	95.00%	96.92%	93.33%	92.65%	97.22%	0.07	0.95
	KNN	91.79%	94.49%	89.54%	88.24%	95.14%	0.11	0.93
	BN	93.33%	95.36%	91.59%	90.69%	95.83%	0.04	0.95
Standard-ED-3L	SVM	91.43%	88.89%	94.12%	94.12%	88.89%	0.06	0.92
	KNN	90.00%	88.57%	91.43%	91.18%	88.89%	0.11	0.91
	BN	91.43%	90.00%	92.86%	92.65%	90.28%	0.10	0.93
Standard-ED-4L	SVM	93.57%	92.75%	94.37%	94.12%	93.06%	0.06	0.94
	KNN	93.57%	92.14%	95.00%	94.85%	92.36%	0.07	0.94
	BN	93.81%	91.98%	95.67%	95.59%	92.13%	0.08	0.94
Standard-ED-5L	SVM	95.00%	94.20%	95.77%	95.59%	94.44%	0.04	0.95
	KNN	93.93%	93.43%	94.41%	94.12%	93.75%	0.06	0.94
	BN	94.29%	92.86%	95.71%	95.59%	93.06%	0.07	0.95

Standard-ED-6L	SVM	96.43%	94.37%	98.55%	98.53%	94.44%	0.02	0.96
	KNN	95.00%	95.52%	94.52%	94.12%	95.83%	0.04	0.96
	BN	95.00%	94.20%	95.77%	95.59%	94.44%	0.04	0.96
Standard-DTW-3L	SVM	90.71%	91.04%	90.41%	89.71%	91.67%	0.10	0.91
	KNN	85.71%	85.29%	86.11%	85.29%	86.11%	0.15	0.88
	BN	88.33%	87.44%	89.20%	88.73%	87.96%	0.11	0.91
Standard-DTW-4L	SVM	85.00%	86.15%	84.00%	82.35%	87.50%	0.17	0.85
	KNN	81.79%	80.14%	83.45%	83.09%	80.56%	0.17	0.83
	BN	84.29%	83.17%	85.38%	84.80%	83.80%	0.16	0.86
Standard-DTW-5L	SVM	89.29%	90.77%	88.00%	86.76%	91.67%	0.13	0.89
	KNN	85.00%	82.64%	87.50%	87.50%	82.64%	0.13	0.87
	BN	87.86%	86.26%	89.47%	89.22%	86.57%	0.11	0.9
Standard-DTW-6L	SVM	94.29%	94.12%	94.44%	94.12%	94.44%	0.06	0.94
	KNN	89.29%	88.41%	90.14%	89.71%	88.89%	0.10	0.92
	BN	90.95%	89.90%	91.98%	91.67%	90.28%	0.08	0.94
Standard-LCS-3L	SVM	92.86%	93.94%	91.89%	91.18%	94.44%	0.09	0.93
	KNN	87.50%	89.15%	86.09%	84.56%	90.28%	0.14	0.9
	BN	90.71%	91.04%	90.41%	89.71%	91.67%	0.08	0.93
Standard-LCS-4L	SVM	88.57%	90.62%	86.84%	85.29%	91.67%	0.14	0.88
	KNN	89.64%	91.47%	88.08%	86.76%	92.36%	0.13	0.89
	BN	91.67%	92.04%	91.32%	90.69%	92.59%	0.07	0.92
Standard-LCS-5L	SVM	94.29%	96.88%	92.11%	91.18%	97.22%	0.08	0.94
	KNN	90.71%	92.97%	88.82%	87.50%	93.75%	0.12	0.92
	BN	92.38%	94.79%	90.35%	89.22%	95.37%	0.10	0.94
Standard-LCS-6L	SVM	94.29%	100.00%	90.00%	88.24%	100.00%	0.11	0.94
	KNN	90.71%	95.08%	87.34%	85.29%	95.83%	0.13	0.92
	BN	91.90%	95.21%	89.22%	87.75%	95.83%	0.12	0.94
Standard-KLD-3L	SVM	87.86%	88.06%	87.67%	86.76%	88.89%	0.13	0.88
	KNN	89.64%	87.94%	91.37%	91.18%	88.19%	0.09	0.89
	BN	90.48%	88.68%	92.31%	92.16%	88.89%	0.11	0.91
Standard-KLD-4L	SVM	89.29%	88.41%	90.14%	89.71%	88.89%	0.10	0.89
	KNN	85.36%	83.22%	87.59%	87.50%	83.33%	0.16	0.87
	BN	87.62%	85.19%	90.20%	90.20%	85.19%	0.15	0.9
Standard-KLD-5L	SVM	85.71%	88.71%	83.33%	80.88%	90.28%	0.17	0.86
	KNN	78.21%	78.20%	78.23%	76.47%	79.86%	0.23	0.82
	BN	82.14%	81.16%	83.10%	82.35%	81.94%	0.18	0.86
Standard-KLD-6L	SVM	88.57%	90.62%	86.84%	85.29%	91.67%	0.14	0.88
	KNN	85.00%	87.30%	83.12%	80.88%	88.89%	0.17	0.87
	BN	87.14%	87.50%	86.82%	85.78%	88.43%	0.12	0.89
Overlapped-0NCF-3L	SVM	84.29%	81.94%	86.76%	86.76%	81.94%	0.14	0.84
	KNN	82.50%	80.00%	85.19%	85.29%	79.86%	0.19	0.83
	BN	85.48%	83.26%	87.80%	87.75%	83.33%	0.17	0.87
Overlapped-0NCF-4L	SVM	84.29%	81.94%	86.76%	86.76%	81.94%	0.14	0.84
	KNN	82.50%	80.00%	85.19%	85.29%	79.86%	0.19	0.83
	BN	85.48%	83.26%	87.80%	87.75%	83.33%	0.17	0.87
Overlapped-0NCF-5L	SVM	84.29%	81.94%	86.76%	86.76%	81.94%	0.14	0.84
	KNN	82.50%	80.00%	85.19%	85.29%	79.86%	0.19	0.83
	BN	85.48%	83.26%	87.80%	87.75%	83.33%	0.17	0.87
Overlapped-0NCF-6L	SVM	84.29%	81.94%	86.76%	86.76%	81.94%	0.14	0.84
	KNN	82.50%	80.00%	85.19%	85.29%	79.86%	0.19	0.83
	BN	85.48%	83.26%	87.80%	87.75%	83.33%	0.17	0.87

Overlapped-AIV-3L	SVM	90.71%	91.04%	90.41%	89.71%	91.67%	0.10	0.91
	KNN	85.71%	83.33%	88.24%	88.24%	83.33%	0.12	0.88
	BN	87.86%	86.26%	89.47%	89.22%	86.57%	0.13	0.91
Overlapped-AIV-4L	SVM	82.86%	84.38%	81.58%	79.41%	86.11%	0.19	0.83
	KNN	80.36%	85.22%	76.97%	72.06%	88.19%	0.23	0.81
	BN	83.57%	86.10%	81.55%	78.92%	87.96%	0.21	0.85
Overlapped-AIV-5L	SVM	82.86%	84.38%	81.58%	79.41%	86.11%	0.19	0.83
	KNN	80.36%	85.22%	76.97%	72.06%	88.19%	0.23	0.81
	BN	83.57%	86.10%	81.55%	78.92%	87.96%	0.21	0.85
Overlapped-AIV-6L	SVM	82.86%	84.38%	81.58%	79.41%	86.11%	0.19	0.83
	KNN	80.36%	85.22%	76.97%	72.06%	88.19%	0.23	0.81
	BN	83.57%	86.10%	81.55%	78.92%	87.96%	0.21	0.85
Overlapped-GLCM-3L	SVM	87.14%	86.76%	87.50%	86.76%	87.50%	0.13	0.87
	KNN	86.43%	84.03%	88.97%	88.97%	84.03%	0.12	0.87
	BN	88.81%	86.85%	90.82%	90.69%	87.04%	0.09	0.9
Overlapped-GLCM-4L	SVM	88.57%	89.39%	87.84%	86.76%	90.28%	0.13	0.89
	KNN	86.43%	87.69%	85.33%	83.82%	88.89%	0.15	0.87
	BN	86.67%	87.37%	86.04%	84.80%	88.43%	0.15	0.89
Overlapped-GLCM-5L	SVM	89.29%	90.77%	88.00%	86.76%	91.67%	0.13	0.89
	KNN	86.79%	88.37%	85.43%	83.82%	89.58%	0.15	0.88
	BN	87.14%	88.27%	86.16%	84.80%	89.35%	0.15	0.89
Overlapped-GLCM-6L	SVM	89.29%	90.77%	88.00%	86.76%	91.67%	0.13	0.89
	KNN	86.79%	88.37%	85.43%	83.82%	89.58%	0.15	0.88
	BN	87.14%	88.27%	86.16%	84.80%	89.35%	0.15	0.89
Overlapped-KCC-3L	SVM	93.57%	94.03%	93.15%	92.65%	94.44%	0.07	0.94
	KNN	92.14%	91.30%	92.96%	92.65%	91.67%	0.07	0.93
	BN	93.10%	91.87%	94.31%	94.12%	92.13%	0.08	0.94
Overlapped-KCC-4L	SVM	87.14%	91.67%	83.75%	80.88%	93.06%	0.17	0.87
	KNN	83.21%	89.38%	79.04%	74.26%	91.67%	0.21	0.85
	BN	85.24%	89.01%	82.35%	79.41%	90.74%	0.09	0.88
Overlapped-KCC-5L	SVM	85.71%	90.00%	82.50%	79.41%	91.67%	0.18	0.86
	KNN	81.79%	87.61%	77.84%	72.79%	90.28%	0.22	0.84
	BN	84.29%	87.91%	81.51%	78.43%	89.81%	0.22	0.86
Overlapped-KCC-6L	SVM	87.14%	89.06%	85.53%	83.82%	90.28%	0.15	0.87
	KNN	81.79%	85.12%	79.25%	75.74%	87.50%	0.21	0.84
	BN	84.05%	85.86%	82.53%	80.39%	87.50%	0.20	0.87
Overlapped-ED-3L	SVM	87.86%	86.96%	88.73%	88.24%	87.50%	0.12	0.88
	KNN	81.79%	77.78%	86.61%	87.50%	76.39%	0.20	0.85
	BN	86.43%	83.26%	89.95%	90.20%	82.87%	0.17	0.9
Overlapped-ED-4L	SVM	90.00%	89.71%	90.28%	89.71%	90.28%	0.10	0.9
	KNN	83.21%	81.12%	85.40%	85.29%	81.25%	0.16	0.87
	BN	85.95%	83.72%	88.29%	88.24%	83.80%	0.12	0.89
Overlapped-ED-5L	SVM	85.71%	84.29%	87.14%	86.76%	84.72%	0.14	0.86
	KNN	81.07%	79.02%	83.21%	83.09%	79.17%	0.20	0.83
	BN	83.57%	81.40%	85.85%	85.78%	81.48%	0.15	0.87
Overlapped-ED-6L	SVM	85.71%	84.29%	87.14%	86.76%	84.72%	0.14	0.86
	KNN	81.07%	79.02%	83.21%	83.09%	79.17%	0.20	0.83
	BN	83.57%	81.40%	85.85%	85.78%	81.48%	0.15	0.87
Overlapped-DTW-3L	SVM	84.29%	81.08%	87.88%	88.24%	80.56%	0.13	0.84
	KNN	82.50%	79.19%	86.26%	86.76%	78.47%	0.20	0.84
	BN	85.00%	82.19%	88.06%	88.24%	81.94%	0.12	0.87

Overlapped-DTW-4L	SVM	85.71%	84.29%	87.14%	86.76%	84.72%	0.14	0.86
	KNN	83.93%	81.82%	86.13%	86.03%	81.94%	0.17	0.85
	BN	86.43%	84.51%	88.41%	88.24%	84.72%	0.15	0.88
Overlapped-DTW-5L	SVM	85.71%	84.29%	87.14%	86.76%	84.72%	0.14	0.86
	KNN	83.93%	81.82%	86.13%	86.03%	81.94%	0.17	0.85
	BN	86.43%	84.51%	88.41%	88.24%	84.72%	0.15	0.88
Overlapped-DTW-6L	SVM	85.71%	84.29%	87.14%	86.76%	84.72%	0.14	0.86
	KNN	83.93%	81.82%	86.13%	86.03%	81.94%	0.17	0.85
	BN	86.43%	84.51%	88.41%	88.24%	84.72%	0.15	0.88
Overlapped-LCS-3L	SVM	88.57%	89.39%	87.84%	86.76%	90.28%	0.13	0.89
	KNN	86.07%	85.93%	86.21%	85.29%	86.81%	0.14	0.87
	BN	88.10%	87.75%	88.43%	87.75%	88.43%	0.12	0.9
Overlapped-LCS-4L	SVM	83.57%	85.71%	81.82%	79.41%	87.50%	0.19	0.83
	KNN	78.93%	85.32%	74.85%	68.38%	88.89%	0.25	0.81
	BN	79.05%	81.52%	77.12%	73.53%	84.26%	0.26	0.83
Overlapped-LCS-5L	SVM	83.57%	85.71%	81.82%	79.41%	87.50%	0.19	0.83
	KNN	78.93%	85.32%	74.85%	68.38%	88.89%	0.25	0.81
	BN	79.52%	82.42%	77.31%	73.53%	85.19%	0.15	0.83
Overlapped-LCS-6L	SVM	83.57%	85.71%	81.82%	79.41%	87.50%	0.19	0.83
	KNN	78.93%	85.32%	74.85%	68.38%	88.89%	0.25	0.81
	BN	79.52%	82.42%	77.31%	73.53%	85.19%	0.15	0.83
Overlapped-KLD-3L	SVM	85.71%	86.36%	85.14%	83.82%	87.50%	0.16	0.86
	KNN	82.14%	81.16%	83.10%	82.35%	81.94%	0.18	0.84
	BN	85.24%	83.81%	86.67%	86.27%	84.26%	0.15	0.87
Overlapped-KLD-4L	SVM	84.29%	83.82%	84.72%	83.82%	84.72%	0.16	0.84
	KNN	85.36%	83.22%	87.59%	87.50%	83.33%	0.13	0.85
	BN	87.14%	85.05%	89.32%	89.22%	85.19%	0.14	0.87
Overlapped-KLD-5L	SVM	84.29%	83.82%	84.72%	83.82%	84.72%	0.16	0.84
	KNN	85.36%	83.22%	87.59%	87.50%	83.33%	0.13	0.85
	BN	87.14%	85.05%	89.32%	89.22%	85.19%	0.14	0.87
Overlapped-KLD-6L	SVM	84.29%	83.82%	84.72%	83.82%	84.72%	0.16	0.84
	KNN	85.36%	83.22%	87.59%	87.50%	83.33%	0.13	0.85
	BN	87.14%	85.05%	89.32%	89.22%	85.19%	0.14	0.87

Table A.3: The results using VRLM with PCA.

Method	Classifiers	Acc	Sen	Spec	PPV	NPV	EER	AUC
Standard-0NCF-3L	SVM	89.29%	93.44%	86.08%	83.82%	94.44%	0.15	0.89
	KNN	83.93%	87.60%	81.13%	77.94%	89.58%	0.19	0.86
	BN	85.48%	89.50%	82.43%	79.41%	91.20%	0.09	0.89
Standard-0NCF-4L	SVM	89.29%	90.77%	88.00%	86.76%	91.67%	0.13	0.89
	KNN	83.93%	84.73%	83.22%	81.62%	86.11%	0.17	0.87
	BN	84.76%	86.08%	83.63%	81.86%	87.50%	0.12	0.88
Standard-0NCF-5L	SVM	87.14%	87.88%	86.49%	85.29%	88.89%	0.14	0.87
	KNN	82.14%	84.13%	80.52%	77.94%	86.11%	0.20	0.85
	BN	82.38%	83.85%	81.14%	78.92%	85.65%	0.14	0.86
Standard-0NCF-6L	SVM	85.71%	88.71%	83.33%	80.88%	90.28%	0.17	0.86
	KNN	80.71%	84.17%	78.12%	74.26%	86.81%	0.22	0.83
	BN	81.19%	83.42%	79.40%	76.47%	85.65%	0.24	0.85

Standard-AIV-3L	SVM	88.57%	93.33%	85.00%	82.35%	94.44%	0.16	0.88
	KNN	85.36%	89.92%	81.99%	78.68%	91.67%	0.18	0.87
	BN	86.90%	90.71%	83.97%	81.37%	92.13%	0.09	0.89
Standard-AIV-4L	SVM	80.71%	82.54%	79.22%	76.47%	84.72%	0.22	0.81
	KNN	80.71%	84.17%	78.12%	74.26%	86.81%	0.23	0.81
	BN	81.43%	85.00%	78.75%	75.00%	87.50%	0.12	0.83
Standard-AIV-5L	SVM	89.29%	92.06%	87.01%	85.29%	93.06%	0.14	0.89
	KNN	81.07%	85.47%	77.91%	73.53%	88.19%	0.22	0.85
	BN	82.38%	86.11%	79.58%	75.98%	88.43%	0.23	0.87
Standard-AIV-6L	SVM	86.43%	91.53%	82.72%	79.41%	93.06%	0.18	0.86
	KNN	82.50%	87.83%	78.79%	74.26%	90.28%	0.22	0.84
	BN	83.33%	87.22%	80.42%	76.96%	89.35%	0.23	0.86
Standard-GLCM-3L	SVM	87.86%	94.74%	83.13%	79.41%	95.83%	0.18	0.88
	KNN	83.93%	88.89%	80.37%	76.47%	90.97%	0.20	0.86
	BN	84.76%	89.77%	81.15%	77.45%	91.67%	0.22	0.87
Standard-GLCM-4L	SVM	86.43%	85.51%	87.32%	86.76%	86.11%	0.13	0.86
	KNN	77.86%	78.03%	77.70%	75.74%	79.86%	0.21	0.82
	BN	80.95%	81.96%	80.09%	77.94%	83.80%	0.22	0.86
Standard-GLCM-5L	SVM	87.86%	86.96%	88.73%	88.24%	87.50%	0.12	0.88
	KNN	82.14%	82.58%	81.76%	80.15%	84.03%	0.17	0.85
	BN	83.10%	84.10%	82.22%	80.39%	85.65%	0.15	0.87
Standard-GLCM-6L	SVM	87.14%	87.88%	86.49%	85.29%	88.89%	0.14	0.87
	KNN	84.29%	85.38%	83.33%	81.62%	86.81%	0.17	0.86
	BN	85.48%	86.29%	84.75%	83.33%	87.50%	0.17	0.87
Standard-KCC-3L	SVM	92.86%	95.31%	90.79%	89.71%	95.83%	0.10	0.93
	KNN	87.86%	91.80%	84.81%	82.35%	93.06%	0.15	0.9
	BN	87.86%	90.48%	85.71%	83.82%	91.67%	0.08	0.91
Standard-KCC-4L	SVM	93.57%	94.03%	93.15%	92.65%	94.44%	0.07	0.94
	KNN	92.86%	93.28%	92.47%	91.91%	93.75%	0.08	0.93
	BN	92.14%	91.71%	92.56%	92.16%	92.13%	0.08	0.94
Standard-KCC-5L	SVM	87.14%	90.32%	84.62%	82.35%	91.67%	0.16	0.87
	KNN	86.79%	89.60%	84.52%	82.35%	90.97%	0.16	0.87
	BN	86.90%	86.34%	87.44%	86.76%	87.04%	0.13	0.88
Standard-KCC-6L	SVM	88.57%	90.62%	86.84%	85.29%	91.67%	0.14	0.88
	KNN	87.86%	89.84%	86.18%	84.56%	90.97%	0.14	0.88
	BN	87.86%	88.83%	87.00%	85.78%	89.81%	0.14	0.88
Standard-ED-3L	SVM	90.71%	92.31%	89.33%	88.24%	93.06%	0.11	0.91
	KNN	84.29%	88.98%	80.86%	77.21%	90.97%	0.19	0.87
	BN	85.95%	89.62%	83.12%	80.39%	91.20%	0.09	0.9
Standard-ED-4L	SVM	91.43%	91.18%	91.67%	91.18%	91.67%	0.09	0.91
	KNN	88.93%	90.08%	87.92%	86.76%	90.97%	0.13	0.9
	BN	91.19%	91.54%	90.87%	90.20%	92.13%	0.10	0.93
Standard-ED-5L	SVM	85.00%	87.30%	83.12%	80.88%	88.89%	0.18	0.85
	KNN	83.57%	87.50%	80.62%	77.21%	89.58%	0.20	0.84
	BN	86.67%	90.22%	83.90%	81.37%	91.67%	0.08	0.88
Standard-ED-6L	SVM	92.14%	95.24%	89.61%	88.24%	95.83%	0.11	0.92
	KNN	91.79%	95.20%	89.03%	87.50%	95.83%	0.11	0.92
	BN	91.43%	93.75%	89.47%	88.24%	94.44%	0.06	0.92
Standard-DTW-3L	SVM	90.00%	95.00%	86.25%	83.82%	95.83%	0.14	0.9
	KNN	83.93%	87.60%	81.13%	77.94%	89.58%	0.19	0.87
	BN	85.48%	89.50%	82.43%	79.41%	91.20%	0.09	0.89

Standard-DTW-4L	SVM	90.71%	92.31%	89.33%	88.24%	93.06%	0.11	0.91
	KNN	86.79%	88.98%	84.97%	83.09%	90.28%	0.15	0.89
	BN	86.19%	88.83%	84.05%	81.86%	90.28%	0.10	0.89
Standard-DTW-5L	SVM	91.43%	93.75%	89.47%	88.24%	94.44%	0.11	0.91
	KNN	87.50%	90.40%	85.16%	83.09%	91.67%	0.15	0.89
	BN	87.86%	90.05%	86.03%	84.31%	91.20%	0.16	0.9
Standard-DTW-6L	SVM	86.43%	87.69%	85.33%	83.82%	88.89%	0.15	0.86
	KNN	80.00%	83.90%	77.16%	72.79%	86.81%	0.23	0.83
	BN	80.71%	83.98%	78.24%	74.51%	86.57%	0.25	0.85
Standard-LCS-3L	SVM	86.43%	90.16%	83.54%	80.88%	91.67%	0.17	0.86
	KNN	84.64%	89.08%	81.37%	77.94%	90.97%	0.19	0.85
	BN	87.86%	91.80%	84.81%	82.35%	93.06%	0.07	0.89
Standard-LCS-4L	SVM	93.57%	92.75%	94.37%	94.12%	93.06%	0.06	0.94
	KNN	88.93%	89.47%	88.44%	87.50%	90.28%	0.10	0.91
	BN	89.52%	90.00%	89.09%	88.24%	90.74%	0.10	0.93
Standard-LCS-5L	SVM	96.43%	98.46%	94.67%	94.12%	98.61%	0.06	0.96
	KNN	91.79%	95.93%	88.54%	86.76%	96.53%	0.11	0.94
	BN	92.62%	94.36%	91.11%	90.20%	94.91%	0.10	0.95
Standard-LCS-6L	SVM	88.57%	90.62%	86.84%	85.29%	91.67%	0.14	0.88
	KNN	85.00%	87.90%	82.69%	80.15%	89.58%	0.18	0.87
	BN	88.33%	90.58%	86.46%	84.80%	91.67%	0.15	0.9
Standard-KLD-3L	SVM	95.00%	92.96%	97.10%	97.06%	93.06%	0.03	0.95
	KNN	91.43%	91.79%	91.10%	90.44%	92.36%	0.08	0.93
	BN	92.14%	93.40%	91.03%	90.20%	93.98%	0.07	0.95
Standard-KLD-4L	SVM	87.86%	90.48%	85.71%	83.82%	91.67%	0.15	0.88
	KNN	81.43%	85.59%	78.40%	74.26%	88.19%	0.22	0.84
	BN	81.67%	84.32%	79.57%	76.47%	86.57%	0.23	0.86
Standard-KLD-5L	SVM	85.00%	88.52%	82.28%	79.41%	90.28%	0.19	0.85
	KNN	81.07%	84.87%	78.26%	74.26%	87.50%	0.22	0.83
	BN	81.43%	83.87%	79.49%	76.47%	86.11%	0.24	0.84
Standard-KLD-6L	SVM	79.29%	79.10%	79.45%	77.94%	80.56%	0.21	0.79
	KNN	77.86%	78.03%	77.70%	75.74%	79.86%	0.23	0.79
	BN	78.10%	78.57%	77.68%	75.49%	80.56%	0.19	0.81
Overlapped-0NCF-3L	SVM	90.00%	93.55%	87.18%	85.29%	94.44%	0.13	0.9
	KNN	83.93%	86.40%	81.94%	79.41%	88.19%	0.18	0.87
	BN	83.33%	85.64%	81.47%	78.92%	87.50%	0.21	0.87
Overlapped-0NCF-4L	SVM	90.00%	93.55%	87.18%	85.29%	94.44%	0.13	0.9
	KNN	83.93%	86.40%	81.94%	79.41%	88.19%	0.18	0.87
	BN	83.33%	85.64%	81.47%	78.92%	87.50%	0.21	0.87
Overlapped-0NCF-5L	SVM	90.00%	93.55%	87.18%	85.29%	94.44%	0.13	0.9
	KNN	83.93%	86.40%	81.94%	79.41%	88.19%	0.18	0.87
	BN	83.33%	85.64%	81.47%	78.92%	87.50%	0.21	0.87
Overlapped-0NCF-6L	SVM	90.00%	93.55%	87.18%	85.29%	94.44%	0.13	0.9
	KNN	83.93%	86.40%	81.94%	79.41%	88.19%	0.18	0.87
	BN	83.33%	85.64%	81.47%	78.92%	87.50%	0.21	0.87
Overlapped-AIV-3L	SVM	90.71%	91.04%	90.41%	89.71%	91.67%	0.10	0.91
	KNN	86.43%	90.16%	83.54%	80.88%	91.67%	0.17	0.88
	BN	86.90%	90.27%	84.26%	81.86%	91.67%	0.08	0.9
Overlapped-AIV-4L	SVM	87.14%	90.32%	84.62%	82.35%	91.67%	0.16	0.87
	KNN	83.21%	88.03%	79.75%	75.74%	90.28%	0.21	0.85
	BN	83.10%	86.74%	80.33%	76.96%	88.89%	0.23	0.86

Overlapped-AIV-5L	SVM	87.14%	90.32%	84.62%	82.35%	91.67%	0.16	0.87
	KNN	83.21%	88.03%	79.75%	75.74%	90.28%	0.21	0.85
	BN	83.10%	86.74%	80.33%	76.96%	88.89%	0.23	0.86
Overlapped-AIV-6L	SVM	87.14%	90.32%	84.62%	82.35%	91.67%	0.16	0.87
	KNN	83.21%	88.03%	79.75%	75.74%	90.28%	0.21	0.85
	BN	83.10%	86.74%	80.33%	76.96%	88.89%	0.23	0.86
Overlapped-GLCM-3L	SVM	85.00%	87.30%	83.12%	80.88%	88.89%	0.18	0.85
	KNN	81.43%	86.21%	78.05%	73.53%	88.89%	0.22	0.83
	BN	81.43%	86.21%	78.05%	73.53%	88.89%	0.12	0.84
Overlapped-GLCM-4L	SVM	87.14%	90.32%	84.62%	82.35%	91.67%	0.16	0.87
	KNN	82.50%	87.83%	78.79%	74.26%	90.28%	0.21	0.85
	BN	81.90%	86.36%	78.69%	74.51%	88.89%	0.24	0.85
Overlapped-GLCM-5L	SVM	87.14%	90.32%	84.62%	82.35%	91.67%	0.16	0.87
	KNN	82.50%	87.83%	78.79%	74.26%	90.28%	0.21	0.85
	BN	81.90%	86.36%	78.69%	74.51%	88.89%	0.24	0.85
Overlapped-GLCM-6L	SVM	87.14%	90.32%	84.62%	82.35%	91.67%	0.16	0.87
	KNN	82.50%	87.83%	78.79%	74.26%	90.28%	0.21	0.85
	BN	81.90%	86.36%	78.69%	74.51%	88.89%	0.24	0.85
Overlapped-KCC-3L	SVM	90.71%	93.65%	88.31%	86.76%	94.44%	0.12	0.91
	KNN	88.21%	93.28%	84.47%	81.62%	94.44%	0.16	0.89
	BN	86.43%	89.30%	84.12%	81.86%	90.74%	0.09	0.89
Overlapped-KCC-4L	SVM	84.29%	87.10%	82.05%	79.41%	88.89%	0.19	0.84
	KNN	82.14%	85.25%	79.75%	76.47%	87.50%	0.21	0.83
	BN	83.33%	86.02%	81.20%	78.43%	87.96%	0.22	0.85
Overlapped-KCC-5L	SVM	84.29%	87.10%	82.05%	79.41%	88.89%	0.19	0.84
	KNN	82.86%	86.07%	80.38%	77.21%	88.19%	0.20	0.83
	BN	83.33%	86.02%	81.20%	78.43%	87.96%	0.22	0.85
Overlapped-KCC-6L	SVM	83.57%	84.62%	82.67%	80.88%	86.11%	0.18	0.83
	KNN	81.79%	84.00%	80.00%	77.21%	86.11%	0.21	0.83
	BN	82.86%	85.11%	81.03%	78.43%	87.04%	0.22	0.84
Overlapped-ED-3L	SVM	85.71%	86.36%	85.14%	83.82%	87.50%	0.16	0.86
	KNN	83.57%	85.16%	82.24%	80.15%	86.81%	0.18	0.85
	BN	83.57%	86.49%	81.28%	78.43%	88.43%	0.12	0.87
Overlapped-ED-4L	SVM	84.29%	84.85%	83.78%	82.35%	86.11%	0.17	0.84
	KNN	81.79%	81.48%	82.07%	80.88%	82.64%	0.19	0.83
	BN	82.62%	82.27%	82.95%	81.86%	83.33%	0.18	0.85
Overlapped-ED-5L	SVM	85.71%	86.36%	85.14%	83.82%	87.50%	0.16	0.86
	KNN	82.50%	82.22%	82.76%	81.62%	83.33%	0.18	0.84
	BN	83.57%	83.25%	83.87%	82.84%	84.26%	0.17	0.86
Overlapped-ED-6L	SVM	85.71%	86.36%	85.14%	83.82%	87.50%	0.16	0.86
	KNN	82.50%	82.22%	82.76%	81.62%	83.33%	0.18	0.84
	BN	83.57%	83.25%	83.87%	82.84%	84.26%	0.17	0.86
Overlapped-DTW-3L	SVM	90.00%	93.55%	87.18%	85.29%	94.44%	0.13	0.9
	KNN	83.57%	86.29%	81.41%	78.68%	88.19%	0.19	0.87
	BN	83.33%	85.64%	81.47%	78.92%	87.50%	0.21	0.87
Overlapped-DTW-4L	SVM	90.00%	93.55%	87.18%	85.29%	94.44%	0.13	0.9
	KNN	83.93%	86.40%	81.94%	79.41%	88.19%	0.18	0.87
	BN	83.33%	85.64%	81.47%	78.92%	87.50%	0.21	0.87
Overlapped-DTW-5L	SVM	90.00%	93.55%	87.18%	85.29%	94.44%	0.13	0.9
	KNN	83.93%	86.40%	81.94%	79.41%	88.19%	0.18	0.87
	BN	83.33%	85.64%	81.47%	78.92%	87.50%	0.21	0.87

Overlapped-DTW-6L	SVM	90.00%	93.55%	87.18%	85.29%	94.44%	0.13	0.9
	KNN	83.93%	86.40%	81.94%	79.41%	88.19%	0.18	0.87
	BN	83.33%	85.64%	81.47%	78.92%	87.50%	0.21	0.87
Overlapped-LCS-3L	SVM	86.43%	86.57%	86.30%	85.29%	87.50%	0.14	0.86
	KNN	85.36%	87.40%	83.66%	81.62%	88.89%	0.17	0.86
	BN	86.19%	88.83%	84.05%	81.86%	90.28%	0.10	0.88
Overlapped-LCS-4L	SVM	88.57%	88.24%	88.89%	88.24%	88.89%	0.12	0.89
	KNN	81.43%	83.33%	79.87%	77.21%	85.42%	0.20	0.85
	BN	81.67%	82.23%	81.17%	79.41%	83.80%	0.17	0.86
Overlapped-LCS-5L	SVM	87.14%	87.88%	86.49%	85.29%	88.89%	0.14	0.87
	KNN	81.07%	83.20%	79.35%	76.47%	85.42%	0.21	0.84
	BN	81.19%	82.05%	80.44%	78.43%	83.80%	0.17	0.86
Overlapped-LCS-6L	SVM	87.14%	87.88%	86.49%	85.29%	88.89%	0.14	0.87
	KNN	81.07%	83.20%	79.35%	76.47%	85.42%	0.21	0.84
	BN	81.19%	82.05%	80.44%	78.43%	83.80%	0.17	0.86
Overlapped-KLD-3L	SVM	90.00%	90.91%	89.19%	88.24%	91.67%	0.11	0.9
	KNN	83.57%	84.62%	82.67%	80.88%	86.11%	0.18	0.87
	BN	83.57%	84.97%	82.38%	80.39%	86.57%	0.20	0.87
Overlapped-KLD-4L	SVM	88.57%	90.62%	86.84%	85.29%	91.67%	0.14	0.88
	KNN	82.86%	85.48%	80.77%	77.94%	87.50%	0.20	0.86
	BN	82.62%	85.03%	80.69%	77.94%	87.04%	0.13	0.86
Overlapped-KLD-5L	SVM	88.57%	90.62%	86.84%	85.29%	91.67%	0.14	0.88
	KNN	82.86%	85.48%	80.77%	77.94%	87.50%	0.20	0.86
	BN	82.62%	85.03%	80.69%	77.94%	87.04%	0.13	0.86
Overlapped-KLD-6L	SVM	88.57%	90.62%	86.84%	85.29%	91.67%	0.14	0.88
	KNN	82.86%	85.48%	80.77%	77.94%	87.50%	0.20	0.86
	BN	82.62%	85.03%	80.69%	77.94%	87.04%	0.13	0.86

Table A.4: The results using HOG with PCA.

Method	Classifiers	Acc	Sen	Spec	PPV	NPV	EER	AUC
Standard-0NCF-3L	SVM	89.29%	92.06%	87.01%	85.29%	93.06%	0.14	0.89
	KNN	79.64%	84.35%	76.36%	71.32%	87.50%	0.23	0.84
	BN	83.57%	87.71%	80.50%	76.96%	89.81%	0.23	0.88
Standard-0NCF-4L	SVM	92.86%	95.31%	90.79%	89.71%	95.83%	0.10	0.93
	KNN	81.79%	85.71%	78.88%	75.00%	88.19%	0.21	0.87
	BN	84.76%	88.04%	82.20%	79.41%	89.81%	0.11	0.9
Standard-0NCF-5L	SVM	92.14%	95.24%	89.61%	88.24%	95.83%	0.11	0.92
	KNN	82.50%	86.55%	79.50%	75.74%	88.89%	0.20	0.87
	BN	85.24%	88.59%	82.63%	79.90%	90.28%	0.17	0.9
Standard-0NCF-6L	SVM	92.14%	95.24%	89.61%	88.24%	95.83%	0.11	0.92
	KNN	82.50%	86.55%	79.50%	75.74%	88.89%	0.20	0.87
	BN	85.24%	88.59%	82.63%	79.90%	90.28%	0.17	0.9
Standard-AIV-3L	SVM	92.86%	98.33%	88.75%	86.76%	98.61%	0.12	0.93
	KNN	86.07%	91.45%	82.21%	78.68%	93.06%	0.18	0.89
	BN	89.05%	92.93%	86.02%	83.82%	93.98%	0.16	0.92
Standard-AIV-4L	SVM	91.43%	96.67%	87.50%	85.29%	97.22%	0.13	0.91
	KNN	85.00%	89.17%	81.88%	78.68%	90.97%	0.18	0.88
	BN	87.14%	90.32%	84.62%	82.35%	91.67%	0.08	0.9

Standard-AIV-5L	SVM	91.43%	93.75%	89.47%	88.24%	94.44%	0.11	0.91
	KNN	81.07%	83.20%	79.35%	76.47%	85.42%	0.21	0.86
	BN	84.29%	85.94%	82.89%	80.88%	87.50%	0.19	0.89
Standard-AIV-6L	SVM	91.43%	93.75%	89.47%	88.24%	94.44%	0.11	0.91
	KNN	81.07%	83.20%	79.35%	76.47%	85.42%	0.21	0.86
	BN	84.29%	85.94%	82.89%	80.88%	87.50%	0.19	0.89
Standard-GLCM-3L	SVM	89.29%	92.06%	87.01%	85.29%	93.06%	0.14	0.89
	KNN	80.71%	84.75%	77.78%	73.53%	87.50%	0.22	0.85
	BN	84.05%	87.43%	81.43%	78.43%	89.35%	0.11	0.88
Standard-GLCM-4L	SVM	87.14%	90.32%	84.62%	82.35%	91.67%	0.16	0.87
	KNN	79.29%	82.50%	76.88%	72.79%	85.42%	0.23	0.83
	BN	83.10%	86.34%	80.59%	77.45%	88.43%	0.23	0.87
Standard-GLCM-5L	SVM	91.43%	95.16%	88.46%	86.76%	95.83%	0.12	0.91
	KNN	82.14%	85.83%	79.38%	75.74%	88.19%	0.20	0.87
	BN	85.24%	88.59%	82.63%	79.90%	90.28%	0.20	0.9
Standard-GLCM-6L	SVM	91.43%	95.16%	88.46%	86.76%	95.83%	0.12	0.91
	KNN	82.14%	85.83%	79.38%	75.74%	88.19%	0.20	0.87
	BN	85.24%	88.59%	82.63%	79.90%	90.28%	0.10	0.9
Standard-KCC-3L	SVM	90.00%	95.00%	86.25%	83.82%	95.83%	0.14	0.9
	KNN	82.86%	90.74%	77.91%	72.06%	93.06%	0.22	0.86
	BN	86.43%	92.98%	81.93%	77.94%	94.44%	0.06	0.9
Standard-KCC-4L	SVM	93.57%	98.36%	89.87%	88.24%	98.61%	0.11	0.93
	KNN	86.07%	94.50%	80.70%	75.74%	95.83%	0.19	0.9
	BN	87.62%	93.68%	83.33%	79.90%	94.91%	0.20	0.91
Standard-KCC-5L	SVM	89.29%	94.92%	85.19%	82.35%	95.83%	0.16	0.89
	KNN	81.43%	88.18%	77.06%	71.32%	90.97%	0.22	0.85
	BN	84.52%	89.27%	81.07%	77.45%	91.20%	0.23	0.89
Standard-KCC-6L	SVM	92.14%	95.24%	89.61%	88.24%	95.83%	0.11	0.92
	KNN	82.50%	89.19%	78.11%	72.79%	91.67%	0.21	0.87
	BN	84.76%	89.77%	81.15%	77.45%	91.67%	0.23	0.89
Standard-ED-3L	SVM	92.86%	98.33%	88.75%	86.76%	98.61%	0.12	0.93
	KNN	87.14%	91.67%	83.75%	80.88%	93.06%	0.16	0.9
	BN	88.57%	92.86%	85.29%	82.84%	93.98%	0.17	0.92
Standard-ED-4L	SVM	92.14%	98.31%	87.65%	85.29%	98.61%	0.13	0.92
	KNN	82.50%	86.55%	79.50%	75.74%	88.89%	0.20	0.87
	BN	85.71%	89.56%	82.77%	79.90%	91.20%	0.20	0.9
Standard-ED-5L	SVM	94.29%	100.00%	90.00%	88.24%	100.00%	0.11	0.94
	KNN	81.79%	84.55%	79.62%	76.47%	86.81%	0.20	0.88
	BN	84.29%	85.94%	82.89%	80.88%	87.50%	0.17	0.9
Standard-ED-6L	SVM	93.57%	98.36%	89.87%	88.24%	98.61%	0.11	0.93
	KNN	82.14%	85.25%	79.75%	76.47%	87.50%	0.20	0.88
	BN	84.52%	86.39%	82.97%	80.88%	87.96%	0.17	0.9
Standard-DTW-3L	SVM	89.29%	92.06%	87.01%	85.29%	93.06%	0.14	0.89
	KNN	79.64%	83.76%	76.69%	72.06%	86.81%	0.23	0.84
	BN	83.57%	86.89%	81.01%	77.94%	88.89%	0.11	0.88
Standard-DTW-4L	SVM	92.86%	95.31%	90.79%	89.71%	95.83%	0.10	0.93
	KNN	82.14%	86.44%	79.01%	75.00%	88.89%	0.20	0.87
	BN	85.24%	88.59%	82.63%	79.90%	90.28%	0.20	0.9
Standard-DTW-5L	SVM	91.43%	95.16%	88.46%	86.76%	95.83%	0.12	0.91
	KNN	81.79%	86.32%	78.53%	74.26%	88.89%	0.21	0.86
	BN	85.24%	89.01%	82.35%	79.41%	90.74%	0.10	0.9

Standard-DTW-6L	SVM	90.71%	93.65%	88.31%	86.76%	94.44%	0.12	0.91
	KNN	81.43%	85.59%	78.40%	74.26%	88.19%	0.21	0.86
	BN	85.00%	88.52%	82.28%	79.41%	90.28%	0.11	0.9
Standard-LCS-3L	SVM	92.86%	98.33%	88.75%	86.76%	98.61%	0.12	0.93
	KNN	84.29%	89.66%	80.49%	76.47%	91.67%	0.19	0.88
	BN	87.38%	92.18%	83.82%	80.88%	93.52%	0.19	0.92
Standard-LCS-4L	SVM	93.57%	96.83%	90.91%	89.71%	97.22%	0.10	0.93
	KNN	85.36%	89.26%	82.39%	79.41%	90.97%	0.18	0.89
	BN	88.10%	91.40%	85.47%	83.33%	92.59%	0.07	0.92
Standard-LCS-5L	SVM	94.29%	98.39%	91.03%	89.71%	98.61%	0.09	0.94
	KNN	86.07%	92.17%	81.82%	77.94%	93.75%	0.18	0.9
	BN	87.62%	92.70%	83.88%	80.88%	93.98%	0.19	0.92
Standard-LCS-6L	SVM	94.29%	98.39%	91.03%	89.71%	98.61%	0.09	0.94
	KNN	85.71%	91.38%	81.71%	77.94%	93.06%	0.18	0.9
	BN	87.38%	92.18%	83.82%	80.88%	93.52%	0.19	0.92
Standard-KLD-3L	SVM	90.71%	93.65%	88.31%	86.76%	94.44%	0.12	0.91
	KNN	80.00%	85.09%	76.51%	71.32%	88.19%	0.23	0.85
	BN	84.05%	88.27%	80.91%	77.45%	90.28%	0.10	0.89
Standard-KLD-4L	SVM	92.86%	95.31%	90.79%	89.71%	95.83%	0.10	0.93
	KNN	82.50%	87.83%	78.79%	74.26%	90.28%	0.20	0.88
	BN	85.71%	89.56%	82.77%	79.90%	91.20%	0.09	0.91
Standard-KLD-5L	SVM	92.14%	93.85%	90.67%	89.71%	94.44%	0.10	0.92
	KNN	83.57%	86.89%	81.01%	77.94%	88.89%	0.19	0.88
	BN	85.95%	88.36%	83.98%	81.86%	89.81%	0.11	0.9
Standard-KLD-6L	SVM	92.14%	93.85%	90.67%	89.71%	94.44%	0.10	0.92
	KNN	83.57%	86.89%	81.01%	77.94%	88.89%	0.19	0.88
	BN	85.95%	88.36%	83.98%	81.86%	89.81%	0.11	0.9
Overlapped-0NCF-3L	SVM	93.57%	98.36%	89.87%	88.24%	98.61%	0.11	0.93
	KNN	87.50%	92.44%	83.85%	80.88%	93.75%	0.16	0.9
	BN	89.29%	93.44%	86.08%	83.82%	94.44%	0.14	0.92
Overlapped-0NCF-4L	SVM	95.71%	100.00%	92.31%	91.18%	100.00%	0.08	0.96
	KNN	91.43%	96.67%	87.50%	85.29%	97.22%	0.13	0.93
	BN	92.14%	96.72%	88.61%	86.76%	97.22%	0.03	0.94
Overlapped-0NCF-5L	SVM	96.43%	98.46%	94.67%	94.12%	98.61%	0.06	0.96
	KNN	91.79%	97.48%	87.58%	85.29%	97.92%	0.12	0.94
	BN	91.90%	96.20%	88.56%	86.76%	96.76%	0.13	0.95
Standard-0NCF-6L	SVM	97.14%	100.00%	94.74%	94.12%	100.00%	0.06	0.97
	KNN	92.14%	97.50%	88.12%	86.03%	97.92%	0.12	0.95
	BN	92.38%	96.74%	88.98%	87.25%	97.22%	0.13	0.95
Standard-AIV-3L	SVM	97.86%	98.51%	97.26%	97.06%	98.61%	0.03	0.98
	KNN	92.86%	93.28%	92.47%	91.91%	93.75%	0.08	0.95
	BN	94.05%	94.53%	93.61%	93.14%	94.91%	0.05	0.97
Standard-AIV-4L	SVM	95.71%	100.00%	92.31%	91.18%	100.00%	0.08	0.96
	KNN	88.57%	93.33%	85.00%	82.35%	94.44%	0.15	0.92
	BN	90.24%	94.54%	86.92%	84.80%	95.37%	0.15	0.93
Standard-AIV-5L	SVM	94.29%	98.39%	91.03%	89.71%	98.61%	0.09	0.94
	KNN	87.86%	91.80%	84.81%	82.35%	93.06%	0.15	0.91
	BN	89.52%	92.55%	87.07%	85.29%	93.52%	0.06	0.93
Overlapped-AIV-6L	SVM	93.57%	98.36%	89.87%	88.24%	98.61%	0.11	0.93
	KNN	87.50%	91.74%	84.28%	81.62%	93.06%	0.16	0.9
	BN	89.05%	92.47%	86.32%	84.31%	93.52%	0.14	0.92

Overlapped-GLCM-3L	SVM	94.29%	96.88%	92.11%	91.18%	97.22%	0.08	0.94
	KNN	87.86%	92.50%	84.38%	81.62%	93.75%	0.16	0.91
	BN	89.52%	93.48%	86.44%	84.31%	94.44%	0.16	0.93
Overlapped-GLCM-4L	SVM	94.29%	98.39%	91.03%	89.71%	98.61%	0.09	0.94
	KNN	90.00%	93.55%	87.18%	85.29%	94.44%	0.13	0.92
	BN	91.19%	94.65%	88.41%	86.76%	95.37%	0.13	0.93
Overlapped-GLCM-5L	SVM	95.71%	98.44%	93.42%	92.65%	98.61%	0.07	0.96
	KNN	88.93%	93.39%	85.53%	83.09%	94.44%	0.14	0.92
	BN	90.71%	94.12%	87.98%	86.27%	94.91%	0.05	0.94
Overlapped-GLCM-6L	SVM	96.43%	98.46%	94.67%	94.12%	98.61%	0.06	0.96
	KNN	88.93%	93.39%	85.53%	83.09%	94.44%	0.14	0.93
	BN	90.24%	94.05%	87.23%	85.29%	94.91%	0.05	0.94
Overlapped-KCC-3L	SVM	97.86%	97.10%	98.59%	98.53%	97.22%	0.01	0.98
	KNN	91.07%	93.02%	89.40%	88.24%	93.75%	0.07	0.94
	BN	92.38%	94.33%	90.71%	89.71%	94.91%	0.09	0.96
Overlapped-KCC-4L	SVM	95.71%	96.97%	94.59%	94.12%	97.22%	0.06	0.96
	KNN	89.29%	90.77%	88.00%	86.76%	91.67%	0.12	0.92
	BN	91.19%	92.39%	90.13%	89.22%	93.06%	0.10	0.94
Overlapped-KCC-5L	SVM	97.86%	100.00%	96.00%	95.59%	100.00%	0.04	0.98
	KNN	93.21%	93.33%	93.10%	92.65%	93.75%	0.07	0.95
	BN	92.86%	93.50%	92.27%	91.67%	93.98%	0.06	0.95
Overlapped-KCC-6L	SVM	95.00%	96.92%	93.33%	92.65%	97.22%	0.07	0.95
	KNN	90.36%	92.25%	88.74%	87.50%	93.06%	0.12	0.93
	BN	91.19%	93.26%	89.43%	88.24%	93.98%	0.12	0.94
Overlapped-ED-3L	SVM	97.86%	98.51%	97.26%	97.06%	98.61%	0.03	0.98
	KNN	91.07%	94.40%	88.39%	86.76%	95.14%	0.12	0.94
	BN	92.62%	95.29%	90.39%	89.22%	95.83%	0.04	0.96
Overlapped-ED-4L	SVM	96.43%	97.01%	95.89%	95.59%	97.22%	0.04	0.96
	KNN	91.79%	93.13%	90.60%	89.71%	93.75%	0.10	0.94
	BN	93.33%	94.44%	92.34%	91.67%	94.91%	0.08	0.96
Overlapped-ED-5L	SVM	95.71%	95.59%	95.83%	95.59%	95.83%	0.04	0.96
	KNN	90.00%	91.54%	88.67%	87.50%	92.36%	0.12	0.93
	BN	91.90%	93.37%	90.62%	89.71%	93.98%	0.06	0.95
Overlapped-ED-6L	SVM	95.71%	96.97%	94.59%	94.12%	97.22%	0.06	0.96
	KNN	90.71%	92.31%	89.33%	88.24%	93.06%	0.11	0.93
	BN	92.38%	93.88%	91.07%	90.20%	94.44%	0.06	0.95
Overlapped-DTW-3L	SVM	94.29%	100.00%	90.00%	88.24%	100.00%	0.11	0.94
	KNN	87.86%	92.50%	84.38%	81.62%	93.75%	0.16	0.91
	BN	89.52%	93.48%	86.44%	84.31%	94.44%	0.16	0.93
Overlapped-DTW-4L	SVM	96.43%	98.46%	94.67%	94.12%	98.61%	0.06	0.96
	KNN	90.00%	92.19%	88.16%	86.76%	93.06%	0.12	0.93
	BN	90.71%	93.19%	88.65%	87.25%	93.98%	0.06	0.94
Overlapped-DTW-5L	SVM	97.14%	100.00%	94.74%	94.12%	100.00%	0.06	0.97
	KNN	91.43%	95.90%	87.97%	86.03%	96.53%	0.12	0.94
	BN	92.14%	96.22%	88.94%	87.25%	96.76%	0.13	0.95
Overlapped-DTW-6L	SVM	97.14%	100.00%	94.74%	94.12%	100.00%	0.06	0.97
	KNN	90.36%	92.25%	88.74%	87.50%	93.06%	0.11	0.94
	BN	91.19%	94.18%	88.74%	87.25%	94.91%	0.05	0.95
Overlapped-LCS-3L	SVM	95.71%	95.59%	95.83%	95.59%	95.83%	0.04	0.96
	KNN	93.93%	96.12%	92.05%	91.18%	96.53%	0.08	0.95
	BN	95.24%	96.94%	93.75%	93.14%	97.22%	0.06	0.96

Overlapped-LCS-4L	SVM	97.14%	98.48%	95.95%	95.59%	98.61%	0.04	0.97
	KNN	92.14%	94.53%	90.13%	88.97%	95.14%	0.10	0.95
	BN	93.57%	95.38%	92.00%	91.18%	95.83%	0.04	0.96
Overlapped-LCS-5L	SVM	95.71%	98.44%	93.42%	92.65%	98.61%	0.07	0.96
	KNN	87.86%	90.48%	85.71%	83.82%	91.67%	0.14	0.92
	BN	90.48%	92.71%	88.60%	87.25%	93.52%	0.11	0.94
Overlapped-LCS-6L	SVM	95.00%	98.41%	92.21%	91.18%	98.61%	0.08	0.95
	KNN	88.93%	92.00%	86.45%	84.56%	93.06%	0.14	0.92
	BN	90.71%	92.75%	88.99%	87.75%	93.52%	0.12	0.93
Overlapped-KLD-3L	SVM	96.43%	98.46%	94.67%	94.12%	98.61%	0.06	0.96
	KNN	93.57%	96.09%	91.45%	90.44%	96.53%	0.09	0.95
	BN	94.76%	96.91%	92.92%	92.16%	97.22%	0.07	0.96
Overlapped-KLD-4L	SVM	96.43%	100.00%	93.51%	92.65%	100.00%	0.07	0.96
	KNN	88.57%	90.62%	86.84%	85.29%	91.67%	0.13	0.92
	BN	89.52%	92.11%	87.39%	85.78%	93.06%	0.07	0.93
Overlapped-KLD-5L	SVM	95.71%	98.44%	93.42%	92.65%	98.61%	0.07	0.96
	KNN	87.50%	89.15%	86.09%	84.56%	90.28%	0.14	0.92
	BN	88.81%	90.26%	87.56%	86.27%	91.20%	0.09	0.93
Overlapped-KLD-6L	SVM	95.00%	98.41%	92.21%	91.18%	98.61%	0.08	0.95
	KNN	88.21%	89.31%	87.25%	86.03%	90.28%	0.13	0.92
	BN	89.29%	90.77%	88.00%	86.76%	91.67%	0.13	0.93

Table A.5: The results using LBP with PCA.

Method	Classifiers	Acc	Sen	Spec	PPV	NPV	EER	AUC
Standard-0NCF-3L	SVM	78.57%	75.00%	82.81%	83.82%	73.61%	0.18	0.79
	KNN	65.36%	59.33%	83.10%	91.18%	40.97%	0.35	0.72
	BN	73.81%	67.03%	86.81%	90.69%	57.87%	0.42	0.81
Standard-0NCF-4L	SVM	68.57%	66.67%	70.59%	70.59%	66.67%	0.31	0.69
	KNN	65.36%	60.43%	75.27%	83.09%	48.61%	0.37	0.67
	BN	72.62%	68.02%	79.19%	82.35%	63.43%	0.37	0.76
Standard-0NCF-5L	SVM	75.00%	75.38%	74.67%	72.06%	77.78%	0.26	0.75
	KNN	71.43%	66.47%	79.09%	83.09%	60.42%	0.20	0.73
	BN	77.38%	73.59%	82.01%	83.33%	71.76%	0.28	0.8
Standard-0NCF-6L	SVM	80.00%	77.03%	83.33%	83.82%	76.39%	0.17	0.8
	KNN	74.29%	69.28%	81.58%	84.56%	64.58%	0.28	0.77
	BN	78.57%	74.78%	83.16%	84.31%	73.15%	0.17	0.83
Standard-AIV-3L	SVM	79.29%	76.00%	83.08%	83.82%	75.00%	0.18	0.79
	KNN	71.79%	64.92%	86.52%	91.18%	53.47%	0.31	0.76
	BN	79.05%	72.31%	90.00%	92.16%	66.67%	0.33	0.84
Standard-AIV-4L	SVM	92.14%	91.30%	92.96%	92.65%	91.67%	0.07	0.92
	KNN	86.79%	81.13%	94.21%	94.85%	79.17%	0.17	0.9
	BN	89.76%	85.46%	94.82%	95.10%	84.72%	0.13	0.93
Standard-AIV-5L	SVM	93.57%	91.55%	95.65%	95.59%	91.67%	0.05	0.94
	KNN	93.21%	90.91%	95.62%	95.59%	90.97%	0.09	0.93
	BN	94.52%	92.49%	96.62%	96.57%	92.59%	0.07	0.95
Standard-AIV-6L	SVM	90.00%	88.57%	91.43%	91.18%	88.89%	0.09	0.9
	KNN	88.21%	86.52%	89.93%	89.71%	86.81%	0.13	0.89
	BN	90.71%	89.47%	91.94%	91.67%	89.81%	0.08	0.92

Standard-GLCM-3L	SVM	83.57%	79.22%	88.89%	89.71%	77.78%	0.12	0.84
	KNN	70.00%	62.75%	89.47%	94.12%	47.22%	0.31	0.77
	BN	76.43%	69.37%	89.26%	92.16%	61.57%	0.09	0.84
Standard-GLCM-4L	SVM	78.57%	75.00%	82.81%	83.82%	73.61%	0.18	0.79
	KNN	75.00%	68.13%	87.76%	91.18%	59.72%	0.29	0.77
	BN	79.29%	73.88%	86.86%	88.73%	70.37%	0.30	0.83
Standard-GLCM-5L	SVM	98.57%	97.14%	100.00%	100.00%	97.22%	0.00	0.99
	KNN	90.36%	83.44%	100.00%	100.00%	81.25%	0.14	0.95
	BN	92.86%	87.83%	98.95%	99.02%	87.04%	0.10	0.97
Standard-GLCM-6L	SVM	97.86%	95.77%	100.00%	100.00%	95.83%	0.00	0.98
	KNN	94.64%	90.07%	100.00%	100.00%	89.58%	0.09	0.96
	BN	96.43%	93.15%	100.00%	100.00%	93.06%	0.06	0.98
Standard-KCC-3L	SVM	74.29%	72.22%	76.47%	76.47%	72.22%	0.25	0.74
	KNN	63.21%	58.13%	76.62%	86.76%	40.97%	0.37	0.69
	BN	72.14%	66.05%	83.22%	87.75%	57.41%	0.13	0.79
Standard-KCC-4L	SVM	86.43%	84.51%	88.41%	88.24%	84.72%	0.12	0.86
	KNN	78.93%	73.05%	87.61%	89.71%	68.75%	0.24	0.83
	BN	84.05%	79.40%	89.84%	90.69%	77.78%	0.18	0.88
Standard-KCC-5L	SVM	88.57%	89.39%	87.84%	86.76%	90.28%	0.13	0.89
	KNN	87.50%	88.55%	86.58%	85.29%	89.58%	0.14	0.88
	BN	90.24%	91.37%	89.24%	88.24%	92.13%	0.12	0.92
Standard-KCC-6L	SVM	91.43%	93.75%	89.47%	88.24%	94.44%	0.11	0.91
	KNN	90.36%	91.60%	89.26%	88.24%	92.36%	0.11	0.91
	BN	91.43%	92.86%	90.18%	89.22%	93.52%	0.10	0.92
Standard-ED-3L	SVM	87.14%	85.71%	88.57%	88.24%	86.11%	0.12	0.87
	KNN	72.86%	65.31%	90.48%	94.12%	52.78%	0.29	0.8
	BN	79.29%	72.76%	89.57%	91.67%	67.59%	0.32	0.87
Standard-ED-4L	SVM	94.29%	91.67%	97.06%	97.06%	91.67%	0.03	0.94
	KNN	82.14%	73.89%	97.00%	97.79%	67.36%	0.21	0.88
	BN	85.48%	79.42%	93.79%	94.61%	76.85%	0.06	0.92
Standard-ED-5L	SVM	95.00%	92.96%	97.10%	97.06%	93.06%	0.03	0.95
	KNN	91.43%	88.89%	94.12%	94.12%	88.89%	0.10	0.93
	BN	92.62%	90.23%	95.12%	95.10%	90.28%	0.09	0.95
Standard-ED-6L	SVM	95.71%	96.97%	94.59%	94.12%	97.22%	0.06	0.96
	KNN	92.86%	92.65%	93.06%	92.65%	93.06%	0.07	0.94
	BN	93.33%	92.72%	93.93%	93.63%	93.06%	0.06	0.95
Standard-DTW-3L	SVM	77.86%	74.67%	81.54%	82.35%	73.61%	0.19	0.78
	KNN	65.36%	59.42%	82.19%	90.44%	41.67%	0.35	0.72
	BN	74.05%	67.27%	86.90%	90.69%	58.33%	0.11	0.81
Standard-DTW-4L	SVM	75.00%	72.60%	77.61%	77.94%	72.22%	0.23	0.75
	KNN	68.21%	62.70%	78.95%	85.29%	52.08%	0.34	0.72
	BN	74.29%	69.20%	81.76%	84.80%	64.35%	0.35	0.79
Standard-DTW-5L	SVM	93.57%	92.75%	94.37%	94.12%	93.06%	0.06	0.94
	KNN	90.00%	91.54%	88.67%	87.50%	92.36%	0.08	0.92
	BN	90.71%	91.88%	89.69%	88.73%	92.59%	0.07	0.93
Standard-DTW-6L	SVM	93.57%	92.75%	94.37%	94.12%	93.06%	0.06	0.94
	KNN	90.00%	86.99%	93.28%	93.38%	86.81%	0.12	0.92
	BN	90.24%	88.63%	91.87%	91.67%	88.89%	0.11	0.93
Standard-LCS-3L	SVM	87.86%	88.06%	87.67%	86.76%	88.89%	0.13	0.88
	KNN	73.21%	65.80%	89.66%	93.38%	54.17%	0.07	0.81
	BN	80.00%	73.44%	90.24%	92.16%	68.52%	0.31	0.87

Standard-LCS-4L	SVM	89.29%	88.41%	90.14%	89.71%	88.89%	0.10	0.89
	KNN	88.57%	87.14%	90.00%	89.71%	87.50%	0.12	0.89
	BN	91.19%	90.34%	92.02%	91.67%	90.74%	0.08	0.92
Standard-LCS-5L	SVM	87.14%	83.78%	90.91%	91.18%	83.33%	0.10	0.87
	KNN	88.21%	86.01%	90.51%	90.44%	86.11%	0.13	0.88
	BN	89.76%	88.89%	90.61%	90.20%	89.35%	0.10	0.91
Standard-LCS-6L	SVM	94.29%	95.45%	93.24%	92.65%	95.83%	0.07	0.94
	KNN	91.79%	94.49%	89.54%	88.24%	95.14%	0.11	0.93
	BN	91.67%	94.24%	89.52%	88.24%	94.91%	0.11	0.93
Standard-KLD-3L	SVM	87.86%	86.96%	88.73%	88.24%	87.50%	0.12	0.88
	KNN	70.71%	63.37%	89.74%	94.12%	48.61%	0.30	0.8
	BN	77.86%	70.79%	90.20%	92.65%	63.89%	0.07	0.87
Standard-KLD-4L	SVM	92.14%	91.30%	92.96%	92.65%	91.67%	0.07	0.92
	KNN	85.71%	79.63%	94.07%	94.85%	77.08%	0.18	0.89
	BN	88.57%	83.62%	94.68%	95.10%	82.41%	0.05	0.93
Standard-KLD-5L	SVM	87.14%	86.76%	87.50%	86.76%	87.50%	0.13	0.87
	KNN	84.64%	81.21%	88.55%	88.97%	80.56%	0.12	0.86
	BN	88.10%	85.32%	91.09%	91.18%	85.19%	0.09	0.9
Standard-KLD-6L	SVM	90.00%	88.57%	91.43%	91.18%	88.89%	0.09	0.9
	KNN	88.21%	83.66%	93.70%	94.12%	82.64%	0.15	0.89
	BN	89.29%	85.33%	93.85%	94.12%	84.72%	0.06	0.91
Overlapped-0NCF-3L	SVM	75.71%	72.37%	79.69%	80.88%	70.83%	0.21	0.76
	KNN	65.36%	59.42%	82.19%	90.44%	41.67%	0.36	0.71
	BN	72.14%	66.29%	82.35%	86.76%	58.33%	0.41	0.78
Overlapped-0NCF-4L	SVM	75.71%	72.37%	79.69%	80.88%	70.83%	0.21	0.76
	KNN	65.36%	59.42%	82.19%	90.44%	41.67%	0.36	0.71
	BN	72.14%	66.29%	82.35%	86.76%	58.33%	0.41	0.78
Overlapped-0NCF-5L	SVM	75.71%	72.37%	79.69%	80.88%	70.83%	0.21	0.76
	KNN	65.36%	59.42%	82.19%	90.44%	41.67%	0.36	0.71
	BN	72.14%	66.29%	82.35%	86.76%	58.33%	0.41	0.78
Overlapped-0NCF-6L	SVM	75.71%	72.37%	79.69%	80.88%	70.83%	0.21	0.76
	KNN	65.36%	59.42%	82.19%	90.44%	41.67%	0.36	0.71
	BN	72.14%	66.29%	82.35%	86.76%	58.33%	0.41	0.78
Overlapped-AIV-3L	SVM	84.29%	81.08%	87.88%	88.24%	80.56%	0.13	0.84
	KNN	69.29%	62.25%	88.16%	93.38%	46.53%	0.31	0.77
	BN	76.67%	69.34%	90.41%	93.14%	61.11%	0.24	0.85
Overlapped-AIV-4L	SVM	79.29%	76.71%	82.09%	82.35%	76.39%	0.19	0.79
	KNN	76.79%	72.33%	82.64%	84.56%	69.44%	0.26	0.78
	BN	79.29%	75.32%	84.13%	85.29%	73.61%	0.17	0.82
Overlapped-AIV-5L	SVM	79.29%	76.71%	82.09%	82.35%	76.39%	0.19	0.79
	KNN	76.79%	72.33%	82.64%	84.56%	69.44%	0.26	0.78
	BN	79.29%	75.32%	84.13%	85.29%	73.61%	0.17	0.82
Overlapped-AIV-6L	SVM	79.29%	76.71%	82.09%	82.35%	76.39%	0.19	0.79
	KNN	76.79%	72.33%	82.64%	84.56%	69.44%	0.26	0.78
	BN	79.29%	75.32%	84.13%	85.29%	73.61%	0.17	0.82
Overlapped-GLCM-3L	SVM	75.71%	74.29%	77.14%	76.47%	75.00%	0.24	0.76
	KNN	63.93%	58.62%	77.92%	87.50%	41.67%	0.36	0.7
	BN	70.71%	65.28%	80.00%	84.80%	57.41%	0.43	0.77
Overlapped-GLCM-4L	SVM	75.71%	72.37%	79.69%	80.88%	70.83%	0.21	0.76
	KNN	69.29%	63.02%	82.95%	88.97%	50.69%	0.33	0.73
	BN	73.81%	68.22%	82.72%	86.27%	62.04%	0.35	0.78

Overlapped-GLCM-5L	SVM	75.71%	72.37%	79.69%	80.88%	70.83%	0.21	0.76
	KNN	70.71%	64.36%	83.70%	88.97%	53.47%	0.32	0.74
	BN	74.76%	69.29%	83.13%	86.27%	63.89%	0.33	0.79
Overlapped-GLCM-6L	SVM	75.71%	72.37%	79.69%	80.88%	70.83%	0.21	0.76
	KNN	70.71%	64.36%	83.70%	88.97%	53.47%	0.32	0.74
	BN	74.76%	69.29%	83.13%	86.27%	63.89%	0.33	0.79
Overlapped-KCC-3L	SVM	82.86%	81.43%	84.29%	83.82%	81.94%	0.16	0.83
	KNN	67.14%	60.78%	84.21%	91.18%	44.44%	0.33	0.75
	BN	74.52%	67.77%	87.07%	90.69%	59.26%	0.09	0.83
Overlapped-KCC-4L	SVM	75.71%	75.00%	76.39%	75.00%	76.39%	0.25	0.76
	KNN	75.71%	72.97%	78.79%	79.41%	72.22%	0.22	0.76
	BN	76.19%	73.64%	79.00%	79.41%	73.15%	0.27	0.77
Overlapped-KCC-5L	SVM	77.14%	76.47%	77.78%	76.47%	77.78%	0.23	0.77
	KNN	77.86%	75.69%	80.15%	80.15%	75.69%	0.21	0.78
	BN	77.86%	75.81%	80.00%	79.90%	75.93%	0.24	0.79
Overlapped-KCC-6L	SVM	75.00%	77.05%	73.42%	69.12%	80.56%	0.28	0.75
	KNN	75.71%	74.64%	76.76%	75.74%	75.69%	0.24	0.75
	BN	76.19%	75.00%	77.36%	76.47%	75.93%	0.24	0.77
Overlapped-ED-3L	SVM	86.43%	83.56%	89.55%	89.71%	83.33%	0.11	0.87
	KNN	72.50%	64.82%	91.36%	94.85%	51.39%	0.29	0.8
	BN	79.52%	72.35%	91.67%	93.63%	66.20%	0.34	0.86
Overlapped-ED-4L	SVM	82.86%	80.56%	85.29%	85.29%	80.56%	0.15	0.83
	KNN	74.29%	67.20%	88.30%	91.91%	57.64%	0.29	0.79
	BN	76.19%	69.70%	87.18%	90.20%	62.96%	0.10	0.82
Overlapped-ED-5L	SVM	80.00%	77.03%	83.33%	83.82%	76.39%	0.17	0.8
	KNN	72.86%	65.96%	86.96%	91.18%	55.56%	0.30	0.77
	BN	75.24%	68.80%	86.36%	89.71%	61.57%	0.11	0.8
Overlapped-ED-6L	SVM	80.00%	77.03%	83.33%	83.82%	76.39%	0.17	0.8
	KNN	72.86%	65.96%	86.96%	91.18%	55.56%	0.30	0.77
	BN	75.24%	68.80%	86.36%	89.71%	61.57%	0.11	0.8
Overlapped-DTW-3L	SVM	77.14%	73.68%	81.25%	82.35%	72.22%	0.20	0.77
	KNN	66.07%	59.90%	83.56%	91.18%	42.36%	0.35	0.72
	BN	73.10%	67.04%	83.66%	87.75%	59.26%	0.40	0.79
Overlapped-DTW-4L	SVM	77.14%	73.68%	81.25%	82.35%	72.22%	0.20	0.77
	KNN	66.07%	59.90%	83.56%	91.18%	42.36%	0.35	0.72
	BN	72.86%	66.79%	83.55%	87.75%	58.80%	0.14	0.79
Overlapped-DTW-5L	SVM	77.14%	73.68%	81.25%	82.35%	72.22%	0.20	0.77
	KNN	66.07%	59.90%	83.56%	91.18%	42.36%	0.35	0.72
	BN	72.86%	66.79%	83.55%	87.75%	58.80%	0.14	0.79
Overlapped-DTW-6L	SVM	77.14%	73.68%	81.25%	82.35%	72.22%	0.20	0.77
	KNN	66.07%	59.90%	83.56%	91.18%	42.36%	0.35	0.72
	BN	72.86%	66.79%	83.55%	87.75%	58.80%	0.14	0.79
Overlapped-LCS-3L	SVM	88.57%	88.24%	88.89%	88.24%	88.89%	0.12	0.89
	KNN	72.86%	65.31%	90.48%	94.12%	52.78%	0.06	0.81
	BN	77.38%	71.21%	87.12%	89.71%	65.74%	0.33	0.86
Overlapped-LCS-4L	SVM	75.00%	73.91%	76.06%	75.00%	75.00%	0.25	0.75
	KNN	72.50%	68.10%	78.63%	81.62%	63.89%	0.22	0.74
	BN	75.71%	72.37%	79.69%	80.88%	70.83%	0.25	0.78
Overlapped-LCS-5L	SVM	75.00%	74.63%	75.34%	73.53%	76.39%	0.26	0.75
	KNN	72.14%	67.90%	77.97%	80.88%	63.89%	0.22	0.74
	BN	75.71%	72.57%	79.38%	80.39%	71.30%	0.26	0.77

Overlapped-LCS-6L	SVM	75.00%	74.63%	75.34%	73.53%	76.39%	0.26	0.75
	KNN	72.14%	67.90%	77.97%	80.88%	63.89%	0.22	0.74
	BN	75.71%	72.57%	79.38%	80.39%	71.30%	0.26	0.77
Overlapped-KLD-3L	SVM	80.71%	78.87%	82.61%	82.35%	79.17%	0.18	0.81
	KNN	68.21%	61.69%	84.81%	91.18%	46.53%	0.33	0.75
	BN	74.29%	68.18%	84.62%	88.24%	61.11%	0.38	0.81
Overlapped-KLD-4L	SVM	78.57%	75.00%	82.81%	83.82%	73.61%	0.18	0.79
	KNN	66.43%	60.10%	84.72%	91.91%	42.36%	0.34	0.73
	BN	73.10%	66.43%	86.01%	90.20%	56.94%	0.12	0.8
Overlapped-KLD-5L	SVM	78.57%	75.00%	82.81%	83.82%	73.61%	0.18	0.79
	KNN	66.43%	60.10%	84.72%	91.91%	42.36%	0.34	0.73
	BN	73.10%	66.43%	86.01%	90.20%	56.94%	0.12	0.8
Overlapped-KLD-6L	SVM	78.57%	75.00%	82.81%	83.82%	73.61%	0.18	0.79
	KNN	66.43%	60.10%	84.72%	91.91%	42.36%	0.34	0.73
	BN	73.10%	66.43%	86.01%	90.20%	56.94%	0.12	0.8

Table A.6: The results using HOG-LBP with PCA.

Method	Classifiers	Acc	Sen	Spec	PPV	NPV	EER	AUC
Standard-0NCF-3L	SVM	93.57%	98.36%	89.87%	88.24%	98.61%	0.11	0.93
	KNN	86.43%	92.24%	82.32%	78.68%	93.75%	0.17	0.9
	BN	87.14%	90.76%	84.32%	81.86%	92.13%	0.18	0.91
Standard-0NCF-4L	SVM	91.43%	98.28%	86.59%	83.82%	98.61%	0.14	0.91
	KNN	83.21%	90.09%	78.70%	73.53%	92.36%	0.21	0.87
	BN	85.00%	90.29%	81.22%	77.45%	92.13%	0.18	0.89
Standard-0NCF-5L	SVM	92.14%	98.31%	87.65%	85.29%	98.61%	0.13	0.92
	KNN	84.64%	90.43%	80.61%	76.47%	92.36%	0.19	0.88
	BN	85.71%	90.45%	82.23%	78.92%	92.13%	0.21	0.89
Standard-0NCF-6L	SVM	93.57%	98.36%	89.87%	88.24%	98.61%	0.11	0.93
	KNN	84.29%	89.66%	80.49%	76.47%	91.67%	0.19	0.89
	BN	85.71%	90.45%	82.23%	78.92%	92.13%	0.08	0.9
Standard-AIV-3L	SVM	95.00%	96.92%	93.33%	92.65%	97.22%	0.07	0.95
	KNN	87.14%	92.37%	83.33%	80.15%	93.75%	0.16	0.91
	BN	89.05%	92.47%	86.32%	84.31%	93.52%	0.15	0.93
Standard-AIV-4L	SVM	91.43%	96.67%	87.50%	85.29%	97.22%	0.13	0.91
	KNN	83.93%	91.74%	78.95%	73.53%	93.75%	0.20	0.87
	BN	86.19%	92.44%	81.85%	77.94%	93.98%	0.22	0.89
Standard-AIV-5L	SVM	90.00%	96.55%	85.37%	82.35%	97.22%	0.15	0.9
	KNN	83.57%	93.27%	77.84%	71.32%	95.14%	0.22	0.87
	BN	84.52%	91.12%	80.08%	75.49%	93.06%	0.07	0.88
Standard-AIV-6L	SVM	90.00%	93.55%	87.18%	85.29%	94.44%	0.13	0.9
	KNN	82.86%	90.00%	78.24%	72.79%	92.36%	0.21	0.86
	BN	84.52%	89.27%	81.07%	77.45%	91.20%	0.23	0.88
Standard-GLCM-3L	SVM	92.86%	96.77%	89.74%	88.24%	97.22%	0.11	0.93
	KNN	86.07%	89.43%	83.44%	80.88%	90.97%	0.17	0.89
	BN	87.38%	90.37%	84.98%	82.84%	91.67%	0.17	0.9
Standard-GLCM-4L	SVM	92.14%	96.72%	88.61%	86.76%	97.22%	0.12	0.92
	KNN	85.36%	91.30%	81.21%	77.21%	93.06%	0.19	0.89
	BN	86.67%	91.57%	83.06%	79.90%	93.06%	0.07	0.9

Standard-GLCM-5L	SVM	91.43%	98.28%	86.59%	83.82%	98.61%	0.14	0.91
	KNN	80.71%	88.68%	75.86%	69.12%	91.67%	0.23	0.86
	BN	83.33%	89.41%	79.20%	74.51%	91.67%	0.08	0.88
Standard-GLCM-6L	SVM	93.57%	98.36%	89.87%	88.24%	98.61%	0.11	0.93
	KNN	84.64%	91.15%	80.24%	75.74%	93.06%	0.19	0.89
	BN	85.48%	90.86%	81.63%	77.94%	92.59%	0.22	0.89
Standard-KCC-3L	SVM	95.00%	98.41%	92.21%	91.18%	98.61%	0.08	0.95
	KNN	86.07%	92.92%	81.44%	77.21%	94.44%	0.18	0.9
	BN	86.43%	91.06%	82.99%	79.90%	92.59%	0.19	0.91
Standard-KCC-4L	SVM	92.14%	93.85%	90.67%	89.71%	94.44%	0.10	0.92
	KNN	87.50%	91.06%	84.71%	82.35%	92.36%	0.15	0.9
	BN	89.52%	92.11%	87.39%	85.78%	93.06%	0.14	0.92
Standard-KCC-5L	SVM	91.43%	95.16%	88.46%	86.76%	95.83%	0.12	0.91
	KNN	83.93%	90.27%	79.64%	75.00%	92.36%	0.20	0.87
	BN	85.48%	90.40%	81.89%	78.43%	92.13%	0.08	0.89
Standard-KCC-6L	SVM	90.00%	96.55%	85.37%	82.35%	97.22%	0.15	0.9
	KNN	83.57%	89.47%	79.52%	75.00%	91.67%	0.20	0.87
	BN	84.29%	88.33%	81.25%	77.94%	90.28%	0.10	0.88
Standard-ED-3L	SVM	94.29%	96.88%	92.11%	91.18%	97.22%	0.08	0.94
	KNN	85.36%	92.79%	80.47%	75.74%	94.44%	0.19	0.9
	BN	86.90%	92.09%	83.13%	79.90%	93.52%	0.20	0.91
Standard-ED-4L	SVM	93.57%	95.38%	92.00%	91.18%	95.83%	0.08	0.94
	KNN	88.57%	91.94%	85.90%	83.82%	93.06%	0.14	0.91
	BN	90.71%	92.31%	89.33%	88.24%	93.06%	0.11	0.93
Standard-ED-5L	SVM	92.14%	95.24%	89.61%	88.24%	95.83%	0.11	0.92
	KNN	86.07%	91.45%	82.21%	78.68%	93.06%	0.18	0.89
	BN	86.19%	90.11%	83.19%	80.39%	91.67%	0.19	0.9
Standard-ED-6L	SVM	91.43%	92.42%	90.54%	89.71%	93.06%	0.10	0.91
	KNN	86.79%	89.60%	84.52%	82.35%	90.97%	0.16	0.89
	BN	86.67%	88.95%	84.78%	82.84%	90.28%	0.10	0.89
Standard-DTW-3L	SVM	93.57%	98.36%	89.87%	88.24%	98.61%	0.11	0.93
	KNN	86.43%	92.24%	82.32%	78.68%	93.75%	0.17	0.9
	BN	86.19%	90.56%	82.92%	79.90%	92.13%	0.08	0.9
Standard-DTW-4L	SVM	92.14%	98.31%	87.65%	85.29%	98.61%	0.13	0.92
	KNN	85.36%	90.60%	81.60%	77.94%	92.36%	0.18	0.89
	BN	86.90%	91.16%	83.68%	80.88%	92.59%	0.07	0.9
Standard-DTW-5L	SVM	92.14%	98.31%	87.65%	85.29%	98.61%	0.13	0.92
	KNN	82.86%	92.31%	77.27%	70.59%	94.44%	0.22	0.87
	BN	84.29%	91.57%	79.53%	74.51%	93.52%	0.25	0.88
Standard-DTW-6L	SVM	90.71%	95.08%	87.34%	85.29%	95.83%	0.13	0.91
	KNN	81.43%	86.84%	77.71%	72.79%	89.58%	0.22	0.86
	BN	83.10%	88.00%	79.59%	75.49%	90.28%	0.10	0.88
Standard-LCS-3L	SVM	93.57%	91.55%	95.65%	95.59%	91.67%	0.05	0.94
	KNN	90.36%	91.60%	89.26%	88.24%	92.36%	0.08	0.92
	BN	91.90%	92.50%	91.36%	90.69%	93.06%	0.07	0.94
Standard-LCS-4L	SVM	92.86%	93.94%	91.89%	91.18%	94.44%	0.09	0.93
	KNN	87.86%	92.50%	84.38%	81.62%	93.75%	0.16	0.9
	BN	88.57%	91.94%	85.90%	83.82%	93.06%	0.14	0.92
Standard-LCS-5L	SVM	91.43%	96.67%	87.50%	85.29%	97.22%	0.13	0.91
	KNN	82.14%	89.81%	77.33%	71.32%	92.36%	0.22	0.87
	BN	83.33%	88.51%	79.67%	75.49%	90.74%	0.25	0.88

Standard-LCS-6L	SVM	90.71%	96.61%	86.42%	83.82%	97.22%	0.14	0.91
	KNN	83.21%	90.83%	78.36%	72.79%	93.06%	0.21	0.87
	BN	84.29%	89.66%	80.49%	76.47%	91.67%	0.09	0.88
Standard-KLD-3L	SVM	95.71%	100.00%	92.31%	91.18%	100.00%	0.08	0.96
	KNN	90.36%	92.25%	88.74%	87.50%	93.06%	0.12	0.93
	BN	90.95%	92.35%	89.73%	88.73%	93.06%	0.11	0.93
Standard-KLD-4L	SVM	92.86%	96.77%	89.74%	88.24%	97.22%	0.11	0.93
	KNN	84.29%	91.82%	79.41%	74.26%	93.75%	0.20	0.88
	BN	85.71%	91.38%	81.71%	77.94%	93.06%	0.22	0.89
Standard-KLD-5L	SVM	92.86%	96.77%	89.74%	88.24%	97.22%	0.11	0.93
	KNN	83.57%	90.18%	79.17%	74.26%	92.36%	0.20	0.88
	BN	84.05%	88.70%	80.66%	76.96%	90.74%	0.23	0.89
Standard-KLD-6L	SVM	92.86%	98.33%	88.75%	86.76%	98.61%	0.12	0.93
	KNN	82.86%	90.00%	78.24%	72.79%	92.36%	0.21	0.88
	BN	83.33%	88.07%	79.92%	75.98%	90.28%	0.10	0.89
Overlapped-0NCF-3L	SVM	88.57%	96.43%	83.33%	79.41%	97.22%	0.17	0.88
	KNN	79.29%	86.79%	74.71%	67.65%	90.28%	0.25	0.84
	BN	80.48%	85.06%	77.24%	72.55%	87.96%	0.27	0.85
Overlapped-0NCF-4L	SVM	88.57%	96.43%	83.33%	79.41%	97.22%	0.17	0.88
	KNN	79.29%	86.79%	74.71%	67.65%	90.28%	0.25	0.84
	BN	80.48%	85.06%	77.24%	72.55%	87.96%	0.27	0.85
Overlapped-0NCF-5L	SVM	88.57%	96.43%	83.33%	79.41%	97.22%	0.17	0.88
	KNN	79.29%	86.79%	74.71%	67.65%	90.28%	0.25	0.84
	BN	80.48%	85.06%	77.24%	72.55%	87.96%	0.27	0.85
Overlapped-0NCF-6L	SVM	88.57%	96.43%	83.33%	79.41%	97.22%	0.17	0.88
	KNN	79.29%	86.79%	74.71%	67.65%	90.28%	0.25	0.84
	BN	80.48%	85.06%	77.24%	72.55%	87.96%	0.27	0.85
Overlapped-AIV-3L	SVM	85.00%	92.73%	80.00%	75.00%	94.44%	0.21	0.85
	KNN	76.79%	83.81%	72.57%	64.71%	88.19%	0.27	0.81
	BN	80.48%	85.47%	77.02%	72.06%	88.43%	0.27	0.85
Overlapped-AIV-4L	SVM	85.71%	92.86%	80.95%	76.47%	94.44%	0.20	0.85
	KNN	76.43%	82.41%	72.67%	65.44%	86.81%	0.27	0.81
	BN	79.29%	83.05%	76.54%	72.06%	86.11%	0.28	0.84
Overlapped-AIV-5L	SVM	85.71%	92.86%	80.95%	76.47%	94.44%	0.20	0.85
	KNN	76.43%	82.41%	72.67%	65.44%	86.81%	0.27	0.81
	BN	79.29%	83.05%	76.54%	72.06%	86.11%	0.28	0.84
Overlapped-AIV-6L	SVM	85.71%	92.86%	80.95%	76.47%	94.44%	0.20	0.85
	KNN	76.43%	82.41%	72.67%	65.44%	86.81%	0.27	0.81
	BN	79.29%	83.05%	76.54%	72.06%	86.11%	0.28	0.84
Overlapped-GLCM-3L	SVM	86.43%	92.98%	81.93%	77.94%	94.44%	0.19	0.86
	KNN	77.50%	83.49%	73.68%	66.91%	87.50%	0.26	0.82
	BN	80.00%	84.09%	77.05%	72.55%	87.04%	0.14	0.84
Overlapped-GLCM-4L	SVM	85.71%	92.86%	80.95%	76.47%	94.44%	0.20	0.85
	KNN	77.86%	84.91%	73.56%	66.18%	88.89%	0.26	0.81
	BN	79.52%	84.30%	76.21%	71.08%	87.50%	0.27	0.84
Overlapped-GLCM-5L	SVM	86.43%	92.98%	81.93%	77.94%	94.44%	0.19	0.86
	KNN	78.21%	85.05%	73.99%	66.91%	88.89%	0.25	0.82
	BN	79.52%	83.91%	76.42%	71.57%	87.04%	0.14	0.84
Overlapped-GLCM-6L	SVM	86.43%	92.98%	81.93%	77.94%	94.44%	0.19	0.86
	KNN	78.21%	85.05%	73.99%	66.91%	88.89%	0.25	0.82
	BN	79.52%	83.91%	76.42%	71.57%	87.04%	0.14	0.84

Overlapped-KCC-3L	SVM	85.00%	91.23%	80.72%	76.47%	93.06%	0.20	0.85
	KNN	76.07%	82.24%	72.25%	64.71%	86.81%	0.27	0.8
	BN	77.86%	81.71%	75.10%	70.10%	85.19%	0.16	0.83
Overlapped-KCC-4L	SVM	85.00%	94.34%	79.31%	73.53%	95.83%	0.22	0.85
	KNN	78.57%	85.85%	74.14%	66.91%	89.58%	0.26	0.81
	BN	79.76%	84.39%	76.52%	71.57%	87.50%	0.28	0.83
Overlapped-KCC-5L	SVM	85.71%	96.15%	79.55%	73.53%	97.22%	0.21	0.85
	KNN	78.57%	85.85%	74.14%	66.91%	89.58%	0.26	0.82
	BN	80.00%	84.48%	76.83%	72.06%	87.50%	0.13	0.84
Overlapped-KCC-6L	SVM	85.71%	96.15%	79.55%	73.53%	97.22%	0.21	0.85
	KNN	78.21%	85.05%	73.99%	66.91%	88.89%	0.26	0.82
	BN	80.24%	84.57%	77.14%	72.55%	87.50%	0.27	0.84
Overlapped-ED-3L	SVM	87.86%	94.74%	83.13%	79.41%	95.83%	0.18	0.88
	KNN	75.71%	84.00%	71.11%	61.76%	88.89%	0.27	0.81
	BN	78.33%	83.83%	74.70%	68.63%	87.50%	0.31	0.84
Overlapped-ED-4L	SVM	84.29%	91.07%	79.76%	75.00%	93.06%	0.21	0.84
	KNN	76.43%	80.17%	73.78%	68.38%	84.03%	0.26	0.8
	BN	77.14%	79.35%	75.42%	71.57%	82.41%	0.26	0.82
Overlapped-ED-5L	SVM	85.00%	91.23%	80.72%	76.47%	93.06%	0.20	0.85
	KNN	76.07%	79.49%	73.62%	68.38%	83.33%	0.26	0.8
	BN	77.38%	79.46%	75.74%	72.06%	82.41%	0.19	0.82
Overlapped-ED-6L	SVM	85.00%	91.23%	80.72%	76.47%	93.06%	0.20	0.85
	KNN	76.07%	79.49%	73.62%	68.38%	83.33%	0.26	0.8
	BN	77.38%	79.46%	75.74%	72.06%	82.41%	0.19	0.82
Overlapped-DTW-3L	SVM	88.57%	94.83%	84.15%	80.88%	95.83%	0.17	0.88
	KNN	79.64%	86.24%	75.44%	69.12%	89.58%	0.24	0.84
	BN	80.24%	84.57%	77.14%	72.55%	87.50%	0.27	0.85
Overlapped-DTW-4L	SVM	88.57%	96.43%	83.33%	79.41%	97.22%	0.17	0.88
	KNN	79.64%	86.92%	75.14%	68.38%	90.28%	0.24	0.84
	BN	80.71%	85.55%	77.33%	72.55%	88.43%	0.27	0.85
Overlapped-DTW-5L	SVM	88.57%	96.43%	83.33%	79.41%	97.22%	0.17	0.88
	KNN	79.64%	86.92%	75.14%	68.38%	90.28%	0.24	0.84
	BN	80.71%	85.55%	77.33%	72.55%	88.43%	0.27	0.85
Overlapped-DTW-6L	SVM	88.57%	96.43%	83.33%	79.41%	97.22%	0.17	0.88
	KNN	79.64%	86.92%	75.14%	68.38%	90.28%	0.24	0.84
	BN	80.71%	85.55%	77.33%	72.55%	88.43%	0.27	0.85
Overlapped-LCS-3L	SVM	89.29%	96.49%	84.34%	80.88%	97.22%	0.16	0.89
	KNN	83.57%	88.79%	79.88%	75.74%	90.97%	0.20	0.86
	BN	85.00%	87.70%	82.83%	80.39%	89.35%	0.20	0.88
Overlapped-LCS-4L	SVM	84.29%	92.59%	79.07%	73.53%	94.44%	0.22	0.84
	KNN	78.21%	84.40%	74.27%	67.65%	88.19%	0.26	0.81
	BN	79.76%	85.21%	76.10%	70.59%	88.43%	0.28	0.83
Overlapped-LCS-5L	SVM	85.00%	92.73%	80.00%	75.00%	94.44%	0.21	0.85
	KNN	78.21%	84.40%	74.27%	67.65%	88.19%	0.26	0.81
	BN	80.00%	84.88%	76.61%	71.57%	87.96%	0.28	0.83
Overlapped-LCS-6L	SVM	85.00%	92.73%	80.00%	75.00%	94.44%	0.21	0.85
	KNN	78.21%	84.40%	74.27%	67.65%	88.19%	0.26	0.81
	BN	80.00%	84.88%	76.61%	71.57%	87.96%	0.28	0.83
Overlapped-KLD-3L	SVM	84.29%	91.07%	79.76%	75.00%	93.06%	0.21	0.84
	KNN	77.86%	84.26%	73.84%	66.91%	88.19%	0.26	0.81
	BN	78.33%	82.66%	75.30%	70.10%	86.11%	0.29	0.82

Overlapped-KLD-4L	SVM	87.86%	94.74%	83.13%	79.41%	95.83%	0.18	0.88
	KNN	78.57%	85.19%	74.42%	67.65%	88.89%	0.25	0.83
	BN	79.52%	83.52%	76.64%	72.06%	86.57%	0.27	0.85
Overlapped-KLD-5L	SVM	87.86%	94.74%	83.13%	79.41%	95.83%	0.18	0.88
	KNN	78.57%	85.19%	74.42%	67.65%	88.89%	0.25	0.83
	BN	79.52%	83.52%	76.64%	72.06%	86.57%	0.27	0.85
Overlapped-KLD-6L	SVM	87.86%	94.74%	83.13%	79.41%	95.83%	0.18	0.88
	KNN	78.57%	85.19%	74.42%	67.65%	88.89%	0.25	0.83
	BN	79.52%	83.52%	76.64%	72.06%	86.57%	0.27	0.85

Table A.7: The results using LPQ with PCA.

Method	Classifiers	Acc	Sen	Spec	PPV	NPV	EER	AUC
Standard-0NCF-3L	SVM	73.57%	68.67%	80.70%	83.82%	63.89%	0.20	0.74
	KNN	62.50%	57.21%	80.00%	90.44%	36.11%	0.38	0.69
	BN	67.38%	62.01%	78.01%	84.80%	50.93%	0.46	0.73
Standard-0NCF-4L	SVM	68.57%	63.64%	76.92%	82.35%	55.56%	0.24	0.69
	KNN	59.29%	54.95%	75.86%	89.71%	30.56%	0.40	0.65
	BN	65.24%	60.07%	76.52%	84.80%	46.76%	0.21	0.7
Standard-0NCF-5L	SVM	72.14%	67.47%	78.95%	82.35%	62.50%	0.22	0.72
	KNN	62.14%	56.88%	80.65%	91.18%	34.72%	0.38	0.68
	BN	67.38%	61.59%	80.15%	87.25%	48.61%	0.35	0.72
Standard-0NCF-6L	SVM	65.00%	61.45%	70.18%	75.00%	55.56%	0.31	0.65
	KNN	57.86%	54.09%	71.67%	87.50%	29.86%	0.42	0.62
	BN	66.90%	61.40%	78.52%	85.78%	49.07%	0.50	0.69
Standard-AIV-3L	SVM	75.71%	70.24%	83.93%	86.76%	65.28%	0.17	0.76
	KNN	62.86%	57.84%	76.32%	86.76%	40.28%	0.37	0.7
	BN	69.05%	63.70%	78.67%	84.31%	54.63%	0.21	0.75
Standard-AIV-4L	SVM	83.57%	79.22%	88.89%	89.71%	77.78%	0.12	0.84
	KNN	72.50%	65.95%	85.26%	89.71%	56.25%	0.30	0.78
	BN	76.43%	70.27%	86.34%	89.22%	64.35%	0.11	0.84
Standard-AIV-5L	SVM	80.71%	78.87%	82.61%	82.35%	79.17%	0.18	0.81
	KNN	68.93%	62.69%	82.76%	88.97%	50.00%	0.32	0.75
	BN	74.05%	67.53%	85.91%	89.71%	59.26%	0.13	0.81
Standard-AIV-6L	SVM	87.86%	84.93%	91.04%	91.18%	84.72%	0.09	0.88
	KNN	78.93%	72.00%	90.48%	92.65%	65.97%	0.24	0.84
	BN	80.00%	74.59%	87.50%	89.22%	71.30%	0.29	0.85
Standard-GLCM-3L	SVM	75.71%	71.25%	81.67%	83.82%	68.06%	0.19	0.76
	KNN	63.57%	58.02%	80.88%	90.44%	38.19%	0.36	0.7
	BN	71.43%	65.44%	82.43%	87.25%	56.48%	0.43	0.76
Standard-GLCM-4L	SVM	72.14%	67.06%	80.00%	83.82%	61.11%	0.21	0.72
	KNN	61.07%	56.11%	79.66%	91.18%	32.64%	0.38	0.67
	BN	66.90%	61.48%	78.10%	85.29%	49.54%	0.47	0.73
Standard-GLCM-5L	SVM	72.86%	67.86%	80.36%	83.82%	62.50%	0.21	0.73
	KNN	60.71%	56.07%	75.76%	88.24%	34.72%	0.38	0.67
	BN	69.52%	63.29%	82.84%	88.73%	51.39%	0.44	0.76
Standard-GLCM-6L	SVM	75.00%	72.60%	77.61%	77.94%	72.22%	0.23	0.75
	KNN	61.07%	59.85%	62.24%	60.29%	61.81%	0.39	0.68
	BN	69.52%	68.45%	70.56%	69.12%	69.91%	0.31	0.76

Standard-KCC-3L	SVM	70.00%	64.77%	78.85%	83.82%	56.94%	0.22	0.7
	KNN	59.64%	55.20%	76.27%	89.71%	31.25%	0.40	0.65
	BN	67.38%	61.36%	81.60%	88.73%	47.22%	0.50	0.72
Standard-KCC-4L	SVM	72.14%	67.47%	78.95%	82.35%	62.50%	0.22	0.72
	KNN	60.36%	55.87%	74.63%	87.50%	34.72%	0.39	0.67
	BN	67.86%	62.55%	77.93%	84.31%	52.31%	0.47	0.74
Standard-KCC-5L	SVM	87.14%	85.71%	88.57%	88.24%	86.11%	0.12	0.87
	KNN	75.36%	71.61%	80.00%	81.62%	69.44%	0.26	0.81
	BN	79.52%	77.06%	82.18%	82.35%	76.85%	0.22	0.86
Standard-KCC-6L	SVM	71.43%	70.00%	72.86%	72.06%	70.83%	0.28	0.71
	KNN	65.36%	61.27%	71.96%	77.94%	53.47%	0.36	0.69
	BN	71.43%	68.26%	75.26%	76.96%	66.20%	0.33	0.75
Standard-ED-3L	SVM	81.43%	76.92%	87.10%	88.24%	75.00%	0.14	0.82
	KNN	71.07%	63.82%	88.89%	93.38%	50.00%	0.31	0.77
	BN	76.67%	70.87%	85.54%	88.24%	65.74%	0.34	0.83
Standard-ED-4L	SVM	79.29%	76.00%	83.08%	83.82%	75.00%	0.18	0.79
	KNN	67.14%	60.68%	85.14%	91.91%	43.75%	0.34	0.74
	BN	76.19%	69.26%	88.67%	91.67%	61.57%	0.38	0.82
Standard-ED-5L	SVM	81.43%	75.61%	89.66%	91.18%	72.22%	0.11	0.82
	KNN	68.57%	61.43%	90.00%	94.85%	43.75%	0.33	0.76
	BN	74.05%	67.40%	86.39%	90.20%	58.80%	0.39	0.81
Standard-ED-6L	SVM	80.71%	79.71%	81.69%	80.88%	80.56%	0.19	0.81
	KNN	78.21%	73.58%	84.30%	86.03%	70.83%	0.25	0.8
	BN	82.62%	79.91%	85.57%	85.78%	79.63%	0.20	0.85
Standard-DTW-3L	SVM	71.43%	66.67%	78.57%	82.35%	61.11%	0.22	0.72
	KNN	59.29%	55.29%	70.83%	84.56%	35.42%	0.40	0.66
	BN	65.24%	60.58%	73.97%	81.37%	50.00%	0.46	0.71
Standard-DTW-4L	SVM	55.71%	53.75%	58.33%	63.24%	48.61%	0.43	0.56
	KNN	52.86%	50.93%	59.38%	80.88%	26.39%	0.47	0.55
	BN	60.71%	56.94%	68.35%	78.43%	43.98%	0.51	0.63
Standard-DTW-5L	SVM	60.00%	58.11%	62.12%	63.24%	56.94%	0.39	0.6
	KNN	56.07%	53.37%	62.07%	75.74%	37.50%	0.44	0.58
	BN	63.10%	59.18%	69.93%	77.45%	49.54%	0.30	0.65
Standard-DTW-6L	SVM	70.71%	71.43%	70.13%	66.18%	75.00%	0.31	0.71
	KNN	64.29%	63.04%	65.49%	63.97%	64.58%	0.36	0.67
	BN	69.52%	68.63%	70.37%	68.63%	70.37%	0.31	0.72
Standard-LCS-3L	SVM	90.00%	90.91%	89.19%	88.24%	91.67%	0.11	0.9
	KNN	80.00%	73.26%	90.74%	92.65%	68.06%	0.09	0.85
	BN	83.81%	79.06%	89.78%	90.69%	77.31%	0.23	0.89
Standard-LCS-4L	SVM	92.86%	92.65%	93.06%	92.65%	93.06%	0.07	0.93
	KNN	81.79%	74.29%	94.29%	95.59%	68.75%	0.05	0.88
	BN	85.48%	78.95%	94.80%	95.59%	75.93%	0.04	0.91
Standard-LCS-5L	SVM	87.86%	88.06%	87.67%	86.76%	88.89%	0.13	0.88
	KNN	86.79%	83.22%	90.84%	91.18%	82.64%	0.09	0.87
	BN	87.86%	85.58%	90.24%	90.20%	85.65%	0.10	0.89
Standard-LCS-6L	SVM	89.29%	89.55%	89.04%	88.24%	90.28%	0.12	0.89
	KNN	89.29%	90.15%	88.51%	87.50%	90.97%	0.12	0.89
	BN	90.71%	91.04%	90.41%	89.71%	91.67%	0.10	0.92
Standard-KLD-3L	SVM	73.57%	69.62%	78.69%	80.88%	66.67%	0.22	0.74
	KNN	61.79%	56.68%	79.37%	90.44%	34.72%	0.38	0.68
	BN	69.29%	63.25%	81.75%	87.75%	51.85%	0.47	0.75

Standard-KLD-4L	SVM	67.86%	64.56%	72.13%	75.00%	61.11%	0.29	0.68
	KNN	57.86%	54.25%	69.12%	84.56%	32.64%	0.41	0.63
	BN	64.29%	59.64%	73.57%	81.86%	47.69%	0.22	0.7
Standard-KLD-5L	SVM	70.00%	68.06%	72.06%	72.06%	68.06%	0.29	0.7
	KNN	62.50%	57.87%	73.49%	83.82%	42.36%	0.38	0.67
	BN	69.52%	64.29%	78.57%	83.82%	56.02%	0.42	0.72
Standard-KLD-6L	SVM	70.71%	69.57%	71.83%	70.59%	70.83%	0.29	0.71
	KNN	66.43%	63.64%	69.84%	72.06%	61.11%	0.32	0.69
	BN	70.71%	69.19%	72.25%	71.57%	69.91%	0.29	0.74
Overlapped-0NCF-3L	SVM	67.86%	64.56%	72.13%	75.00%	61.11%	0.29	0.68
	KNN	59.29%	55.29%	70.83%	84.56%	35.42%	0.41	0.64
	BN	64.52%	59.93%	73.43%	81.37%	48.61%	0.47	0.68
Overlapped-0NCF-4L	SVM	67.86%	64.56%	72.13%	75.00%	61.11%	0.29	0.68
	KNN	59.29%	55.29%	70.83%	84.56%	35.42%	0.41	0.64
	BN	64.52%	59.93%	73.43%	81.37%	48.61%	0.47	0.68
Overlapped-0NCF-5L	SVM	67.86%	64.56%	72.13%	75.00%	61.11%	0.29	0.68
	KNN	59.29%	55.29%	70.83%	84.56%	35.42%	0.41	0.64
	BN	64.52%	59.93%	73.43%	81.37%	48.61%	0.47	0.68
Overlapped-0NCF-6L	SVM	67.86%	64.56%	72.13%	75.00%	61.11%	0.29	0.68
	KNN	59.29%	55.29%	70.83%	84.56%	35.42%	0.41	0.64
	BN	64.52%	59.93%	73.43%	81.37%	48.61%	0.47	0.68
Overlapped-AIV-3L	SVM	75.71%	70.24%	83.93%	86.76%	65.28%	0.17	0.76
	KNN	65.00%	59.13%	81.94%	90.44%	40.97%	0.36	0.71
	BN	68.81%	63.77%	77.42%	82.84%	55.56%	0.40	0.74
Overlapped-AIV-4L	SVM	72.14%	71.01%	73.24%	72.06%	72.22%	0.28	0.72
	KNN	66.79%	62.29%	74.29%	80.15%	54.17%	0.26	0.7
	BN	70.71%	66.67%	76.27%	79.41%	62.50%	0.35	0.73
Overlapped-AIV-5L	SVM	72.14%	71.01%	73.24%	72.06%	72.22%	0.28	0.72
	KNN	66.79%	62.29%	74.29%	80.15%	54.17%	0.26	0.7
	BN	70.71%	66.67%	76.27%	79.41%	62.50%	0.35	0.73
Overlapped-AIV-6L	SVM	72.14%	71.01%	73.24%	72.06%	72.22%	0.28	0.72
	KNN	66.79%	62.29%	74.29%	80.15%	54.17%	0.26	0.7
	BN	70.71%	66.67%	76.27%	79.41%	62.50%	0.35	0.73
Overlapped-GLCM-3L	SVM	76.43%	71.08%	84.21%	86.76%	66.67%	0.17	0.77
	KNN	66.07%	59.81%	84.51%	91.91%	41.67%	0.35	0.72
	BN	72.38%	66.06%	84.25%	88.73%	56.94%	0.41	0.77
Overlapped-GLCM-4L	SVM	67.14%	67.19%	67.11%	63.24%	70.83%	0.34	0.67
	KNN	59.29%	56.18%	64.71%	73.53%	45.83%	0.39	0.63
	BN	67.38%	63.90%	72.07%	75.49%	59.72%	0.38	0.71
Overlapped-GLCM-5L	SVM	70.00%	70.97%	69.23%	64.71%	75.00%	0.32	0.7
	KNN	61.07%	57.63%	66.99%	75.00%	47.92%	0.36	0.66
	BN	68.81%	65.15%	73.74%	76.96%	61.11%	0.37	0.72
Overlapped-GLCM-6L	SVM	70.00%	70.97%	69.23%	64.71%	75.00%	0.32	0.7
	KNN	61.07%	57.63%	66.99%	75.00%	47.92%	0.36	0.66
	BN	68.81%	65.15%	73.74%	76.96%	61.11%	0.37	0.72
Overlapped-KCC-3L	SVM	75.71%	69.77%	85.19%	88.24%	63.89%	0.16	0.76
	KNN	62.86%	57.41%	81.25%	91.18%	36.11%	0.37	0.7
	BN	72.14%	64.85%	88.98%	93.14%	52.31%	0.15	0.78
Overlapped-KCC-4L	SVM	67.86%	67.69%	68.00%	64.71%	70.83%	0.33	0.68
	KNN	63.57%	61.33%	66.15%	67.65%	59.72%	0.35	0.66
	BN	68.57%	66.98%	70.19%	69.61%	67.59%	0.31	0.71

Overlapped-KCC-5L	SVM	67.86%	68.85%	67.09%	61.76%	73.61%	0.34	0.68
	KNN	65.00%	66.38%	64.02%	56.62%	72.92%	0.37	0.66
	BN	69.52%	70.88%	68.49%	63.24%	75.46%	0.26	0.72
Overlapped-KCC-6L	SVM	69.29%	70.49%	68.35%	63.24%	75.00%	0.33	0.69
	KNN	66.07%	67.52%	65.03%	58.09%	73.61%	0.36	0.67
	BN	69.76%	71.27%	68.62%	63.24%	75.93%	0.25	0.72
Overlapped-ED-3L	SVM	94.29%	94.12%	94.44%	94.12%	94.44%	0.06	0.94
	KNN	74.29%	66.00%	95.00%	97.06%	52.78%	0.03	0.85
	BN	80.24%	73.00%	92.36%	94.12%	67.13%	0.06	0.9
Overlapped-ED-4L	SVM	72.86%	66.67%	84.00%	88.24%	58.33%	0.17	0.73
	KNN	65.36%	60.32%	75.82%	83.82%	47.92%	0.36	0.7
	BN	71.67%	66.04%	81.29%	85.78%	58.33%	0.38	0.76
Overlapped-ED-5L	SVM	75.00%	68.97%	84.91%	88.24%	62.50%	0.16	0.75
	KNN	66.79%	62.15%	74.76%	80.88%	53.47%	0.35	0.71
	BN	72.62%	67.73%	79.88%	83.33%	62.50%	0.36	0.76
Overlapped-ED-6L	SVM	75.00%	68.97%	84.91%	88.24%	62.50%	0.16	0.75
	KNN	66.79%	62.15%	74.76%	80.88%	53.47%	0.35	0.71
	BN	72.62%	67.73%	79.88%	83.33%	62.50%	0.36	0.76
Overlapped-DTW-3L	SVM	70.71%	67.09%	75.41%	77.94%	63.89%	0.26	0.71
	KNN	60.00%	55.83%	71.62%	84.56%	36.81%	0.39	0.66
	BN	64.76%	60.07%	73.94%	81.86%	48.61%	0.45	0.7
Overlapped-DTW-4L	SVM	68.57%	64.63%	74.14%	77.94%	59.72%	0.27	0.69
	KNN	59.64%	55.45%	72.46%	86.03%	34.72%	0.40	0.65
	BN	64.29%	59.64%	73.57%	81.86%	47.69%	0.47	0.69
Overlapped-DTW-5L	SVM	68.57%	64.63%	74.14%	77.94%	59.72%	0.27	0.69
	KNN	59.64%	55.45%	72.46%	86.03%	34.72%	0.40	0.65
	BN	64.29%	59.64%	73.57%	81.86%	47.69%	0.47	0.69
Overlapped-DTW-6L	SVM	68.57%	64.63%	74.14%	77.94%	59.72%	0.27	0.69
	KNN	59.64%	55.45%	72.46%	86.03%	34.72%	0.40	0.65
	BN	64.29%	59.64%	73.57%	81.86%	47.69%	0.47	0.69
Overlapped-LCS-3L	SVM	86.43%	87.69%	85.33%	83.82%	88.89%	0.15	0.86
	KNN	73.93%	67.03%	87.37%	91.18%	57.64%	0.11	0.8
	BN	79.52%	72.87%	90.12%	92.16%	67.59%	0.31	0.86
Overlapped-LCS-4L	SVM	68.57%	68.75%	68.42%	64.71%	72.22%	0.33	0.68
	KNN	66.07%	68.14%	64.67%	56.62%	75.00%	0.36	0.67
	BN	65.71%	67.86%	64.29%	55.88%	75.00%	0.36	0.67
Overlapped-LCS-5L	SVM	67.86%	67.69%	68.00%	64.71%	70.83%	0.33	0.68
	KNN	65.00%	66.67%	63.86%	55.88%	73.61%	0.37	0.66
	BN	65.00%	66.86%	63.75%	55.39%	74.07%	0.36	0.67
Overlapped-LCS-6L	SVM	67.86%	67.69%	68.00%	64.71%	70.83%	0.33	0.68
	KNN	65.00%	66.67%	63.86%	55.88%	73.61%	0.37	0.66
	BN	65.00%	66.86%	63.75%	55.39%	74.07%	0.36	0.67
Overlapped-KLD-3L	SVM	70.71%	66.27%	77.19%	80.88%	61.11%	0.24	0.71
	KNN	60.00%	55.71%	72.86%	86.03%	35.42%	0.39	0.66
	BN	65.00%	60.29%	74.13%	81.86%	49.07%	0.47	0.71
Overlapped-KLD-4L	SVM	69.29%	64.71%	76.36%	80.88%	58.33%	0.25	0.7
	KNN	60.36%	55.81%	75.38%	88.24%	34.03%	0.40	0.65
	BN	65.48%	60.57%	75.18%	82.84%	49.07%	0.48	0.7
Overlapped-KLD-5L	SVM	69.29%	64.71%	76.36%	80.88%	58.33%	0.25	0.7
	KNN	60.36%	55.81%	75.38%	88.24%	34.03%	0.40	0.65
	BN	65.48%	60.57%	75.18%	82.84%	49.07%	0.48	0.7

Overlapped-KLD-6L	SVM	69.29%	64.71%	76.36%	80.88%	58.33%	0.25	0.7
	KNN	60.36%	55.81%	75.38%	88.24%	34.03%	0.40	0.65
	BN	65.48%	60.57%	75.18%	82.84%	49.07%	0.48	0.7

A.3 Feature Selection-based Results

In this part additional results for the evaluation of the IFK single feature generation mechanism are considered with respect to true seven proposed critical functions and no critical functions. The results included in this part are presented in eight different tables (Tables A.8 to A.15) for each critical function. Recall that the original reported experiments reported in Chapter 6 only featured overlapping decomposition, the LCS critical function and SVM classification. Additional results are thus presented using:

1. No critical function (0NCF),
2. Average Intensity Value (AIV),
3. Kendall's Coefficient Concordance (KCC),
4. Gray Level Co-occurrence Matrix (GLCM),
5. Euclidean Distance (ED),
6. Dynamic Time Warping (DTW),
7. Longest Common Subsequence (LCS) and
8. Kullback-Leibler divergence (KLD).

The results are presented in a series of tables using the range of dictionary sizes each K considered previously, $\{32, 64, 128, 256, 512\}$, and a range of values for L.

Table A.8: IFK results without using a critical function (0NCF).

Method	Classifiers	Acc	Sen	Spec	PPV	NPV	EER	AUC
Standard-64K-3L	SVM	90.71%	91.04%	90.41%	89.71%	91.67%	0.10	0.91
	KNN	88.21%	88.72%	87.76%	86.76%	89.58%	0.13	0.89
	BN	89.05%	90.31%	87.95%	86.76%	91.20%	0.13	0.91
Standard-128K-3L	SVM	92.14%	95.24%	89.61%	88.24%	95.83%	0.11	0.92
	KNN	89.29%	89.55%	89.04%	88.24%	90.28%	0.12	0.91
	BN	90.00%	91.33%	88.84%	87.75%	92.13%	0.12	0.91
Standard-256K-3L	SVM	85.71%	87.50%	84.21%	82.35%	88.89%	0.17	0.86
	KNN	85.36%	84.67%	86.01%	85.29%	85.42%	0.15	0.85
	BN	77.62%	84.38%	73.46%	66.18%	88.43%	0.31	0.78

Standard-512K-3L	SVM	95.00%	96.92%	93.33%	92.65%	97.22%	0.07	0.95
	KNN	95.00%	95.52%	94.52%	94.12%	95.83%	0.06	0.95
	BN	93.57%	95.38%	92.00%	91.18%	95.83%	0.09	0.93
Standard-128K-4L	SVM	90.71%	92.31%	89.33%	88.24%	93.06%	0.11	0.91
	KNN	87.86%	86.43%	89.29%	88.97%	86.81%	0.11	0.89
	BN	88.33%	87.80%	88.84%	88.24%	88.43%	0.12	0.9
Standard-256K-4L	SVM	92.86%	93.94%	91.89%	91.18%	94.44%	0.09	0.93
	KNN	90.00%	91.54%	88.67%	87.50%	92.36%	0.12	0.91
	BN	89.52%	89.60%	89.45%	88.73%	90.28%	0.10	0.91
Standard-512K-4L	SVM	97.14%	100.00%	94.74%	94.12%	100.00%	0.06	0.97
	KNN	93.93%	94.74%	93.20%	92.65%	95.14%	0.07	0.95
	BN	92.14%	94.30%	90.31%	89.22%	94.91%	0.10	0.93
Standard-64K-4L	SVM	92.86%	95.31%	90.79%	89.71%	95.83%	0.10	0.93
	KNN	91.43%	94.44%	88.96%	87.50%	95.14%	0.11	0.92
	BN	91.67%	94.24%	89.52%	88.24%	94.91%	0.12	0.93
Standard-128K-5L	SVM	94.29%	95.45%	93.24%	92.65%	95.83%	0.07	0.94
	KNN	91.43%	93.75%	89.47%	88.24%	94.44%	0.11	0.93
	BN	89.29%	89.16%	89.40%	88.73%	89.81%	0.10	0.9
Standard-256K-5L	SVM	92.86%	96.77%	89.74%	88.24%	97.22%	0.11	0.93
	KNN	88.93%	92.00%	86.45%	84.56%	93.06%	0.14	0.91
	BN	86.43%	87.31%	85.65%	84.31%	88.43%	0.15	0.88
Standard-512K-5L	SVM	91.43%	93.75%	89.47%	88.24%	94.44%	0.11	0.91
	KNN	88.57%	92.62%	85.44%	83.09%	93.75%	0.15	0.9
	BN	85.95%	87.18%	84.89%	83.33%	88.43%	0.16	0.87
Standard-64K-5L	SVM	92.86%	93.94%	91.89%	91.18%	94.44%	0.09	0.93
	KNN	90.71%	92.97%	88.82%	87.50%	93.75%	0.12	0.92
	BN	89.05%	88.73%	89.35%	88.73%	89.35%	0.11	0.9
Standard-128K-6L	SVM	92.14%	93.85%	90.67%	89.71%	94.44%	0.10	0.92
	KNN	92.86%	95.31%	90.79%	89.71%	95.83%	0.10	0.92
	BN	89.52%	91.24%	88.05%	86.76%	92.13%	0.13	0.89
Standard-256K-6L	SVM	91.43%	93.75%	89.47%	88.24%	94.44%	0.11	0.91
	KNN	89.29%	92.74%	86.54%	84.56%	93.75%	0.14	0.9
	BN	85.71%	86.73%	84.82%	83.33%	87.96%	0.17	0.86
Standard-512K-6L	SVM	91.43%	93.75%	89.47%	88.24%	94.44%	0.11	0.91
	KNN	87.50%	87.41%	87.59%	86.76%	88.19%	0.13	0.89
	BN	84.52%	83.57%	85.45%	84.80%	84.26%	0.16	0.85
Standard-64K-6L	SVM	94.29%	96.88%	92.11%	91.18%	97.22%	0.08	0.94
	KNN	92.14%	94.53%	90.13%	88.97%	95.14%	0.10	0.93
	BN	87.86%	88.44%	87.33%	86.27%	89.35%	0.14	0.89
Overlapped-32K-3L	SVM	92.86%	96.77%	89.74%	88.24%	97.22%	0.11	0.93
	KNN	90.36%	94.31%	87.26%	85.29%	95.14%	0.13	0.91
	BN	89.05%	92.93%	86.02%	83.82%	93.98%	0.06	0.9
Overlapped-64K-3L	SVM	94.29%	98.39%	91.03%	89.71%	98.61%	0.09	0.94
	KNN	92.14%	95.24%	89.61%	88.24%	95.83%	0.11	0.93
	BN	90.95%	94.15%	88.36%	86.76%	94.91%	0.12	0.91
Overlapped-128K-3L	SVM	92.86%	96.77%	89.74%	88.24%	97.22%	0.11	0.93
	KNN	91.79%	93.80%	90.07%	88.97%	94.44%	0.10	0.92
	BN	90.48%	93.16%	88.26%	86.76%	93.98%	0.13	0.9
Overlapped-256K-3L	SVM	90.71%	92.31%	89.33%	88.24%	93.06%	0.11	0.91
	KNN	78.93%	80.80%	77.42%	74.26%	83.33%	0.23	0.85
	BN	74.05%	73.40%	74.65%	73.04%	75.00%	0.26	0.77

Overlapped-512K-3L	SVM	91.43%	92.42%	90.54%	89.71%	93.06%	0.10	0.91
	KNN	92.14%	92.54%	91.78%	91.18%	93.06%	0.09	0.92
	BN	91.43%	92.86%	90.18%	89.22%	93.52%	0.10	0.92
Overlapped-32K-4L	SVM	97.14%	98.48%	95.95%	95.59%	98.61%	0.04	0.97
	KNN	90.71%	95.08%	87.34%	85.29%	95.83%	0.12	0.94
	BN	90.00%	95.00%	86.25%	83.82%	95.83%	0.14	0.93
Overlapped-64K-4L	SVM	90.00%	89.71%	90.28%	89.71%	90.28%	0.10	0.9
	KNN	87.86%	89.23%	86.67%	85.29%	90.28%	0.14	0.89
	BN	88.57%	91.05%	86.52%	84.80%	92.13%	0.15	0.9
Overlapped-128K-4L	SVM	87.86%	86.96%	88.73%	88.24%	87.50%	0.12	0.88
	KNN	85.71%	85.29%	86.11%	85.29%	86.11%	0.14	0.87
	BN	86.67%	87.76%	85.71%	84.31%	88.89%	0.15	0.88
Overlapped-256K-4L	SVM	90.71%	93.65%	88.31%	86.76%	94.44%	0.12	0.91
	KNN	89.29%	91.41%	87.50%	86.03%	92.36%	0.13	0.9
	BN	86.90%	89.84%	84.55%	82.35%	91.20%	0.16	0.87
Overlapped-512K-4L	SVM	86.43%	87.69%	85.33%	83.82%	88.89%	0.15	0.86
	KNN	84.64%	84.44%	84.83%	83.82%	85.42%	0.16	0.85
	BN	81.43%	80.58%	82.24%	81.37%	81.48%	0.19	0.81
Overlapped-32K-5L	SVM	93.57%	95.38%	92.00%	91.18%	95.83%	0.08	0.94
	KNN	94.64%	96.18%	93.29%	92.65%	96.53%	0.07	0.94
	BN	92.14%	94.30%	90.31%	89.22%	94.91%	0.11	0.92
Overlapped-64K-5L	SVM	95.00%	95.52%	94.52%	94.12%	95.83%	0.06	0.95
	KNN	93.21%	95.35%	91.39%	90.44%	95.83%	0.09	0.94
	BN	91.43%	94.21%	89.13%	87.75%	94.91%	0.11	0.93
Overlapped-128K-5L	SVM	88.57%	90.62%	86.84%	85.29%	91.67%	0.14	0.88
	KNN	88.21%	89.92%	86.75%	85.29%	90.97%	0.14	0.88
	BN	87.86%	90.05%	86.03%	84.31%	91.20%	0.15	0.89
Overlapped-256K-5L	SVM	92.14%	93.85%	90.67%	89.71%	94.44%	0.10	0.92
	KNN	89.29%	88.97%	89.58%	88.97%	89.58%	0.11	0.91
	BN	88.10%	88.50%	87.73%	86.76%	89.35%	0.13	0.9
Overlapped-512K-5L	SVM	93.57%	95.38%	92.00%	91.18%	95.83%	0.08	0.94
	KNN	90.36%	92.25%	88.74%	87.50%	93.06%	0.12	0.92
	BN	85.95%	86.07%	85.84%	84.80%	87.04%	0.15	0.86
Overlapped-32K-6L	SVM	91.43%	96.67%	87.50%	85.29%	97.22%	0.13	0.91
	KNN	90.71%	93.65%	88.31%	86.76%	94.44%	0.12	0.91
	BN	89.76%	92.59%	87.45%	85.78%	93.52%	0.07	0.91
Overlapped-64K-6L	SVM	92.86%	96.77%	89.74%	88.24%	97.22%	0.11	0.93
	KNN	91.79%	94.49%	89.54%	88.24%	95.14%	0.11	0.92
	BN	89.76%	92.59%	87.45%	85.78%	93.52%	0.13	0.91
Overlapped-128K-6L	SVM	93.57%	96.83%	90.91%	89.71%	97.22%	0.10	0.93
	KNN	91.79%	95.20%	89.03%	87.50%	95.83%	0.11	0.93
	BN	90.24%	93.12%	87.88%	86.27%	93.98%	0.13	0.91
Overlapped-256K-6L	SVM	86.43%	86.57%	86.30%	85.29%	87.50%	0.14	0.86
	KNN	86.43%	87.12%	85.81%	84.56%	88.19%	0.15	0.86
	BN	85.95%	87.18%	84.89%	83.33%	88.43%	0.17	0.87
Overlapped-512K-6L	SVM	92.14%	92.54%	91.78%	91.18%	93.06%	0.09	0.92
	KNN	90.36%	90.37%	90.34%	89.71%	90.97%	0.10	0.91
	BN	90.24%	91.79%	88.89%	87.75%	92.59%	0.12	0.92

Table A.9: The results of using the AIV critical function in the context of IFK.

Method	Classifiers	Acc	Sen	Spec	PPV	NPV	EER	AUC
Standard-32K-3L	SVM	96.43%	97.01%	95.89%	95.59%	97.22%	0.04	0.96
	KNN	95.00%	96.92%	93.33%	92.65%	97.22%	0.07	0.96
	BN	95.48%	96.95%	94.17%	93.63%	97.22%	0.06	0.96
Standard-64K-3L	SVM	92.86%	92.65%	93.06%	92.65%	93.06%	0.07	0.93
	KNN	92.86%	92.65%	93.06%	92.65%	93.06%	0.07	0.93
	BN	93.10%	93.53%	92.69%	92.16%	93.98%	0.08	0.94
Standard-32K-4L	SVM	98.57%	98.53%	98.61%	98.53%	98.61%	0.01	0.99
	KNN	96.79%	98.47%	95.30%	94.85%	98.61%	0.05	0.98
	BN	95.48%	96.95%	94.17%	93.63%	97.22%	0.06	0.96
Standard-128K-3L	SVM	99.29%	100.00%	98.63%	98.53%	100.00%	0.01	0.99
	KNN	98.57%	100.00%	97.30%	97.06%	100.00%	0.03	0.99
	BN	96.19%	98.96%	93.86%	93.14%	99.07%	0.07	0.96
Standard-256K-3L	SVM	99.29%	100.00%	98.63%	98.53%	100.00%	0.01	0.99
	KNN	98.21%	98.52%	97.93%	97.79%	98.61%	0.02	0.99
	BN	97.62%	98.02%	97.25%	97.06%	98.15%	0.03	0.98
Standard-512K-3L	SVM	97.86%	100.00%	96.00%	95.59%	100.00%	0.04	0.98
	KNN	96.07%	97.71%	94.63%	94.12%	97.92%	0.06	0.97
	BN	95.24%	96.94%	93.75%	93.14%	97.22%	0.07	0.95
Standard-128K-4L	SVM	99.29%	100.00%	98.63%	98.53%	100.00%	0.01	0.99
	KNN	98.57%	100.00%	97.30%	97.06%	100.00%	0.03	0.99
	BN	96.19%	97.00%	95.45%	95.10%	97.22%	0.05	0.97
Standard-256K-4L	SVM	95.71%	95.59%	95.83%	95.59%	95.83%	0.04	0.96
	KNN	97.14%	96.38%	97.89%	97.79%	96.53%	0.02	0.96
	BN	96.67%	95.67%	97.64%	97.55%	95.83%	0.04	0.96
Standard-512K-4L	SVM	96.43%	95.65%	97.18%	97.06%	95.83%	0.03	0.96
	KNN	92.14%	93.85%	90.67%	89.71%	94.44%	0.06	0.94
	BN	87.62%	89.18%	86.28%	84.80%	90.28%	0.14	0.89
Standard-64K-4L	SVM	99.29%	98.55%	100.00%	100.00%	98.61%	0.00	0.99
	KNN	95.71%	98.44%	93.42%	92.65%	98.61%	0.01	0.97
	BN	94.52%	96.41%	92.89%	92.16%	96.76%	0.08	0.96
Standard-128K-5L	SVM	99.29%	100.00%	98.63%	98.53%	100.00%	0.01	0.99
	KNN	99.29%	100.00%	98.63%	98.53%	100.00%	0.01	0.99
	BN	97.38%	98.01%	96.80%	96.57%	98.15%	0.03	0.98
Standard-256K-5L	SVM	100.00%	100.00%	100.00%	100.00%	100.00%	0.00	1
	KNN	100.00%	100.00%	100.00%	100.00%	100.00%	0.00	1
	BN	99.52%	99.03%	100.00%	100.00%	99.07%	0.01	0.99
Standard-32K-5L	SVM	94.29%	96.88%	92.11%	91.18%	97.22%	0.08	0.94
	KNN	93.57%	96.83%	90.91%	89.71%	97.22%	0.09	0.94
	BN	93.33%	95.36%	91.59%	90.69%	95.83%	0.09	0.94
Standard-512K-5L	SVM	100.00%	100.00%	100.00%	100.00%	100.00%	0.00	1
	KNN	100.00%	100.00%	100.00%	100.00%	100.00%	0.00	1
	BN	99.76%	99.51%	100.00%	100.00%	99.54%	0.00	1
Standard-64K-5L	SVM	97.86%	98.51%	97.26%	97.06%	98.61%	0.03	0.98
	KNN	97.50%	98.50%	96.60%	96.32%	98.61%	0.04	0.98
	BN	95.71%	95.59%	95.83%	95.59%	95.83%	0.04	0.96
Standard-128K-6L	SVM	100.00%	100.00%	100.00%	100.00%	100.00%	0.00	1
	KNN	99.64%	100.00%	99.31%	99.26%	100.00%	0.01	1
	BN	97.86%	97.56%	98.14%	98.04%	97.69%	0.02	0.98
Standard-256K-6L	SVM	100.00%	100.00%	100.00%	100.00%	100.00%	0.00	1

	KNN	99.29%	99.26%	99.31%	99.26%	99.31%	0.01	1
	BN	98.33%	98.05%	98.60%	98.53%	98.15%	0.02	0.99
Standard-32K-6L	SVM	99.29%	100.00%	98.63%	98.53%	100.00%	0.01	0.99
	KNN	98.93%	100.00%	97.96%	97.79%	100.00%	0.02	0.99
	BN	97.86%	98.99%	96.83%	96.57%	99.07%	0.03	0.98
Standard-512K-6L	SVM	100.00%	100.00%	100.00%	100.00%	100.00%	0.00	1
	KNN	99.29%	98.55%	100.00%	100.00%	98.61%	0.00	1
	BN	99.29%	98.55%	100.00%	100.00%	98.61%	0.00	1
Standard-64K-6L	SVM	99.29%	100.00%	98.63%	98.53%	100.00%	0.01	0.99
	KNN	98.93%	100.00%	97.96%	97.79%	100.00%	0.02	0.99
	BN	97.62%	98.50%	96.82%	96.57%	98.61%	0.03	0.98
Overlapped-128K-3L	SVM	91.43%	92.42%	90.54%	89.71%	93.06%	0.10	0.91
	KNN	91.79%	93.13%	90.60%	89.71%	93.75%	0.10	0.92
	BN	90.71%	91.88%	89.69%	88.73%	92.59%	0.11	0.91
Overlapped-256K-3L	SVM	98.57%	100.00%	97.30%	97.06%	100.00%	0.03	0.99
	KNN	96.43%	97.73%	95.27%	94.85%	97.92%	0.05	0.97
	BN	93.57%	94.03%	93.15%	92.65%	94.44%	0.06	0.95
Overlapped-32K-3L	SVM	97.14%	98.48%	95.95%	95.59%	98.61%	0.04	0.97
	KNN	96.43%	99.22%	94.08%	93.38%	99.31%	0.06	0.97
	BN	94.76%	97.89%	92.17%	91.18%	98.15%	0.08	0.95
Overlapped-512K-3L	SVM	92.86%	95.31%	90.79%	89.71%	95.83%	0.10	0.93
	KNN	90.36%	91.60%	89.26%	88.24%	92.36%	0.11	0.92
	BN	89.76%	90.86%	88.79%	87.75%	91.67%	0.12	0.91
Overlapped-64K-3L	SVM	94.29%	98.39%	91.03%	89.71%	98.61%	0.09	0.94
	KNN	92.50%	96.00%	89.68%	88.24%	96.53%	0.11	0.93
	BN	90.71%	93.65%	88.31%	86.76%	94.44%	0.12	0.91
Overlapped-128K-4L	SVM	95.00%	96.92%	93.33%	92.65%	97.22%	0.07	0.95
	KNN	96.43%	98.46%	94.67%	94.12%	98.61%	0.06	0.96
	BN	95.71%	96.50%	95.00%	94.61%	96.76%	0.05	0.95
Overlapped-256K-4L	SVM	97.86%	98.51%	97.26%	97.06%	98.61%	0.03	0.98
	KNN	96.79%	97.04%	96.55%	96.32%	97.22%	0.04	0.97
	BN	96.43%	96.55%	96.31%	96.08%	96.76%	0.04	0.97
Overlapped-32K-4L	SVM	95.00%	96.92%	93.33%	92.65%	97.22%	0.07	0.95
	KNN	94.29%	97.62%	91.56%	90.44%	97.92%	0.09	0.95
	BN	93.57%	96.34%	91.27%	90.20%	96.76%	0.10	0.94
Overlapped-512K-4L	SVM	95.71%	95.59%	95.83%	95.59%	95.83%	0.04	0.96
	KNN	96.43%	97.01%	95.89%	95.59%	97.22%	0.04	0.96
	BN	96.67%	97.03%	96.33%	96.08%	97.22%	0.04	0.97
Overlapped-64K-4L	SVM	93.57%	94.03%	93.15%	92.65%	94.44%	0.07	0.94
	KNN	93.21%	95.35%	91.39%	90.44%	95.83%	0.09	0.93
	BN	93.81%	95.41%	92.41%	91.67%	95.83%	0.08	0.94
Overlapped-128K-5L	SVM	97.86%	98.51%	97.26%	97.06%	98.61%	0.03	0.98
	KNN	97.14%	99.23%	95.33%	94.85%	99.31%	0.05	0.97
	BN	96.67%	98.47%	95.09%	94.61%	98.61%	0.05	0.97
Overlapped-256K-5L	SVM	98.57%	98.53%	98.61%	98.53%	98.61%	0.01	0.99
	KNN	98.93%	99.26%	98.62%	98.53%	99.31%	0.01	0.99
	BN	98.33%	98.52%	98.16%	98.04%	98.61%	0.02	0.98
Overlapped-32K-5L	SVM	97.86%	98.51%	97.26%	97.06%	98.61%	0.03	0.98
	KNN	95.36%	96.95%	93.96%	93.38%	97.22%	0.06	0.97
	BN	92.62%	93.91%	91.48%	90.69%	94.44%	0.09	0.94
Overlapped-512K-5L	SVM	99.29%	98.55%	100.00%	100.00%	98.61%	0.00	0.99

	KNN	98.57%	98.53%	98.61%	98.53%	98.61%	0.01	0.99
	BN	98.33%	98.05%	98.60%	98.53%	98.15%	0.02	0.99
Overlapped-64K-5L	SVM	98.57%	98.53%	98.61%	98.53%	98.61%	0.01	0.99
	KNN	98.21%	99.25%	97.28%	97.06%	99.31%	0.03	0.98
	BN	96.67%	97.50%	95.91%	95.59%	97.69%	0.02	0.97
Overlapped-128K-6L	SVM	97.86%	97.10%	98.59%	98.53%	97.22%	0.01	0.98
	KNN	98.57%	98.53%	98.61%	98.53%	98.61%	0.01	0.98
	BN	98.33%	98.05%	98.60%	98.53%	98.15%	0.02	0.98
Overlapped-256K-6L	SVM	98.57%	98.53%	98.61%	98.53%	98.61%	0.01	0.99
	KNN	98.57%	98.53%	98.61%	98.53%	98.61%	0.01	0.99
	BN	98.33%	98.05%	98.60%	98.53%	98.15%	0.02	0.98
Overlapped-32K-6L	SVM	97.86%	97.10%	98.59%	98.53%	97.22%	0.01	0.98
	KNN	96.07%	96.30%	95.86%	95.59%	96.53%	0.04	0.97
	BN	95.00%	95.98%	94.12%	93.63%	96.30%	0.06	0.96
Overlapped-512K-6L	SVM	98.57%	100.00%	97.30%	97.06%	100.00%	0.03	0.99
	KNN	98.21%	99.25%	97.28%	97.06%	99.31%	0.03	0.98
	BN	98.33%	99.00%	97.72%	97.55%	99.07%	0.02	0.99
Overlapped-64K-6L	SVM	97.86%	97.10%	98.59%	98.53%	97.22%	0.01	0.98
	KNN	97.50%	97.08%	97.90%	97.79%	97.22%	0.03	0.98
	BN	96.90%	96.59%	97.21%	97.06%	96.76%	0.03	0.97

Table A.10: The results of using the GLCM critical function using IFK.

Method	Classifiers	Acc	Sen	Spec	PPV	NPV	EER	AUC
Standard-128K-3L	SVM	93.57%	96.83%	90.91%	89.71%	97.22%	0.10	0.93
	KNN	92.50%	94.57%	90.73%	89.71%	95.14%	0.10	0.93
	BN	92.14%	94.76%	89.96%	88.73%	95.37%	0.11	0.92
Standard-256K-3L	SVM	95.00%	98.41%	92.21%	91.18%	98.61%	0.08	0.95
	KNN	92.50%	95.28%	90.20%	88.97%	95.83%	0.10	0.94
	BN	91.19%	92.82%	89.78%	88.73%	93.52%	0.11	0.92
Standard-32K-3L	SVM	92.14%	95.24%	89.61%	88.24%	95.83%	0.11	0.92
	KNN	89.64%	94.21%	86.16%	83.82%	95.14%	0.14	0.91
	BN	90.48%	93.62%	87.93%	86.27%	94.44%	0.06	0.92
Standard-512K-3L	SVM	90.00%	89.71%	90.28%	89.71%	90.28%	0.10	0.9
	KNN	92.50%	93.23%	91.84%	91.18%	93.75%	0.09	0.91
	BN	89.29%	89.16%	89.40%	88.73%	89.81%	0.10	0.87
Standard-64K-3L	SVM	92.86%	96.77%	89.74%	88.24%	97.22%	0.11	0.93
	KNN	90.36%	91.60%	89.26%	88.24%	92.36%	0.11	0.92
	BN	90.95%	93.23%	89.04%	87.75%	93.98%	0.06	0.92
Standard-128K-4L	SVM	93.57%	95.38%	92.00%	91.18%	95.83%	0.08	0.94
	KNN	91.07%	93.70%	88.89%	87.50%	94.44%	0.11	0.92
	BN	91.19%	93.72%	89.08%	87.75%	94.44%	0.11	0.92
Standard-256K-4L	SVM	90.71%	92.31%	89.33%	88.24%	93.06%	0.11	0.91
	KNN	92.50%	93.89%	91.28%	90.44%	94.44%	0.09	0.92
	BN	92.14%	94.76%	89.96%	88.73%	95.37%	0.11	0.91
Standard-32K-4L	SVM	93.57%	94.03%	93.15%	92.65%	94.44%	0.07	0.94
	KNN	92.86%	93.94%	91.89%	91.18%	94.44%	0.09	0.93
	BN	92.38%	93.43%	91.44%	90.69%	93.98%	0.09	0.93

Standard-512K-4L	SVM	95.71%	98.44%	93.42%	92.65%	98.61%	0.07	0.96
	KNN	95.00%	96.21%	93.92%	93.38%	96.53%	0.06	0.95
	BN	94.05%	95.90%	92.44%	91.67%	96.30%	0.08	0.94
Standard-64K-4L	SVM	96.43%	97.01%	95.89%	95.59%	97.22%	0.04	0.96
	KNN	92.86%	94.62%	91.33%	90.44%	95.14%	0.09	0.95
	BN	91.43%	91.18%	91.67%	91.18%	91.67%	0.09	0.93
Standard-128K-5L	SVM	96.43%	98.46%	94.67%	94.12%	98.61%	0.06	0.96
	KNN	95.00%	97.66%	92.76%	91.91%	97.92%	0.08	0.96
	BN	93.33%	94.44%	92.34%	91.67%	94.91%	0.08	0.94
Standard-256K-5L	SVM	97.14%	98.48%	95.95%	95.59%	98.61%	0.04	0.97
	KNN	95.00%	98.41%	92.21%	91.18%	98.61%	0.08	0.96
	BN	94.52%	96.41%	92.89%	92.16%	96.76%	0.07	0.95
Standard-32K-5L	SVM	96.43%	97.01%	95.89%	95.59%	97.22%	0.04	0.96
	KNN	95.36%	96.24%	94.56%	94.12%	96.53%	0.06	0.96
	BN	94.29%	95.45%	93.24%	92.65%	95.83%	0.07	0.95
Standard-512K-5L	SVM	97.14%	98.48%	95.95%	95.59%	98.61%	0.04	0.97
	KNN	95.36%	98.43%	92.81%	91.91%	98.61%	0.07	0.96
	BN	94.05%	95.90%	92.44%	91.67%	96.30%	0.08	0.95
Standard-64K-5L	SVM	94.29%	96.88%	92.11%	91.18%	97.22%	0.08	0.94
	KNN	91.79%	96.69%	88.05%	86.03%	97.22%	0.12	0.93
	BN	90.95%	94.15%	88.36%	86.76%	94.91%	0.12	0.92
Standard-128K-6L	SVM	97.14%	97.06%	97.22%	97.06%	97.22%	0.03	0.97
	KNN	94.64%	96.90%	92.72%	91.91%	97.22%	0.07	0.96
	BN	93.81%	95.88%	92.04%	91.18%	96.30%	0.08	0.95
Standard-256K-6L	SVM	97.14%	97.06%	97.22%	97.06%	97.22%	0.03	0.97
	KNN	95.71%	97.69%	94.00%	93.38%	97.92%	0.06	0.96
	BN	94.29%	95.92%	92.86%	92.16%	96.30%	0.07	0.95
Standard-32K-6L	SVM	97.14%	98.48%	95.95%	95.59%	98.61%	0.04	0.97
	KNN	95.00%	97.66%	92.76%	91.91%	97.92%	0.07	0.96
	BN	93.57%	96.34%	91.27%	90.20%	96.76%	0.03	0.95
Standard-512K-6L	SVM	97.14%	97.06%	97.22%	97.06%	97.22%	0.03	0.97
	KNN	96.79%	98.47%	95.30%	94.85%	98.61%	0.05	0.97
	BN	95.71%	96.97%	94.59%	94.12%	97.22%	0.06	0.96
Standard-64K-6L	SVM	95.71%	96.97%	94.59%	94.12%	97.22%	0.06	0.96
	KNN	94.64%	96.18%	93.29%	92.65%	96.53%	0.07	0.95
	BN	93.10%	94.87%	91.56%	90.69%	95.37%	0.09	0.94
Overlapped-128K-3L	SVM	93.57%	98.36%	89.87%	88.24%	98.61%	0.11	0.93
	KNN	88.93%	90.08%	87.92%	86.76%	90.97%	0.13	0.91
	BN	87.86%	90.05%	86.03%	84.31%	91.20%	0.15	0.89
Overlapped-256K-3L	SVM	93.57%	98.36%	89.87%	88.24%	98.61%	0.11	0.93
	KNN	92.14%	95.97%	89.10%	87.50%	96.53%	0.11	0.93
	BN	91.67%	96.17%	88.19%	86.27%	96.76%	0.12	0.92
Overlapped-32K-3L	SVM	91.43%	96.67%	87.50%	85.29%	97.22%	0.13	0.91
	KNN	89.29%	94.17%	85.62%	83.09%	95.14%	0.15	0.9
	BN	88.33%	92.35%	85.23%	82.84%	93.52%	0.17	0.9
Overlapped-512K-3L	SVM	92.86%	95.31%	90.79%	89.71%	95.83%	0.10	0.93
	KNN	90.71%	90.44%	90.97%	90.44%	90.97%	0.10	0.92
	BN	90.71%	91.88%	89.69%	88.73%	92.59%	0.11	0.92
Overlapped-64K-3L	SVM	92.14%	96.72%	88.61%	86.76%	97.22%	0.12	0.92
	KNN	88.93%	93.39%	85.53%	83.09%	94.44%	0.15	0.9
	BN	88.10%	91.40%	85.47%	83.33%	92.59%	0.07	0.9

Overlapped-128K-4L	SVM	90.00%	92.19%	88.16%	86.76%	93.06%	0.12	0.9
	KNN	88.57%	90.00%	87.33%	86.03%	90.97%	0.13	0.89
	BN	87.38%	89.53%	85.59%	83.82%	90.74%	0.15	0.89
Overlapped-256K-4L	SVM	89.29%	89.55%	89.04%	88.24%	90.28%	0.12	0.89
	KNN	86.43%	85.51%	87.32%	86.76%	86.11%	0.13	0.88
	BN	81.19%	84.92%	78.42%	74.51%	87.50%	0.25	0.8
Overlapped-32K-4L	SVM	95.00%	95.52%	94.52%	94.12%	95.83%	0.06	0.95
	KNN	93.21%	95.35%	91.39%	90.44%	95.83%	0.09	0.94
	BN	92.14%	95.24%	89.61%	88.24%	95.83%	0.04	0.93
Overlapped-512K-4L	SVM	92.14%	92.54%	91.78%	91.18%	93.06%	0.09	0.92
	KNN	89.64%	90.23%	89.12%	88.24%	90.97%	0.11	0.91
	BN	88.57%	90.62%	86.84%	85.29%	91.67%	0.14	0.89
Overlapped-64K-4L	SVM	89.29%	89.55%	89.04%	88.24%	90.28%	0.12	0.89
	KNN	87.86%	88.64%	87.16%	86.03%	89.58%	0.13	0.89
	BN	88.81%	90.26%	87.56%	86.27%	91.20%	0.13	0.9
Overlapped-128K-5L	SVM	90.71%	89.86%	91.55%	91.18%	90.28%	0.09	0.91
	KNN	86.43%	88.28%	84.87%	83.09%	89.58%	0.11	0.89
	BN	86.90%	89.84%	84.55%	82.35%	91.20%	0.16	0.9
Overlapped-256K-5L	SVM	92.86%	92.65%	93.06%	92.65%	93.06%	0.07	0.93
	KNN	90.00%	90.91%	89.19%	88.24%	91.67%	0.11	0.91
	BN	90.00%	92.19%	88.16%	86.76%	93.06%	0.13	0.92
Overlapped-32K-5L	SVM	94.29%	95.45%	93.24%	92.65%	95.83%	0.07	0.94
	KNN	92.50%	94.57%	90.73%	89.71%	95.14%	0.10	0.93
	BN	91.19%	94.65%	88.41%	86.76%	95.37%	0.05	0.92
Overlapped-512K-5L	SVM	96.43%	97.01%	95.89%	95.59%	97.22%	0.04	0.96
	KNN	93.57%	95.38%	92.00%	91.18%	95.83%	0.08	0.95
	BN	86.43%	94.01%	81.42%	76.96%	95.37%	0.21	0.87
Overlapped-64K-5L	SVM	90.71%	93.65%	88.31%	86.76%	94.44%	0.12	0.91
	KNN	89.64%	94.21%	86.16%	83.82%	95.14%	0.14	0.9
	BN	89.29%	93.92%	85.77%	83.33%	94.91%	0.05	0.91
Overlapped-128K-6L	SVM	92.14%	93.85%	90.67%	89.71%	94.44%	0.10	0.92
	KNN	88.57%	92.62%	85.44%	83.09%	93.75%	0.15	0.9
	BN	87.62%	91.76%	84.45%	81.86%	93.06%	0.18	0.9
Overlapped-256K-6L	SVM	90.00%	92.19%	88.16%	86.76%	93.06%	0.12	0.9
	KNN	84.64%	91.89%	79.88%	75.00%	93.75%	0.20	0.87
	BN	85.48%	91.81%	81.12%	76.96%	93.52%	0.18	0.88
Overlapped-32K-6L	SVM	90.00%	90.91%	89.19%	88.24%	91.67%	0.11	0.9
	KNN	88.57%	89.39%	87.84%	86.76%	90.28%	0.13	0.89
	BN	89.29%	90.77%	88.00%	86.76%	91.67%	0.13	0.9
Overlapped-512K-6L	SVM	88.57%	91.94%	85.90%	83.82%	93.06%	0.15	0.88
	KNN	83.57%	89.47%	79.52%	75.00%	91.67%	0.20	0.86
	BN	84.29%	89.20%	80.74%	76.96%	91.20%	0.19	0.87
Overlapped-64K-6L	SVM	87.86%	89.23%	86.67%	85.29%	90.28%	0.14	0.88
	KNN	86.79%	91.60%	83.23%	80.15%	93.06%	0.17	0.87
	BN	86.90%	91.16%	83.68%	80.88%	92.59%	0.07	0.88

Table A.11: The results of using the KCC critical function using IFK.

Method	Classifiers	Acc	Sen	Spec	PPV	NPV	EER	AUC

Standard-128K-3L	SVM	97.86%	98.51%	97.26%	97.06%	98.61%	0.03	0.98
	KNN	94.29%	94.78%	93.84%	93.38%	95.14%	0.06	0.96
	BN	93.81%	94.06%	93.58%	93.14%	94.44%	0.07	0.95
Standard-256K-3L	SVM	97.14%	100.00%	94.74%	94.12%	100.00%	0.06	0.97
	KNN	93.57%	96.09%	91.45%	90.44%	96.53%	0.09	0.95
	BN	93.10%	95.81%	90.83%	89.71%	96.30%	0.04	0.95
Standard-32K-3L	SVM	94.29%	96.88%	92.11%	91.18%	97.22%	0.08	0.94
	KNN	93.21%	96.80%	90.32%	88.97%	97.22%	0.10	0.94
	BN	92.86%	94.85%	91.15%	90.20%	95.37%	0.09	0.94
Standard-512K-3L	SVM	96.43%	97.01%	95.89%	95.59%	97.22%	0.04	0.96
	KNN	96.07%	96.99%	95.24%	94.85%	97.22%	0.05	0.96
	BN	95.00%	96.92%	93.33%	92.65%	97.22%	0.07	0.95
Standard-64K-3L	SVM	94.29%	96.88%	92.11%	91.18%	97.22%	0.08	0.94
	KNN	92.50%	93.89%	91.28%	90.44%	94.44%	0.09	0.93
	BN	89.29%	89.95%	88.69%	87.75%	90.74%	0.12	0.9
Standard-128K-4L	SVM	98.57%	98.53%	98.61%	98.53%	98.61%	0.01	0.99
	KNN	97.50%	98.50%	96.60%	96.32%	98.61%	0.04	0.98
	BN	97.62%	97.55%	97.69%	97.55%	97.69%	0.02	0.98
Standard-256K-4L	SVM	95.71%	96.97%	94.59%	94.12%	97.22%	0.06	0.96
	KNN	96.43%	96.32%	96.53%	96.32%	96.53%	0.04	0.96
	BN	88.81%	92.90%	85.65%	83.33%	93.98%	0.17	0.9
Standard-32K-4L	SVM	98.57%	98.53%	98.61%	98.53%	98.61%	0.01	0.99
	KNN	97.50%	98.50%	96.60%	96.32%	98.61%	0.04	0.98
	BN	97.62%	97.55%	97.69%	97.55%	97.69%	0.02	0.98
Standard-512K-4L	SVM	96.43%	97.01%	95.89%	95.59%	97.22%	0.04	0.96
	KNN	93.57%	96.09%	91.45%	90.44%	96.53%	0.09	0.95
	BN	91.43%	93.30%	89.82%	88.73%	93.98%	0.11	0.92
Standard-64K-4L	SVM	97.14%	97.06%	97.22%	97.06%	97.22%	0.03	0.97
	KNN	96.79%	97.74%	95.92%	95.59%	97.92%	0.04	0.97
	BN	96.19%	95.63%	96.73%	96.57%	95.83%	0.04	0.96
Standard-128K-5L	SVM	96.43%	97.01%	95.89%	95.59%	97.22%	0.04	0.96
	KNN	97.14%	97.76%	96.58%	96.32%	97.92%	0.04	0.97
	BN	97.14%	96.60%	97.66%	97.55%	96.76%	0.03	0.97
Standard-256K-5L	SVM	97.14%	97.06%	97.22%	97.06%	97.22%	0.03	0.97
	KNN	97.50%	97.78%	97.24%	97.06%	97.92%	0.03	0.97
	BN	97.38%	96.62%	98.12%	98.04%	96.76%	0.03	0.97
Standard-32K-5L	SVM	98.57%	98.53%	98.61%	98.53%	98.61%	0.01	0.99
	KNN	97.14%	98.48%	95.95%	95.59%	98.61%	0.04	0.98
	BN	97.14%	97.06%	97.22%	97.06%	97.22%	0.03	0.98
Standard-512K-5L	SVM	98.57%	98.53%	98.61%	98.53%	98.61%	0.01	0.99
	KNN	98.21%	98.52%	97.93%	97.79%	98.61%	0.02	0.98
	BN	97.86%	97.56%	98.14%	98.04%	97.69%	0.02	0.98
Standard-64K-5L	SVM	98.57%	98.53%	98.61%	98.53%	98.61%	0.01	0.99
	KNN	98.57%	98.53%	98.61%	98.53%	98.61%	0.01	0.99
	BN	98.33%	97.58%	99.06%	99.02%	97.69%	0.02	0.98
Standard-128K-6L	SVM	97.86%	98.51%	97.26%	97.06%	98.61%	0.03	0.98
	KNN	97.50%	98.50%	96.60%	96.32%	98.61%	0.04	0.98
	BN	97.62%	98.02%	97.25%	97.06%	98.15%	0.03	0.98
Standard-256K-6L	SVM	97.14%	97.06%	97.22%	97.06%	97.22%	0.03	0.97
	KNN	97.50%	97.78%	97.24%	97.06%	97.92%	0.03	0.97
	BN	97.86%	97.56%	98.14%	98.04%	97.69%	0.02	0.98

Standard-32K-6L	SVM	97.86%	98.51%	97.26%	97.06%	98.61%	0.03	0.98
	KNN	96.43%	98.46%	94.67%	94.12%	98.61%	0.06	0.97
	BN	96.67%	97.03%	96.33%	96.08%	97.22%	0.03	0.97
Standard-512K-6L	SVM	97.86%	98.51%	97.26%	97.06%	98.61%	0.03	0.98
	KNN	97.86%	98.51%	97.26%	97.06%	98.61%	0.03	0.98
	BN	98.10%	98.51%	97.71%	97.55%	98.61%	0.02	0.98
Standard-64K-6L	SVM	98.57%	98.53%	98.61%	98.53%	98.61%	0.01	0.99
	KNN	97.86%	98.51%	97.26%	97.06%	98.61%	0.03	0.98
	BN	98.10%	98.04%	98.15%	98.04%	98.15%	0.02	0.98
Overlapped-128K-3L	SVM	94.29%	96.88%	92.11%	91.18%	97.22%	0.08	0.94
	KNN	93.21%	96.06%	90.85%	89.71%	96.53%	0.10	0.94
	BN	91.43%	94.21%	89.13%	87.75%	94.91%	0.11	0.91
Overlapped-256K-3L	SVM	92.86%	96.77%	89.74%	88.24%	97.22%	0.11	0.93
	KNN	91.79%	94.49%	89.54%	88.24%	95.14%	0.11	0.92
	BN	90.71%	94.59%	87.66%	85.78%	95.37%	0.13	0.92
Overlapped-32K-3L	SVM	92.86%	96.77%	89.74%	88.24%	97.22%	0.11	0.93
	KNN	91.07%	95.87%	87.42%	85.29%	96.53%	0.13	0.92
	BN	90.00%	94.51%	86.55%	84.31%	95.37%	0.16	0.91
Overlapped-512K-3L	SVM	95.00%	95.52%	94.52%	94.12%	95.83%	0.06	0.95
	KNN	92.50%	95.28%	90.20%	88.97%	95.83%	0.10	0.94
	BN	90.48%	93.16%	88.26%	86.76%	93.98%	0.12	0.91
Overlapped-64K-3L	SVM	94.29%	96.88%	92.11%	91.18%	97.22%	0.08	0.94
	KNN	87.14%	90.32%	84.62%	82.35%	91.67%	0.15	0.91
	BN	81.43%	82.47%	80.53%	78.43%	84.26%	0.20	0.82
Overlapped-128K-4L	SVM	98.57%	98.53%	98.61%	98.53%	98.61%	0.01	0.99
	KNN	96.07%	98.45%	94.04%	93.38%	98.61%	0.06	0.97
	BN	95.71%	95.59%	95.83%	95.59%	95.83%	0.04	0.97
Overlapped-256K-4L	SVM	97.14%	98.48%	95.95%	95.59%	98.61%	0.04	0.97
	KNN	95.00%	96.92%	93.33%	92.65%	97.22%	0.07	0.96
	BN	93.33%	95.36%	91.59%	90.69%	95.83%	0.09	0.94
Overlapped-32K-4L	SVM	98.57%	98.53%	98.61%	98.53%	98.61%	0.01	0.99
	KNN	98.57%	98.53%	98.61%	98.53%	98.61%	0.01	0.99
	BN	97.86%	96.65%	99.05%	99.02%	96.76%	0.03	0.98
Overlapped-512K-4L	SVM	98.57%	98.53%	98.61%	98.53%	98.61%	0.01	0.99
	KNN	96.07%	96.99%	95.24%	94.85%	97.22%	0.05	0.97
	BN	93.57%	94.47%	92.76%	92.16%	94.91%	0.08	0.94
Overlapped-64K-4L	SVM	96.43%	98.46%	94.67%	94.12%	98.61%	0.06	0.96
	KNN	95.71%	98.44%	93.42%	92.65%	98.61%	0.07	0.96
	BN	96.19%	97.00%	95.45%	95.10%	97.22%	0.03	0.97
Overlapped-128K-5L	SVM	97.14%	98.48%	95.95%	95.59%	98.61%	0.04	0.97
	KNN	96.79%	98.47%	95.30%	94.85%	98.61%	0.05	0.97
	BN	96.90%	97.04%	96.77%	96.57%	97.22%	0.03	0.97
Overlapped-256K-5L	SVM	98.57%	98.53%	98.61%	98.53%	98.61%	0.01	0.99
	KNN	97.50%	98.50%	96.60%	96.32%	98.61%	0.04	0.98
	BN	96.90%	96.14%	97.65%	97.55%	96.30%	0.04	0.97
Overlapped-32K-5L	SVM	96.43%	98.46%	94.67%	94.12%	98.61%	0.06	0.96
	KNN	92.86%	98.33%	88.75%	86.76%	98.61%	0.11	0.95
	BN	93.10%	96.79%	90.13%	88.73%	97.22%	0.10	0.95
Overlapped-512K-5L	SVM	97.14%	98.48%	95.95%	95.59%	98.61%	0.04	0.97
	KNN	96.07%	98.45%	94.04%	93.38%	98.61%	0.06	0.97
	BN	90.24%	94.54%	86.92%	84.80%	95.37%	0.14	0.91

Overlapped-64K-5L	SVM	97.86%	98.51%	97.26%	97.06%	98.61%	0.03	0.98
	KNN	96.79%	98.47%	95.30%	94.85%	98.61%	0.05	0.97
	BN	96.67%	96.57%	96.76%	96.57%	96.76%	0.03	0.97
Overlapped-128K-6L	SVM	88.57%	90.62%	86.84%	85.29%	91.67%	0.14	0.88
	KNN	88.21%	91.87%	85.35%	83.09%	93.06%	0.15	0.88
	BN	89.29%	92.51%	86.70%	84.80%	93.52%	0.14	0.9
Overlapped-256K-6L	SVM	90.00%	93.55%	87.18%	85.29%	94.44%	0.13	0.9
	KNN	89.64%	94.21%	86.16%	83.82%	95.14%	0.14	0.9
	BN	89.76%	93.51%	86.81%	84.80%	94.44%	0.14	0.9
Overlapped-32K-6L	SVM	91.43%	93.75%	89.47%	88.24%	94.44%	0.11	0.91
	KNN	91.07%	94.40%	88.39%	86.76%	95.14%	0.12	0.91
	BN	91.19%	93.72%	89.08%	87.75%	94.44%	0.12	0.92
Overlapped-512K-6L	SVM	88.57%	90.62%	86.84%	85.29%	91.67%	0.14	0.88
	KNN	88.93%	93.39%	85.53%	83.09%	94.44%	0.15	0.89
	BN	89.52%	93.01%	86.75%	84.80%	93.98%	0.15	0.9
Overlapped-64K-6L	SVM	91.43%	93.75%	89.47%	88.24%	94.44%	0.11	0.91
	KNN	88.93%	95.65%	84.24%	80.88%	96.53%	0.16	0.9
	BN	89.29%	94.41%	85.48%	82.84%	95.37%	0.15	0.91

Table A.12: The results of using the ED critical function using IFK.

Method	Classifiers	Acc	Sen	Spec	PPV	NPV	EER	AUC
Standard-128K-3L	SVM	93.57%	92.75%	94.37%	94.12%	93.06%	0.06	0.94
	KNN	90.36%	89.78%	90.91%	90.44%	90.28%	0.10	0.92
	BN	87.86%	87.32%	88.37%	87.75%	87.96%	0.12	0.89
Standard-256K-3L	SVM	95.00%	98.41%	92.21%	91.18%	98.61%	0.08	0.95
	KNN	95.71%	99.21%	92.86%	91.91%	99.31%	0.08	0.95
	BN	95.00%	97.91%	92.58%	91.67%	98.15%	0.08	0.95
Standard-32K-3L	SVM	92.86%	90.28%	95.59%	95.59%	90.28%	0.05	0.93
	KNN	92.14%	91.30%	92.96%	92.65%	91.67%	0.08	0.93
	BN	92.14%	92.54%	91.78%	91.18%	93.06%	0.09	0.93
Standard-512K-3L	SVM	92.14%	92.54%	91.78%	91.18%	93.06%	0.09	0.92
	KNN	87.86%	87.50%	88.19%	87.50%	88.19%	0.12	0.9
	BN	84.05%	81.86%	86.34%	86.27%	81.94%	0.17	0.84
Standard-64K-3L	SVM	92.86%	96.77%	89.74%	88.24%	97.22%	0.11	0.93
	KNN	92.86%	96.03%	90.26%	88.97%	96.53%	0.10	0.93
	BN	92.86%	95.79%	90.43%	89.22%	96.30%	0.11	0.93
Standard-128K-4L	SVM	99.29%	98.55%	100.00%	100.00%	98.61%	0.00	0.99
	KNN	98.21%	97.81%	98.60%	98.53%	97.92%	0.02	0.99
	BN	98.33%	97.58%	99.06%	99.02%	97.69%	0.01	0.99
Standard-256K-4L	SVM	99.29%	98.55%	100.00%	100.00%	98.61%	0.00	0.99
	KNN	98.57%	97.83%	99.30%	99.26%	97.92%	0.02	0.99
	BN	98.57%	97.60%	99.53%	99.51%	97.69%	0.02	0.99
Standard-32K-4L	SVM	99.29%	98.55%	100.00%	100.00%	98.61%	0.00	0.99
	KNN	97.50%	98.50%	96.60%	96.32%	98.61%	0.01	0.98
	BN	96.90%	96.59%	97.21%	97.06%	96.76%	0.03	0.98
Standard-512K-4L	SVM	97.86%	97.10%	98.59%	98.53%	97.22%	0.01	0.98
	KNN	96.43%	95.00%	97.86%	97.79%	95.14%	0.05	0.97
	BN	89.29%	89.95%	88.69%	87.75%	90.74%	0.12	0.87

Standard-64K-4L	SVM	99.29%	98.55%	100.00%	100.00%	98.61%	0.00	0.99
	KNN	98.57%	97.83%	99.30%	99.26%	97.92%	0.02	0.99
	BN	98.57%	97.60%	99.53%	99.51%	97.69%	0.02	0.99
Standard-128K-5L	SVM	100.00%	100.00%	100.00%	100.00%	100.00%	0.00	1
	KNN	99.29%	100.00%	98.63%	98.53%	100.00%	0.01	1
	BN	98.57%	98.06%	99.07%	99.02%	98.15%	0.02	0.99
Standard-256K-5L	SVM	100.00%	100.00%	100.00%	100.00%	100.00%	0.00	1
	KNN	100.00%	100.00%	100.00%	100.00%	100.00%	0.00	1
	BN	99.29%	98.55%	100.00%	100.00%	98.61%	0.01	0.99
Standard-32K-5L	SVM	98.57%	98.53%	98.61%	98.53%	98.61%	0.01	0.99
	KNN	98.21%	98.52%	97.93%	97.79%	98.61%	0.02	0.98
	BN	97.14%	97.06%	97.22%	97.06%	97.22%	0.03	0.98
Standard-512K-5L	SVM	100.00%	100.00%	100.00%	100.00%	100.00%	0.00	1
	KNN	99.64%	100.00%	99.31%	99.26%	100.00%	0.01	1
	BN	98.81%	100.00%	97.74%	97.55%	100.00%	0.02	0.99
Standard-64K-5L	SVM	99.29%	100.00%	98.63%	98.53%	100.00%	0.01	0.99
	KNN	98.93%	100.00%	97.96%	97.79%	100.00%	0.02	0.99
	BN	98.10%	97.57%	98.60%	98.53%	97.69%	0.02	0.98
Standard-128K-6L	SVM	99.29%	100.00%	98.63%	98.53%	100.00%	0.01	0.99
	KNN	99.29%	100.00%	98.63%	98.53%	100.00%	0.01	0.99
	BN	97.62%	96.19%	99.05%	99.02%	96.30%	0.04	0.97
Standard-256K-6L	SVM	99.29%	100.00%	98.63%	98.53%	100.00%	0.01	0.99
	KNN	98.93%	100.00%	97.96%	97.79%	100.00%	0.02	0.99
	BN	96.90%	95.69%	98.10%	98.04%	95.83%	0.04	0.97
Standard-32K-6L	SVM	99.29%	98.55%	100.00%	100.00%	98.61%	0.00	0.99
	KNN	97.86%	97.79%	97.92%	97.79%	97.92%	0.02	0.99
	BN	95.24%	94.23%	96.23%	96.08%	94.44%	0.06	0.96
Standard-512K-6L	SVM	100.00%	100.00%	100.00%	100.00%	100.00%	0.00	1
	KNN	99.64%	100.00%	99.31%	99.26%	100.00%	0.01	1
	BN	97.62%	95.75%	99.52%	99.51%	95.83%	0.04	0.97
Standard-64K-6L	SVM	99.29%	100.00%	98.63%	98.53%	100.00%	0.01	0.99
	KNN	99.29%	100.00%	98.63%	98.53%	100.00%	0.01	0.99
	BN	97.38%	95.73%	99.04%	99.02%	95.83%	0.04	0.97
Overlapped-128K-3L	SVM	95.71%	98.44%	93.42%	92.65%	98.61%	0.07	0.96
	KNN	93.93%	96.12%	92.05%	91.18%	96.53%	0.08	0.95
	BN	94.52%	95.94%	93.27%	92.65%	96.30%	0.07	0.96
Overlapped-256K-3L	SVM	95.71%	96.97%	94.59%	94.12%	97.22%	0.06	0.96
	KNN	96.79%	96.35%	97.20%	97.06%	96.53%	0.03	0.96
	BN	96.19%	96.53%	95.87%	95.59%	96.76%	0.04	0.96
Overlapped-32K-3L	SVM	95.71%	98.44%	93.42%	92.65%	98.61%	0.07	0.96
	KNN	95.36%	97.67%	93.38%	92.65%	97.92%	0.07	0.95
	BN	94.76%	95.96%	93.69%	93.14%	96.30%	0.07	0.95
Overlapped-512K-3L	SVM	92.86%	93.94%	91.89%	91.18%	94.44%	0.09	0.93
	KNN	88.57%	88.81%	88.36%	87.50%	89.58%	0.12	0.91
	BN	88.10%	89.29%	87.05%	85.78%	90.28%	0.13	0.89
Overlapped-64K-3L	SVM	95.00%	98.41%	92.21%	91.18%	98.61%	0.08	0.95
	KNN	93.93%	96.85%	91.50%	90.44%	97.22%	0.09	0.94
	BN	92.38%	95.74%	89.66%	88.24%	96.30%	0.11	0.92
Overlapped-128K-4L	SVM	97.86%	95.77%	100.00%	100.00%	95.83%	0.00	0.98
	KNN	97.86%	96.43%	99.29%	99.26%	96.53%	0.03	0.98
	BN	98.10%	97.57%	98.60%	98.53%	97.69%	0.02	0.98

Overlapped-256K-4L	SVM	97.86%	97.10%	98.59%	98.53%	97.22%	0.01	0.98
	KNN	96.43%	95.65%	97.18%	97.06%	95.83%	0.04	0.97
	BN	93.81%	95.88%	92.04%	91.18%	96.30%	0.09	0.93
Overlapped-32K-4L	SVM	98.57%	98.53%	98.61%	98.53%	98.61%	0.01	0.99
	KNN	98.93%	98.54%	99.30%	99.26%	98.61%	0.01	0.99
	BN	98.81%	98.07%	99.53%	99.51%	98.15%	0.02	0.99
Overlapped-512K-4L	SVM	97.14%	97.06%	97.22%	97.06%	97.22%	0.03	0.97
	KNN	96.79%	97.04%	96.55%	96.32%	97.22%	0.04	0.97
	BN	93.10%	90.32%	96.06%	96.08%	90.28%	0.10	0.92
Overlapped-64K-4L	SVM	100.00%	100.00%	100.00%	100.00%	100.00%	0.00	1
	KNN	100.00%	100.00%	100.00%	100.00%	100.00%	0.00	1
	BN	99.76%	99.51%	100.00%	100.00%	99.54%	0.00	1
Overlapped-128K-5L	SVM	99.29%	98.55%	100.00%	100.00%	98.61%	0.00	0.99
	KNN	99.64%	99.27%	100.00%	100.00%	99.31%	0.01	0.99
	BN	98.57%	99.01%	98.17%	98.04%	99.07%	0.02	0.99
Overlapped-256K-5L	SVM	100.00%	100.00%	100.00%	100.00%	100.00%	0.00	1
	KNN	99.29%	100.00%	98.63%	98.53%	100.00%	0.01	1
	BN	99.29%	99.51%	99.08%	99.02%	99.54%	0.00	1
Overlapped-32K-5L	SVM	98.57%	97.14%	100.00%	100.00%	97.22%	0.00	0.99
	KNN	98.57%	97.83%	99.30%	99.26%	97.92%	0.02	0.99
	BN	98.10%	97.12%	99.06%	99.02%	97.22%	0.03	0.98
Overlapped-512K-5L	SVM	97.86%	97.10%	98.59%	98.53%	97.22%	0.01	0.98
	KNN	98.57%	97.83%	99.30%	99.26%	97.92%	0.02	0.98
	BN	98.81%	98.07%	99.53%	99.51%	98.15%	0.02	0.99
Overlapped-64K-5L	SVM	100.00%	100.00%	100.00%	100.00%	100.00%	0.00	1
	KNN	99.64%	99.27%	100.00%	100.00%	99.31%	0.00	1
	BN	99.52%	99.03%	100.00%	100.00%	99.07%	0.01	1
Overlapped-128K-6L	SVM	97.14%	97.06%	97.22%	97.06%	97.22%	0.03	0.97
	KNN	97.50%	96.40%	98.58%	98.53%	96.53%	0.01	0.97
	BN	97.14%	96.15%	98.11%	98.04%	96.30%	0.04	0.97
Overlapped-256K-6L	SVM	98.57%	98.53%	98.61%	98.53%	98.61%	0.01	0.99
	KNN	97.86%	97.79%	97.92%	97.79%	97.92%	0.02	0.98
	BN	97.86%	97.10%	98.59%	98.53%	97.22%	0.03	0.98
Overlapped-32K-6L	SVM	98.57%	97.14%	100.00%	100.00%	97.22%	0.00	0.99
	KNN	98.57%	97.14%	100.00%	100.00%	97.22%	0.03	0.99
	BN	97.62%	96.63%	98.58%	98.53%	96.76%	0.03	0.98
Overlapped-512K-6L	SVM	99.29%	100.00%	98.63%	98.53%	100.00%	0.01	0.99
	KNN	99.29%	100.00%	98.63%	98.53%	100.00%	0.01	0.99
	BN	99.29%	99.51%	99.08%	99.02%	99.54%	0.01	0.99
Overlapped-64K-6L	SVM	97.86%	97.10%	98.59%	98.53%	97.22%	0.01	0.98
	KNN	97.86%	97.10%	98.59%	98.53%	97.22%	0.03	0.98
	BN	97.62%	96.19%	99.05%	99.02%	96.30%	0.04	0.98

Table A.13: The results of using the DTW critical function using IFK.

Method	Classifiers	Acc	Sen	Spec	PPV	NPV	EER	AUC
Standard-128K-3L	SVM	94.29%	96.88%	92.11%	91.18%	97.22%	0.08	0.94
	KNN	89.29%	90.15%	88.51%	87.50%	90.97%	0.12	0.92
	BN	90.24%	91.79%	88.89%	87.75%	92.59%	0.07	0.93

Standard-256K-3L	SVM	92.14%	95.24%	89.61%	88.24%	95.83%	0.11	0.92
	KNN	90.00%	90.91%	89.19%	88.24%	91.67%	0.11	0.91
	BN	90.48%	91.41%	89.64%	88.73%	92.13%	0.11	0.92
Standard-32K-3L	SVM	89.29%	92.06%	87.01%	85.29%	93.06%	0.14	0.89
	KNN	86.79%	88.98%	84.97%	83.09%	90.28%	0.16	0.88
	BN	87.62%	88.78%	86.61%	85.29%	89.81%	0.15	0.89
Standard-512K-3L	SVM	94.29%	95.45%	93.24%	92.65%	95.83%	0.07	0.94
	KNN	94.64%	96.18%	93.29%	92.65%	96.53%	0.07	0.94
	BN	92.86%	95.31%	90.79%	89.71%	95.83%	0.10	0.92
Standard-64K-3L	SVM	94.29%	98.39%	91.03%	89.71%	98.61%	0.09	0.94
	KNN	89.29%	91.41%	87.50%	86.03%	92.36%	0.13	0.92
	BN	89.05%	90.72%	87.61%	86.27%	91.67%	0.08	0.92
Standard-128K-4L	SVM	93.57%	95.38%	92.00%	91.18%	95.83%	0.08	0.94
	KNN	90.00%	89.71%	90.28%	89.71%	90.28%	0.10	0.92
	BN	90.24%	90.55%	89.95%	89.22%	91.20%	0.11	0.92
Standard-256K-4L	SVM	93.57%	94.03%	93.15%	92.65%	94.44%	0.07	0.94
	KNN	91.79%	91.85%	91.72%	91.18%	92.36%	0.09	0.93
	BN	89.76%	90.05%	89.50%	88.73%	90.74%	0.11	0.91
Standard-32K-4L	SVM	96.43%	98.46%	94.67%	94.12%	98.61%	0.06	0.96
	KNN	93.57%	95.38%	92.00%	91.18%	95.83%	0.08	0.95
	BN	92.86%	94.39%	91.52%	90.69%	94.91%	0.09	0.94
Standard-512K-4L	SVM	92.86%	92.65%	93.06%	92.65%	93.06%	0.07	0.93
	KNN	87.14%	85.21%	89.13%	88.97%	85.42%	0.12	0.9
	BN	88.33%	87.44%	89.20%	88.73%	87.96%	0.11	0.91
Standard-64K-4L	SVM	92.86%	93.94%	91.89%	91.18%	94.44%	0.09	0.93
	KNN	88.93%	88.89%	88.97%	88.24%	89.58%	0.12	0.91
	BN	89.76%	90.05%	89.50%	88.73%	90.74%	0.11	0.92
Standard-128K-5L	SVM	96.43%	97.01%	95.89%	95.59%	97.22%	0.04	0.96
	KNN	95.00%	96.92%	93.33%	92.65%	97.22%	0.07	0.96
	BN	93.10%	93.97%	92.31%	91.67%	94.44%	0.08	0.93
Standard-256K-5L	SVM	97.86%	98.51%	97.26%	97.06%	98.61%	0.03	0.98
	KNN	96.43%	97.73%	95.27%	94.85%	97.92%	0.05	0.97
	BN	95.48%	96.48%	94.57%	94.12%	96.76%	0.06	0.96
Standard-32K-5L	SVM	94.29%	94.12%	94.44%	94.12%	94.44%	0.06	0.94
	KNN	93.57%	92.14%	95.00%	94.85%	92.36%	0.05	0.94
	BN	92.86%	93.07%	92.66%	92.16%	93.52%	0.08	0.93
Standard-512K-5L	SVM	97.86%	98.51%	97.26%	97.06%	98.61%	0.03	0.98
	KNN	96.79%	98.47%	95.30%	94.85%	98.61%	0.05	0.97
	BN	94.05%	94.09%	94.01%	93.63%	94.44%	0.06	0.94
Standard-64K-5L	SVM	95.00%	96.92%	93.33%	92.65%	97.22%	0.07	0.95
	KNN	93.57%	96.09%	91.45%	90.44%	96.53%	0.09	0.94
	BN	92.62%	94.36%	91.11%	90.20%	94.91%	0.05	0.94
Standard-128K-6L	SVM	96.43%	98.46%	94.67%	94.12%	98.61%	0.06	0.96
	KNN	95.00%	95.52%	94.52%	94.12%	95.83%	0.06	0.96
	BN	91.90%	91.67%	92.13%	91.67%	92.13%	0.08	0.92
Standard-256K-6L	SVM	96.43%	98.46%	94.67%	94.12%	98.61%	0.06	0.96
	KNN	96.43%	97.73%	95.27%	94.85%	97.92%	0.05	0.96
	BN	93.81%	93.63%	93.98%	93.63%	93.98%	0.06	0.93
Standard-32K-6L	SVM	96.43%	98.46%	94.67%	94.12%	98.61%	0.06	0.96
	KNN	94.64%	96.18%	93.29%	92.65%	96.53%	0.07	0.95
	BN	90.71%	90.24%	91.16%	90.69%	90.74%	0.09	0.91

Standard-512K-6L	SVM	97.14%	98.48%	95.95%	95.59%	98.61%	0.04	0.97
	KNN	95.71%	96.97%	94.59%	94.12%	97.22%	0.06	0.96
	BN	92.86%	93.07%	92.66%	92.16%	93.52%	0.08	0.93
Standard-64K-6L	SVM	94.29%	92.86%	95.71%	95.59%	93.06%	0.05	0.94
	KNN	92.86%	91.43%	94.29%	94.12%	91.67%	0.08	0.94
	BN	90.71%	88.73%	92.75%	92.65%	88.89%	0.11	0.92
Overlapped-128K-3L	SVM	89.29%	94.92%	85.19%	82.35%	95.83%	0.16	0.89
	KNN	85.00%	85.61%	84.46%	83.09%	86.81%	0.16	0.87
	BN	85.71%	87.11%	84.51%	82.84%	88.43%	0.12	0.88
Overlapped-256K-3L	SVM	95.00%	96.92%	93.33%	92.65%	97.22%	0.07	0.95
	KNN	91.07%	93.02%	89.40%	88.24%	93.75%	0.11	0.93
	BN	89.29%	92.97%	86.38%	84.31%	93.98%	0.14	0.92
Overlapped-32K-3L	SVM	87.86%	90.48%	85.71%	83.82%	91.67%	0.15	0.88
	KNN	88.57%	91.27%	86.36%	84.56%	92.36%	0.14	0.88
	BN	89.05%	91.58%	86.96%	85.29%	92.59%	0.15	0.89
Overlapped-512K-3L	SVM	93.57%	98.36%	89.87%	88.24%	98.61%	0.11	0.93
	KNN	90.00%	92.19%	88.16%	86.76%	93.06%	0.12	0.92
	BN	89.29%	90.36%	88.34%	87.25%	91.20%	0.13	0.91
Overlapped-64K-3L	SVM	93.57%	96.83%	90.91%	89.71%	97.22%	0.10	0.93
	KNN	89.29%	88.97%	89.58%	88.97%	89.58%	0.11	0.91
	BN	88.33%	88.18%	88.48%	87.75%	88.89%	0.11	0.91
Overlapped-128K-4L	SVM	92.86%	96.77%	89.74%	88.24%	97.22%	0.11	0.93
	KNN	89.29%	94.92%	85.19%	82.35%	95.83%	0.15	0.91
	BN	89.29%	93.92%	85.77%	83.33%	94.91%	0.05	0.91
Overlapped-256K-4L	SVM	91.43%	91.18%	91.67%	91.18%	91.67%	0.09	0.91
	KNN	87.86%	86.43%	89.29%	88.97%	86.81%	0.11	0.9
	BN	87.14%	87.13%	87.16%	86.27%	87.96%	0.13	0.88
Overlapped-32K-4L	SVM	90.00%	95.00%	86.25%	83.82%	95.83%	0.14	0.9
	KNN	87.86%	91.80%	84.81%	82.35%	93.06%	0.16	0.89
	BN	88.33%	93.30%	84.65%	81.86%	94.44%	0.16	0.9
Overlapped-512K-4L	SVM	89.29%	90.77%	88.00%	86.76%	91.67%	0.13	0.89
	KNN	82.14%	84.68%	80.13%	77.21%	86.81%	0.20	0.86
	BN	79.76%	82.87%	77.41%	73.53%	85.65%	0.23	0.81
Overlapped-64K-4L	SVM	92.86%	95.31%	90.79%	89.71%	95.83%	0.10	0.93
	KNN	90.36%	91.60%	89.26%	88.24%	92.36%	0.11	0.92
	BN	90.24%	93.12%	87.88%	86.27%	93.98%	0.13	0.92
Overlapped-128K-5L	SVM	95.00%	96.92%	93.33%	92.65%	97.22%	0.07	0.95
	KNN	93.93%	96.12%	92.05%	91.18%	96.53%	0.08	0.94
	BN	91.67%	95.19%	88.84%	87.25%	95.83%	0.12	0.92
Overlapped-256K-5L	SVM	95.00%	95.52%	94.52%	94.12%	95.83%	0.06	0.95
	KNN	92.86%	93.94%	91.89%	91.18%	94.44%	0.08	0.94
	BN	91.43%	93.75%	89.47%	88.24%	94.44%	0.11	0.92
Overlapped-32K-5L	SVM	92.86%	93.94%	91.89%	91.18%	94.44%	0.09	0.93
	KNN	92.50%	92.59%	92.41%	91.91%	93.06%	0.08	0.93
	BN	90.24%	91.37%	89.24%	88.24%	92.13%	0.11	0.91
Overlapped-512K-5L	SVM	95.00%	95.52%	94.52%	94.12%	95.83%	0.06	0.95
	KNN	93.93%	94.07%	93.79%	93.38%	94.44%	0.07	0.94
	BN	92.62%	94.82%	90.75%	89.71%	95.37%	0.10	0.93
Overlapped-64K-5L	SVM	89.29%	90.77%	88.00%	86.76%	91.67%	0.13	0.89
	KNN	90.00%	90.30%	89.73%	88.97%	90.97%	0.11	0.9
	BN	89.05%	90.31%	87.95%	86.76%	91.20%	0.13	0.89

Overlapped-128K-6L	SVM	96.43%	98.46%	94.67%	94.12%	98.61%	0.06	0.96
	KNN	94.29%	96.88%	92.11%	91.18%	97.22%	0.08	0.95
	BN	92.62%	95.77%	90.04%	88.73%	96.30%	0.10	0.94
Overlapped-256K-6L	SVM	97.14%	97.06%	97.22%	97.06%	97.22%	0.03	0.97
	KNN	96.07%	94.96%	97.16%	97.06%	95.14%	0.03	0.97
	BN	94.52%	95.02%	94.06%	93.63%	95.37%	0.06	0.96
Overlapped-32K-6L	SVM	95.71%	96.97%	94.59%	94.12%	97.22%	0.06	0.96
	KNN	95.00%	96.92%	93.33%	92.65%	97.22%	0.07	0.95
	BN	91.67%	92.89%	90.58%	89.71%	93.52%	0.10	0.92
Overlapped-512K-6L	SVM	95.00%	95.52%	94.52%	94.12%	95.83%	0.06	0.95
	KNN	94.64%	96.18%	93.29%	92.65%	96.53%	0.07	0.95
	BN	92.86%	95.31%	90.79%	89.71%	95.83%	0.10	0.93
Overlapped-64K-6L	SVM	97.14%	98.48%	95.95%	95.59%	98.61%	0.04	0.97
	KNN	93.93%	95.42%	92.62%	91.91%	95.83%	0.08	0.95
	BN	91.43%	92.86%	90.18%	89.22%	93.52%	0.10	0.93

Table A.14: The results of using the LCS critical function using IFK.

Method	Classifiers	Acc	Sen	Spec	PPV	NPV	EER	AUC
Standard-128K-3L	SVM	97.86%	97.10%	98.59%	98.53%	97.22%	0.01	0.98
	KNN	94.29%	95.45%	93.24%	92.65%	95.83%	0.04	0.96
	BN	94.05%	95.43%	92.83%	92.16%	95.83%	0.04	0.97
Standard-256K-3L	SVM	96.43%	98.46%	94.67%	94.12%	98.61%	0.06	0.96
	KNN	94.64%	96.90%	92.72%	91.91%	97.22%	0.08	0.95
	BN	93.81%	96.35%	91.67%	90.69%	96.76%	0.09	0.95
Standard-512K-3L	SVM	100.00%	100.00%	100.00%	100.00%	100.00%	0.00	1
	KNN	97.50%	98.50%	96.60%	96.32%	98.61%	0.04	0.99
	BN	94.05%	96.86%	91.70%	90.69%	97.22%	0.09	0.94
Standard-64K-3L	SVM	99.29%	98.55%	100.00%	100.00%	98.61%	0.00	0.99
	KNN	98.57%	99.25%	97.95%	97.79%	99.31%	0.01	0.99
	BN	95.95%	97.46%	94.62%	94.12%	97.69%	0.06	0.97
Standard-128K-4L	SVM	99.29%	100.00%	98.63%	98.53%	100.00%	0.01	0.99
	KNN	98.21%	100.00%	96.64%	96.32%	100.00%	0.03	0.99
	BN	98.57%	100.00%	97.30%	97.06%	100.00%	0.00	0.99
Standard-256K-4L	SVM	97.86%	98.51%	97.26%	97.06%	98.61%	0.03	0.98
	KNN	96.79%	97.04%	96.55%	96.32%	97.22%	0.04	0.97
	BN	96.19%	95.63%	96.73%	96.57%	95.83%	0.04	0.97
Standard-512K-4L	SVM	99.29%	100.00%	98.63%	98.53%	100.00%	0.01	0.99
	KNN	97.50%	98.50%	96.60%	96.32%	98.61%	0.04	0.98
	BN	95.00%	96.45%	93.72%	93.14%	96.76%	0.07	0.95
Standard-64K-4L	SVM	98.57%	98.53%	98.61%	98.53%	98.61%	0.01	0.99
	KNN	98.57%	99.25%	97.95%	97.79%	99.31%	0.02	0.99
	BN	98.57%	99.50%	97.73%	97.55%	99.54%	0.02	0.99
Standard-128K-5L	SVM	98.57%	100.00%	97.30%	97.06%	100.00%	0.03	0.99
	KNN	97.86%	100.00%	96.00%	95.59%	100.00%	0.04	0.98
	BN	98.10%	100.00%	96.43%	96.08%	100.00%	0.04	0.99
Standard-256K-5L	SVM	97.86%	100.00%	96.00%	95.59%	100.00%	0.04	0.98
	KNN	97.14%	100.00%	94.74%	94.12%	100.00%	0.05	0.97
	BN	97.62%	100.00%	95.58%	95.10%	100.00%	0.05	0.98

Standard-512K-5L	SVM	98.57%	100.00%	97.30%	97.06%	100.00%	0.03	0.99
	KNN	98.21%	100.00%	96.64%	96.32%	100.00%	0.04	0.98
	BN	98.10%	100.00%	96.43%	96.08%	100.00%	0.04	0.98
Standard-64K-5L	SVM	98.57%	100.00%	97.30%	97.06%	100.00%	0.03	0.99
	KNN	97.50%	100.00%	95.36%	94.85%	100.00%	0.05	0.98
	BN	98.10%	100.00%	96.43%	96.08%	100.00%	0.04	0.99
Standard-128K-6L	SVM	98.57%	100.00%	97.30%	97.06%	100.00%	0.03	0.99
	KNN	95.36%	99.20%	92.26%	91.18%	99.31%	0.08	0.97
	BN	96.43%	99.48%	93.89%	93.14%	99.54%	0.06	0.98
Standard-256K-6L	SVM	98.57%	100.00%	97.30%	97.06%	100.00%	0.03	0.99
	KNN	97.86%	100.00%	96.00%	95.59%	100.00%	0.04	0.98
	BN	98.10%	100.00%	96.43%	96.08%	100.00%	0.04	0.98
Standard-512K-6L	SVM	97.86%	98.51%	97.26%	97.06%	98.61%	0.03	0.98
	KNN	97.14%	97.06%	97.22%	97.06%	97.22%	0.03	0.97
	BN	97.62%	98.02%	97.25%	97.06%	98.15%	0.03	0.98
Standard-64K-6L	SVM	99.29%	100.00%	98.63%	98.53%	100.00%	0.01	0.99
	KNN	96.43%	100.00%	93.51%	92.65%	100.00%	0.06	0.98
	BN	97.62%	100.00%	95.58%	95.10%	100.00%	0.04	0.99
Overlapped-128K-3L	SVM	99.29%	100.00%	98.63%	98.53%	100.00%	0.01	0.99
	KNN	97.50%	99.24%	95.97%	95.59%	99.31%	0.04	0.98
	BN	94.52%	97.38%	92.14%	91.18%	97.69%	0.08	0.94
Overlapped-256K-3L	SVM	95.71%	96.97%	94.59%	94.12%	97.22%	0.06	0.96
	KNN	94.29%	96.88%	92.11%	91.18%	97.22%	0.08	0.95
	BN	90.00%	88.94%	91.04%	90.69%	89.35%	0.11	0.89
Overlapped-32K-3L	SVM	95.71%	98.44%	93.42%	92.65%	98.61%	0.07	0.96
	KNN	95.36%	96.95%	93.96%	93.38%	97.22%	0.06	0.95
	BN	95.95%	97.46%	94.62%	94.12%	97.69%	0.06	0.96
Overlapped-512K-3L	SVM	95.00%	96.92%	93.33%	92.65%	97.22%	0.07	0.95
	KNN	94.64%	96.18%	93.29%	92.65%	96.53%	0.07	0.95
	BN	94.05%	95.90%	92.44%	91.67%	96.30%	0.04	0.95
Overlapped-64K-3L	SVM	97.86%	98.51%	97.26%	97.06%	98.61%	0.03	0.98
	KNN	96.79%	97.74%	95.92%	95.59%	97.92%	0.04	0.97
	BN	91.67%	97.21%	87.55%	85.29%	97.69%	0.14	0.91
Overlapped-128K-4L	SVM	99.29%	100.00%	98.63%	98.53%	100.00%	0.01	0.99
	KNN	98.93%	98.54%	99.30%	99.26%	98.61%	0.01	0.99
	BN	99.05%	98.54%	99.53%	99.51%	98.61%	0.00	0.99
Overlapped-256K-4L	SVM	97.86%	97.10%	98.59%	98.53%	97.22%	0.01	0.98
	KNN	95.71%	94.93%	96.48%	96.32%	95.14%	0.05	0.97
	BN	91.19%	88.84%	93.66%	93.63%	88.89%	0.11	0.91
Overlapped-32K-4L	SVM	97.86%	98.51%	97.26%	97.06%	98.61%	0.03	0.98
	KNN	97.86%	98.51%	97.26%	97.06%	98.61%	0.03	0.98
	BN	97.62%	97.55%	97.69%	97.55%	97.69%	0.02	0.98
Overlapped-512K-4L	SVM	100.00%	100.00%	100.00%	100.00%	100.00%	0.00	1
	KNN	98.21%	100.00%	96.64%	96.32%	100.00%	0.03	0.99
	BN	90.00%	93.55%	87.18%	85.29%	94.44%	0.14	0.88
Overlapped-64K-4L	SVM	97.86%	98.51%	97.26%	97.06%	98.61%	0.03	0.98
	KNN	97.14%	97.06%	97.22%	97.06%	97.22%	0.03	0.97
	BN	97.62%	97.55%	97.69%	97.55%	97.69%	0.02	0.98
Overlapped-128K-5L	SVM	97.86%	100.00%	96.00%	95.59%	100.00%	0.04	0.98
	KNN	97.14%	99.23%	95.33%	94.85%	99.31%	0.05	0.97
	BN	97.62%	99.49%	95.98%	95.59%	99.54%	0.04	0.98

Overlapped-256K-5L	SVM	95.71%	94.29%	97.14%	97.06%	94.44%	0.03	0.96
	KNN	96.43%	95.65%	97.18%	97.06%	95.83%	0.04	0.96
	BN	97.14%	97.06%	97.22%	97.06%	97.22%	0.03	0.97
Overlapped-32K-5L	SVM	97.14%	98.48%	95.95%	95.59%	98.61%	0.04	0.97
	KNN	96.43%	98.46%	94.67%	94.12%	98.61%	0.06	0.97
	BN	96.43%	97.49%	95.48%	95.10%	97.69%	0.05	0.97
Overlapped-512K-5L	SVM	98.57%	97.14%	100.00%	100.00%	97.22%	0.00	0.99
	KNN	97.86%	97.10%	98.59%	98.53%	97.22%	0.03	0.98
	BN	97.14%	97.52%	96.79%	96.57%	97.69%	0.02	0.98
Overlapped-64K-5L	SVM	99.29%	100.00%	98.63%	98.53%	100.00%	0.01	0.99
	KNN	97.86%	99.24%	96.62%	96.32%	99.31%	0.04	0.99
	BN	98.10%	99.00%	97.27%	97.06%	99.07%	0.03	0.99
Overlapped-128K-6L	SVM	97.86%	95.77%	100.00%	100.00%	95.83%	0.00	0.98
	KNN	98.21%	96.45%	100.00%	100.00%	96.53%	0.03	0.98
	BN	98.57%	97.60%	99.53%	99.51%	97.69%	0.02	0.99
Overlapped-256K-6L	SVM	99.29%	100.00%	98.63%	98.53%	100.00%	0.01	0.99
	KNN	98.21%	98.52%	97.93%	97.79%	98.61%	0.02	0.99
	BN	98.33%	98.52%	98.16%	98.04%	98.61%	0.02	0.99
Overlapped-32K-6L	SVM	99.29%	98.55%	100.00%	100.00%	98.61%	0.00	0.99
	KNN	99.29%	98.55%	100.00%	100.00%	98.61%	0.01	0.99
	BN	97.86%	96.65%	99.05%	99.02%	96.76%	0.03	0.98
Overlapped-512K-6L	SVM	97.14%	100.00%	94.74%	94.12%	100.00%	0.06	0.97
	KNN	95.71%	100.00%	92.31%	91.18%	100.00%	0.08	0.96
	BN	96.43%	100.00%	93.51%	92.65%	100.00%	0.07	0.98
Overlapped-64K-6L	SVM	97.86%	97.10%	98.59%	98.53%	97.22%	0.01	0.98
	KNN	98.21%	97.81%	98.60%	98.53%	97.92%	0.02	0.98
	BN	98.33%	97.58%	99.06%	99.02%	97.69%	0.02	0.98

Table A.15: The results of using the KLD critical function using IFK.

Method	Classifiers	Acc	Sen	Spec	PPV	NPV	EER	AUC
Standard-128K-3L	SVM	97.14%	95.71%	98.57%	98.53%	95.83%	0.02	0.97
	KNN	94.64%	93.53%	95.74%	95.59%	93.75%	0.06	0.96
	BN	93.57%	91.94%	95.22%	95.10%	92.13%	0.08	0.95
Standard-256K-3L	SVM	95.00%	95.52%	94.52%	94.12%	95.83%	0.06	0.95
	KNN	95.00%	94.20%	95.77%	95.59%	94.44%	0.04	0.95
	BN	94.76%	92.52%	97.09%	97.06%	92.59%	0.07	0.95
Standard-32K-3L	SVM	95.00%	96.92%	93.33%	92.65%	97.22%	0.07	0.95
	KNN	96.07%	96.30%	95.86%	95.59%	96.53%	0.04	0.95
	BN	95.00%	93.78%	96.21%	96.08%	93.98%	0.06	0.94
Standard-512K-3L	SVM	95.71%	95.59%	95.83%	95.59%	95.83%	0.04	0.96
	KNN	95.00%	95.52%	94.52%	94.12%	95.83%	0.06	0.95
	BN	93.33%	95.83%	91.23%	90.20%	96.30%	0.09	0.93
Standard-64K-3L	SVM	95.00%	95.52%	94.52%	94.12%	95.83%	0.06	0.95
	KNN	95.71%	96.27%	95.21%	94.85%	96.53%	0.05	0.95
	BN	94.76%	96.43%	93.30%	92.65%	96.76%	0.07	0.95
Standard-128K-4L	SVM	96.43%	94.37%	98.55%	98.53%	94.44%	0.02	0.96
	KNN	96.07%	94.96%	97.16%	97.06%	95.14%	0.05	0.96
	BN	95.24%	93.81%	96.67%	96.57%	93.98%	0.06	0.96

Standard-256K-4L	SVM	95.00%	91.78%	98.51%	98.53%	91.67%	0.02	0.95
	KNN	95.36%	93.62%	97.12%	97.06%	93.75%	0.06	0.95
	BN	95.00%	92.17%	98.03%	98.04%	92.13%	0.08	0.95
Standard-32K-4L	SVM	94.29%	94.12%	94.44%	94.12%	94.44%	0.06	0.94
	KNN	92.14%	90.14%	94.20%	94.12%	90.28%	0.06	0.93
	BN	90.71%	89.86%	91.55%	91.18%	90.28%	0.09	0.92
Standard-512K-4L	SVM	93.57%	92.75%	94.37%	94.12%	93.06%	0.06	0.94
	KNN	94.29%	94.12%	94.44%	94.12%	94.44%	0.06	0.94
	BN	93.10%	94.42%	91.93%	91.18%	94.91%	0.09	0.92
Standard-64K-4L	SVM	95.71%	98.44%	93.42%	92.65%	98.61%	0.07	0.96
	KNN	93.57%	94.03%	93.15%	92.65%	94.44%	0.07	0.95
	BN	92.62%	92.20%	93.02%	92.65%	92.59%	0.07	0.93
Standard-128K-5L	SVM	97.86%	98.51%	97.26%	97.06%	98.61%	0.03	0.98
	KNN	95.71%	94.93%	96.48%	96.32%	95.14%	0.04	0.97
	BN	93.57%	92.75%	94.37%	94.12%	93.06%	0.07	0.95
Standard-256K-5L	SVM	97.86%	97.10%	98.59%	98.53%	97.22%	0.01	0.98
	KNN	96.07%	95.62%	96.50%	96.32%	95.83%	0.04	0.97
	BN	93.10%	91.87%	94.31%	94.12%	92.13%	0.08	0.93
Standard-32K-5L	SVM	94.29%	95.45%	93.24%	92.65%	95.83%	0.07	0.94
	KNN	92.50%	92.59%	92.41%	91.91%	93.06%	0.08	0.93
	BN	92.38%	93.43%	91.44%	90.69%	93.98%	0.06	0.94
Standard-512K-5L	SVM	96.43%	94.37%	98.55%	98.53%	94.44%	0.02	0.96
	KNN	96.43%	95.00%	97.86%	97.79%	95.14%	0.05	0.96
	BN	94.76%	92.92%	96.63%	96.57%	93.06%	0.03	0.95
Standard-64K-5L	SVM	93.57%	91.55%	95.65%	95.59%	91.67%	0.05	0.94
	KNN	90.71%	89.29%	92.14%	91.91%	89.58%	0.10	0.92
	BN	90.24%	89.00%	91.47%	91.18%	89.35%	0.09	0.92
Standard-128K-6L	SVM	97.86%	98.51%	97.26%	97.06%	98.61%	0.03	0.98
	KNN	96.43%	96.32%	96.53%	96.32%	96.53%	0.04	0.97
	BN	93.81%	92.79%	94.81%	94.61%	93.06%	0.07	0.94
Standard-256K-6L	SVM	97.14%	98.48%	95.95%	95.59%	98.61%	0.04	0.97
	KNN	96.43%	98.46%	94.67%	94.12%	98.61%	0.06	0.97
	BN	93.57%	93.60%	93.55%	93.14%	93.98%	0.06	0.93
Standard-32K-6L	SVM	92.86%	92.65%	93.06%	92.65%	93.06%	0.07	0.93
	KNN	92.50%	92.59%	92.41%	91.91%	93.06%	0.08	0.93
	BN	92.14%	92.12%	92.17%	91.67%	92.59%	0.08	0.93
Standard-512K-6L	SVM	97.86%	95.77%	100.00%	100.00%	95.83%	0.00	0.98
	KNN	97.14%	97.06%	97.22%	97.06%	97.22%	0.03	0.98
	BN	95.71%	95.15%	96.26%	96.08%	95.37%	0.05	0.96
Standard-64K-6L	SVM	96.43%	97.01%	95.89%	95.59%	97.22%	0.04	0.96
	KNN	94.64%	94.16%	95.10%	94.85%	94.44%	0.05	0.96
	BN	92.62%	91.79%	93.43%	93.14%	92.13%	0.07	0.93
Overlapped-128K-3L	SVM	92.86%	96.77%	89.74%	88.24%	97.22%	0.11	0.93
	KNN	91.07%	95.12%	87.90%	86.03%	95.83%	0.13	0.92
	BN	89.76%	93.51%	86.81%	84.80%	94.44%	0.06	0.91
Overlapped-256K-3L	SVM	92.14%	95.24%	89.61%	88.24%	95.83%	0.11	0.92
	KNN	91.07%	93.02%	89.40%	88.24%	93.75%	0.11	0.92
	BN	90.00%	91.75%	88.50%	87.25%	92.59%	0.13	0.91
Overlapped-32K-3L	SVM	93.57%	96.83%	90.91%	89.71%	97.22%	0.10	0.93
	KNN	91.07%	95.12%	87.90%	86.03%	95.83%	0.12	0.92
	BN	89.76%	93.51%	86.81%	84.80%	94.44%	0.06	0.91

Overlapped-512K-3L	SVM	94.29%	96.88%	92.11%	91.18%	97.22%	0.08	0.94
	KNN	93.21%	95.35%	91.39%	90.44%	95.83%	0.09	0.94
	BN	91.19%	93.26%	89.43%	88.24%	93.98%	0.11	0.91
Overlapped-64K-3L	SVM	91.43%	93.75%	89.47%	88.24%	94.44%	0.11	0.91
	KNN	89.64%	92.13%	87.58%	86.03%	93.06%	0.13	0.9
	BN	87.14%	90.32%	84.62%	82.35%	91.67%	0.16	0.87
Overlapped-128K-4L	SVM	90.00%	92.19%	88.16%	86.76%	93.06%	0.12	0.9
	KNN	88.21%	89.31%	87.25%	86.03%	90.28%	0.13	0.89
	BN	89.05%	91.15%	87.28%	85.78%	92.13%	0.13	0.9
Overlapped-256K-4L	SVM	93.57%	95.38%	92.00%	91.18%	95.83%	0.08	0.94
	KNN	89.64%	90.23%	89.12%	88.24%	90.97%	0.11	0.92
	BN	89.05%	90.31%	87.95%	86.76%	91.20%	0.13	0.91
Overlapped-32K-4L	SVM	89.29%	90.77%	88.00%	86.76%	91.67%	0.13	0.89
	KNN	89.64%	89.05%	90.21%	89.71%	89.58%	0.10	0.89
	BN	89.76%	90.45%	89.14%	88.24%	91.20%	0.12	0.9
Overlapped-512K-4L	SVM	89.29%	92.06%	87.01%	85.29%	93.06%	0.14	0.89
	KNN	86.07%	88.19%	84.31%	82.35%	89.58%	0.16	0.88
	BN	84.05%	89.14%	80.41%	76.47%	91.20%	0.21	0.84
Overlapped-64K-4L	SVM	90.00%	89.71%	90.28%	89.71%	90.28%	0.10	0.9
	KNN	90.00%	90.30%	89.73%	88.97%	90.97%	0.11	0.9
	BN	89.76%	91.28%	88.44%	87.25%	92.13%	0.12	0.9
Overlapped-128K-5L	SVM	93.57%	95.38%	92.00%	91.18%	95.83%	0.08	0.94
	KNN	92.14%	90.71%	93.57%	93.38%	90.97%	0.07	0.93
	BN	91.19%	91.54%	90.87%	90.20%	92.13%	0.10	0.92
Overlapped-256K-5L	SVM	96.43%	94.37%	98.55%	98.53%	94.44%	0.02	0.96
	KNN	96.07%	95.62%	96.50%	96.32%	95.83%	0.04	0.96
	BN	95.24%	96.00%	94.55%	94.12%	96.30%	0.06	0.96
Overlapped-32K-5L	SVM	97.86%	97.10%	98.59%	98.53%	97.22%	0.01	0.98
	KNN	91.43%	88.89%	94.12%	94.12%	88.89%	0.10	0.95
	BN	89.52%	88.83%	90.19%	89.71%	89.35%	0.11	0.93
Overlapped-512K-5L	SVM	97.14%	95.71%	98.57%	98.53%	95.83%	0.02	0.97
	KNN	96.79%	95.68%	97.87%	97.79%	95.83%	0.04	0.97
	BN	97.14%	95.71%	98.57%	98.53%	95.83%	0.04	0.97
Overlapped-64K-5L	SVM	95.00%	96.92%	93.33%	92.65%	97.22%	0.07	0.95
	KNN	92.50%	91.97%	93.01%	92.65%	92.36%	0.07	0.94
	BN	90.71%	91.88%	89.69%	88.73%	92.59%	0.11	0.92
Overlapped-128K-6L	SVM	97.14%	95.71%	98.57%	98.53%	95.83%	0.02	0.97
	KNN	97.50%	96.40%	98.58%	98.53%	96.53%	0.03	0.97
	BN	96.90%	96.59%	97.21%	97.06%	96.76%	0.03	0.97
Overlapped-256K-6L	SVM	97.86%	97.10%	98.59%	98.53%	97.22%	0.01	0.98
	KNN	98.21%	97.81%	98.60%	98.53%	97.92%	0.02	0.98
	BN	98.10%	97.12%	99.06%	99.02%	97.22%	0.03	0.98
Overlapped-32K-6L	SVM	88.57%	90.62%	86.84%	85.29%	91.67%	0.14	0.88
	KNN	86.07%	83.92%	88.32%	88.24%	84.03%	0.12	0.87
	BN	86.90%	86.70%	87.10%	86.27%	87.50%	0.14	0.89
Overlapped-512K-6L	SVM	98.57%	97.14%	100.00%	100.00%	97.22%	0.00	0.99
	KNN	97.86%	96.43%	99.29%	99.26%	96.53%	0.03	0.98
	BN	97.62%	95.75%	99.52%	99.51%	95.83%	0.04	0.98
Overlapped-64K-6L	SVM	95.00%	96.92%	93.33%	92.65%	97.22%	0.07	0.95
	KNN	92.14%	91.91%	92.36%	91.91%	92.36%	0.08	0.94
	BN	90.95%	91.09%	90.83%	90.20%	91.67%	0.10	0.92

Appendix B

Further Results for Whole Image-based Representation

In this appendix some additional results are presented with respect to the evaluation of the whole image-based volumetric representation presented in Chapter 7. Recall that the whole image-based representation comprised five stages as illustrated previously in Figure 7.1: (i) image decomposition, (ii) tree conceptualisation, (iii) frequent sub-graph mining, (iv) feature vector generation and (v) classifier generation. Each of these stages had a number of techniques associated with it. With respect to the first stage, image decomposition, five critical functions were used:

1. Average Intensity Value (AIV).
2. Kendall's Coefficient Concordance (KCC).
3. Euclidean Distance (ED).
4. Longest Common Subsequence (LCS).
5. Kullback-Leibler divergence (KLD).

For the evaluation presented in Chapter 7 all five techniques were evaluated using static techniques for the remaining stages, these were: (i) Kurtosis node labelling, (ii) gSpan using $\sigma = 20\%$ and (iii) SVM classification. For completeness in this appendix results from additional experiments with respect to these critical function are presented in the following tables (Tables B.1 to B.5). In the evaluation, the results of standard and overlapping decomposition are included. Four levels of decomposition L are also presented ($L = \{3, 4, 5, 6\}$). In addition, four decomposition threshold values $t = \{0.3, 0.5, 0.7, 0.9\}$ were used. With respect to stage two, tree conceptualisation, two types of node labellings were used: (i) Kurtosis and (ii) Mean intensity value. The results presented in this appendix confirm the earlier results that, in the context of the whole image-based representation:

1. Overlapping decomposition outperforms standard decomposition,

2. The best threshold value t were 0.5.

3. The best performing critical functions tend to be LCS,

4. Kurtosis node labelling produced better results than Mean,

5. SVM and BN classification tend to outperform KNN classification.

Table B.1: The results using the AIV critical function in the context of whole image-based methods, where S means standard decomposition, O overlapped decomposition, t is the threshold for the critical function and L is the level.

Method	Classifier	Acc	Sen	Spec	PPV	NPV	EER	AUC
SM 3L t 0.3	SVM	89.29%	88.73%	89.86%	90.00%	88.57%	0.10	0.89
	KNN	82.86%	81.08%	84.85%	85.71%	80.00%	0.17	0.88
	BN	81.90%	81.31%	82.52%	82.86%	80.95%	0.18	0.86
SM 4L t 0.3	SVM	80.00%	79.17%	80.88%	81.43%	78.57%	0.19	0.8
	KNN	75.00%	73.65%	76.52%	77.86%	72.14%	0.28	0.77
	BN	75.00%	74.88%	75.12%	75.24%	74.76%	0.25	0.78
SM 5L t 0.3	SVM	79.29%	79.71%	78.87%	78.57%	80.00%	0.21	0.79
	KNN	77.14%	76.03%	78.36%	79.29%	75.00%	0.23	0.8
	BN	77.38%	76.02%	78.89%	80.00%	74.76%	0.22	0.8
SM 6L t 0.3	SVM	77.86%	77.46%	78.26%	78.57%	77.14%	0.22	0.78
	KNN	73.93%	71.90%	76.38%	78.57%	69.29%	0.25	0.77
	BN	74.76%	72.81%	77.08%	79.05%	70.48%	0.25	0.79
SM 3L t 0.5	SVM	89.29%	88.73%	89.86%	90.00%	88.57%	0.10	0.89
	KNN	88.93%	87.59%	90.37%	90.71%	87.14%	0.11	0.9
	BN	89.29%	87.67%	91.04%	91.43%	87.14%	0.11	0.92
SM 4L t 0.5	SVM	85.00%	82.67%	87.69%	88.57%	81.43%	0.12	0.85
	KNN	80.00%	77.27%	83.33%	85.00%	75.00%	0.22	0.83
	BN	79.29%	77.33%	81.54%	82.86%	75.71%	0.22	0.83
SM 5L t 0.5	SVM	83.57%	78.31%	91.23%	92.86%	74.29%	0.09	0.84
	KNN	81.07%	77.71%	85.37%	87.14%	75.00%	0.22	0.83
	BN	80.95%	78.26%	84.21%	85.71%	76.19%	0.21	0.84
SM 6L t 0.5	SVM	82.14%	80.00%	84.62%	85.71%	78.57%	0.15	0.82
	KNN	80.71%	76.54%	86.44%	88.57%	72.86%	0.20	0.82
	BN	81.19%	77.18%	86.59%	88.57%	73.81%	0.21	0.83
SM 3L t 0.7	SVM	85.71%	82.89%	89.06%	90.00%	81.43%	0.11	0.86
	KNN	84.29%	80.77%	88.71%	90.00%	78.57%	0.21	0.85
	BN	83.57%	80.00%	88.11%	89.52%	77.62%	0.20	0.85
SM 4L t 0.7	SVM	78.57%	80.30%	77.03%	75.71%	81.43%	0.23	0.79
	KNN	78.57%	78.99%	78.17%	77.86%	79.29%	0.21	0.78
	BN	80.24%	79.53%	80.98%	81.43%	79.05%	0.19	0.81
SM 5L t 0.7	SVM	86.43%	84.00%	89.23%	90.00%	82.86%	0.11	0.86
	KNN	85.71%	83.33%	88.46%	89.29%	82.14%	0.17	0.86
	BN	84.76%	82.88%	86.87%	87.62%	81.90%	0.17	0.87

SM 6L t 0.7	SVM	88.57%	85.53%	92.19%	92.86%	84.29%	0.08	0.89
	KNN	86.43%	82.28%	91.80%	92.86%	80.00%	0.16	0.89
	BN	85.24%	80.58%	91.57%	92.86%	77.62%	0.17	0.87
SM 3L t 0.9	SVM	82.86%	81.94%	83.82%	84.29%	81.43%	0.16	0.83
	KNN	82.50%	80.13%	85.27%	86.43%	78.57%	0.19	0.82
	BN	83.81%	81.70%	86.22%	87.14%	80.48%	0.18	0.85
SM 4L t 0.9	SVM	85.71%	82.05%	90.32%	91.43%	80.00%	0.10	0.86
	KNN	86.07%	82.58%	90.40%	91.43%	80.71%	0.19	0.85
	BN	86.90%	82.98%	91.89%	92.86%	80.95%	0.18	0.87
SM 5L t 0.9	SVM	85.00%	82.67%	87.69%	88.57%	81.43%	0.12	0.85
	KNN	85.00%	81.41%	89.52%	90.71%	79.29%	0.18	0.85
	BN	85.71%	81.25%	91.67%	92.86%	78.57%	0.20	0.86
SM 6L t 0.9	SVM	88.57%	85.53%	92.19%	92.86%	84.29%	0.08	0.89
	KNN	86.43%	82.28%	91.80%	92.86%	80.00%	0.16	0.89
	BN	85.24%	80.58%	91.57%	92.86%	77.62%	0.17	0.87
OM 3L t 0.3	SVM	93.57%	91.78%	95.52%	95.71%	91.43%	0.04	0.94
	KNN	93.21%	91.16%	95.49%	95.71%	90.71%	0.08	0.94
	BN	93.33%	91.36%	95.50%	95.71%	90.95%	0.07	0.95
OM 4L t 0.3	SVM	94.29%	94.29%	94.29%	94.29%	94.29%	0.06	0.94
	KNN	93.21%	93.53%	92.91%	92.86%	93.57%	0.06	0.94
	BN	93.10%	92.49%	93.72%	93.81%	92.38%	0.08	0.94
OM 5L t 0.3	SVM	92.86%	92.86%	92.86%	92.86%	92.86%	0.07	0.93
	KNN	93.57%	91.78%	95.52%	95.71%	91.43%	0.06	0.93
	BN	94.29%	92.66%	96.04%	96.19%	92.38%	0.07	0.94
OM 3L t 0.5	SVM	93.57%	91.78%	95.52%	95.71%	91.43%	0.04	0.94
	KNN	93.21%	91.16%	95.49%	95.71%	90.71%	0.08	0.94
	BN	93.33%	91.36%	95.50%	95.71%	90.95%	0.07	0.95
OM 4L t 0.5	SVM	94.29%	94.29%	94.29%	94.29%	94.29%	0.06	0.94
	KNN	93.21%	93.53%	92.91%	92.86%	93.57%	0.06	0.94
	BN	93.10%	92.49%	93.72%	93.81%	92.38%	0.08	0.94
OM 5L t 0.5	SVM	92.86%	92.86%	92.86%	92.86%	92.86%	0.07	0.93
	KNN	93.57%	91.78%	95.52%	95.71%	91.43%	0.06	0.93
	BN	94.29%	92.66%	96.04%	96.19%	92.38%	0.07	0.94
OM 3L t 0.7	SVM	93.57%	91.78%	95.52%	95.71%	91.43%	0.04	0.94
	KNN	93.21%	91.16%	95.49%	95.71%	90.71%	0.08	0.94
	BN	93.33%	91.36%	95.50%	95.71%	90.95%	0.07	0.95
OM4 t 0.7	SVM	94.29%	94.29%	94.29%	94.29%	94.29%	0.06	0.94
	KNN	93.21%	93.53%	92.91%	92.86%	93.57%	0.06	0.94
	BN	93.10%	92.49%	93.72%	93.81%	92.38%	0.08	0.94
OM 5L t 0.7	SVM	92.86%	92.86%	92.86%	92.86%	92.86%	0.07	0.93
	KNN	93.57%	91.78%	95.52%	95.71%	91.43%	0.06	0.93
	BN	94.29%	92.66%	96.04%	96.19%	92.38%	0.07	0.94
OM 3L t 0.9	SVM	88.57%	88.57%	88.57%	88.57%	88.57%	0.11	0.89
	KNN	86.79%	86.01%	87.59%	87.86%	85.71%	0.12	0.9
	BN	87.38%	84.89%	90.26%	90.95%	83.81%	0.11	0.91

OM 4L t 0.9	SVM	91.43%	89.19%	93.94%	94.29%	88.57%	0.06	0.91
	KNN	90.00%	86.84%	93.75%	94.29%	85.71%	0.11	0.91
	BN	89.76%	85.84%	94.65%	95.24%	84.29%	0.14	0.91
OM 5L t 0.9	SVM	97.14%	95.83%	98.53%	98.57%	95.71%	0.01	0.97
	KNN	97.14%	95.83%	98.53%	98.57%	95.71%	0.04	0.97
	BN	97.38%	95.85%	99.01%	99.05%	95.71%	0.03	0.98
SK 3L t0.3	SVM	87.14%	89.39%	85.14%	84.29%	90.00%	0.15	0.87
	KNN	84.64%	86.47%	82.99%	82.14%	87.14%	0.18	0.86
	BN	82.38%	83.66%	81.19%	80.48%	84.29%	0.19	0.86
SK 4L t0.3	SVM	90.00%	88.89%	91.18%	91.43%	88.57%	0.09	0.9
	KNN	84.29%	83.33%	85.29%	85.71%	82.86%	0.15	0.88
	BN	83.33%	84.31%	82.41%	81.90%	84.76%	0.15	0.88
SK 5L t0.3	SVM	78.57%	79.41%	77.78%	77.14%	80.00%	0.22	0.79
	KNN	75.36%	75.91%	74.83%	74.29%	76.43%	0.26	0.78
	BN	75.95%	77.39%	74.66%	73.33%	78.57%	0.25	0.79
SK 6L t0.3	SVM	83.57%	84.06%	83.10%	82.86%	84.29%	0.17	0.84
	KNN	79.64%	79.02%	80.29%	80.71%	78.57%	0.20	0.83
	BN	79.76%	80.19%	79.34%	79.05%	80.48%	0.20	0.84
SK 3L t0.5	SVM	82.86%	83.82%	81.94%	81.43%	84.29%	0.18	0.83
	KNN	79.29%	80.15%	78.47%	77.86%	80.71%	0.19	0.83
	BN	79.29%	79.15%	79.43%	79.52%	79.05%	0.21	0.83
SK 4L t0.5	SVM	86.43%	85.92%	86.96%	87.14%	85.71%	0.13	0.86
	KNN	83.57%	81.76%	85.61%	86.43%	80.71%	0.15	0.86
	BN	83.10%	80.62%	86.01%	87.14%	79.05%	0.18	0.86
SK 5L t0.5	SVM	81.43%	78.21%	85.48%	87.14%	75.71%	0.15	0.81
	KNN	79.64%	76.43%	83.74%	85.71%	73.57%	0.21	0.81
	BN	80.95%	78.02%	84.57%	86.19%	75.71%	0.20	0.83
SK 6L t0.5	SVM	88.57%	87.50%	89.71%	90.00%	87.14%	0.10	0.89
	KNN	85.36%	84.14%	86.67%	87.14%	83.57%	0.15	0.87
	BN	84.76%	82.88%	86.87%	87.62%	81.90%	0.17	0.87
SK 3L t0.7	SVM	87.14%	85.14%	89.39%	90.00%	84.29%	0.11	0.87
	KNN	85.00%	82.67%	87.69%	88.57%	81.43%	0.17	0.87
	BN	83.57%	81.61%	85.79%	86.67%	80.48%	0.19	0.86
SK 4L t0.7	SVM	86.43%	84.93%	88.06%	88.57%	84.29%	0.12	0.86
	KNN	81.43%	79.73%	83.33%	84.29%	78.57%	0.14	0.86
	BN	82.14%	79.48%	85.34%	86.67%	77.62%	0.14	0.86
SK 5L t0.7	SVM	87.86%	87.32%	88.41%	88.57%	87.14%	0.12	0.88
	KNN	84.29%	82.00%	86.92%	87.86%	80.71%	0.14	0.87
	BN	84.52%	81.39%	88.36%	89.52%	79.52%	0.16	0.88
SK 6L t0.7	SVM	88.57%	88.57%	88.57%	88.57%	88.57%	0.11	0.89
	KNN	85.00%	83.56%	86.57%	87.14%	82.86%	0.14	0.86
	BN	85.48%	83.41%	87.82%	88.57%	82.38%	0.15	0.87
SK 5L t0.9	SVM	86.43%	82.28%	91.80%	92.86%	80.00%	0.08	0.86
	KNN	84.29%	79.63%	90.68%	92.14%	76.43%	0.21	0.85
	BN	84.52%	79.35%	91.91%	93.33%	75.71%	0.22	0.86

SK 4L t0.9	SVM	86.43%	81.48%	93.22%	94.29%	78.57%	0.07	0.86
	KNN	86.43%	81.48%	93.22%	94.29%	78.57%	0.18	0.88
	BN	85.95%	80.82%	93.14%	94.29%	77.62%	0.18	0.87
SK 3L t0.9	SVM	87.14%	86.11%	88.24%	88.57%	85.71%	0.12	0.87
	KNN	83.21%	80.39%	86.61%	87.86%	78.57%	0.16	0.87
	BN	83.81%	81.14%	86.98%	88.10%	79.52%	0.15	0.87
SK 6L t0.9	SVM	90.00%	84.15%	98.28%	98.57%	81.43%	0.02	0.9
	KNN	90.00%	84.57%	97.46%	97.86%	82.14%	0.18	0.89
	BN	90.24%	84.77%	97.74%	98.10%	82.38%	0.18	0.9
OK 3L t0.3	SVM	85.00%	86.57%	83.56%	82.86%	87.14%	0.16	0.85
	KNN	82.86%	84.33%	81.51%	80.71%	85.00%	0.18	0.86
	BN	84.52%	86.43%	82.81%	81.90%	87.14%	0.16	0.88
OK 4L t0.3	SVM	92.14%	91.55%	92.75%	92.86%	91.43%	0.07	0.92
	KNN	89.64%	87.76%	91.73%	92.14%	87.14%	0.11	0.91
	BN	87.14%	86.45%	87.86%	88.10%	86.19%	0.13	0.9
OK 5L t0.3	SVM	87.14%	86.11%	88.24%	88.57%	85.71%	0.12	0.87
	KNN	87.14%	86.11%	88.24%	88.57%	85.71%	0.14	0.88
	BN	86.90%	86.05%	87.80%	88.10%	85.71%	0.14	0.89
OK 6L t0.3	SVM	93.57%	92.96%	94.20%	94.29%	92.86%	0.06	0.94
	KNN	88.93%	87.07%	90.98%	91.43%	86.43%	0.11	0.92
	BN	87.86%	86.98%	88.78%	89.05%	86.67%	0.12	0.92
OK 3L t0.5	SVM	89.29%	87.67%	91.04%	91.43%	87.14%	0.09	0.89
	KNN	88.57%	86.49%	90.91%	91.43%	85.71%	0.14	0.88
	BN	89.05%	85.65%	93.16%	93.81%	84.29%	0.15	0.9
OK 4L t0.5	SVM	82.86%	81.94%	83.82%	84.29%	81.43%	0.16	0.83
	KNN	82.14%	81.25%	83.09%	83.57%	80.71%	0.19	0.83
	BN	84.05%	82.95%	85.22%	85.71%	82.38%	0.16	0.85
OK 5L t0.5	SVM	96.43%	95.77%	97.10%	97.14%	95.71%	0.03	0.96
	KNN	93.21%	91.16%	95.49%	95.71%	90.71%	0.08	0.96
	BN	92.62%	90.50%	94.97%	95.24%	90.00%	0.09	0.95
OK 6L t0.5	SVM	85.00%	83.56%	86.57%	87.14%	82.86%	0.13	0.85
	KNN	85.71%	83.33%	88.46%	89.29%	82.14%	0.14	0.85
	BN	86.19%	84.55%	88.00%	88.57%	83.81%	0.12	0.87
OK 3L t0.7	SVM	87.14%	83.33%	91.94%	92.86%	81.43%	0.08	0.87
	KNN	87.86%	83.12%	94.17%	95.00%	80.71%	0.17	0.87
	BN	88.10%	82.79%	95.45%	96.19%	80.00%	0.19	0.88
OK 4L t0.7	SVM	91.43%	89.19%	93.94%	94.29%	88.57%	0.06	0.91
	KNN	91.07%	88.08%	94.57%	95.00%	87.14%	0.06	0.92
	BN	90.48%	86.96%	94.74%	95.24%	85.71%	0.13	0.92
OK 5L t0.7	SVM	89.29%	88.73%	89.86%	90.00%	88.57%	0.10	0.89
	KNN	89.29%	87.67%	91.04%	91.43%	87.14%	0.12	0.89
	BN	89.52%	87.39%	91.92%	92.38%	86.67%	0.13	0.9
OK 6L t0.7	SVM	85.00%	83.56%	86.57%	87.14%	82.86%	0.13	0.85
	KNN	85.71%	83.33%	88.46%	89.29%	82.14%	0.14	0.85
	BN	86.19%	84.55%	88.00%	88.57%	83.81%	0.12	0.87

OK 3L t0.9	SVM	92.86%	91.67%	94.12%	94.29%	91.43%	0.06	0.93
	KNN	93.57%	91.78%	95.52%	95.71%	91.43%	0.09	0.94
	BN	94.05%	91.86%	96.48%	96.67%	91.43%	0.07	0.95
OK 4L t0.9	SVM	94.29%	91.89%	96.97%	97.14%	91.43%	0.03	0.94
	KNN	95.36%	93.20%	97.74%	97.86%	92.86%	0.05	0.95
	BN	95.95%	94.06%	98.01%	98.10%	93.81%	0.04	0.97
OK 5L t0.9	SVM	92.14%	91.55%	92.75%	92.86%	91.43%	0.07	0.92
	KNN	92.50%	91.03%	94.07%	94.29%	90.71%	0.08	0.92
	BN	93.33%	91.74%	95.05%	95.24%	91.43%	0.08	0.93

Table B.2: The results using the ED critical function in the context of whole image-based methods, where S means standard decomposition, O overlapped decomposition, t is the threshold for the critical function and L is the level..

Method	Classifier	Acc	Sen	Spec	PPV	NPV	EER	AUC
SM 3L t0.3	SVM	78.57%	78.57%	78.57%	78.57%	78.57%	0.21	0.79
	KNN	75.36%	74.83%	75.91%	76.43%	74.29%	0.24	0.78
	BN	76.43%	76.30%	76.56%	76.67%	76.19%	0.23	0.79
SM 4L t0.3	SVM	77.14%	79.69%	75.00%	72.86%	81.43%	0.25	0.77
	KNN	71.79%	71.94%	71.63%	71.43%	72.14%	0.29	0.75
	BN	73.57%	74.38%	72.81%	71.90%	75.24%	0.26	0.77
SM 5L t0.3	SVM	78.57%	77.78%	79.41%	80.00%	77.14%	0.21	0.79
	KNN	73.21%	72.41%	74.07%	75.00%	71.43%	0.29	0.77
	BN	73.57%	72.60%	74.63%	75.71%	71.43%	0.26	0.78
SM 6L t0.3	SVM	75.00%	75.36%	74.65%	74.29%	75.71%	0.25	0.75
	KNN	72.14%	70.39%	74.22%	76.43%	67.86%	0.27	0.74
	BN	73.57%	72.00%	75.38%	77.14%	70.00%	0.26	0.76
SM 3L t0.5	SVM	71.43%	70.83%	72.06%	72.86%	70.00%	0.28	0.71
	KNN	69.29%	68.24%	70.45%	72.14%	66.43%	0.28	0.71
	BN	71.90%	71.10%	72.77%	73.81%	70.00%	0.26	0.74
SM 4L t0.5	SVM	82.14%	80.82%	83.58%	84.29%	80.00%	0.16	0.82
	KNN	78.21%	78.01%	78.42%	78.57%	77.86%	0.22	0.81
	BN	78.81%	79.80%	77.88%	77.14%	80.48%	0.20	0.83
SM 5L t0.5	SVM	87.14%	88.24%	86.11%	85.71%	88.57%	0.14	0.87
	KNN	78.21%	76.87%	79.70%	80.71%	75.71%	0.19	0.84
	BN	78.33%	78.20%	78.47%	78.57%	78.10%	0.22	0.85
SM 6L t0.5	SVM	77.86%	79.10%	76.71%	75.71%	80.00%	0.23	0.78
	KNN	74.64%	74.13%	75.18%	75.71%	73.57%	0.24	0.78
	BN	73.81%	73.58%	74.04%	74.29%	73.33%	0.26	0.75
SM 3L t0.7	SVM	78.57%	77.03%	80.30%	81.43%	75.71%	0.20	0.79
	KNN	76.79%	75.86%	77.78%	78.57%	75.00%	0.23	0.78
	BN	75.71%	75.23%	76.21%	76.67%	74.76%	0.25	0.78
SM 4L t0.7	SVM	76.43%	74.03%	79.37%	81.43%	71.43%	0.21	0.76
	KNN	76.43%	74.03%	79.37%	81.43%	71.43%	0.27	0.76
	BN	76.90%	75.80%	78.11%	79.05%	74.76%	0.23	0.78

SM 5L t0.7	SVM	83.57%	84.06%	83.10%	82.86%	84.29%	0.17	0.84
	KNN	80.71%	81.62%	79.86%	79.29%	82.14%	0.20	0.83
	BN	79.29%	81.22%	77.58%	76.19%	82.38%	0.21	0.83
SM 6L t0.7	SVM	74.29%	74.29%	74.29%	74.29%	74.29%	0.26	0.74
	KNN	72.50%	71.72%	73.33%	74.29%	70.71%	0.27	0.76
	BN	74.05%	73.49%	74.63%	75.24%	72.86%	0.27	0.78
OM 3L t0.3	SVM	84.29%	85.29%	83.33%	82.86%	85.71%	0.17	0.84
	KNN	79.64%	79.86%	79.43%	79.29%	80.00%	0.20	0.82
	BN	79.05%	80.20%	77.98%	77.14%	80.95%	0.22	0.82
OM 4L t0.3	SVM	86.43%	85.92%	86.96%	87.14%	85.71%	0.13	0.86
	KNN	87.14%	86.62%	87.68%	87.86%	86.43%	0.12	0.88
	BN	84.29%	84.95%	83.64%	83.33%	85.24%	0.16	0.86
OM 5L t0.3	SVM	79.29%	78.87%	79.71%	80.00%	78.57%	0.20	0.79
	KNN	75.36%	75.18%	75.54%	75.71%	75.00%	0.25	0.78
	BN	76.67%	76.92%	76.42%	76.19%	77.14%	0.23	0.79
OM 6L t0.3	SVM	80.71%	79.45%	82.09%	82.86%	78.57%	0.18	0.81
	KNN	75.00%	73.65%	76.52%	77.86%	72.14%	0.26	0.79
	BN	75.00%	74.65%	75.36%	75.71%	74.29%	0.25	0.8
OM 3L t0.5	SVM	85.71%	84.72%	86.76%	87.14%	84.29%	0.13	0.86
	KNN	84.29%	82.43%	86.36%	87.14%	81.43%	0.15	0.86
	BN	81.90%	80.73%	83.17%	83.81%	80.00%	0.18	0.85
OM 4L t0.5	SVM	75.71%	76.47%	75.00%	74.29%	77.14%	0.25	0.76
	KNN	71.07%	69.54%	72.87%	75.00%	67.14%	0.28	0.74
	BN	72.14%	71.23%	73.13%	74.29%	70.00%	0.28	0.76
OM 5L t0.5	SVM	78.57%	77.78%	79.41%	80.00%	77.14%	0.21	0.79
	KNN	76.43%	74.67%	78.46%	80.00%	72.86%	0.25	0.77
	BN	75.95%	73.80%	78.53%	80.48%	71.43%	0.26	0.78
OM 6L t0.5	SVM	82.14%	79.22%	85.71%	87.14%	77.14%	0.14	0.82
	KNN	76.79%	72.46%	83.19%	86.43%	67.14%	0.25	0.8
	BN	77.86%	74.07%	83.05%	85.71%	70.00%	0.23	0.81
OM 3L t0.7	SVM	80.71%	83.08%	78.67%	77.14%	84.29%	0.21	0.81
	KNN	80.00%	79.58%	80.43%	80.71%	79.29%	0.20	0.81
	BN	80.00%	79.72%	80.29%	80.48%	79.52%	0.20	0.82
OM 4L t0.7	SVM	79.29%	83.61%	75.95%	72.86%	85.71%	0.24	0.79
	KNN	76.43%	78.46%	74.67%	72.86%	80.00%	0.25	0.78
	BN	74.76%	76.00%	73.64%	72.38%	77.14%	0.26	0.77
OM 5L t0.7	SVM	82.14%	80.82%	83.58%	84.29%	80.00%	0.16	0.82
	KNN	79.64%	78.62%	80.74%	81.43%	77.86%	0.21	0.82
	BN	78.81%	77.88%	79.80%	80.48%	77.14%	0.21	0.82
OM 6L t0.7	SVM	77.14%	75.68%	78.79%	80.00%	74.29%	0.21	0.77
	KNN	73.93%	71.34%	77.24%	80.00%	67.86%	0.24	0.76
	BN	75.00%	72.53%	78.07%	80.48%	69.52%	0.25	0.78
OM 3L t0.9	SVM	75.00%	73.97%	76.12%	77.14%	72.86%	0.24	0.75
	KNN	75.36%	74.15%	76.69%	77.86%	72.86%	0.25	0.75
	BN	76.67%	76.17%	77.18%	77.62%	75.71%	0.22	0.77

OM 4L t0.9	SVM	78.57%	78.57%	78.57%	78.57%	78.57%	0.21	0.79
	KNN	77.86%	77.86%	77.86%	77.86%	77.86%	0.22	0.79
	BN	78.10%	78.10%	78.10%	78.10%	78.10%	0.22	0.8
OM 5L t0.9	SVM	81.43%	82.35%	80.56%	80.00%	82.86%	0.19	0.81
	KNN	77.14%	77.54%	76.76%	76.43%	77.86%	0.24	0.8
	BN	76.90%	77.56%	76.28%	75.71%	78.10%	0.24	0.79
OM 6L t0.9	SVM	87.14%	89.39%	85.14%	84.29%	90.00%	0.15	0.87
	KNN	81.79%	83.46%	80.27%	79.29%	84.29%	0.20	0.85
	BN	79.76%	82.72%	77.29%	75.24%	84.29%	0.22	0.84
SK 3L t0.3	SVM	92.86%	95.45%	90.54%	90.00%	95.71%	0.09	0.93
	KNN	89.29%	90.44%	88.19%	87.86%	90.71%	0.10	0.93
	BN	88.57%	91.75%	85.84%	84.76%	92.38%	0.12	0.93
SK 4L t0.3	SVM	88.57%	89.71%	87.50%	87.14%	90.00%	0.12	0.89
	KNN	85.71%	85.71%	85.71%	85.71%	85.71%	0.14	0.88
	BN	85.95%	87.94%	84.16%	83.33%	88.57%	0.17	0.89
SK 5L t0.3	SVM	80.00%	83.87%	76.92%	74.29%	85.71%	0.23	0.8
	KNN	76.79%	79.07%	74.83%	72.86%	80.71%	0.25	0.78
	BN	77.14%	80.65%	74.36%	71.43%	82.86%	0.26	0.8
SK 6L t0.3	SVM	85.71%	89.06%	82.89%	81.43%	90.00%	0.17	0.86
	KNN	82.50%	85.83%	79.74%	77.86%	87.14%	0.19	0.84
	BN	83.10%	88.83%	78.84%	75.71%	90.48%	0.20	0.86
SK 3L t0.5	SVM	89.29%	95.08%	84.81%	82.86%	95.71%	0.15	0.89
	KNN	87.50%	92.68%	83.44%	81.43%	93.57%	0.19	0.87
	BN	87.38%	93.37%	82.85%	80.48%	94.29%	0.19	0.88
SK 4L t0.5	SVM	90.71%	90.14%	91.30%	91.43%	90.00%	0.09	0.91
	KNN	85.71%	85.21%	86.23%	86.43%	85.00%	0.15	0.88
	BN	85.71%	86.06%	85.38%	85.24%	86.19%	0.14	0.89
SK 5L t0.5	SVM	78.57%	80.30%	77.03%	75.71%	81.43%	0.23	0.79
	KNN	74.29%	75.00%	73.61%	72.86%	75.71%	0.25	0.79
	BN	75.95%	78.84%	73.59%	70.95%	80.95%	0.24	0.81
SK 6L t0.5	SVM	85.71%	86.76%	84.72%	84.29%	87.14%	0.15	0.86
	KNN	80.36%	79.31%	81.48%	82.14%	78.57%	0.19	0.86
	BN	81.67%	82.13%	81.22%	80.95%	82.38%	0.18	0.87
SK 3L t0.7	SVM	89.29%	91.04%	87.67%	87.14%	91.43%	0.12	0.89
	KNN	85.71%	87.31%	84.25%	83.57%	87.86%	0.16	0.86
	BN	84.76%	88.42%	81.74%	80.00%	89.52%	0.19	0.87
SK 4L t0.7	SVM	88.57%	93.55%	84.62%	82.86%	94.29%	0.15	0.89
	KNN	85.71%	88.46%	83.33%	82.14%	89.29%	0.17	0.87
	BN	85.95%	90.81%	82.13%	80.00%	91.90%	0.19	0.88
SK 5L t0.7	SVM	83.57%	87.30%	80.52%	78.57%	88.57%	0.19	0.84
	KNN	78.57%	80.30%	77.03%	75.71%	81.43%	0.22	0.84
	BN	80.48%	83.68%	77.83%	75.71%	85.24%	0.20	0.85
SK 6L t0.7	SVM	85.00%	83.56%	86.57%	87.14%	82.86%	0.13	0.85
	KNN	82.86%	81.94%	83.82%	84.29%	81.43%	0.17	0.84
	BN	83.10%	83.57%	82.63%	82.38%	83.81%	0.17	0.86

OK 3L t0.3	SVM	82.86%	85.94%	80.26%	78.57%	87.14%	0.20	0.83
	KNN	80.71%	80.71%	80.71%	80.71%	80.71%	0.19	0.84
	BN	83.33%	83.98%	82.71%	82.38%	84.29%	0.18	0.86
OK 4L t0.3	SVM	83.57%	85.07%	82.19%	81.43%	85.71%	0.18	0.84
	KNN	80.36%	81.02%	79.72%	79.29%	81.43%	0.19	0.85
	BN	83.33%	85.00%	81.82%	80.95%	85.71%	0.15	0.88
OK 5L t0.3	SVM	91.43%	93.94%	89.19%	88.57%	94.29%	0.11	0.91
	KNN	87.86%	88.97%	86.81%	86.43%	89.29%	0.13	0.91
	BN	86.67%	88.12%	85.32%	84.76%	88.57%	0.14	0.9
OK 6L t0.3	SVM	85.00%	87.69%	82.67%	81.43%	88.57%	0.17	0.85
	KNN	85.00%	85.51%	84.51%	84.29%	85.71%	0.15	0.86
	BN	85.00%	85.17%	84.83%	84.76%	85.24%	0.15	0.87
OK 3L t0.5	SVM	90.00%	88.89%	91.18%	91.43%	88.57%	0.09	0.9
	KNN	85.00%	83.56%	86.57%	87.14%	82.86%	0.15	0.9
	BN	86.19%	85.85%	86.54%	86.67%	85.71%	0.13	0.91
OK 4L t0.5	SVM	87.86%	87.32%	88.41%	88.57%	87.14%	0.12	0.88
	KNN	85.71%	84.25%	87.31%	87.86%	83.57%	0.13	0.88
	BN	86.43%	85.58%	87.32%	87.62%	85.24%	0.13	0.89
OK 5L t0.5	SVM	85.00%	84.51%	85.51%	85.71%	84.29%	0.14	0.85
	KNN	84.29%	83.80%	84.78%	85.00%	83.57%	0.16	0.85
	BN	85.48%	85.31%	85.65%	85.71%	85.24%	0.15	0.87
OK 6L t0.5	SVM	84.29%	85.29%	83.33%	82.86%	85.71%	0.17	0.84
	KNN	82.14%	83.09%	81.25%	80.71%	83.57%	0.18	0.85
	BN	83.81%	85.50%	82.27%	81.43%	86.19%	0.16	0.87
OK 3L t0.7	SVM	83.57%	85.07%	82.19%	81.43%	85.71%	0.18	0.84
	KNN	81.43%	80.56%	82.35%	82.86%	80.00%	0.18	0.83
	BN	83.81%	83.81%	83.81%	83.81%	83.81%	0.16	0.86
OK 4L t0.7	SVM	78.57%	78.57%	78.57%	78.57%	78.57%	0.21	0.79
	KNN	78.21%	78.42%	78.01%	77.86%	78.57%	0.22	0.81
	BN	81.43%	83.00%	80.00%	79.05%	83.81%	0.20	0.83
OK 5L t0.7	SVM	89.29%	88.73%	89.86%	90.00%	88.57%	0.10	0.89
	KNN	84.64%	84.40%	84.89%	85.00%	84.29%	0.16	0.89
	BN	84.52%	85.37%	83.72%	83.33%	85.71%	0.15	0.89
OK 6L t0.7	SVM	83.57%	83.10%	84.06%	84.29%	82.86%	0.16	0.84
	KNN	80.71%	79.45%	82.09%	82.86%	78.57%	0.18	0.85
	BN	82.38%	82.08%	82.69%	82.86%	81.90%	0.18	0.87
OK 3L t0.9	SVM	80.71%	79.45%	82.09%	82.86%	78.57%	0.18	0.81
	KNN	78.21%	76.87%	79.70%	80.71%	75.71%	0.25	0.82
	BN	81.19%	80.47%	81.95%	82.38%	80.00%	0.18	0.85
OK 4L t0.9	SVM	83.57%	81.33%	86.15%	87.14%	80.00%	0.14	0.84
	KNN	80.00%	78.38%	81.82%	82.86%	77.14%	0.19	0.82
	BN	81.90%	80.45%	83.50%	84.29%	79.52%	0.17	0.85
OK 5L t0.9	SVM	82.14%	82.61%	81.69%	81.43%	82.86%	0.18	0.82
	KNN	78.21%	78.42%	78.01%	77.86%	78.57%	0.22	0.81
	BN	80.00%	80.00%	80.00%	80.00%	80.00%	0.20	0.83

OK 6L t0.9	SVM	84.29%	82.43%	86.36%	87.14%	81.43%	0.14	0.84
	KNN	82.86%	81.08%	84.85%	85.71%	80.00%	0.18	0.85
	BN	84.52%	83.41%	85.71%	86.19%	82.86%	0.17	0.87

Table B.3: The results using the KCC in the context of whole image-based methods, where S means standard decomposition, O overlapped decomposition, t is the threshold for the critical function and L is the level..

Method	Classifier	Acc	Sen	Spec	PPV	NPV	EER	AUC
SM 3L t0.3	SVM	84.29%	82.43%	86.36%	87.14%	81.43%	0.14	0.84
	KNN	81.43%	79.33%	83.85%	85.00%	77.86%	0.20	0.84
	BN	80.24%	79.26%	81.28%	81.90%	78.57%	0.20	0.83
SM 4L t0.3	SVM	85.00%	83.56%	86.57%	87.14%	82.86%	0.13	0.85
	KNN	76.43%	75.00%	78.03%	79.29%	73.57%	0.24	0.81
	BN	76.19%	75.70%	76.70%	77.14%	75.24%	0.24	0.81
SM 5L t0.3	SVM	73.57%	73.24%	73.91%	74.29%	72.86%	0.26	0.74
	KNN	69.64%	69.23%	70.07%	70.71%	68.57%	0.31	0.73
	BN	71.67%	70.59%	72.86%	74.29%	69.05%	0.27	0.75
SM 6L t0.3	SVM	79.29%	79.71%	78.87%	78.57%	80.00%	0.21	0.79
	KNN	76.07%	74.17%	78.29%	80.00%	72.14%	0.23	0.78
	BN	76.43%	74.45%	78.76%	80.48%	72.38%	0.24	0.8
SM 3L t0.5	SVM	73.57%	73.24%	73.91%	74.29%	72.86%	0.26	0.74
	KNN	70.00%	69.18%	70.90%	72.14%	67.86%	0.28	0.73
	BN	72.62%	71.89%	73.40%	74.29%	70.95%	0.27	0.75
SM 4L t0.5	SVM	82.14%	79.22%	85.71%	87.14%	77.14%	0.14	0.82
	KNN	78.93%	78.72%	79.14%	79.29%	78.57%	0.21	0.83
	BN	79.76%	80.19%	79.34%	79.05%	80.48%	0.20	0.83
SM 5L t0.5	SVM	85.00%	86.57%	83.56%	82.86%	87.14%	0.16	0.85
	KNN	79.64%	79.43%	79.86%	80.00%	79.29%	0.20	0.84
	BN	78.81%	78.40%	79.23%	79.52%	78.10%	0.21	0.84
SM 6L t0.5	SVM	75.71%	74.32%	77.27%	78.57%	72.86%	0.23	0.76
	KNN	73.57%	72.30%	75.00%	76.43%	70.71%	0.27	0.75
	BN	74.05%	72.65%	75.63%	77.14%	70.95%	0.27	0.74
SM 3L t0.7	SVM	82.14%	82.61%	81.69%	81.43%	82.86%	0.18	0.82
	KNN	79.29%	79.71%	78.87%	78.57%	80.00%	0.20	0.81
	BN	77.14%	77.14%	77.14%	77.14%	77.14%	0.23	0.8
SM 4L t0.7	SVM	82.86%	79.49%	87.10%	88.57%	77.14%	0.13	0.83
	KNN	82.14%	80.00%	84.62%	85.71%	78.57%	0.20	0.83
	BN	80.71%	79.72%	81.77%	82.38%	79.05%	0.20	0.82
SM 6L t0.7	SVM	82.14%	83.58%	80.82%	80.00%	84.29%	0.19	0.82
	KNN	78.21%	81.10%	75.82%	73.57%	82.86%	0.26	0.81
	BN	77.38%	79.19%	75.78%	74.29%	80.48%	0.21	0.82
SM 5L t0.7	SVM	75.71%	76.47%	75.00%	74.29%	77.14%	0.25	0.76
	KNN	73.57%	72.60%	74.63%	75.71%	71.43%	0.27	0.75
	BN	73.33%	73.33%	73.33%	73.33%	73.33%	0.27	0.76

SM 3L t0.9	SVM	75.71%	73.08%	79.03%	81.43%	70.00%	0.21	0.76
	KNN	75.36%	73.83%	77.10%	78.57%	72.14%	0.26	0.76
	BN	75.71%	73.89%	77.84%	79.52%	71.90%	0.23	0.78
SM 4L t0.9	SVM	81.43%	80.56%	82.35%	82.86%	80.00%	0.18	0.81
	KNN	74.29%	73.29%	75.37%	76.43%	72.14%	0.25	0.78
	BN	74.05%	72.85%	75.38%	76.67%	71.43%	0.26	0.79
SM 5L t0.9	SVM	73.57%	74.63%	72.60%	71.43%	75.71%	0.27	0.74
	KNN	71.79%	71.63%	71.94%	72.14%	71.43%	0.28	0.74
	BN	72.38%	72.38%	72.38%	72.38%	72.38%	0.28	0.76
SM 6L t0.9	SVM	78.57%	78.57%	78.57%	78.57%	78.57%	0.21	0.79
	KNN	75.00%	75.36%	74.65%	74.29%	75.71%	0.25	0.78
	BN	75.95%	76.85%	75.12%	74.29%	77.62%	0.24	0.79
OM 3L t0.3	SVM	79.29%	79.71%	78.87%	78.57%	80.00%	0.21	0.79
	KNN	76.43%	75.00%	78.03%	79.29%	73.57%	0.24	0.79
	BN	76.19%	75.46%	76.96%	77.62%	74.76%	0.23	0.79
OM 4L t0.3	SVM	80.00%	80.00%	80.00%	80.00%	80.00%	0.20	0.8
	KNN	76.43%	75.34%	77.61%	78.57%	74.29%	0.24	0.78
	BN	75.95%	74.22%	77.95%	79.52%	72.38%	0.25	0.79
OM 5L t0.3	SVM	81.43%	80.56%	82.35%	82.86%	80.00%	0.18	0.81
	KNN	77.86%	74.68%	81.97%	84.29%	71.43%	0.23	0.79
	BN	78.10%	75.00%	82.07%	84.29%	71.90%	0.23	0.81
OM 6L t0.3	SVM	80.00%	80.00%	80.00%	80.00%	80.00%	0.20	0.8
	KNN	78.21%	78.42%	78.01%	77.86%	78.57%	0.22	0.79
	BN	78.57%	78.04%	79.13%	79.52%	77.62%	0.22	0.8
OM 3L t0.5	SVM	79.29%	78.08%	80.60%	81.43%	77.14%	0.19	0.79
	KNN	76.07%	75.52%	76.64%	77.14%	75.00%	0.24	0.8
	BN	78.10%	77.83%	78.37%	78.57%	77.62%	0.22	0.82
OM 6L t0.5	SVM	78.57%	79.41%	77.78%	77.14%	80.00%	0.22	0.79
	KNN	77.86%	77.86%	77.86%	77.86%	77.86%	0.22	0.79
	BN	76.43%	75.81%	77.07%	77.62%	75.24%	0.24	0.8
OM 4L t0.5	SVM	80.71%	78.67%	83.08%	84.29%	77.14%	0.17	0.81
	KNN	77.50%	75.84%	79.39%	80.71%	74.29%	0.23	0.81
	BN	78.10%	76.82%	79.50%	80.48%	75.71%	0.22	0.81
OM 5L t0.5	SVM	77.14%	77.14%	77.14%	77.14%	77.14%	0.23	0.77
	KNN	74.29%	72.37%	76.56%	78.57%	70.00%	0.28	0.76
	BN	73.10%	70.82%	75.94%	78.57%	67.62%	0.28	0.75
OM 3L t0.7	SVM	82.86%	81.94%	83.82%	84.29%	81.43%	0.16	0.83
	KNN	82.14%	80.41%	84.09%	85.00%	79.29%	0.18	0.83
	BN	80.95%	79.82%	82.18%	82.86%	79.05%	0.19	0.83
OM 6L t0.7	SVM	75.00%	73.33%	76.92%	78.57%	71.43%	0.23	0.75
	KNN	75.00%	73.65%	76.52%	77.86%	72.14%	0.25	0.76
	BN	76.43%	75.81%	77.07%	77.62%	75.24%	0.24	0.78
OM 4L t0.7	SVM	82.14%	80.82%	83.58%	84.29%	80.00%	0.16	0.82
	KNN	76.79%	74.83%	79.07%	80.71%	72.86%	0.22	0.8
	BN	76.90%	76.28%	77.56%	78.10%	75.71%	0.22	0.81

OM 5L t0.7	SVM	87.14%	90.62%	84.21%	82.86%	91.43%	0.16	0.87
	KNN	81.79%	83.97%	79.87%	78.57%	85.00%	0.21	0.85
	BN	79.52%	81.00%	78.18%	77.14%	81.90%	0.22	0.84
OM 3L t0.9	SVM	75.71%	75.71%	75.71%	75.71%	75.71%	0.24	0.76
	KNN	76.43%	75.69%	77.21%	77.86%	75.00%	0.24	0.77
	BN	76.67%	76.17%	77.18%	77.62%	75.71%	0.24	0.78
OM 4L t0.9	SVM	80.71%	80.28%	81.16%	81.43%	80.00%	0.19	0.81
	KNN	76.43%	76.06%	76.81%	77.14%	75.71%	0.24	0.8
	BN	76.43%	76.56%	76.30%	76.19%	76.67%	0.24	0.79
OM 5L t0.9	SVM	87.86%	90.77%	85.33%	84.29%	91.43%	0.15	0.88
	KNN	82.50%	84.21%	80.95%	80.00%	85.00%	0.19	0.86
	BN	80.24%	83.25%	77.73%	75.71%	84.76%	0.22	0.85
OM 6L t0.9	SVM	87.86%	88.41%	87.32%	87.14%	88.57%	0.13	0.88
	KNN	83.57%	82.19%	85.07%	85.71%	81.43%	0.16	0.86
	BN	82.38%	81.48%	83.33%	83.81%	80.95%	0.18	0.86
SK 3L t0.3	SVM	82.86%	81.94%	83.82%	84.29%	81.43%	0.16	0.83
	KNN	80.36%	80.14%	80.58%	80.71%	80.00%	0.20	0.8
	BN	81.43%	82.67%	80.28%	79.52%	83.33%	0.18	0.83
SK 4L t0.3	SVM	82.86%	81.94%	83.82%	84.29%	81.43%	0.16	0.83
	KNN	79.29%	78.47%	80.15%	80.71%	77.86%	0.19	0.81
	BN	81.19%	81.64%	80.75%	80.48%	81.90%	0.19	0.84
SK 5L t0.3	SVM	86.43%	91.80%	82.28%	80.00%	92.86%	0.18	0.86
	KNN	81.43%	85.48%	78.21%	75.71%	87.14%	0.24	0.84
	BN	81.43%	86.26%	77.73%	74.76%	88.10%	0.23	0.84
SK 6L t0.3	SVM	80.71%	82.09%	79.45%	78.57%	82.86%	0.21	0.81
	KNN	78.93%	80.00%	77.93%	77.14%	80.71%	0.23	0.8
	BN	79.29%	81.87%	77.09%	75.24%	83.33%	0.24	0.81
SK 3L t0.5	SVM	80.71%	77.92%	84.13%	85.71%	75.71%	0.16	0.81
	KNN	75.00%	73.33%	76.92%	78.57%	71.43%	0.24	0.79
	BN	75.00%	75.86%	74.19%	73.33%	76.67%	0.23	0.81
SK 4L t0.5	SVM	75.00%	80.70%	71.08%	65.71%	84.29%	0.29	0.75
	KNN	69.64%	72.73%	67.30%	62.86%	76.43%	0.34	0.73
	BN	73.10%	77.40%	69.96%	65.24%	80.95%	0.32	0.76
SK 5L t0.5	SVM	86.43%	89.23%	84.00%	82.86%	90.00%	0.16	0.86
	KNN	78.57%	78.17%	78.99%	79.29%	77.86%	0.21	0.83
	BN	78.57%	81.25%	76.32%	74.29%	82.86%	0.22	0.83
SK 6L t0.5	SVM	80.71%	80.28%	81.16%	81.43%	80.00%	0.19	0.81
	KNN	77.14%	77.14%	77.14%	77.14%	77.14%	0.23	0.78
	BN	77.38%	79.19%	75.78%	74.29%	80.48%	0.24	0.81
SK 3L t0.7	SVM	81.43%	81.43%	81.43%	81.43%	81.43%	0.19	0.81
	KNN	77.14%	77.54%	76.76%	76.43%	77.86%	0.23	0.8
	BN	77.86%	79.70%	76.23%	74.76%	80.95%	0.20	0.81
SK 4L t0.7	SVM	79.29%	78.87%	79.71%	80.00%	78.57%	0.20	0.79
	KNN	78.93%	80.00%	77.93%	77.14%	80.71%	0.21	0.79
	BN	79.52%	81.96%	77.43%	75.71%	83.33%	0.20	0.82

SK 5L t0.7	SVM	89.29%	86.67%	92.31%	92.86%	85.71%	0.08	0.89
	KNN	83.93%	83.22%	84.67%	85.00%	82.86%	0.17	0.85
	BN	84.52%	84.36%	84.69%	84.76%	84.29%	0.15	0.87
SK 6L t0.7	SVM	87.14%	90.62%	84.21%	82.86%	91.43%	0.16	0.87
	KNN	82.14%	84.09%	80.41%	79.29%	85.00%	0.21	0.84
	BN	82.14%	86.10%	78.97%	76.67%	87.62%	0.22	0.85
SK 3L t0.9	SVM	86.43%	94.74%	80.72%	77.14%	95.71%	0.19	0.86
	KNN	81.79%	88.03%	77.30%	73.57%	90.00%	0.21	0.85
	BN	81.67%	89.82%	76.28%	71.43%	91.90%	0.23	0.85
SK 4L t0.9	SVM	85.00%	83.56%	86.57%	87.14%	82.86%	0.13	0.85
	KNN	81.43%	80.56%	82.35%	82.86%	80.00%	0.19	0.82
	BN	81.43%	81.43%	81.43%	81.43%	81.43%	0.19	0.84
SK 5L t0.9	SVM	87.86%	88.41%	87.32%	87.14%	88.57%	0.13	0.88
	KNN	83.57%	85.07%	82.19%	81.43%	85.71%	0.19	0.85
	BN	83.57%	86.91%	80.79%	79.05%	88.10%	0.21	0.86
SK 6L t0.9	SVM	85.00%	85.51%	84.51%	84.29%	85.71%	0.15	0.85
	KNN	81.07%	80.85%	81.29%	81.43%	80.71%	0.19	0.85
	BN	81.67%	82.76%	80.65%	80.00%	83.33%	0.18	0.86
OK 3L t0.3	SVM	83.57%	82.19%	85.07%	85.71%	81.43%	0.15	0.84
	KNN	79.64%	78.62%	80.74%	81.43%	77.86%	0.19	0.83
	BN	81.90%	81.02%	82.84%	83.33%	80.48%	0.17	0.85
OK 4L t0.3	SVM	82.14%	83.58%	80.82%	80.00%	84.29%	0.19	0.82
	KNN	78.57%	79.41%	77.78%	77.14%	80.00%	0.21	0.81
	BN	80.24%	80.68%	79.81%	79.52%	80.95%	0.20	0.83
OK 5L t0.3	SVM	85.00%	84.51%	85.51%	85.71%	84.29%	0.14	0.85
	KNN	83.21%	82.52%	83.94%	84.29%	82.14%	0.17	0.85
	BN	84.76%	84.43%	85.10%	85.24%	84.29%	0.15	0.87
OK 6L t0.3	SVM	83.57%	84.06%	83.10%	82.86%	84.29%	0.17	0.84
	KNN	79.29%	79.71%	78.87%	78.57%	80.00%	0.21	0.83
	BN	79.52%	80.69%	78.44%	77.62%	81.43%	0.21	0.84
OK 3L t0.9	SVM	85.00%	82.67%	87.69%	88.57%	81.43%	0.12	0.85
	KNN	80.36%	78.15%	82.95%	84.29%	76.43%	0.21	0.85
	BN	82.38%	80.91%	84.00%	84.76%	80.00%	0.19	0.86
OK 4L t0.9	SVM	80.00%	80.00%	80.00%	80.00%	80.00%	0.20	0.8
	KNN	79.64%	79.02%	80.29%	80.71%	78.57%	0.21	0.81
	BN	81.90%	82.52%	81.31%	80.95%	82.86%	0.18	0.84
OK 5L t0.9	SVM	75.71%	78.12%	73.68%	71.43%	80.00%	0.26	0.76
	KNN	74.29%	74.29%	74.29%	74.29%	74.29%	0.26	0.76
	BN	75.71%	76.73%	74.77%	73.81%	77.62%	0.26	0.79
OK 6L t0.9	SVM	88.57%	84.62%	93.55%	94.29%	82.86%	0.06	0.89
	KNN	85.71%	82.47%	89.68%	90.71%	80.71%	0.17	0.87
	BN	86.19%	83.63%	89.18%	90.00%	82.38%	0.14	0.89

Table B.4: The results using the KLD critical function in the context of whole image-based, where S means standard decomposition, O overlapped decomposition, t is the threshold for the critical function and L is the level.

Method	Classifier	Acc	Sen	Spec	PPV	NPV	EER	AUC
SM 3L t0.3	SVM	77.14%	76.39%	77.94%	78.57%	75.71%	0.22	0.77
	KNN	74.64%	72.85%	76.74%	78.57%	70.71%	0.26	0.76
	BN	73.57%	72.20%	75.13%	76.67%	70.48%	0.26	0.77
SM 4L t0.3	SVM	66.43%	67.69%	65.33%	62.86%	70.00%	0.35	0.66
	KNN	66.07%	65.73%	66.42%	67.14%	65.00%	0.34	0.67
	BN	68.10%	67.76%	68.45%	69.05%	67.14%	0.31	0.71
SM 5L t0.3	SVM	72.14%	73.13%	71.23%	70.00%	74.29%	0.29	0.72
	KNN	66.79%	66.67%	66.91%	67.14%	66.43%	0.33	0.7
	BN	68.57%	68.75%	68.40%	68.10%	69.05%	0.32	0.71
SM 6L t0.3	SVM	82.14%	84.62%	80.00%	78.57%	85.71%	0.20	0.82
	KNN	79.29%	81.54%	77.33%	75.71%	82.86%	0.23	0.81
	BN	78.10%	80.41%	76.11%	74.29%	81.90%	0.23	0.81
SM 3L t0.5	SVM	80.71%	82.09%	79.45%	78.57%	82.86%	0.21	0.81
	KNN	75.00%	76.52%	73.65%	72.14%	77.86%	0.22	0.78
	BN	75.95%	78.53%	73.80%	71.43%	80.48%	0.27	0.8
SM 4L t0.5	SVM	75.71%	77.27%	74.32%	72.86%	78.57%	0.26	0.76
	KNN	73.21%	73.38%	73.05%	72.86%	73.57%	0.27	0.75
	BN	74.29%	74.06%	74.52%	74.76%	73.81%	0.26	0.77
SM 5L t0.5	SVM	77.86%	76.71%	79.10%	80.00%	75.71%	0.21	0.78
	KNN	74.64%	75.18%	74.13%	73.57%	75.71%	0.24	0.77
	BN	76.67%	78.57%	75.00%	73.33%	80.00%	0.22	0.79
SM 6L t0.5	SVM	83.57%	85.07%	82.19%	81.43%	85.71%	0.18	0.84
	KNN	84.29%	86.92%	82.00%	80.71%	87.86%	0.19	0.83
	BN	85.48%	89.42%	82.25%	80.48%	90.48%	0.19	0.86
SM 3L t0.7	SVM	87.14%	89.39%	85.14%	84.29%	90.00%	0.15	0.87
	KNN	84.29%	82.88%	85.82%	86.43%	82.14%	0.16	0.86
	BN	83.33%	83.33%	83.33%	83.33%	83.33%	0.17	0.86
SM 4L t0.7	SVM	78.57%	80.30%	77.03%	75.71%	81.43%	0.23	0.79
	KNN	75.36%	75.54%	75.18%	75.00%	75.71%	0.24	0.78
	BN	77.14%	78.79%	75.68%	74.29%	80.00%	0.23	0.8
SM 5L t0.7	SVM	88.57%	98.21%	82.14%	78.57%	98.57%	0.18	0.89
	KNN	86.43%	96.36%	80.00%	75.71%	97.14%	0.18	0.89
	BN	85.00%	94.55%	78.82%	74.29%	95.71%	0.18	0.87
SM 6L t0.7	SVM	81.43%	84.38%	78.95%	77.14%	85.71%	0.21	0.81
	KNN	80.00%	81.34%	78.77%	77.86%	82.14%	0.21	0.81
	BN	81.19%	83.25%	79.37%	78.10%	84.29%	0.21	0.83
SM 3L t0.9	SVM	88.57%	92.19%	85.53%	84.29%	92.86%	0.14	0.89
	KNN	86.07%	89.15%	83.44%	82.14%	90.00%	0.16	0.88
	BN	85.00%	88.48%	82.10%	80.48%	89.52%	0.17	0.88
SM 4L t0.9	SVM	87.86%	92.06%	84.42%	82.86%	92.86%	0.16	0.88
	KNN	88.21%	92.13%	84.97%	83.57%	92.86%	0.16	0.88
	BN	86.43%	92.27%	82.01%	79.52%	93.33%	0.19	0.88

SM 5L t0.9	SVM	92.86%	95.45%	90.54%	90.00%	95.71%	0.09	0.93
	KNN	92.14%	96.09%	88.82%	87.86%	96.43%	0.11	0.93
	BN	90.48%	96.20%	86.02%	84.29%	96.67%	0.13	0.92
SM 6L t0.9	SVM	90.71%	95.24%	87.01%	85.71%	95.71%	0.13	0.91
	KNN	88.93%	92.25%	86.09%	85.00%	92.86%	0.13	0.9
	BN	89.05%	94.09%	85.04%	83.33%	94.76%	0.15	0.91
OM 3L t0.3	SVM	87.86%	87.32%	88.41%	88.57%	87.14%	0.12	0.88
	KNN	86.43%	86.96%	85.92%	85.71%	87.14%	0.14	0.88
	BN	85.24%	87.00%	83.64%	82.86%	87.62%	0.14	0.88
OM 4L t0.3	SVM	86.43%	86.96%	85.92%	85.71%	87.14%	0.14	0.86
	KNN	85.00%	86.57%	83.56%	82.86%	87.14%	0.16	0.85
	BN	85.48%	87.06%	84.02%	83.33%	87.62%	0.16	0.88
OM 5L t0.3	SVM	91.43%	93.94%	89.19%	88.57%	94.29%	0.11	0.91
	KNN	90.36%	88.97%	91.85%	92.14%	88.57%	0.10	0.93
	BN	89.52%	90.69%	88.43%	88.10%	90.95%	0.11	0.92
OM 6L t0.3	SVM	92.14%	96.83%	88.31%	87.14%	97.14%	0.12	0.92
	KNN	91.43%	96.77%	87.18%	85.71%	97.14%	0.14	0.91
	BN	91.67%	97.81%	86.92%	85.24%	98.10%	0.14	0.92
OM 3L t0.5	SVM	93.57%	94.20%	92.96%	92.86%	94.29%	0.07	0.94
	KNN	93.21%	93.53%	92.91%	92.86%	93.57%	0.06	0.94
	BN	91.67%	91.87%	91.47%	91.43%	91.90%	0.09	0.93
OM 4L t0.5	SVM	89.29%	91.04%	87.67%	87.14%	91.43%	0.12	0.89
	KNN	88.57%	91.54%	86.00%	85.00%	92.14%	0.12	0.91
	BN	89.76%	92.82%	87.11%	86.19%	93.33%	0.13	0.92
OM 5L t0.5	SVM	95.71%	97.06%	94.44%	94.29%	97.14%	0.06	0.96
	KNN	96.43%	97.79%	95.14%	95.00%	97.86%	0.04	0.97
	BN	96.90%	98.52%	95.39%	95.24%	98.57%	0.03	0.97
OM 6L t0.5	SVM	99.29%	100.00%	98.59%	98.57%	100.00%	0.01	0.99
	KNN	99.29%	100.00%	98.59%	98.57%	100.00%	0.00	0.99
	BN	99.05%	100.00%	98.13%	98.10%	100.00%	0.00	0.99
SK 3L t0.3	SVM	83.57%	83.10%	84.06%	84.29%	82.86%	0.16	0.84
	KNN	79.29%	80.60%	78.08%	77.14%	81.43%	0.21	0.81
	BN	80.24%	83.60%	77.49%	75.24%	85.24%	0.23	0.83
SK 4L t0.3	SVM	88.57%	90.91%	86.49%	85.71%	91.43%	0.14	0.89
	KNN	85.71%	88.46%	83.33%	82.14%	89.29%	0.17	0.87
	BN	86.19%	90.00%	83.04%	81.43%	90.95%	0.15	0.88
SK 5L t0.3	SVM	84.29%	85.29%	83.33%	82.86%	85.71%	0.17	0.84
	KNN	82.86%	83.33%	82.39%	82.14%	83.57%	0.18	0.84
	BN	83.10%	84.58%	81.74%	80.95%	85.24%	0.19	0.85
SK 6L t0.3	SVM	86.43%	85.92%	86.96%	87.14%	85.71%	0.13	0.86
	KNN	83.21%	83.45%	82.98%	82.86%	83.57%	0.17	0.85
	BN	85.00%	86.93%	83.26%	82.38%	87.62%	0.16	0.88
SK 3L t0.5	SVM	90.00%	92.42%	87.84%	87.14%	92.86%	0.12	0.9
	KNN	89.29%	91.67%	87.16%	86.43%	92.14%	0.12	0.9
	BN	89.76%	93.72%	86.46%	85.24%	94.29%	0.12	0.92

SK 4L t0.5	SVM	83.57%	84.06%	83.10%	82.86%	84.29%	0.17	0.84
	KNN	79.64%	79.02%	80.29%	80.71%	78.57%	0.19	0.83
	BN	81.67%	83.42%	80.09%	79.05%	84.29%	0.19	0.85
SK 5L t0.5	SVM	80.71%	79.45%	82.09%	82.86%	78.57%	0.18	0.81
	KNN	78.93%	79.14%	78.72%	78.57%	79.29%	0.21	0.8
	BN	81.19%	83.25%	79.37%	78.10%	84.29%	0.21	0.83
SK 6L t0.5	SVM	85.71%	87.88%	83.78%	82.86%	88.57%	0.16	0.86
	KNN	82.14%	84.09%	80.41%	79.29%	85.00%	0.19	0.84
	BN	83.33%	86.84%	80.43%	78.57%	88.10%	0.20	0.86
SK 3L t0.7	SVM	79.29%	82.54%	76.62%	74.29%	84.29%	0.23	0.79
	KNN	76.79%	80.00%	74.19%	71.43%	82.14%	0.25	0.79
	BN	77.86%	83.82%	73.68%	69.05%	86.67%	0.27	0.81
SK 4L t0.7	SVM	82.86%	83.82%	81.94%	81.43%	84.29%	0.18	0.83
	KNN	83.93%	83.22%	84.67%	85.00%	82.86%	0.17	0.85
	BN	85.00%	86.21%	83.87%	83.33%	86.67%	0.15	0.87
SK 5L t0.7	SVM	85.71%	86.76%	84.72%	84.29%	87.14%	0.15	0.86
	KNN	82.86%	83.82%	81.94%	81.43%	84.29%	0.19	0.87
	BN	83.57%	86.53%	81.06%	79.52%	87.62%	0.14	0.88
SK 6L t0.7	SVM	90.71%	95.24%	87.01%	85.71%	95.71%	0.13	0.91
	KNN	88.21%	92.13%	84.97%	83.57%	92.86%	0.16	0.89
	BN	88.10%	93.96%	83.61%	81.43%	94.76%	0.18	0.9
SK 3L t0.9	SVM	85.00%	85.51%	84.51%	84.29%	85.71%	0.15	0.85
	KNN	83.21%	83.45%	82.98%	82.86%	83.57%	0.17	0.86
	BN	84.52%	86.07%	83.11%	82.38%	86.67%	0.16	0.88
SK 4L t0.9	SVM	90.00%	93.75%	86.84%	85.71%	94.29%	0.13	0.9
	KNN	89.29%	92.97%	86.18%	85.00%	93.57%	0.14	0.89
	BN	89.05%	94.57%	84.75%	82.86%	95.24%	0.15	0.9
SK 5L t0.9	SVM	89.29%	88.73%	89.86%	90.00%	88.57%	0.10	0.89
	KNN	88.21%	88.49%	87.94%	87.86%	88.57%	0.11	0.89
	BN	88.33%	91.28%	85.78%	84.76%	91.90%	0.14	0.9
SK 6L t0.9	SVM	89.29%	95.08%	84.81%	82.86%	95.71%	0.15	0.89
	KNN	88.57%	94.26%	84.18%	82.14%	95.00%	0.18	0.88
	BN	88.57%	95.00%	83.75%	81.43%	95.71%	0.18	0.89
OK 3L t0.3	SVM	86.43%	85.92%	86.96%	87.14%	85.71%	0.13	0.86
	KNN	86.07%	85.31%	86.86%	87.14%	85.00%	0.13	0.88
	BN	86.67%	85.98%	87.38%	87.62%	85.71%	0.13	0.88
OK 4L t0.3	SVM	85.71%	86.76%	84.72%	84.29%	87.14%	0.15	0.86
	KNN	85.36%	87.79%	83.22%	82.14%	88.57%	0.17	0.87
	BN	85.95%	86.47%	85.45%	85.24%	86.67%	0.14	0.89
OK 5L t0.3	SVM	86.43%	88.06%	84.93%	84.29%	88.57%	0.15	0.86
	KNN	86.79%	88.15%	85.52%	85.00%	88.57%	0.12	0.87
	BN	88.33%	89.27%	87.44%	87.14%	89.52%	0.12	0.9
OK 6L t0.3	SVM	95.00%	98.46%	92.00%	91.43%	98.57%	0.08	0.95
	KNN	92.86%	96.15%	90.00%	89.29%	96.43%	0.10	0.94
	BN	92.14%	97.33%	87.98%	86.67%	97.62%	0.12	0.94

OK 3L t0.5	SVM	92.86%	92.86%	92.86%	92.86%	92.86%	0.07	0.93
	KNN	90.71%	89.58%	91.91%	92.14%	89.29%	0.10	0.93
	BN	90.71%	89.04%	92.54%	92.86%	88.57%	0.10	0.93
OK 4L t0.5	SVM	97.14%	97.14%	97.14%	97.14%	97.14%	0.03	0.97
	KNN	97.50%	97.16%	97.84%	97.86%	97.14%	0.03	0.98
	BN	97.62%	97.17%	98.08%	98.10%	97.14%	0.03	0.98
OK 5L t0.5	SVM	100.00%	100.00%	100.00%	100.00%	100.00%	0.00	1
	KNN	100.00%	100.00%	100.00%	100.00%	100.00%	0.00	1
	BN	99.76%	100.00%	99.53%	99.52%	100.00%	0.00	1
OK 6L t0.5	SVM	97.86%	98.55%	97.18%	97.14%	98.57%	0.03	0.98
	KNN	97.86%	98.55%	97.18%	97.14%	98.57%	0.01	0.98
	BN	98.10%	99.03%	97.20%	97.14%	99.05%	0.01	0.98

Table B.5: The results using the LCS critical function in the context of whole image-based, where S means standard decomposition, O overlapped decomposition, t is the threshold for the critical function and L is the level.

Method	Classifier	Acc	Sen	Spec	PPV	NPV	EER	AUC
SM 3L t0.3	SVM	93.57%	95.52%	91.78%	91.43%	95.71%	0.08	0.94
	KNN	92.50%	93.43%	91.61%	91.43%	93.57%	0.07	0.95
	BN	91.43%	92.23%	90.65%	90.48%	92.38%	0.08	0.94
SM 4L t0.3	SVM	97.14%	97.14%	97.14%	97.14%	97.14%	0.03	0.97
	KNN	97.50%	97.16%	97.84%	97.86%	97.14%	0.02	0.98
	BN	97.86%	97.63%	98.09%	98.10%	97.62%	0.02	0.98
SM 5L t0.3	SVM	98.57%	98.57%	98.57%	98.57%	98.57%	0.01	0.99
	KNN	98.57%	99.28%	97.89%	97.86%	99.29%	0.01	0.99
	BN	98.57%	99.04%	98.11%	98.10%	99.05%	0.01	0.99
SM 6L t0.3	SVM	96.43%	98.51%	94.52%	94.29%	98.57%	0.05	0.96
	KNN	96.07%	97.08%	95.10%	95.00%	97.14%	0.05	0.97
	BN	96.67%	97.57%	95.79%	95.71%	97.62%	0.04	0.98
SM 3L t0.5	SVM	95.00%	94.37%	95.65%	95.71%	94.29%	0.04	0.95
	KNN	95.71%	95.07%	96.38%	96.43%	95.00%	0.05	0.96
	BN	94.29%	93.87%	94.71%	94.76%	93.81%	0.06	0.95
SM 4L t0.5	SVM	100.00%	100.00%	100.00%	100.00%	100.00%	0.00	1
	KNN	99.64%	100.00%	99.29%	99.29%	100.00%	0.00	1
	BN	99.29%	100.00%	98.59%	98.57%	100.00%	0.00	1
SM 5L t0.5	SVM	99.29%	100.00%	98.59%	98.57%	100.00%	0.01	0.99
	KNN	99.29%	100.00%	98.59%	98.57%	100.00%	0.01	0.99
	BN	99.29%	100.00%	98.59%	98.57%	100.00%	0.00	1
SM 6L t0.5	SVM	100.00%	100.00%	100.00%	100.00%	100.00%	0.00	1
	KNN	100.00%	100.00%	100.00%	100.00%	100.00%	0.00	1
	BN	100.00%	100.00%	100.00%	100.00%	100.00%	0.00	1
SM 3L t0.7	SVM	96.43%	94.52%	98.51%	98.57%	94.29%	0.01	0.96
	KNN	95.00%	93.75%	96.32%	96.43%	93.57%	0.04	0.96
	BN	94.52%	93.49%	95.61%	95.71%	93.33%	0.05	0.96

SM 4L t0.7	SVM	100.00%	100.00%	100.00%	100.00%	100.00%	0.00	1
	KNN	100.00%	100.00%	100.00%	100.00%	100.00%	0.00	1
	BN	100.00%	100.00%	100.00%	100.00%	100.00%	0.00	1
SM 5L t0.7	SVM	100.00%	100.00%	100.00%	100.00%	100.00%	0.00	1
	KNN	100.00%	100.00%	100.00%	100.00%	100.00%	0.00	1
	BN	100.00%	100.00%	100.00%	100.00%	100.00%	0.00	1
SM 6L t0.7	SVM	100.00%	100.00%	100.00%	100.00%	100.00%	0.00	1
	KNN	100.00%	100.00%	100.00%	100.00%	100.00%	0.00	1
	BN	100.00%	100.00%	100.00%	100.00%	100.00%	0.00	1
SM 3L t0.9	SVM	92.86%	92.86%	92.86%	92.86%	92.86%	0.07	0.93
	KNN	93.57%	92.96%	94.20%	94.29%	92.86%	0.06	0.93
	BN	94.29%	93.46%	95.15%	95.24%	93.33%	0.06	0.95
SM 4L t0.9	SVM	97.86%	100.00%	95.89%	95.71%	100.00%	0.04	0.98
	KNN	98.21%	100.00%	96.55%	96.43%	100.00%	0.03	0.98
	BN	98.10%	100.00%	96.33%	96.19%	100.00%	0.03	0.98
SM 5L t0.9	SVM	99.29%	100.00%	98.59%	98.57%	100.00%	0.01	0.99
	KNN	99.64%	100.00%	99.29%	99.29%	100.00%	0.00	0.99
	BN	99.76%	100.00%	99.53%	99.52%	100.00%	0.00	1
SM 6L t0.9	SVM	100.00%	100.00%	100.00%	100.00%	100.00%	0.00	1
	KNN	100.00%	100.00%	100.00%	100.00%	100.00%	0.00	1
	BN	100.00%	100.00%	100.00%	100.00%	100.00%	0.00	1
OM 3L t0.3	SVM	93.57%	95.52%	91.78%	91.43%	95.71%	0.08	0.94
	KNN	93.93%	94.89%	93.01%	92.86%	95.00%	0.07	0.94
	BN	94.52%	95.61%	93.49%	93.33%	95.71%	0.07	0.95
OM 4L t0.3	SVM	100.00%	100.00%	100.00%	100.00%	100.00%	0.00	1
	KNN	100.00%	100.00%	100.00%	100.00%	100.00%	0.00	1
	BN	100.00%	100.00%	100.00%	100.00%	100.00%	0.00	1
OM 5L t0.3	SVM	100.00%	100.00%	100.00%	100.00%	100.00%	0.00	1
	KNN	99.64%	100.00%	99.29%	99.29%	100.00%	0.01	1
	BN	99.52%	100.00%	99.06%	99.05%	100.00%	0.01	1
OM 6L t0.3	SVM	97.86%	98.55%	97.18%	97.14%	98.57%	0.03	0.98
	KNN	98.57%	99.28%	97.89%	97.86%	99.29%	0.02	0.98
	BN	98.57%	99.51%	97.66%	97.62%	99.52%	0.02	0.99
OM 3L t0.5	SVM	96.43%	97.10%	95.77%	95.71%	97.14%	0.04	0.96
	KNN	96.43%	97.10%	95.77%	95.71%	97.14%	0.03	0.97
	BN	96.67%	97.57%	95.79%	95.71%	97.62%	0.02	0.97
OM 4L t0.5	SVM	98.57%	100.00%	97.22%	97.14%	100.00%	0.03	0.99
	KNN	98.57%	100.00%	97.22%	97.14%	100.00%	0.02	0.99
	BN	98.57%	100.00%	97.22%	97.14%	100.00%	0.02	0.99
OM 5L t0.5	SVM	100.00%	100.00%	100.00%	100.00%	100.00%	0.00	1
	KNN	100.00%	100.00%	100.00%	100.00%	100.00%	0.00	1
	BN	100.00%	100.00%	100.00%	100.00%	100.00%	0.00	1
OM 6L t0.5	SVM	100.00%	100.00%	100.00%	100.00%	100.00%	0.00	1
	KNN	100.00%	100.00%	100.00%	100.00%	100.00%	0.00	1
	BN	100.00%	100.00%	100.00%	100.00%	100.00%	0.00	1

OM 3L t0.7	SVM	93.57%	92.96%	94.20%	94.29%	92.86%	0.06	0.94
	KNN	95.71%	95.71%	95.71%	95.71%	95.71%	0.04	0.95
	BN	95.48%	96.59%	94.42%	94.29%	96.67%	0.04	0.96
OM 4L t0.7	SVM	99.29%	100.00%	98.59%	98.57%	100.00%	0.01	0.99
	KNN	99.29%	100.00%	98.59%	98.57%	100.00%	0.00	0.99
	BN	99.29%	100.00%	98.59%	98.57%	100.00%	0.00	0.99
OM 5L t0.7	SVM	100.00%	100.00%	100.00%	100.00%	100.00%	0.00	1
	KNN	100.00%	100.00%	100.00%	100.00%	100.00%	0.00	1
	BN	100.00%	100.00%	100.00%	100.00%	100.00%	0.00	1
OM 6L t0.7	SVM	100.00%	100.00%	100.00%	100.00%	100.00%	0.00	1
	KNN	100.00%	100.00%	100.00%	100.00%	100.00%	0.00	1
	BN	100.00%	100.00%	100.00%	100.00%	100.00%	0.00	1
OM 3L t0.9	SVM	93.57%	95.52%	91.78%	91.43%	95.71%	0.08	0.94
	KNN	95.71%	96.38%	95.07%	95.00%	96.43%	0.05	0.95
	BN	96.19%	97.09%	95.33%	95.24%	97.14%	0.05	0.96
OM 4L t0.9	SVM	98.57%	98.57%	98.57%	98.57%	98.57%	0.01	0.99
	KNN	98.93%	98.58%	99.28%	99.29%	98.57%	0.01	0.99
	BN	98.81%	98.12%	99.52%	99.52%	98.10%	0.01	0.99
OM 5L t0.9	SVM	100.00%	100.00%	100.00%	100.00%	100.00%	0.00	1
	KNN	100.00%	100.00%	100.00%	100.00%	100.00%	0.00	1
	BN	100.00%	100.00%	100.00%	100.00%	100.00%	0.00	1
OM 6L t0.9	SVM	100.00%	100.00%	100.00%	100.00%	100.00%	0.00	1
	KNN	100.00%	100.00%	100.00%	100.00%	100.00%	0.00	1
	BN	100.00%	100.00%	100.00%	100.00%	100.00%	0.00	1
SK 3L t0.3	SVM	92.14%	91.55%	92.75%	92.86%	91.43%	0.07	0.92
	KNN	91.79%	90.91%	92.70%	92.86%	90.71%	0.07	0.92
	BN	92.38%	91.20%	93.63%	93.81%	90.95%	0.06	0.93
SK 4L t0.3	SVM	96.43%	95.77%	97.10%	97.14%	95.71%	0.03	0.96
	KNN	95.71%	94.44%	97.06%	97.14%	94.29%	0.04	0.97
	BN	95.48%	93.21%	97.99%	98.10%	92.86%	0.03	0.97
SK 5L t0.3	SVM	100.00%	100.00%	100.00%	100.00%	100.00%	0.00	1
	KNN	99.64%	99.29%	100.00%	100.00%	99.29%	0.00	1
	BN	99.29%	98.59%	100.00%	100.00%	98.57%	0.00	1
SK 6L t0.3	SVM	99.29%	98.59%	100.00%	100.00%	98.57%	0.00	0.99
	KNN	98.93%	97.90%	100.00%	100.00%	97.86%	0.01	0.99
	BN	98.33%	96.77%	100.00%	100.00%	96.67%	0.03	0.98
SK 3L t0.5	SVM	90.71%	90.14%	91.30%	91.43%	90.00%	0.09	0.91
	KNN	91.43%	90.85%	92.03%	92.14%	90.71%	0.08	0.93
	BN	92.14%	90.78%	93.60%	93.81%	90.48%	0.09	0.93
SK 4L t0.5	SVM	98.57%	98.57%	98.57%	98.57%	98.57%	0.01	0.99
	KNN	98.57%	98.57%	98.57%	98.57%	98.57%	0.01	0.99
	BN	98.57%	98.57%	98.57%	98.57%	98.57%	0.01	0.99
SK 5L t0.5	SVM	100.00%	100.00%	100.00%	100.00%	100.00%	0.00	1
	KNN	100.00%	100.00%	100.00%	100.00%	100.00%	0.00	1
	BN	100.00%	100.00%	100.00%	100.00%	100.00%	0.00	1

SK 6L t0.5	SVM	100.00%	100.00%	100.00%	100.00%	100.00%	0.00	1
	KNN	100.00%	100.00%	100.00%	100.00%	100.00%	0.00	1
	BN	100.00%	100.00%	100.00%	100.00%	100.00%	0.00	1
SK 3L t0.7	SVM	95.00%	94.37%	95.65%	95.71%	94.29%	0.04	0.95
	KNN	95.71%	94.44%	97.06%	97.14%	94.29%	0.05	0.96
	BN	95.48%	94.84%	96.14%	96.19%	94.76%	0.05	0.96
SK 4L t0.7	SVM	97.14%	95.83%	98.53%	98.57%	95.71%	0.01	0.97
	KNN	97.14%	95.83%	98.53%	98.57%	95.71%	0.04	0.98
	BN	97.38%	95.85%	99.01%	99.05%	95.71%	0.04	0.98
SK 5L t0.7	SVM	100.00%	100.00%	100.00%	100.00%	100.00%	0.00	1
	KNN	100.00%	100.00%	100.00%	100.00%	100.00%	0.00	1
	BN	100.00%	100.00%	100.00%	100.00%	100.00%	0.00	1
SK 6L t0.7	SVM	100.00%	100.00%	100.00%	100.00%	100.00%	0.00	1
	KNN	100.00%	100.00%	100.00%	100.00%	100.00%	0.00	1
	BN	100.00%	100.00%	100.00%	100.00%	100.00%	0.00	1
SK 3L t0.9	SVM	95.00%	93.15%	97.01%	97.14%	92.86%	0.03	0.95
	KNN	94.64%	93.10%	96.30%	96.43%	92.86%	0.04	0.95
	BN	94.76%	93.12%	96.53%	96.67%	92.86%	0.06	0.95
SK 4L t0.9	SVM	97.86%	97.18%	98.55%	98.57%	97.14%	0.01	0.98
	KNN	97.14%	97.14%	97.14%	97.14%	97.14%	0.03	0.98
	BN	97.38%	97.61%	97.16%	97.14%	97.62%	0.03	0.98
SK 5L t0.9	SVM	100.00%	100.00%	100.00%	100.00%	100.00%	0.00	1
	KNN	100.00%	100.00%	100.00%	100.00%	100.00%	0.00	1
	BN	100.00%	100.00%	100.00%	100.00%	100.00%	0.00	1
SK 6L t0.9	SVM	100.00%	100.00%	100.00%	100.00%	100.00%	0.00	1
	KNN	100.00%	100.00%	100.00%	100.00%	100.00%	0.00	1
	BN	100.00%	100.00%	100.00%	100.00%	100.00%	0.00	1
OK 3L t0.3	SVM	99.29%	98.59%	100.00%	100.00%	98.57%	0.00	0.99
	KNN	99.29%	98.59%	100.00%	100.00%	98.57%	0.01	0.99
	BN	99.29%	98.59%	100.00%	100.00%	98.57%	0.01	0.99
OK 4L t0.3	SVM	100.00%	100.00%	100.00%	100.00%	100.00%	0.00	1
	KNN	100.00%	100.00%	100.00%	100.00%	100.00%	0.00	1
	BN	100.00%	100.00%	100.00%	100.00%	100.00%	0.00	1
OK 5L t0.3	SVM	100.00%	100.00%	100.00%	100.00%	100.00%	0.00	1
	KNN	100.00%	100.00%	100.00%	100.00%	100.00%	0.00	1
	BN	100.00%	100.00%	100.00%	100.00%	100.00%	0.00	1
OK 6L t0.3	SVM	100.00%	100.00%	100.00%	100.00%	100.00%	0.00	1
	KNN	100.00%	100.00%	100.00%	100.00%	100.00%	0.00	1
	BN	100.00%	100.00%	100.00%	100.00%	100.00%	0.00	1
OK 3L t0.5	SVM	99.29%	100.00%	98.59%	98.57%	100.00%	0.01	0.99
	KNN	99.29%	100.00%	98.59%	98.57%	100.00%	0.00	0.99
	BN	99.29%	100.00%	98.59%	98.57%	100.00%	0.00	0.99
OK 4L t0.5	SVM	100.00%	100.00%	100.00%	100.00%	100.00%	0.00	1
	KNN	100.00%	100.00%	100.00%	100.00%	100.00%	0.00	1
	BN	100.00%	100.00%	100.00%	100.00%	100.00%	0.00	1

OK 5L t0.5	SVM	100.00%	100.00%	100.00%	100.00%	100.00%	0.00	1
	KNN	100.00%	100.00%	100.00%	100.00%	100.00%	0.00	1
	BN	100.00%	100.00%	100.00%	100.00%	100.00%	0.00	1
OK 6L t0.5	SVM	100.00%	100.00%	100.00%	100.00%	100.00%	0.00	1
	KNN	100.00%	100.00%	100.00%	100.00%	100.00%	0.00	1
	BN	100.00%	100.00%	100.00%	100.00%	100.00%	0.00	1
OK 3L t0.7	SVM	97.86%	98.55%	97.18%	97.14%	98.57%	0.03	0.98
	KNN	97.86%	98.55%	97.18%	97.14%	98.57%	0.01	0.98
	BN	97.62%	98.54%	96.73%	96.67%	98.57%	0.03	0.98
OK 4L t0.7	SVM	100.00%	100.00%	100.00%	100.00%	100.00%	0.00	1
	KNN	100.00%	100.00%	100.00%	100.00%	100.00%	0.00	1
	BN	100.00%	100.00%	100.00%	100.00%	100.00%	0.00	1
OK 5L t0.7	SVM	100.00%	100.00%	100.00%	100.00%	100.00%	0.00	1
	KNN	100.00%	100.00%	100.00%	100.00%	100.00%	0.00	1
	BN	100.00%	100.00%	100.00%	100.00%	100.00%	0.00	1
OK 6L t0.7	SVM	100.00%	100.00%	100.00%	100.00%	100.00%	0.00	1
	KNN	100.00%	100.00%	100.00%	100.00%	100.00%	0.00	1
	BN	100.00%	100.00%	100.00%	100.00%	100.00%	0.00	1

Bibliography

[1] U Rajendra Acharya, Filippo Molinari, Roberto Garberoglio, Agnieszka Witkowska, Jasjit S Suri, et al. Automated benign & malignant thyroid lesion characterization and classification in 3d contrast-enhanced ultrasound. In *Annual International Conference of the IEEE Engineering in Medicine and Biology Society*, pages 452–455. IEEE, 2012.

[2] David W. Aha. Tolerating noisy, irrelevant and novel attributes in instance-based learning algorithms. *International Journal of Man-Machine Studies*, 36(2):267 – 287, 1992.

[3] Timo Ahonen, Jiri Matas, Chu He, and Matti Pietikainen. Rotation invariant image description with local binary pattern histogram fourier features. In *Proceedings of the 16th Scandinavian Conference on Image Analysis*, pages 61–70, Berlin, Heidelberg, 2009. Springer-Verlag.

[4] Bruce G Batchelor and Frederick M Waltz. Morphological image processing. In Bruce G. Batchelor, editor, *Machine Vision Handbook*, pages 801–870. Springer, 2012.

[5] Liefeng Bo, Xiaofeng Ren, and Dieter Fox. Hierarchical matching pursuit for image classification: Architecture and fast algorithms. In *Advances in Neural Information Processing Systems*, pages 2115–2123, 2011.

[6] A. Bosch, A. Zisserman, and X. Muoz. Image classification using random forests and ferns. In *IEEE 11th International Conference on Computer Vision*, pages 1–8, 2007.

[7] Bernhard E. Boser, Isabelle M. Guyon, and Vladimir N. Vapnik. A training algorithm for optimal margin classifiers. In *Proceedings of the 5th Annual ACM Workshop on Computational Learning Theory*, pages 144–152. ACM Press, 1992.

[8] Y.-L. Boureau, F. Bach, Y. LeCun, and J. Ponce. Learning mid-level features for recognition. In *IEEE Conference on Computer Vision and Pattern Recognition*, pages 2559–2566, 2010.

[9] Susan Bridges, Julia Hodges, Bruce Wooley, Donald Karpovich, and George-Brannon Smith. Knowledge discovery in an oceanographic database. *Applied Intelligence*, 11(2):135–148, 1999.

[10] L. Bruzzone and L. Carlin. A multilevel context-based system for classification of very high spatial resolution images. *IEEE Transactions on Geoscience and Remote Sensing*, 44(9):2587–2600, 2006.

[11] Michael C Burl, Charless Fowlkes, and Joseph Roden. Mining for image content. *Systemics, Cybernetics, and Informatics/Information Systems: Analysis and Synthesis*, 1999.

[12] Erick Cantu-paz. Feature subset selection, class separability, and genetic algorithms. In *Genetic and Evolutionary Computation Conference*, pages 959–970. Springer-Verlag, 2004.

[13] I. Carlbom, I. Chakravarty, and D. Vanderschel. A hierarchical data structure for representing the spatial decomposition of 3-d objects. *IEEE Computer Graphics and Applications*, 5(4):24–31, 1985.

[14] Chih-Chung Chang and Chih-Jen Lin. LIBSVM: A library for support vector machines. *ACM Transactions on Intelligent Systems and Technology*, 2:27:1–27:27, 2011. Software available at `http://www.csie.ntu.edu.tw/~cjlin/libsvm`.

[15] Yin-Wen Chang and Chih-Jen Lin. Feature ranking using linear svm. *Causation and Prediction Challenge Challenges in Machine Learning*, 2:5364, 2008.

[16] Jing Chen, Kip M. Connor, and Lois E.H. Smith. Overstaying their welcome: defective cx3cr1 microglia eyed in macular degeneration. *The Journal of Clinical Investigation*, 117(10):2758–2762, 10 2007.

[17] M. Chen, D. Silver, A. S. Winter, V. Singh, and N. Cornea. Spatial transfer functions: A unified approach to specifying deformation in volume modeling and animation. In *Proceedings of the 2003 Eurographics/IEEE TVCG Workshop on Volume Graphics*, pages 35–44, New York, NY, USA, 2003. ACM.

[18] Weijie Chen, Maryellen L. Giger, Hui Li, Ulrich Bick, and Gillian M. Newstead. Volumetric texture analysis of breast lesions on contrast-enhanced magnetic resonance images. *Magnetic Resonance in Medicine*, 58(3):562–571, 2007.

[19] A. Chu, C. M. Sehgal, and J. F. Greenleaf. Use of gray value distribution of run lengths for texture analysis. *Pattern Recognition Letters.*, 11:415–420, 1990.

[20] Corinna Cortes and Vladimir Vapnik. Support-vector networks. *Machine Learning*, 20:273–297, 1995.

[21] Florence Coscas, Gabriel Coscas, Eric Souied, Sarah Tick, and Gisele Soubrane. Optical coherence tomography identification of occult choroidal neovascularization in age-related macular degeneration. *American Journal of Ophthalmology*, 144(4):592 – 599, 2007.

[22] Gabriel Coscas. Principles of oct examination techniques main oct systems. In *Optical Coherence Tomography in Age-Related Macular Degeneration*, pages 5–14. Springer Berlin Heidelberg, 2009.

[23] J. Cousty, G. Bertrand, L. Najman, and M. Couprie. Watershed cuts: Minimum spanning forests and the drop of water principle. *Pattern Analysis and Machine Intelligence, IEEE Transactions on*, 31(8):1362–1374, 2009.

[24] N. Dalal and B. Triggs. Histograms of oriented gradients for human detection. In *IEEE Computer Society Conference on Computer Vision and Pattern Recognition*, volume 1, pages 886–893, 2005.

[25] Navneet Dalal and Bill Triggs. Histograms of oriented gradients for human detection. In *IEEE Computer Society Conference on Computer Vision and Pattern Recognition*, volume 1, pages 886–893. IEEE, 2005.

[26] Belur V. Dasarathy and Edwin B. Holder. Image characterizations based on joint gray level-run length distributions. *Pattern Recognition Letters.*, 12:497–502, 1991.

[27] Paulus T.V.M. De Jong. Age-related macular degeneration. *New England Journal of Medicine*, 355(14):1474–1485, 2006.

[28] A. P. Dempster, N. M. Laird, and D. B. Rubin. Maximum likelihood from incomplete data via the EM algorithm. *Journal of Royal Statistical Society, Series B*, 39(1):1–38, 1977.

[29] Janez Demšar. Statistical comparisons of classifiers over multiple data sets. *Journal of Machine Learning Research*, 7:1–30, December 2006.

[30] Yining Deng and B.S. Manjunath. Unsupervised segmentation of color-texture regions in images and video. *IEEE Transactions on Pattern Analysis and Machine Intelligence*, 23(8):800–810, 2001.

[31] A. Elsayed, F. Coenen, C. Jiang, M. García-Fiñana, and V. Sluming. Corpus callosum mr image classification. *Knowledge-Based Systems*, 23(4):330–336, 2010.

[32] Hadi Fadaifard and George Wolberg. Multiscale 3d feature extraction and matching. In *International Conference on 3D Imaging, Modeling, Processing, Visualization and Transmission*, pages 228–235. IEEE, 2011.

[33] Tom Fawcett. An introduction to {ROC} analysis. *Pattern Recognition Letters*, 27(8):861 – 874, 2006.

[34] Usama Fayyad, David Haussler, and Paul Stolorz. Kdd for science data analysis: Issues and examples. In *Proceedings of the Second International Conference on Knowledge Discovery and Data Mining*, pages 50–56. AAAI Press, 1996.

[35] Usama Fayyad, Gregory Piatetsky-Shapiro, and Padhraic Smyth. From data mining to knowledge discovery in databases. *AI magazine*, 17(3):37, 1996.

[36] Usama M. Fayyad, Gregory Piatetsky-Shapiro, Padhraic Smyth, and Ramasamy Uthurusamy, editors. *Advances in knowledge discovery and data mining*. American Association for Artificial Intelligence, 1996.

[37] M. Dominik Fischer, Gesine Huber, Susanne C. Beck, Naoyuki Tanimoto, Regine Muehlfriedel, Edda Fahl, Christian Grimm, Andreas Wenzel, Charlotte E. Reme, Serge A. van de Pavert, Jan Wijnholds, Marek Pacal, Rod Bremner, and Mathias W. Seeliger. Noninvasive, in vivo assessment of mouse retinal structure using optical coherence tomography. *PLoS ONE*, 4(10):7507, 10 2009.

[38] Evelyn Fix and Jr. Hodges, J. L. Discriminatory analysis. nonparametric discrimination: Consistency properties. *International Statistical Review / Revue Internationale de Statistique*, 57(3):pp. 238–247, 1989.

[39] Monika Fleckenstein, Peter Charbel Issa, Hans-Martin Helb, Steffen Schmitz-Valckenberg, Robert P. Finger, Hendrik P. N. Scholl, Karin U. Loeffler, and Frank G. Holz. High-resolution spectral domain-oct imaging in geographic atrophy associated with age-related macular degeneration. *Investigative Ophthalmology & Visual Science*, 49(9):4137–4144, 2008.

[40] Gregory T Flitton, Toby P Breckon, and Najla Megherbi Bouallagu. Object recognition using 3d sift in complex ct volumes. In *British Machine Vision Conference*, pages 1–12, 2010.

[41] J. Freixenet, X. Muoz, D. Raba, J. Mart, and X. Cuf. Yet another survey on image segmentation: Region and boundary information integration. In Anders Heyden, Gunnar Sparr, Mads Nielsen, and Peter Johansen, editors, *Computer Vision ECCV 2002*, volume 2352 of *Lecture Notes in Computer Science*, pages 408–422. Springer Berlin Heidelberg, 2002.

[42] Sarah F. Frisken, Ronald N. Perry, Alyn P. Rockwood, and Thouis R. Jones. Adaptively sampled distance fields: A general representation of shape for computer graphics. In *Proceedings of the 27th Annual Conference on Computer Graphics and Interactive Techniques*, pages 249–254, 2000.

[43] Mary M. Galloway. Texture analysis using gray level run lengths. *Computer Graphics and Image Processing*, 4(2):172–179, 1975.

[44] Dengliang Gao. Volume texture extraction for 3d seismic visualization and interpretation. *Geophysics*, 68(4):1294–1302, 2003.

[45] Andrea Giani, Matteo Cereda, and Giovanni Staurenghi. Spectral-domain oct spectralis hra-oct and cirrus zeiss. In *Optical Coherence Tomography in Age-Related Macular Degeneration*, pages 35–48. Springer Berlin Heidelberg, 2009.

[46] Michael Goebel and Le Gruenwald. A survey of data mining and knowledge discovery software tools. *ACM SIGKDD Explorations Newsletter*, 1:20–33, 1999.

[47] Tom Goldstein, Xavier Bresson, and Stanley Osher. Geometric applications of the split bregman method: Segmentation and surface reconstruction. *Journal of Scientific Computing*, 45(1-3):272–293, 2009.

[48] Rafael C. Gonzalez and Richard E. Woods. *Digital Image Processing (3rd Edition)*. Prentice Hall, 3 edition, 2007.

[49] Kirk W. Gossage, Tomasz S. Tkaczyk, Jeffrey J. Rodriguez, and Jennifer K. Barton. Texture analysis of optical coherence tomography images: feasibility for tissue classification. *Journal of Biomedical Optics*, 8(3):570–575, 2003.

[50] Richard A. Groeneveld and Glen Meeden. Measuring skewness and kurtosis. *Journal of the Royal Statistical Society. Series D (The Statistician)*, 33(4):391–399.

[51] Mark Hall, Eibe Frank, Geoffrey Holmes, Bernhard Pfahringer, Peter Reutemann, and Ian H. Witten. The weka data mining software: An update. *SIGKDD Explorations Newsletter*, 11(1):10–18, 2009.

[52] Jiawei Han, Micheline Kamber, and Jian Pei. *Data mining concepts and techniques*. The Morgan Kaufmann series in data management systems. Morgan Kaufmann, third edition edition, 2011.

[53] Robert M. Haralick, K. Shanmugam, and Its'Hak Dinstein. Textural features for image classification. *IEEE Transactions on Systems, Man and Cybernetics*, 3(6):610–621, 1973.

[54] Robert M. Haralick and Linda G. Shapiro. *Computer and Robot Vision*. Addison-Wesley Longman Publishing Co., Inc., Boston, MA, USA, 1st edition, 1992.

[55] Frank Heckel, Olaf Konrad, Horst Karl Hahn, and Heinz-Otto Peitgen. Interactive 3d medical image segmentation with energy-minimizing implicit functions. *Computers & Graphics*, 35(2):275–287, 2011.

[56] M. Heikkila and M. Pietikainen. A texture-based method for modeling the background and detecting moving objects. *IEEE Transactions on Pattern Analysis and Machine Intelligence*, 28(4):657–662, April 2006.

[57] Marko Heikkilä, Matti Pietikäinen, and Cordelia Schmid. Description of interest regions with center-symmetric local binary patterns. In *Computer Vision, Graphics and Image Processing*, pages 58–69. Springer, 2006.

[58] Tobias Heimann and Hans-Peter Meinzer. Statistical shape models for 3d medical image segmentation: A review. *Medical image analysis*, 13(4):543–563, 2009.

[59] Mohd Hanafi Ahmad Hijazi, Chuntao Jiang, Frans Coenen, and Yalin Zheng. Image classification for age-related macular degeneration screening using hierarchical image decompositions and graph mining. In *Machine Learning and Knowledge Discovery in Databases*, pages 65–80. Springer, 2011.

[60] Wynne Hsu, Mong Li Lee, and Ji Zhang. Image mining: Trends and developments. *Journal of Intelligent Information Systems*, 19(1):7–23, 2002.

[61] D Huang, EA Swanson, CP Lin, JS Schuman, WG Stinson, W Chang, MR Hee, T Flotte, K Gregory, CA Puliafito, and al. et. Optical coherence tomography. *Science*, 254(5035):1178–1181, 1991.

[62] Yongzhen Huang, Zifeng Wu, Liang Wang, and Tieniu Tan. Feature coding in image classification: A comprehensive study. *IEEE Transactions on Pattern Analysis and Machine Intelligence*, 36(3):493–506, 2014.

[63] Gregory Michael Hunter. *Efficient computation and data structures for graphics*. PhD thesis, 1978.

[64] Anca Loredana Ion. Methods for knowledge discovery in images. *Information Technology and Control*, 38(1):43–49, 2009.

[65] Chris L Jackins and Steven L Tanimoto. Oct-trees and their use in representing three-dimensional objects. *Computer Graphics and Image Processing*, 14(3):249–270, 1980.

[66] Rama D. Jager, William F. Mieler, and Joan W. Miller. Age-related macular degeneration. *New England Journal of Medicine*, 358(24):2606–2617, 2008.

[67] Nathalie Japkowicz and Mohak Shah. *Evaluating Learning Algorithms: A Classification Perspective*. Cambridge University Press, New York, NY, USA, 2011.

[68] Don H. Johnson and Sinan Sinanovic. Symmetrizing the kullback-leibler distance. *IEEE Transactions on Information Theory*, 2001.

[69] Ian Jolliffe. *Principal component analysis*. Wiley Online Library, 2005.

[70] Raheleh Kafieh, Hossein Rabbani, Michael D Abramoff, and Milan Sonka. Intra-retinal layer segmentation of 3d optical coherence tomography using coarse grained diffusion map. *Medical Image Analysis*, 2013.

[71] Vedran Kajić, Marieh Esmaeelpour, Carl Glittenberg, Martin F Kraus, Joachim Honegger, Richu Othara, Susanne Binder, James G Fujimoto, and Wolfgang Drexler. Automated three-dimensional choroidal vessel segmentation of 3d 1060 nm oct retinal data. *Biomedical optics express*, 4(1):134, 2013.

[72] Eamonn Keogh. Exact indexing of dynamic time warping. In *Proceedings of the 28th international conference on Very Large Data Bases*, pages 406–417, 2002.

[73] Jong Kook Kim and Hyun Wook Park. Statistical textural features for detection of microcalcifications in digitized mammograms. *IEEE Transactions on Medical Imaging,*, 18(3):231 –238, 1999.

[74] Ronald Klein, Tunde Peto, Alan Bird, and Mylan R. Vannewkirk. The epidemiology of age-related macular degeneration. *American Journal of Ophthalmology*, 137(3):486 – 495, 2004.

[75] Willi Klösgen and Jan M. Zytkow. The knowledge discovery process. In Willi Klösgen and Jan M. Zytkow, editors, *Handbook of Data Mining and Knowledge Discovery*, pages 10–21. Oxford University Press, Inc., New York, NY, USA, 2002.

[76] Helga Kolb. Gross anatomy of the eye. In Helga Kolb, Eduardo Fernandez, Ralph Nelson, and Helga Kolb, editors, *Webvision: The Organization of the Retina and Visual System*. 2011.

[77] Helga Kolb. Simple anatomy of the retina. In Helga Kolb, Eduardo Fernandez, Ralph Nelson, and Helga Kolb, editors, *Webvision: The Organization of the Retina and Visual System*. 2011.

[78] Taku Kudo, Eisaku Maeda, and Yuji Matsumoto. An application of boosting to graph classification. In *Advances in neural information processing systems*, pages 729–736, 2004.

[79] Pardeep Kumar, Vivek Kumar Sehgal, and Durg Singh Chauhan. Knowledge discovery in databases (kdd) with images: A novel approach toward image mining and processing. *International Journal of Computer Applications*, 27(6):10–13, 2011.

[80] Lukasz A. Kurgan and Petr Musilek. A survey of knowledge discovery and data mining process models. *The Knowledge Engineering Review*, 21(1):1–24, 2006.

[81] Kirill V Larin, Mohamad G Ghosn, Alexey N Bashkatov, Elina A Genina, Natalia A Trunina, and Valery V Tuchin. Optical clearing for oct image enhancement and in-depth monitoring of molecular diffusion. *IEEE Journal of Selected Topics in Quantum Electronics*, 18(3):1244–1259, 2012.

[82] S. Lazebnik, C. Schmid, and J. Ponce. Beyond bags of features: Spatial pyramid matching for recognizing natural scene categories. In *IEEE Computer Society Conference on Computer Vision and Pattern Recognition*, volume 2, pages 2169–2178, 2006.

[83] Svetlana Lazebnik, Cordelia Schmid, Jean Ponce, et al. Spatial pyramid matching. *Object Categorization: Computer and Human Vision Perspectives*, 3:4, 2009.

[84] Lillian Le-Cointe. Applied statistics: A handbook of techniques. *Technometrics*, 40(2):155–155, 1998.

[85] Jia Li and J.Z. Wang. Automatic linguistic indexing of pictures by a statistical modeling approach. *IEEE Transactions on Pattern Analysis and Machine Intelligence*, 25(9):1075–1088, 2003.

[86] Yihua Liao and V. Rao Vemuri. Use of k-nearest neighbor classifier for intrusion detection. *Computers & Security*, 21(5):439 – 448, 2002.

[87] Zhe Lin and L.S. Davis. Shape-based human detection and segmentation via hierarchical part-template matching. *IEEE Transactions on Pattern Analysis and Machine Intelligence*, 32(4):604–618, 2010.

[88] Yu-Ying Liu, Mei Chen, Hiroshi Ishikawa, Gadi Wollstein, Joel Schuman, and James M. Rehg. Automated macular pathology diagnosis in retinal OCT images using multi-scale spatial pyramid and local binary patterns in texture and shape encoding. *Medical Image Analysis*, 15(5):748–759, 2011.

[89] Seth Long and Lawrence B Holder. Graph-based shape analysis for mri classification. *International Journal of Knowledge Discovery in Bioinformatics*, 2(2):19–33, 2011.

[90] David G Lowe. Object recognition from local scale-invariant features. In *The proceedings of the seventh IEEE international conference on Computer vision*, volume 2, pages 1150–1157. IEEE, 1999.

[91] David G Lowe. Local feature view clustering for 3d object recognition. In *Proceedings of the 2001 IEEE Computer Society Conference on Computer Vision and Pattern Recognition*, volume 1, pages 682–688, 2001.

[92] David G Lowe. Distinctive image features from scale-invariant keypoints. *International journal of computer vision*, 60(2):91–110, 2004.

[93] Dominic Mai, Philipp Fischer, Thomas Blein, Jasmin Dürr, Klaus Palme, Thomas Brox, and Olaf Ronneberger. Discriminative detection and alignment in volumetric data. In *Pattern Recognition*, pages 205–214. Springer, 2013.

[94] Jiri Matas, Ondrej Chum, Martin Urban, and Tomás Pajdla. Robust wide-baseline stereo from maximally stable extremal regions. *Image and vision computing*, 22(10):761–767, 2004.

[95] Krystian Mikolajczyk, Tinne Tuytelaars, Cordelia Schmid, Andrew Zisserman, Jiri Matas, Frederik Schaffalitzky, Timor Kadir, and Luc Van Gool. A comparison of affine region detectors. *International journal of computer vision*, 65(1-2):43–72, 2005.

[96] Nader Nassif, Barry Cense, B. Hyle Park, Seok H. Yun, Teresa C. Chen, Brett E. Bouma, Guillermo J. Tearney, and Johannes F. de Boer. In vivo human retinal imaging by ultrahigh-speed spectral domain optical coherence tomography. *Optics Letters*, 29(5):480–482, 2004.

[97] S. Nowozin, K. Tsuda, T. Uno, T. Kudo, and G. Bakir. Weighted substructure mining for image analysis. In *Computer Vision and Pattern Recognition, 2007. CVPR '07. IEEE Conference on*, pages 1–8, June 2007.

[98] Timo Ojala, Matti Pietikäinen, and Topi Mäenpää. A generalized local binary pattern operator for multiresolution gray scale and rotation invariant texture classification. In *Advances in Pattern Recognition*, pages 399–408. Springer, 2001.

[99] Ville Ojansivu and Janne Heikkilä. Blur insensitive texture classification using local phase quantization. In *Proceedings of the 3rd International Conference on Image and Signal Processing*, pages 236–243. Springer-Verlag, 2008.

[100] TIMOTHY W. OLSEN. Chapter 10 - retina. In David A. Palay and Jay H. Krachmer, editors, *Primary Care Ophthalmology (Second Edition)*, pages 149 – 187. Mosby, Philadelphia, second edition edition, 2005.

[101] Juhani Päivärinta, Esa Rahtu, and Janne Heikkilä. Volume local phase quantization for blur-insensitive dynamic texture classification. In *Proceedings of the 17th Scandinavian Conference on Image Analysis*, pages 360–369. Springer-Verlag, 2011.

[102] Nilesh Patel and Ishwar Sethi. Multimedia data mining: An overview. In ValeryA. Petrushin and Latifur Khan, editors, *Multimedia Data Mining and Knowledge Discovery*, pages 14–41. Springer London, 2007.

[103] Michal Perdoch, Jiri Matas, and Stepán Obdrzálek. Stable affine frames on isophotes. In *IEEE 11th International Conference on Computer Vision*, pages 1–8. IEEE, 2007.

[104] Petra Perner. Image mining: issues, framework, a generic tool and its application to medical-image diagnosis. *Engineering Applications of Artificial Intelligence*, 15(2):205–216, 2002.

[105] Florent Perronnin, Jorge Sánchez, and Thomas Mensink. Improving the fisher kernel for large-scale image classification. In *Computer Vision*, pages 143–156. Springer, 2010.

[106] A. Gh. Podoleanu. Optical coherence tomography. *Journal of Microscopy*, 247(3):209–219, 2012.

[107] Elena Prokofyeva and Eberhart Zrenner. Epidemiology of major eye diseases leading to blindness in europe: a literature review. *Ophthalmic research*, 47(4):171–188, 2011.

[108] DD Purves et al. Neuroscience. edition. edited by: Dale purves, 2004.

[109] Gwénolé Quellec, Kyungmoo Lee, Martin Dolejsi, Mona Kathryn Garvin, Michael D Abràmoff, and Milan Sonka. Three-dimensional analysis of retinal layer texture: identification of fluid-filled regions in sd-oct of the macula. *Medical Imaging, IEEE Transactions on*, 29(6):1321–1330, 2010.

[110] Hossein Rabbani, Milan Sonka, and Michael D Abramoff. Optical coherence tomography noise reduction using anisotropic local bivariate gaussian mixture prior in 3d complex wavelet domain. *International Journal of Biomedical Imaging*, 2013, 2013.

[111] H Rasmussen, KW Chu, P Campochiaro, PL Gehlbach, JA Haller, JT Handa, QD Nguyen, and JU Sung. Clinical protocol. an open-label, phase i, single administration, dose-escalation study of adgvpedf. 11d (adpedf) in neovascular age-related macular degeneration (amd). *Human gene therapy*, 12(16):2029–2032, 2001.

[112] Andreas Reichenbach and Andreas Bringmann. Retina: Neuroanatomy and physiology. In DonaldW. Pfaff, editor, *Neuroscience in the 21st Century*, pages 557–628. Springer New York, 2013.

[113] Lee Ann Remington. Chapter 4 - retina. In Lee Ann Remington, editor, *Clinical Anatomy and Physiology of the Visual System (Third Edition)*, pages 61 – 92. Butterworth-Heinemann, Saint Louis, third edition edition, 2012.

[114] Xiaofeng Ren and J. Malik. Learning a classification model for segmentation. In *Proceedings of Ninth IEEE International Conference on Computer Vision*, pages 10–17 vol.1, 2003.

[115] Alfredo Rodriguez, Douglas B Ehlenberger, Dara L Dickstein, Patrick R Hof, and Susan L Wearne. Automated three-dimensional detection and shape classification of dendritic spines from fluorescence microscopy images. *PLoS One*, 3(4):e1997, 2008.

[116] Leonid I. Rudin, Stanley Osher, and Emad Fatemi. Nonlinear total variation based noise removal algorithms. *Physica D: Nonlinear Phenomena*, 60(1-4):259 – 268, 1992.

[117] Hiroto Saigo, Sebastian Nowozin, Tadashi Kadowaki, Taku Kudo, and Koji Tsuda. gboost: a mathematical programming approach to graph classification and regression. *Machine Learning*, 75(1):69–89, April 2009.

[118] Hanan Samet. The quadtree and related hierarchical data structures. *ACM Computing Surveys (CSUR)*, 16(2):187–260, 1984.

[119] Yoshinobu Sato, Carl-Fredrik Westin, Abhir Bhalerao, Shin Nakajima, Nobuyuki Shiraga, Shinichi Tamura, and Ron Kikinis. Tissue classification based on 3d local intensity structures for volume rendering. *IEEE Transactions on Visualization and Computer Graphics*, 6(2):160–180, 2000.

[120] J. Schneider and R. Westermann. Compression domain volume rendering. In *IEEE Visualization*, pages 293–300, 2003.

[121] Robert Schneiders. Algorithms for quadrilateral and hexahedral mesh generation. *Proceedings of the VKI lecture series on computational fluid cynamics*, 2000.

[122] MichaelE. Schuckers. Receiver operating characteristic curve and equal error rate. In *Computational Methods in Biometric Authentication*, Information Science and Statistics, pages 155–204. Springer London, 2010.

[123] Paul Scovanner, Saad Ali, and Mubarak Shah. A 3-dimensional sift descriptor and its application to action recognition. In *Proceedings of the 15th international conference on Multimedia*, pages 357–360, 2007.

[124] Howard J Seltman. Experimental design and analysis. *Pittsburgh, PA: Carnegie Mellon University*, 2012.

[125] David J Sheskin. *Handbook of parametric and nonparametric statistical procedures*. Chapman & Hall/crc Press, 2003.

[126] J. Sivic and A. Zisserman. Video google: a text retrieval approach to object matching in videos. In *Proceedings of the Ninth IEEE International Conference on Computer Vision*, volume 2, pages 1470–1477, 2003.

[127] Richard Socher, Brody Huval, Bharath Bath, Christopher D Manning, and Andrew Ng. Convolutional-recursive deep learning for 3d object classification. In *Advances in Neural Information Processing Systems*, pages 665–673, 2012.

[128] E Soundararajan, JVM Joseph, C Jayakumar, and M Somasekharan. Knowledge discovery tools and techniques. *Recent Advances in Information Technology*, pages 141–146, 2005.

[129] Bastian Steder, Radu Bogdan Rusu, Kurt Konolige, and Wolfram Burgard. Point feature extraction on 3d range scans taking into account object boundaries. In *IEEE International Conference on Robotics and Automation*, pages 2601–2608. IEEE, 2011.

[130] S Sumathi and SN Sivanandam. Data mining tasks, techniques, and applications. In *Introduction to Data Mining and its Applications*, volume 29 of *Studies in Computational Intelligence*, pages 195–216. Springer Berlin Heidelberg, 2006.

[131] H. Sundar, Rahul S. Sampath, Santi S. Adavani, Christos Davatzikos, and G. Biros. Low-constant parallel algorithms for finite element simulations using linear octrees. In *Proceedings of the 2007 ACM/IEEE Conference on Supercomputing,*, pages 1–12, 2007.

[132] Xiaoou Tang. Texture information in run-length matrices. *IEEE Transactions on Image Processing*, 7(11):1602–1609, 1998.

[133] Steven Tanimoto and Theo Pavlidis. A hierarchical data structure for picture processing. *Computer Graphics and Image Processing*, 4(2):104–119, 1975.

[134] Sergios Theodoridis and Konstantinos Koutroumbas. Chapter 1 - introduction. In Sergios Theodoridis and Konstantinos Koutroumbas, editors, *Pattern Recognition (Fourth Edition)*, pages 1 – 12. Academic Press, Boston, fourth edition edition, 2009.

[135] Alain Tremeau and Nathalie Borel. A region growing and merging algorithm to color segmentation. *Pattern recognition*, 30(7):1191–1203, 1997.

[136] Zhuowen Tu and Xiang Bai. Auto-context and its application to high-level vision tasks and 3d brain image segmentation. *IEEE Transactions on Pattern Analysis and Machine Intelligence*, 32(10):1744–1757, 2010.

[137] Tinne Tuytelaars and Krystian Mikolajczyk. Local invariant feature detectors: A survey. *Foundations and Trends in Computer Graphics and Vision*, 3(3):177–280, 2008.

[138] Vladimir Vapnik. *The nature of statistical learning theory*. springer, 2000.

[139] Diego Viejo, Jose Garcia, Miguel Cazorla, David Gil, and Magnus Johnsson. Using gng to improve 3d feature extraction-application to 6dof egomotion. *Neural Networks*, 32:138–146, 2012.

[140] Michail Vlachos, Marios Hadjieleftheriou, Dimitrios Gunopulos, and Eamonn Keogh. Indexing multi-dimensional time-series with support for multiple distance measures. In *Proceedings of the Ninth ACM SIGKDD International Conference on Knowledge Discovery and Data Mining*, pages 216–225. ACM, 2003.

[141] A. Voisin, V.A. Krylov, G. Moser, S.B. Serpico, and J. Zerubia. Classification of very high resolution sar images of urban areas using copulas and texture in a hierarchical markov random field model. *IEEE Geoscience and Remote Sensing Letters*, 10(1):96–100, 2013.

[142] Jinjun Wang, Jianchao Yang, Kai Yu, Fengjun Lv, Thomas Huang, and Yihong Gong. Locality-constrained linear coding for image classification. In *IEEE Conference on Computer Vision and Pattern Recognition*, pages 3360–3367, 2010.

[143] Xiaoyu Wang, T.X. Han, and Shuicheng Yan. An hog-lbp human detector with partial occlusion handling. In *IEEE 12th International Conference on Computer Vision*, pages 32–39, 2009.

[144] Kenneth Weiss and Leila De Floriani. Simplex and diamond hierarchies: Models and applications. In *Computer Graphics Forum*, volume 30, pages 2127–2155. Wiley Online Library, 2011.

[145] MacIej Wojtkowski, Tomasz Bajraszewski, Iwona Gorczynska, Piotr Targowski, Andrzej Kowalczyk, Wojciech Wasilewski, and Czeslaw Radzewicz. Ophthalmic imaging by spectral optical coherence tomography. *American Journal of Ophthalmology*, 138(3):412 – 419, 2004.

[146] Jianixn Wu and J.M. Rehg. Where am i: Place instance and category recognition using spatial pact. In *IEEE Conference on Computer Vision and Pattern Recognition*, pages 1–8, 2008.

[147] Peng Wu, YongMan Ro, CheeSun Won, and Yanglim Choi. Texture descriptors in mpeg-7. In Wadysaw Skarbek, editor, *Computer Analysis of Images and Patterns*, volume 2124 of *Lecture Notes in Computer Science*, pages 21–28. Springer Berlin Heidelberg, 2001.

[148] X. Yan and Jiawei Han. gspan: graph-based substructure pattern mining. In *Proceedings of IEEE International Conference on Data Mining*, pages 721–724, 2002.

[149] Jianchao Yang, Kai Yu, Yihong Gong, and Thomas Huang. Linear spatial pyramid matching using sparse coding for image classification. In *IEEE Conference on Computer Vision and Pattern Recognition*, pages 1794–1801, 2009.

[150] Qi Yang, Charles A Reisman, Zhenguo Wang, Yasufumi Fukuma, Masanori Hangai, Nagahisa Yoshimura, Atsuo Tomidokoro, Makoto Araie, Ali S Raza, Donald C Hood, et al. Automated layer segmentation of macular oct images using dual-scale gradient information. *Optics express*, 18(20):21293, 2010.

[151] Yi Yang and S. Newsam. Spatial pyramid co-occurrence for image classification. In *IEEE International Conference on Computer Vision*, pages 1465–1472, 2011.

[152] Zahid Yaqoob, Jigang Wu, and Changhuei Yang. Spectral domain optical coherence tomography: a better oct imaging strategy. *Biotechniques*, 2005.

[153] Yufeng Zang, Tianzi Jiang, Yingli Lu, Yong He, and Lixia Tian. Regional homogeneity approach to FMRI data analysis. *NeuroImage*, 22(1):394–400, 2004.

[154] Ji Zhang, Wynne Hsu, and Mong Li Lee. Image mining: Issues, frameworks and techniques. In *Proceedings of the 2nd ACM SIGKDD International Workshop on Multimedia Data Mining*. University of Alberta, 2001.

[155] Yuli Zhang, Huaiyu Wu, and Lei Cheng. Some new deformation formulas about variance and covariance. In *Proceedings of International Conference on Modelling, Identification Control*, pages 987–992, 2012.

[156] Guoying Zhao and M. Pietikainen. Dynamic texture recognition using local binary patterns with an application to facial expressions. *IEEE Transactions on Pattern Analysis and Machine Intelligence*, 29(6):915 –928, june 2007.

[157] Guoying Zhao and Matti Pietikainen. Dynamic texture recognition using local binary patterns with an application to facial expressions. *IEEE Transactions on Pattern Analysis and Machine Intelligence*, 29(6):915–928, 2007.

[158] Xi Zhou, Kai Yu, Tong Zhang, and Thomas S Huang. Image classification using super-vector coding of local image descriptors. In *Computer Vision*, Lecture Notes in Computer Science, pages 141–154. Springer, 2010.